Chapter 1

Introduction

In order to meet the continuously growing electricity demand, the use of nuclear energy is inevitable. The contribution to power production of renewable sources including biomass, wind, hydro and solar will still be limited in short term future (Davis, 1990), while a growth of the use of fossil fuel like oil, gas and coal is unwanted because of the limited resources and environmental impact of emissions. Nuclear energy offers a comparatively clean alternative (El-Hinnawi, 1978) which is technically feasible on the scale needed.

One of the main drawbacks of nuclear energy hitherto has been its safety problem. This had not only a negative effect on public acceptance, the expensive security-measures have also adversely effected the economic performance. Therefore, in the past years the attention of the nuclear industry has shifted from adding redundant safety-systems to designing inherently safe systems. The High Temperature gas-cooled Reactor (HTGR) is a reactor which can be designed to be inherently safe, which means that the worst case accident cannot lead to release of any radio-activity, even in the complete absence of action by operators or control-systems. The HTGR owes its safety characteristics amongst others to two features: its ability to withstand (and thus operate at) high temperatures and its small scale (reactor power is typically less than 300 MW). These features also make the reactor fit for Combined Heat and Power (CHP) production: the high temperature makes it possible to use the waste-heat of the electricity-production, and the typical thermal power of a CHP-plant is low compared to plants for electricity production only. In the Netherlands, CHP production is very popular. Therefore, the Dutch Programme to Intensify Nuclear Competence (PINK) supported the evaluation of a HTGR for cogeneration purposes. This thesis describes research that has been conducted in the framework of PINK. The goal of the study is to investigate the design of the energy conversion system for an HTGR-CHP plant by means of computer modelling.

1.1 The High Temperature Gas-cooled Reactor

In a HTGR fuel is contained in ceramic-coated fuel-particles which itself are contained in a graphite fuel element. The fuel elements can be hexagonal blocks with cooling channels which are stacked in the reactor, or spherical pebbles (6 cm diameter) which form a randomly packed bed. The cooling medium flows through the space between the pebbles (Bedenig, 1972). An impression of the coated particles and the pebbles is given in figure 1 (Kugeler, 1989). The fuel can withstand temperatures up to 1600 °C without any release of fission products. Therefore,

the reactor has to be designed so that in case of complete loss of cooling-flow or even cooling-medium, the fuel temperatures do not exceed 1600 °C. With a small cylindrical core the heat losses by conduction, radiation and natural convection balance the heat production at even lower temperatures.

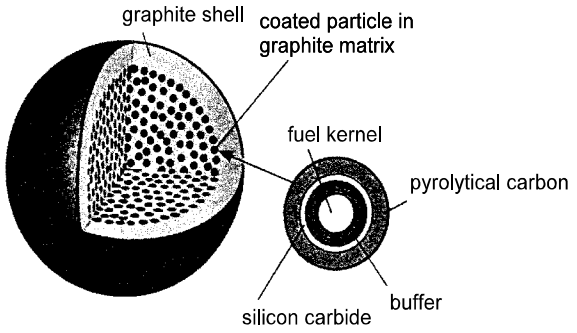

Figure 1.1: Fuel pebble and coated particle.

The cooling medium of the HTGR is helium. Helium is nuclear and chemically inert, which is obviously an asset. Moreover, its heat capacity and conductivity are fairly high, which is favourable for the heat removal. A third advantage of the use of helium in case of a direct gas turbine cycle is the very high velocity of sound. In the turbine design the gas velocity poses no limit on the design (no choking or supersonic-subsonic transitions), hence the stresses in the blades (and thus the blade speeds) are limiting. The main drawback of helium is its low molecular weight, which makes it very hard to produce a leak tight installation (Cohen, 1996).

The HTGR is not a new concept. Already in the nineteen forties it was identified by Keller (Smith, 1945) that 'The closed-cycle gas turbine power plant using helium or helium mixtures appears to be one of the best systems for generating power by the use of the uranium pile.' Several HTGR's have been built and operated in the USA and Great Britain (with prismatic fuel elements) and Germany (pebble bed reactors) since the late fifties. In the German AVR reactor, the inherent safety was even tested by simply switching off the blower, so that the cooling flow completely stagnated. The pebble temperature stayed well below those at which the particles release radio-active elements (Kugeler, 1989). The HTGR power-plants all worked with a secondary steam cycle: the heat was transferred to the steam cycle in a boiler. The direct cycle with a helium turbine that Keller proposed was considered too innovative. However, the high-pressure water in the steam cycle poses a threat to the inherent safety-features. Water ingress can lead to both a reactivity excursion due to additional moderation and corrosion of the graphite. Therefore the substitution of the steam cycle with a closed-cycle gas turbine system is a necessity for the design of an inherently safe plant. Currently, a Japanese HTGR test-reactor is in operation since 1998 (Sanokawa, 1997) and a Chinese test-reactor is under construction (Xu, 1997).

In 1994 a group of Dutch companies and research groups started the INCOGEN (Inherently safe Nuclear COGENeration) pre-feasibility study (van Heek, 1997). Figure 1.2 shows the reactor design which resulted from this study. The plant design of the INCOGEN-study is used as a starting-point for the design produced in this thesis, whereas the reactor design has been slightly modified by Verkerk (2000). The pebble bed reactor core has a diameter of 2.5 m and is initially only 1.25 m high. The pebbles contain 12 gram of 10% enriched uranium. Depletion of fuel during operation is continuously compensated by adding new pebbles at a rate of approximately 60 pebbles per day. This so-called Peu-A-Peu (PAP) fuelling yields a very small overreactivity which is a clear advantage with regard to safety. After four years the reactor cavity is filled up completely and must be emptied. The pebble bed is surrounded with various graphite reflectors; their function is to moderate (slow down) the neutrons and reflect them back to the fuel zone. Helium from the energy conversion system enters the reactor at the bottom and is led to the top

through cooling channels in the side reflector. It flows downward through the pebble bed after which it is redirected to the energy conversion system. Safety studies have shown that this design leads to maximum fuel temperature of 1627 °C during the worst case loss of coolant flow accident (Verkerk, 2000). A slight modification of the design is needed to obtain a temperature under 1600 °C, the fuel temperature which does not lead to fuel degradation.

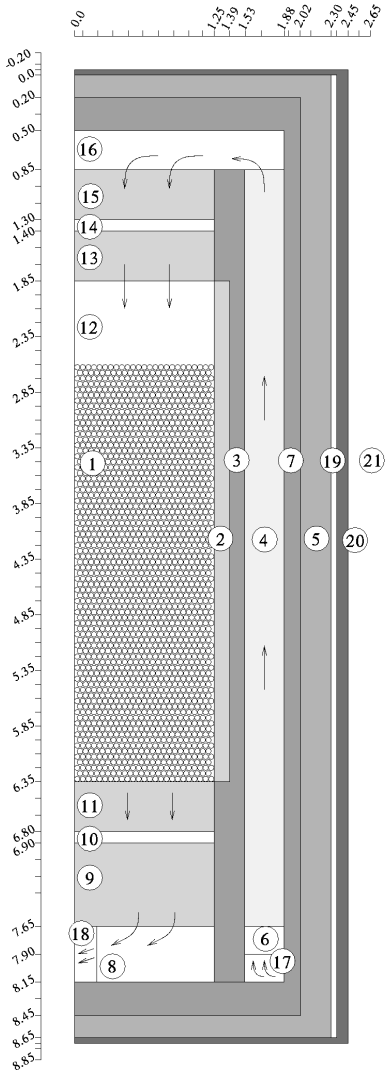

1. pebble-bed core
2. inner reflector
3. middle reflector
4. reflector with coolant channels
5. outer reflector
6. coolant distribution volume
7. separator reflector
8. coolant mixing volume
9. lower bottom reflector
10. bottom reflector plenum
11. upper bottom reflector
12. remaining core volume (to be filled with pebbles)
13. lower top reflector
14. top reflector plenum
15. upper top reflector
16. coolant mixing volume
17. coolant inlet point
18. coolant outlet point
19. gap filled with helium
20. steel vessel wall
21. air

Figure 1.2: INCOGEN reactor design (adapted from Verkerk, 2000).

1.2 The Closed Cycle Gas Turbine System

A typical flowsheet of a Closed Cycle Gas Turbine (CCGT) system is given in figure 1.3. The medium is first brought to high pressure in the compressor. After that it is preheated with the turbine outlet flow in the recuperator. Subsequently the helium is heated with an external heat source, which can for example be fossil, nuclear or solar. The medium expands in the turbine, which drives the generator and compressor. The temperature after this expansion is still quite high, so the residual heat-content of the flow is used to preheat the compressor outlet flow. Finally the gas is cooled before it re-enters the compressor.

Obvious advantages of the CCGT over open-air cycles are the free choice of operating medium and compressor inlet pressure. At elevated pressures pressure losses are reduced (because of lower velocities for a given mass flow) which is beneficial for overall efficiency and design of heat exchanging equipment and turbo-machinery. The medium is kept very clean, which also is favourable for the heat exchanger design. The part-load characteristics of CCGT's are extremely good. At half power, the pressure can be reduced to half the design value. In this way all temperatures and velocities are kept very close to the design values. This results in an efficiency which is even higher than at the design-point, because the recuperator operates more efficiently at lower mass flow. The main disadvantage is the need for a final gas cooler; in an open cycle "cold" air is abundantly available. Several fossil fired CCGT's have operated between 1956 and 1982, of which one had helium as working fluid. The other systems used air (Bammert, 1975 & 1986).

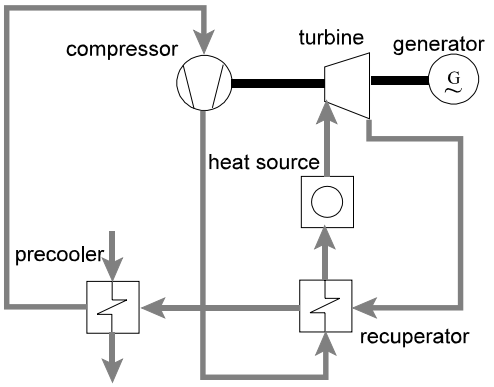

Figure 1.3: Recuperated cycle.

1.3 The Nuclear Gas Turbine System

Only one Nuclear Gas Turbine (NGT) system has ever operated: the USA military ML-1 (McDonald, 1995). This small (330 kWel) mobile power generator employed a non-recuperated nitrogen-cycle, and was built in 1961.

Developments in the eighties and the nineties have led to renewed interest in the NGT system. The most important enabling technologies are magnetic bearings and compact plate-fin heat exchangers (McDonald, 1994). Magnetic bearings are a necessity since oil bearings may lead to oil ingress in the reactor systems, and the rotor of all large plant designs is too heavy for gas bearings. Since 1985 magnetic bearings have been used in conventional gas turbine technology and proven reliable. The recuperator efficiency is of great importance for the plant efficiency and thus economy. This is shown in figure 1.4 in which the efficiency is plotted against pressure ratio for a non-recuperated cycle and for different recuperator efficiencies, given typical component efficiencies and temperatures (from Cohen, 1996). The recuperator size varies strongly with efficiency, for example, to increase the efficiency from 90% to 95% the size is doubled. In the gas-gas heat exchanger, extended surface on both cold and hot side is needed. This is hard to achieve with the tubular heat exchangers which where proposed for NGT-plants up to approx. 1985 (HHT, 1983). However, in the eighties

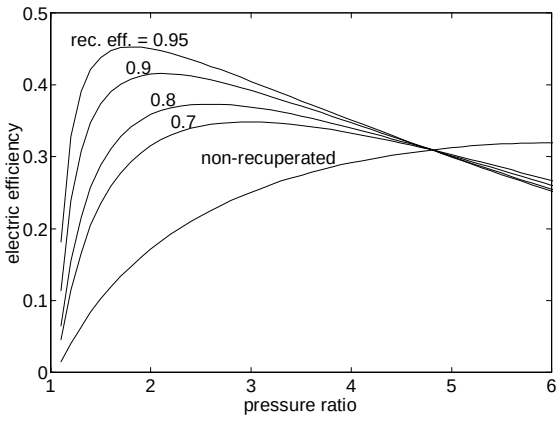

Figure1.4: Efficiency of recuperated and non-recuperated cycle.

compact plate-fin recuperators with very high surface/volume ratio were developed for conventional gas turbines (McDonald, 1996a). These recuperators can easily be adopted for an NGT-plant which makes high efficiencies possible without the cost of high pressure losses, high volumes and high investment costs.

Over the years, proposed designs have changed from extremely large (the GT-HTGR plant of General Atomic in 1975: 3000 MWth (Schoene, 1975)) to very small (the Dutch INCOGEN-design: 40 MWth, (van Heek, 1997)). The designs also have varying degrees of complexity, some important examples are discussed underneath (Kikstra, 1997).

The cycle shown in figure 1.3 is used in several designs (Yan, 1991 & 1992, HHT, 1983, Lidsky, 1988) its biggest asset is its simplicity. Typical values are a pressure ratio of 2 to 2.5, reactor inlet and outlet temperatures of 500 °C and 850 °C and a compressor inlet temperature of 30 °C.

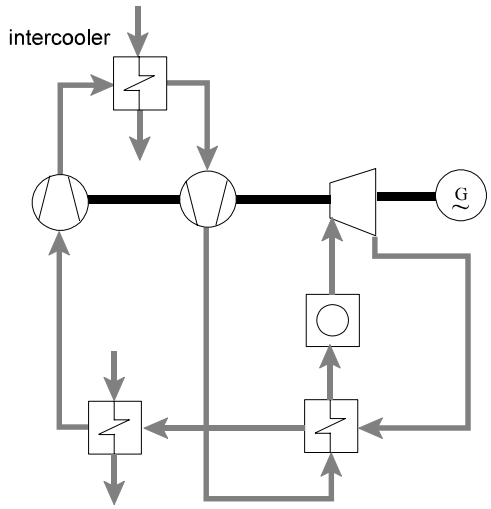

Figure 1.5: Intercooled cycle.

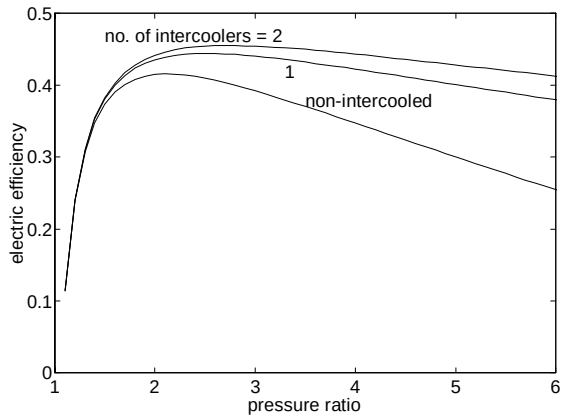

Figure 1.6: Efficiency of intercooled and non-intercooled cycle.

When the compressor is split up and the flow is intercooled between the compression steps, a slight increase in efficiency can be obtained, see figure 1.5 and 1.6. The reason is that the compressor power varies linearly with the volume-flow which increases linearly with the absolute temperature. A reduction in average compression temperature consequently leads to a higher electric efficiency. The GT-MHR of General Atomics (1995) and the South-African PBMR design (Liebenberg, 1996) use this intercooled cycle. Contrary to the GT-MHR design, the PBMR design is a multi-shaft system (see figure 1.7). The thermodynamic cycle is not affected, but the design of a multi-shaft system gives shorter shafts, less stability problems and more degrees of freedom in the mechanical design (three shaft speeds instead of one). Choosing high speeds for

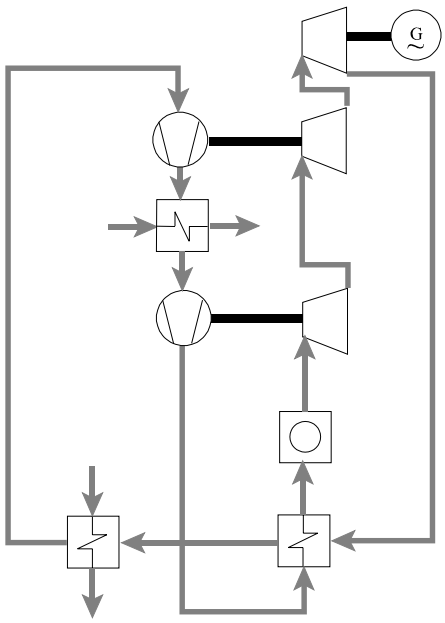

Figure 1.7: Multi-shaft system.

the two turbo-compressors leads to a smaller and simpler design. The dynamics of the system are heavily affected by the choice for a single or multi-shaft system.

Another often proposed variation is the indirect cycle, in which the reactor circuit and the gas turbine circuit are separated (McDonald, 1996b, Lidsky, 1992). This requires an extra blower and a high-temperature intermediate heat exchanger (figure 1.8). Advantages of the indirect cycle are: 1) incidents on the conventional side have less impact on the nuclear part, 2) plate-out of fission products in the turbine is impossible, which simplifies the maintenance, 3) the separation of the nuclear and conventional system which maybe favourable for the licensing and 4) another working fluid can be chosen in the gas turbine cycle. The disadvantages are 1) the intermediate heat exchanger has to operate at very high temperatures, which leads to creep-problems, 2) the need for an extra blower and 3) the intermediate heat exchanger gives a temperature difference between reactor outlet and turbine inlet which gives additional exergy-losses (this is not a major problem, since the material limitations on turbine inlet temperature are stricter than those on the reactor temperature). With a indirect cycle, one could use a closed nitrogen-cycle (Zhang, 1995) or an open secondary air-cycle (McDonald, 1990), thus making use of conventional turbine and compressor designs.

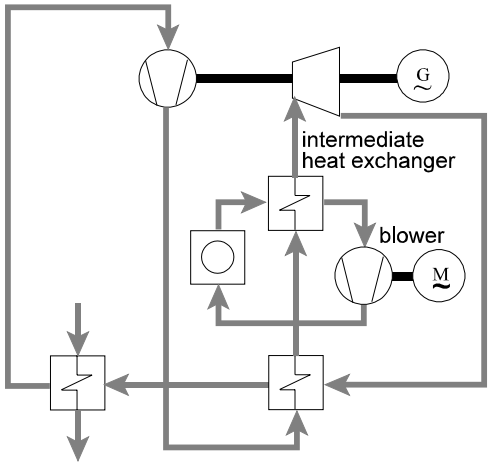

Figure 1.8: Indirect cycle.

Various designs with combined gas and steam cycles have been proposed (Barnert, 1994 & 1995, Gao, 1995). In these designs the recuperator is omitted, the heat-content of the turbine outlet flow is used for steam generation. These systems are much more complex, the risk of water ingress is much higher and only minor improvements in efficiency can be obtained, when comparable component efficiencies and maximum temperatures are used (Agazzina, 1999, Gal, 1998).

Finally, some cycles for combined heat and power production have been proposed in literature. The waste-heat of the CCGT can be used for desalination (Halzl,1968, Kugeler, 1989), production of industrial steam (Bammert, 1971) or production of hot water for industrial purposes or district heating (Yan, 1996). In the INCOGEN-study (van Heek, 1997) a 40 MWth design producing 16.5 MWel and 140 ton/h hot water (temperatures: 40 °C at the inlet, 150 °C at the outlet) was evaluated. The main conclusions were that the system is technically feasible but not economically competitive. One of the deficiencies of the design was the fact that it was optimised for electricity production using the waste-heat for hot water production, without checking whether a demand existed for the quantity and quality of heat produced. The study described in this thesis used the INCOGEN-design as a starting point, but the process has been redesigned to produce heat of a more useful quality.

1.4 Thesis Objectives and Scope

Since extensive studies have proved the excellent safety features of the nuclear gas turbine plant, attention has shifted from safety studies to an optimisation of the overall economy of the plant.

The objective of this thesis is to investigate the design of the energy conversion system for a cogenerating nuclear gas turbine plant by means of computer modelling. The use of the system for combined heat and power production calls for an operating strategy which meets the heat and power demand of the customer rather than producing a constant amount, which eases the reactor operation. The economics are heavily influenced by matters like efficiency, simplicity of design and the ability to quickly meet a wide range of electricity and heat demands. Several models are developed and used to investigate how well the NGT plant can meet the special demands of cogeneration. More specific: What range of heat and power demands can be met? What efficiency is attainable with different design choices? How fast can the plant follow changes in demand? Does this lead to thermal stresses which might reduce the plant life-time? How can the investments of the plant be protected in case of incidents?

Firstly, the design-goals and specifications for the plant are investigated. Then the design-philosophy is described. To analyse the interaction between the plant design and the plant performance and models four models with different levels of complexity have been developed. These models have in common that they all describe the behaviour of the complete plant; no detailed analysis of specific components is done, e.g. no computational fluid dynamics-modelling of the flow over turbine blades or finite element modelling of thermal stresses in the recuperator.

The first model (presented in chapter 2) is a basic model, which is very simple and based on thermodynamic relations only. The important design parameters are established by optimisation with the basic model. Special attention is payed to the flexibility of the plant to meet varying heat demands.

In chapter 3, the second model is developed. This is a steady-state model, in which operating conditions are related to the geometry for all heat exchangers and off-design behaviour of the turbo-machinery is related to its design-conditions. With this model, various components are dimensioned. Subsequently the sensitivity of the efficiency to several design choices is investigated. Finally, the optimal off-design operating conditions have been established.

Chapter 4 describes the development of a dynamic model. First the state-of-the art of dynamic modelling of similar systems is discussed. Then the goal, the assumptions and simplifications of the model are discussed. The structure of the model is described and a description is given of the sub-system and component models.

The dynamical model is validated and verified in chapter 5. Since the design modelled has not been built, validation against experiments is impossible. Therefore the behaviour of components is checked with some logical and sensitivity tests. The reactor model is compared with a rigorous neutronics model, to assess its validity. Finally some responses of the complete primary cycle are compared with calculations with the nuclear thermal-hydraulics code RELAP.

Subsequently, the dynamic model is used to investigate the interactions between design and dynamic response. In chapter 6, firstly it is determined what the optimal dynamic behaviour is. Then the effect of design-decisions like the size of components, volumes between components, choice for a single- or multi-shaft system, location of control-valves etc. on the dynamics is tested with some typical transients.

In chapter 7, a design for the control-system is made. First the process parameters which have to be controlled and possible manipulated variables are identified. Then the interaction between possible control loops ans process non-linearity over the operation-window are investigated. Optimal operating conditions are established. Finally, a control-system is designed and tested with some typical transients.

In chapter 8, the development of the fourth model is described. This dynamic model has been constructed in such a way, that it can be used for online process control. It is a simplified physical model, which is only valid in the normal operating regime. The setup of the model allows completely explicit calculation and the number of states is very limited, in order to allow for fast calculation. In future work, this model can be used to develop a non-linear model predictive control structure.

Chapter 9 presents the conclusions of this study. Finally, three appendices are added which provide information on the heat exchanger and turbo-machinery geometry and on the sizing of inventory vessels.

Chapter 2

Basic Model and Cycle Choice

This chapter starts with a discussion of the design-procedure which will be followed in the rest of this thesis. Then the design-goals and specifications of a nuclear gas turbine plant for combined heat and power production are established. Subsequently it is determined what quality and quantity of heat the plant should deliver. Based on these demands and specifications a choice for a cycle will be made. A simple thermodynamic model of the closed cycle gas turbine system, from now on called the basic model, will be described. This basic model will be used to determine the most important design parameters like the pressure ratio of the cycle and the optimal heat to power ratio.

2.1 Design-procedure

Many books discuss power plant design (e.g. Drbal, 1996, Kuljian, 1968, Hicks, 1986, Morse, 1946 and Li, 1985). However, none of these describe a systematic design-procedure. Systematic methods for the design of chemical plants can be found (Biegler, 1987, Douglas, 1988), unfortunately the guide-lines presented are too specific to apply to power engineering. A systematic approach to the design of conventional gas turbines is discussed very briefly in Cohen (1996).

Since no applicable systematic approach to design could be found in literature, the

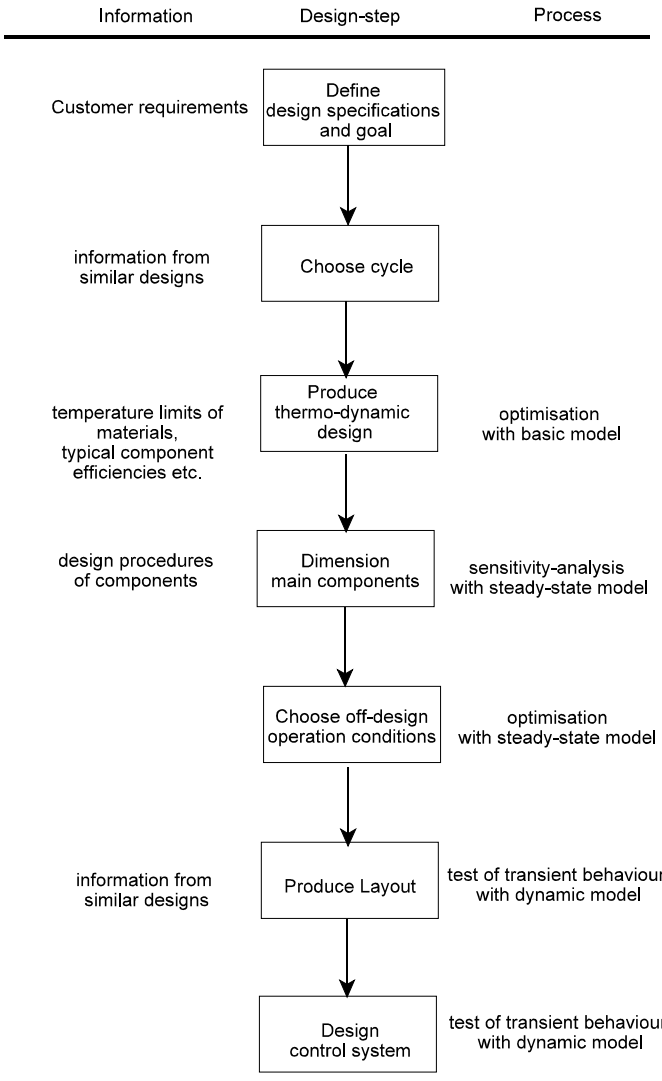

Figure 2.1: Design-procedure.

design-procedure shown in figure 2.1 is followed. In the middle the various design-steps are given. On the left, some information necessary for the design-step is given and on the right the process involved in the design step is described. The design-steps are ordered in a top-down sequence, however unsatisfactory results from design-steps at the bottom may call for re-evaluation of a higher step, thereby making the design-process iterative. In the top-down procedure the design is specified further and further, therefore the complexity of the models used for evaluation also increases from the basic model to the steady-state model and subsequently to the dynamic model. The procedure is not meant to be complete, only the design-steps for which plant-wide analysis by computer-modelling can be helpful are included. Missing steps are for example, the preliminary and aero-dynamical design of turbo-machinery, mechanical design considering strength of pressure boundaries, thermal stresses, vibrations, bearing design etc. No detailed design of components is given. An obviously missing evaluation is the economic assessment, which is because of the lack of input-data.

2.2 Design-goals

The obvious design-goals for the nuclear gas turbine plant for cogeneration are safety and economic competitiveness. These general goals lead to a number of design-specifications which have to be met by the design:

1. Simplicity.
   The design has be simple, both from a safety point-of-view and because of economical reasons. Practical guidelines are:
   - 1.1 Minimisation of number of components.
     Every extra component introduces a possibility of failure of this component. Moreover, because of the small size of CHP plants, the investment costs are high compared to operating costs. Therefore the cycle should be kept as simple as possible, and the number of components should be minimised.
   - 1.2 No use of ‘exotic’ materials.
     Instead of developing high-temperature resistant material, temperatures must be limited to the range in which well-know materials behave satisfactorily.
2. Modularity
   In order to minimise development costs, the same design has to be applicable for different customers. This can be achieved by using the same primary system for generation of different types of heat (e.g. steam, hot water or desalination).
   - 2.1 High efficiency
     A high efficiency is obviously an asset for every power plant. A special virtue of the closed cycle is the ability to keep the efficiency high at part-load. The control system must be designed to make use of this feature.
   - 2.2 Compliance with market demands
     The quality of heat (temperature-level, hot water or steam) and quantities of heat and electricity produced in a cogeneration plant have to meet the customers requirements. Since the heat demand typically exhibits large variations in time, part load and off-design operation are of special importance. This will be discussed in more detail in the next paragraph.

This list is not intended to be exhaustive, additional design-specifications could address subjects like accessibility for maintenance, non-proliferation aspects etc. However, the list is limited to the specifications which are of use in the design-procedure followed in this thesis.

2.3 Heat Demand

If the design-goal is to reach the highest possible total (heat + electricity) efficiency, the cycle can produce low quality heat (Yan, 1996). A better choice would be to take into account the quality of the heat in the design-optimisation, e.g. to optimise to the exergetic efficiency (Woudstra, 1993). However, this may lead to a quality of heat which is not suitable for industrial use as well. Therefore another approach is used, in which the plant will be designed to meet frequently encountered demands of quality and quantity of the heat. Nearly all CHP systems produce either hot water or steam. Therefore, only these two systems will be considered.

Hot water is used in some industrial applications, but mainly in district heating (DH). A normal quality of the heat demand is characterised by return and delivery temperatures of 75 °C and 125 °C respectively (Veen, 1997). There is no typical value for the quantity of heat for district heating, since any number of house-holds can be connected to a district heating plant. However, the heat-demand strongly varies due to seasonal influences, a typical Dutch heat-demand year-curve is given in figure 2.2 (Miedema, 1981). A CHP plant should preferably be able to meet the whole spectrum of heat-demands, otherwise peak-loads have to be met with e.g. supplementary firing. Therefore, the optimal thermal power of the DH plant is not only determined by an economic optimisation for an average heat-demand and full power operating conditions, the frequency characteristic of the heat-demand and part-load efficiencies have to be taken into account as well. An estimation of the optimal ratio of maximum heat demand and thermal power for a NGT-DH plant will be given in paragraph 2.6, with use of the basic model.

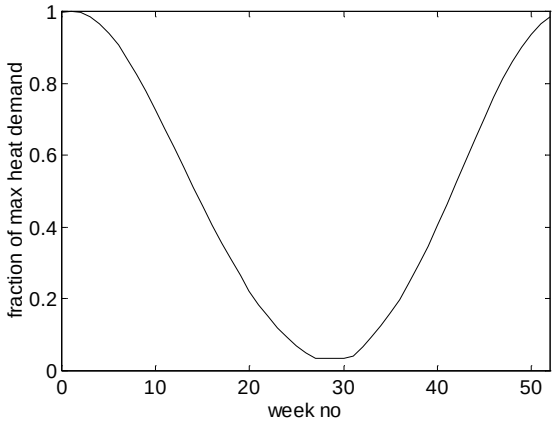

Figure 2.2: Heat-demand year-curve.

Normally slightly superheated steam is used for heating in industrial processes. The aim of superheating is solely to avoid condensation in the supply-pipes. Condensing steam then supplies heat to a process at a constant temperature. Typical industrial steam (IS) conditions (e.g. for breweries and paper mills) are 10 bar and 220 °C, with a return water temperature of 80 °C. Typically demanded steam-flows are 17, 30, 55 and 106 tons/h (Wees, 1986). Of these, 17 tons/h is the most frequently encountered, it will therefore be the target steam production of the NGT-IS plant.

2.4 Cycle Choice

As shown in the previous chapter, a large number of different cycles is proposed in literature. In this paragraph a cycle will be chosen by comparing the characteristics of various cycles with the

design specifications of the combined heat and power plant.

1. Direct or indirect cycle
   The release of fission products from the fuel is expected to be negligible, therefore separation of the reactor and the gas turbine process with an intermediate heat exchanger is not necessary. Moreover, the number of components should be minimised. This rules out the indirect cycle.
2. Bottoming steam cycle or gas turbine process only
   With a bottoming steam-cycle the waste-heat from the turbine may be used a little better for electricity generation than in case of a recuperated cycle. However, for the CHP plant the energy of this flow must not be completely exhausted, because it has to be used for heat production. The option of a back-pressure steam turbine (for electricity and industrial steam production) is also considered too expensive for the small scale.
3. Recuperated or non-recuperated cycle
   With the basic model which will be presented in paragraph 2.5, it can be shown that for the NGT-IS plant a non-recuperated cycle can attain an acceptable efficiency. However, this efficiency can only be reached with a pressure ratio of approx. 8, which is so high that it would severely complicate the turbo-machinery design. Therefore a recuperated cycle is chosen. In contrast to plants for electricity only, there is hardly any benefit from recuperator efficiencies over 90% for CHP-plants, so the recuperator size and costs are limited. The reason for this is that the heat-content of the recuperator hot outlet flow is not cooled away, but used for heat-generation. The exact size and thus efficiency of the recuperator of course has to be determined by an economic trade-off study.
4. Intercooled or non-intercooled cycle
   If an intercooled cycle is used, the compression work is reduced due to the lower volumetric compressor flow. The compressor exit temperature is reduced with intercooling. On account of the recuperator, this leads to a lower recuperator outlet temperature on the hot side. In consequence, a smaller quantity of heat or heat of a lower quality can be produced from the hot recuperator outlet flow. In the intercooler heat is cooled away at a temperature which is too low to be useful. With an intercooled cycle less useful heat can be produced, hence no intercooler is used.

Whether the district heating water and the industrial steam are directly produced in the primary cycle or via some intermediate circuit and whether a single shaft or multi-shaft system should be employed is not essential to the design parameters that will be calculated with the basic model. This issue will therefore be addressed in the next chapter. The direct, recuperated, non-intercooled cycle which is the result from the design choices, is shown in figure 2.3.

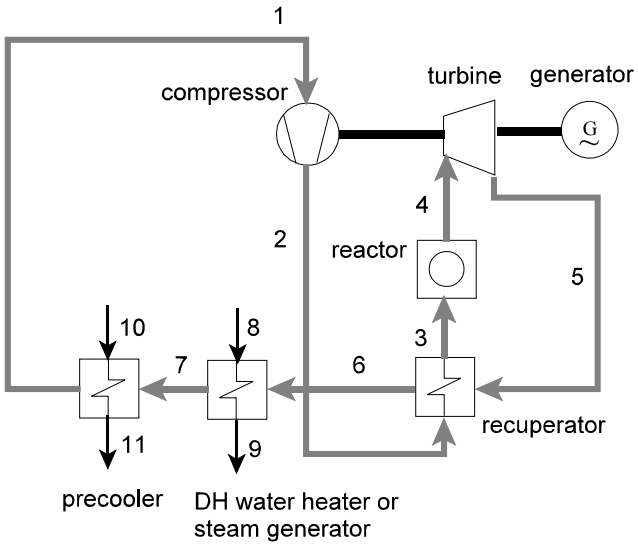

Figure 2.3: Recuperated cycle for CHP production.

2.5 Basic Model

In this paragraph, a basic model will be developed to calculate the main process parameter. This model relates the process conditions using elementary steady-state component models, based on thermodynamic relations only. Polytropic efficiencies of the turbo-machinery, heat exchangers efficiency or minimum temperature difference and the relative pressure loss are assumed to be known and constant, so that all temperatures, mass flows, heat flows and system efficiencies can be calculated.

The compressor and turbine are described as polytropic processes. The temperatures, pressure ratio and power are then related by:

$$\frac{T_2}{T_1} = \varepsilon_{comp}^{\frac{\kappa - 1}{\eta_{comp\ pol}\,\kappa}} \qquad P_{comp} = \phi_{He}\, C_{p\ He}\, (T_2 - T_1)$$

$$\frac{T_5}{T_4} = \varepsilon_{turb}^{\frac{\eta_{turb\ pol}(1 - \kappa)}{\kappa}} \qquad P_{turb} = \phi_{He}\, C_{p\ He}\, (T_4 - T_5) \qquad \varepsilon_{turb} = \varepsilon_{loss}\, \varepsilon_{comp}$$

With:

$T_{1, 2 \ldots}$	=	temperature of flow with corresponding number in figure 2.3 in K
ε	=	pressure ratio (ε_{turb} and $\varepsilon_{comp} > 1$, $\varepsilon_{loss} < 1$)
P	=	power in J s^{-1}
ϕ	=	mass flow in kg s^{-1}
C_p	=	specific heat in J kg^{-1} K^{-1}
κ	=	C_p/C_v = ratio of specific heats
η	=	efficiency

The reactor has simply been modelled as a heat source.

$$P_{reac} = \phi_{He}\, C_{p\ He}\, (T_4 - T_3)$$

Recuperator performance has been modelled using the efficiency η_{rec}, defined as the ratio of transferred heat and transferred heat in case of an infinitely large heat exchanging area (Kays, 1985). The specific heat of helium is temperature-independent, so if all cooling, leakage or bypass-flows are neglected, the heat capacities of both flows are equal and thus:

$$\eta_{rec} = \frac{T_3 - T_2}{T_5 - T_2} = \frac{T_5 - T_6}{T_5 - T_2}$$

The steam generator, DH water heater and final cooler have been modelled with a heat-balance and a minimum temperature difference. For the steam generator this gives:

$$\phi_{steam}\, C_{p\ steam}\, (T_9 - T_{vap}) + \phi_{steam}\, \Delta H_{vap\ water} = \phi_{He}\, C_{p\ He}\, (T_6 - T_{pinch})$$

$$\phi_{steam}\, C_{p\ water\ eco}\, (T_{vap} - T_8) = \phi_{He}\, C_{p\ He}\, (T_{pinch} - T_7)$$

$$P_{heat} = \phi_{steam}\, (C_{p\ water\ eco}\, (T_{vap} - T_8) + \Delta H_{vap\ water} + C_{p\ steam}\, (T_9 - T_{vap}))$$

$$(T_6 - T_9),\ (T_{pinch} - T_{vap})\ \&\ (T_7 - T_8) > \Delta T_{SG\ min}$$

ΔH_{vap} = heat of vaporisation in J kg^{-1}

T_{pinch} is the gas temperature at the start of the evaporation-section as shown in fig 2.4.

For the DH water heater the heat balance and minimum temperature difference are:

$$P_{heat} = \phi_{DH}\, C_{p\ water\ DH}\, (T_9 - T_8) = \phi_{He}\, C_{p\ He}\, (T_6 - T_7)$$

$$(T_6 - T_9)\ \&\ (T_7 - T_8) > \Delta T_{HX\ min}$$

And for the precooler:

$$\phi_{cooling}\, C_{p\ water\ cooling}\, (T_{11} - T_{10}) = \phi_{He}\, C_{p\ He}\, (T_7 - T_1)$$

$$(T_7 - T_{11})\ \&\ (T_1 - T_{10}) > \Delta T_{HX\ min}$$

The electric power production can been calculated with:

$$P_{el} = \eta_{losses}\, (P_{turb} - P_{comp})$$

With:

η_{losses} = correction for mechanical shaft efficiency, generator efficiency and electricity used on plant for e.g. pumps and blowers

The electrical, total and exergetic efficiency and the heat-to-power ratio are defined as:

$$\eta_{el} = \frac{P_{el}}{P_{reac}} \qquad \eta_{total} = \frac{P_{el} + P_{heat}}{P_{reac}} \qquad \eta_{ex} = \frac{P_{el} + \Delta Ex_{heat}}{P_{reac}} \qquad HPR = \frac{P_{heat}}{P_{el}}$$

The exergy gain of the DH water or steam flow is calculated from water and steam entropy S at inlet and outlet and the surrounding temperature ($\Delta Ex = T_{surr}\,(S_9 - S_8)$), whereas the exergy of the neutronic power input and the electric output are equal to the energy. An indication of economic performance takes into account the price ratio of electricity to heat R_p:

$$\eta_{ec} = \frac{R_p\, P_{el} + P_{heat}}{(1 + R_p)\, P_{reac}}$$

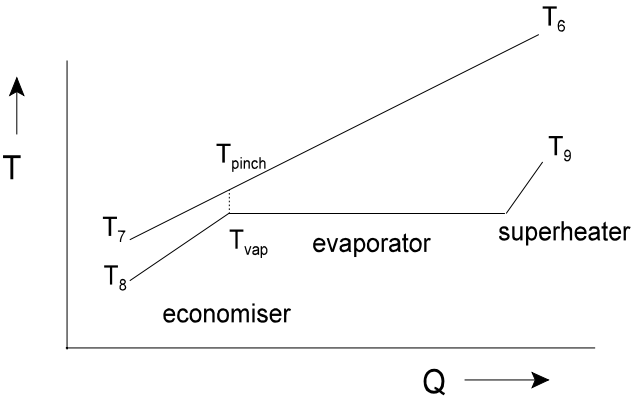

Figure 2.4: Q-T diagram of the steam generator.

2.6 Optimisation of Design Parameters

In order to optimise the electric efficiency some parameters and boundary conditions have to be chosen. For a high efficiency, the reactor outlet temperature T_4 has to be as high as possible. In order not to complicate the turbine design with blade cooling, a temperature of 800 °C is chosen

(Yan, 1996). An active reactor pressure vessel cooling system conflicts with the desired simplicity of design so the reactor vessel is cooled with the reactor inlet gas. The vessel temperature has to be kept out of the creep region which sets an upper limit of 494 °C on the reactor inlet temperature T_3 when 9Cr-1Mo-V steel is used (General Atomic, 1995). Common values for the cooling water are an inlet temperature of 15 °C and an outlet temperature of 25 °C. Typical component efficiencies (from Cohen, 1996 and Lidsky, 1991) and physical properties (from Wagner, 1998, and Yan, 1990) have been listen in table 2.1.

Now the optimal conditions for different heat-to-power ratios can be calculated by optimisation to the electric efficiency. Since the heat-demand is fixed for a given HPR this also gives optimal values for the other efficiency definitions given above. The set of equations has two degrees of freedom, and has been optimised in the pressure ratio and compressor inlet temperature using the modelling-tool Matlab (Matlab, 1992). The results are given in figures 2.5 and 2.8 for DH and the IS system respectively.

Table 2.1: Properties and efficiencies used in the basic model.

physical properties		efficiencies, losses & price ratio	
$C_{p\ He}$	$5.18 \cdot 10^3$ J kg^{-1} K^{-1}	$\eta_{comp\ pol}$	0.89
κ	1.666	$\eta_{turb\ pol}$	0.89
$C_{p\ water\ cooling}$	$4.18 \cdot 10^3$ J kg^{-1} K^{-1}	η_{losses}	0.95
$C_{p\ water\ DH}$	$4.22 \cdot 10^3$ J kg^{-1} K^{-1}	η_{rec}	0.9
$C_{p\ water\ eco}$	$4.26 \cdot 10^3$ J kg^{-1} K^{-1}	ε_{loss}	0.97
$C_{p\ steam}$	$1.87 \cdot 10^3$ J kg^{-1} K^{-1}	$\Delta T_{HX\ min}$	15 °C
$T_{vap\ water}$	180 °C	$\Delta T_{SG\ min}$	10 °C
$\Delta H_{vap\ water}$	$2.333 \cdot 10^6$ J kg^{-1}	R_p	3.2

The efficiency-curves of the DH-system show three distinct regions. In the first region the heat-demand is low and much heat is cooled away in the precooler. The heat is ‘for free’; an increase in heat-demand does not affect the electricity production. The compressor inlet flow is cooled as far as possible to minimise the compression work. In this region the active constraints are those on the precooler temperature difference and the reactor inlet temperature. In the second region the heat flow to the DH heater has to be augmented, which is best done by raising T_6 (active constraint: $T_6 - T_9 > \Delta T_{HX\ min}$). On account of the recuperator T_6 is strongly coupled to T_2 and thus to T_1, therefore the compressor inlet temperature is raised. This increases the compression work, and consequently the electric efficiency is reduced. In the third region no heat is cooled away in the precooler, the only losses are at the electrical side (η_{losses}). The only active constraint is that on the DH heat exchanger. In this region the electricity production is made less efficient with rising heat demand by raising the pressure ratio, thus increasing T_6.

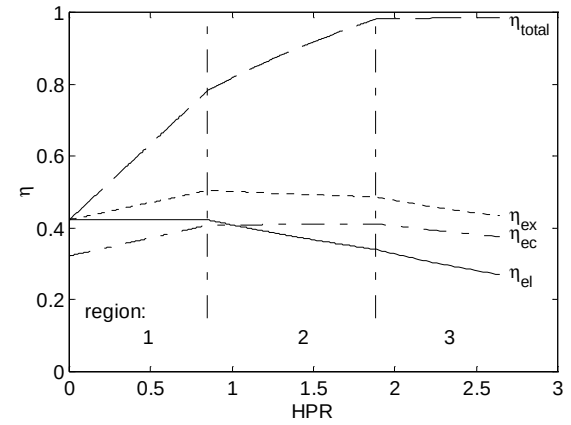

Active constraints:

region 1: $T_1 - T_{11} > \Delta T_{HX\,min}$

$T_3 < T_{3\,max}$

region 2: $T_6 - T_9 > \Delta T_{HX\,min}$

region 3: $T_6 - T_9 > \Delta T_{HX\,min}$

($\phi_{cooling} = 0$)

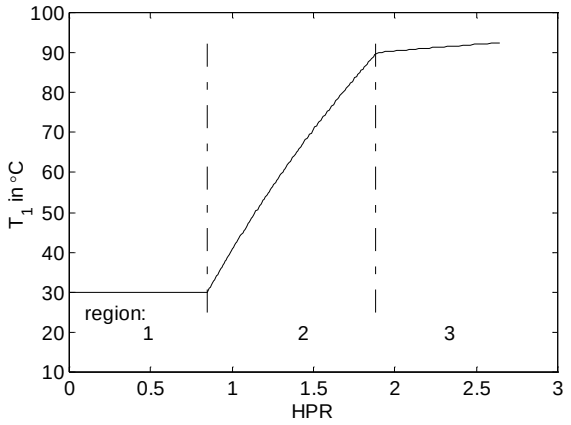

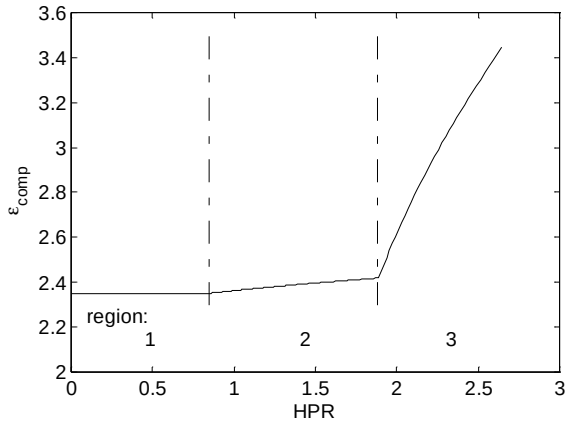

Figure 2.5: Optimal efficiency and conditions of DH-system.

Since the DH plant has not one operating point but a wide range of conditions, its efficiency at 'off-design' conditions is important. In the first and second region, the pressure ratio and volume flow can be held fairly constant. Therefore, the off-design efficiency-curve of a cycle will be similar to the curve shown in figure 2.5 (this will be proven with an off-design model in chapter 3, see figure 3.20). It is assumed that the plant meets the heat-demand and produces as much electricity as possible, thus working at a maximum reactor power all year round.

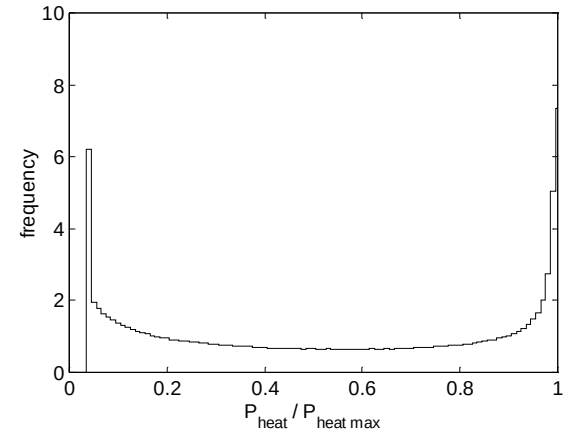

Figure 2.6: Frequency distr. of heat demand.

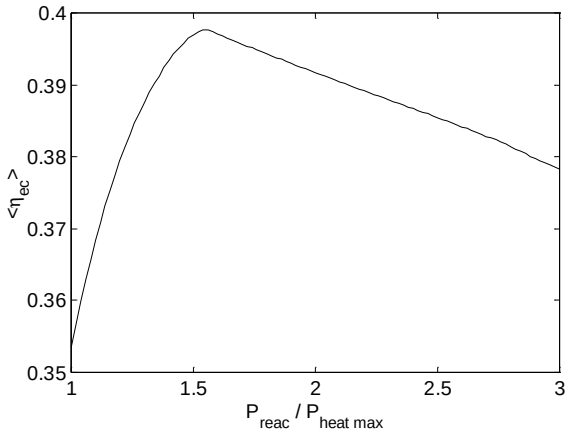

Figure 2.7: Frequency-weighed average η_{ec}.

With the efficiency-HPR curve (fig 2.5) and a frequency distribution (fig 2.6) of heat demand based on figure 2.2, the optimum thermal power of the plant for a given maximum heat demand is established. For different ratios $P_{reac} / P_{heat\ max}$ the frequency-weighted averaged economic performance indicator $<\eta_{ec}>$ is plotted in figure 2.7. It can be seen that there is an optimum at a reactor thermal power of 1.6 times the maximum heat demand.

The optimal parameters of the IS plant and resulting efficiency are given in figure 2.8.

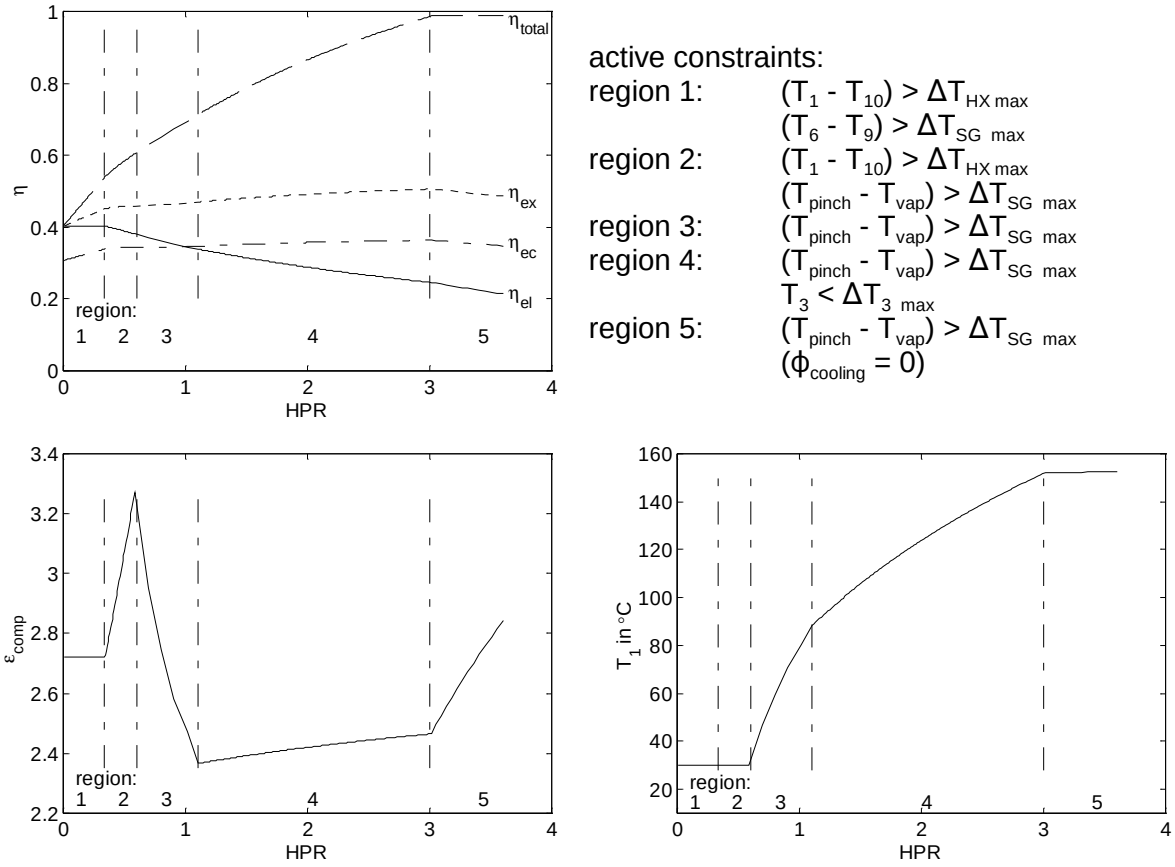

active constraints:

region 1: $(T_1 - T_{10}) > \Delta T_{HX\ max}$
$(T_6 - T_9) > \Delta T_{SG\ max}$

region 2: $(T_1 - T_{10}) > \Delta T_{HX\ max}$
$(T_{pinch} - T_{vap}) > \Delta T_{SG\ max}$

region 3: $(T_{pinch} - T_{vap}) > \Delta T_{SG\ max}$

region 4: $(T_{pinch} - T_{vap}) > \Delta T_{SG\ max}$
$T_3 < \Delta T_{3\ max}$

region 5: $(T_{pinch} - T_{vap}) > \Delta T_{SG\ max}$
$(\phi_{cooling} = 0)$

Figure 2.8: Optimal efficiency and conditions of IS-system.

There are five regions in which different constraints are active, since the steam generator has one constraint more than the DH heat exchanger ($T_{pinch} - T_{vap} > \Delta T_{SG\ min}$). In regions two, three and four the economic performance curve is essentially flat, its slope depends primarily on the chosen price-ratio of electricity and heat. In order to facilitate the turbo-machinery design, the HPR with the lowest pressure ratio (HPR$\approx$ 1, T_1 = 90 °C, ε_{comp}= 2.35) has been chosen as the design-point. The IS system will be designed for an operating window around 17 tons steam/h (P_{heat} = 12 MW). To get the HPR of approximately 1 the plant thermal power should be about 40 MW.

2.7 Conclusions

The design-decisions taken in this chapter have been summarised in table 2.2.

Table 2.2: Design decisions.

Decision	Reason
Target	
design of DH and IS system	customer demand
Cycle	
direct cycle no bottoming steam cycle	minimisation of no. of components
recuperated cycle	high efficiency
no intercooling	need for fairly high recuperator hot outlet temperature
Parameters for IS system	
max. reactor inlet temp. = 494 °C turbine inlet temp. = 800 °C	simplicity of design and material limitations
pressure ratio = 2.35 comp. inlet temp. = 90 °C reactor power = 40 MW	typical steam demand and optimisation
Parameters for DH system	
same design as IS system	modularity of design
variable compressor inlet temp.	varying heat demand
max. heat load = 25 MW	frequency distribution of heat demand and optimisation

Based on the characteristic of CHP, it is decided that a direct, recuperated cycle without bottoming steam cycle is optimal for the NGT-plant for cogeneration. The plant should produce electricity and steam for industrial use (conditions: 10 bar, 220 °C), or electricity and hot water for district heating (temperatures: 75 °C at inlet and 125 °C at outlet).

A DH-cogeneration plant is favourable over a steam-coproducing plant. A cycle which has been optimised for electricity production only, gives a waste-heat flow which still can be used for water heating. On account of to the recuperator however, the heat-content of the recuperator hot outlet flow is too low to produce a decent amount of steam. This can be seen by comparing the low HPR-side of the electric efficiency curve of figures 2.4. and 2.7. In the DH-system the electric efficiency is unaffected by the rising heat demand up to a much higher HPR than in the IS-system.

The optimal reactor power, pressure ratio and temperatures of the IS-plant have been established with the basic model. Unlike plants for electricity production only, the compressor inlet flow must not be cooled as far as possible. For the DH-plant, the optimal conditions and ratio of maximum heat demand and thermal reactor power have been established. Since both plants have approximately the same optimal pressure ratio (2.35), a design can be made which can be used for both applications with the heat generating unit as the only difference. When the optimal thermal power of 40 MW for the IS-plant is also used for the DH-plant, a maximum heat demand of 25 MW can be met.

Chapter 3

Steady-State Model, Design and Operating Conditions

The goal of this chapter is to produce a conceptual design of the energy conversion system (ECS) of the NGT-CHP plant. First a steady-state model is presented, which relates design choices (conditions, geometry component efficiencies) to performance. This model is implemented using the modelling tool ACM (Aspen Custom Modeler, 1999). With this model, a sensitivity-analysis is made of most design parameters. Furthermore, the performance at different operating conditions is optimised.

3.1 Steady-State Model

3.1.1 Turbo-machinery

On account of the complex nature of turbo-machinery, it is complicated to develop a model which relates the geometry (size, number of stages, blade shape etc.) to the performance. An attempt at such a model is made for the dynamic model in the next chapter. The accuracy of the efficiency dependency on geometrical data will not be sufficient to find e.g. the optimal absolute system pressure from the trade-off between efficiency losses due to leakage and friction. In other words, the code cannot be used to make important design decisions. Therefore, the relations from the basic model (relating outlet conditions to inlet conditions, pressure ratio and efficiency) are used at the design-point in the steady-state model. A model is implemented which relates the off-design behaviour to the design-values, so that optimal operating conditions at different heat and power demands can be calculated.

For the compressor this is done by a map which relates the pressure ratio ε_{comp} and isentropic efficiency $\eta_{comp\,isen}$ to the corrected mass flow ($\phi_{corr} = \phi \sqrt{T_{in}}\, p_{atm}/ p_{in}$) and corrected rotational speed ($\omega_{corr} = \omega / \sqrt{T_{in}}$) (Münzberg, 1977). Figure 3.1 shows the map used, which is typical for a radial compressor (Traupel, 1982). The map has been scaled by division by design parameters (ϕ_{scaled} =

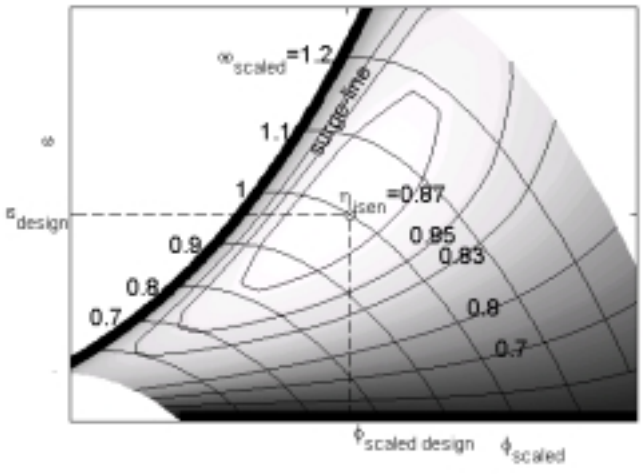

Figure 3.1: Compressor map.

$\phi_{corr} / \phi_{corr\ design}$, $\omega_{scaled} = \omega_{corr} / \omega_{corr\ design}$). The outlet pressure and temperature and the power consumed can be calculated from:

$$p_{out} = \varepsilon_{comp}\, p_{in} \qquad T_{out} = T_{in}\left(1 + \frac{1}{\eta_{comp\ isen}}\left(\varepsilon_{comp}^{\frac{\kappa-1}{\kappa}} - 1\right)\right) \qquad P_{comp} = \phi C_p (T_{out} - T_{in})$$

The off-design model of the turbine is based on the similarity to a nozzle with varying efficiency. The mass flow at varying inlet and outlet conditions is known from the Stodola's law (Traupel, 1982):

$$\phi = \phi_{design}\, \frac{p_{in}}{p_{in\ design}} \left(\frac{T_{in\ design}}{T_{in}}\right)^{\frac{1}{2}} \left(\frac{1 - \varepsilon_{turb}^{\frac{-(n+1)}{n}}}{1 - \varepsilon_{turb\ design}^{\frac{-(n+1)}{n}}}\right)^{\frac{1}{2}} \qquad n = \frac{\kappa}{\kappa - \eta_{turb\ pol}(\kappa - 1)}$$

The efficiency is related to the design efficiency and a dimensionless speed-parameter ν, as shown in figure 3.2 (Attia, 1995).

$$\left(\frac{\eta_{turb\ pol}}{\eta_{turb\ pol\ design}}\right) = f\left(\frac{\nu}{\nu_{design}}\right)$$

$$\nu = \frac{\omega \pi d}{\sqrt{2 C_p (T_{in} - T_{out\ isen})}} \qquad T_{out\ isen} = T_{in}\, \varepsilon_{turb}^{\frac{1-\kappa}{\kappa}}$$

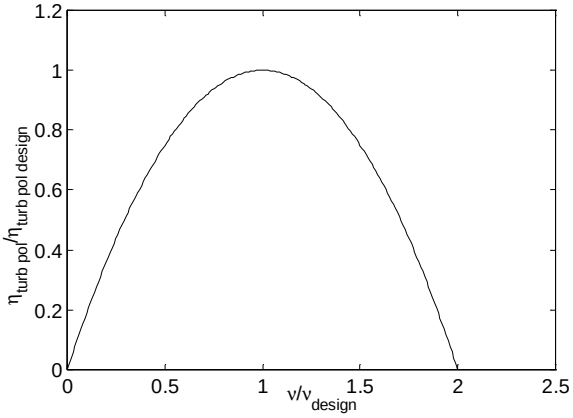

Figure 3.2: Off-design turbine efficiency.

3.1.2 Heat Exchangers

The heat exchangers have been modelled with the efficiency-NTU (Number of Transfer Units) relation (Kays, 1985) for all temperature-relations, and a Reynolds-dependent friction-factor for the pressure drop. The heat exchanger efficiency η is defined as:

$$\eta = \frac{Q_{transf}}{Q_{transf,\ S=\infty}} = \frac{C_{hot}(T_{hot\ in} - T_{hot\ out})}{C_{min}(T_{hot\ in} - T_{cold\ in})} = \frac{C_{cold}(T_{cold\ out} - T_{cold\ in})}{C_{min}(T_{hot\ in} - T_{cold\ in})}$$

η is a function from the NTU, the geometry and the ratio of the heat capacities of the cold and hot flow (C_{min}/C_{max}).

$$C = \phi C_p \qquad C_{min} = \min(C_{hot}, C_{cold}) \qquad NTU = \frac{\alpha S}{C_{min}}$$

With:

α = heat transfer coefficient in J K^{-1} m^{-2} s^{-1}
S = heat transfer surface area in m^2

For a counterflow arrangement:

$$\eta = \frac{1 - e^{-NTU(1 - C_{min}/C_{max})}}{1 - (C_{min}/C_{max})\, e^{-NTU(1 - C_{min}/C_{max})}}$$

The C_p of water which is used in the efficiency-definition is the average value of the C_p at inlet and outlet conditions. For a heat exchanger with a condensing or evaporating medium applies $C_{min} / C_{max} = 0$.

The product αS can be calculated for geometries with extended surface as:

$$\alpha S = \frac{1}{\left(\frac{\delta}{\lambda S}\right)_{wall} + \frac{1}{(\eta_{surf}\, \alpha_{fluid}\, S)_{cold}} + \frac{1}{(\eta_{surf}\, \alpha_{fluid}\, S)_{hot}}}$$

α = heat transfer coefficient in J K^{-1} m^{-2} s^{-1}
δ = thickness in m
λ = thermal conductivity in J m^{-1} K^{-1}
S = heat transfer surface area in m^2

The surface effectiveness η_{surf} is introduced to account for the extended surface and is determined by:

$$\eta_{surf} = 1 - \frac{S_{fin}}{S_{total}}(1 - \eta_{fin}) \qquad \eta_{fin} = \frac{\tanh(m l_{eff})}{m l_{eff}} \qquad m = \sqrt{\frac{2\alpha_{fluid}}{\lambda_{fin}\delta_{fin}}}$$

l_{eff} = effective fin length (= half plate spacing for plate fin heat exchanger) in m

α_{fluid} is calculated from the relation between the Stanton-Prandtl$^{2/3}$ group and the Reynolds number (Kays, 1985). A calculation based on Reynolds-Nusselt correlations would also be possible, but the Stanton-Prandtl$^{2/3}$-Reynolds correlations available are more precise.

$$St\, Pr^{2/3} = f(Re)$$

with:

$$St = \frac{\alpha_{fluid} A}{\phi C_p} \qquad Pr = \frac{\mu C_p}{\lambda} \qquad Re = \frac{D_e |\phi|}{A\mu}$$

The pressure drop over the heat exchanger is determined from velocity v and friction loss factor e_v (Bird, 1960):

$$\Delta p = e_v \frac{1}{2}\rho v^2 \qquad v = \frac{\phi}{\rho A}$$

The friction loss factors of the core and of contraction and expansion in the heads are calculated from the flow length L and the area ratio σ respectively:

$$e_{v\ core} = \frac{4f(Re)L}{D_e} \qquad e_{v\ contr} = 0.45\ (1 - \sigma) \qquad e_{v\ exp} = (\frac{1}{\sigma} - 1)^2$$

For the contractions and expansions, the downstream velocity must be used to calculate the losses.

L, A, S and σ of both sides of the heat exchanger can be determined from the geometry, the relations are given in appendix A.

3.1.3 Other Components

The reactor is simply modelled as a heat-source with a friction factor-Reynolds relation for the pressure loss.

$$P_{reac} = \phi C_p (T_{out} - T_{in})$$

The hydraulic diameter and cross-sectional area (used for the Reynolds-number) of flow through the pebble bed are calculated as:

$$D_e = \frac{2}{3}\frac{\xi}{1-\xi} d_{pebble}$$

$$A = \xi A_{frontal} = \xi \frac{\pi}{4} d_{reactor}$$

With:
ξ = bed porosity

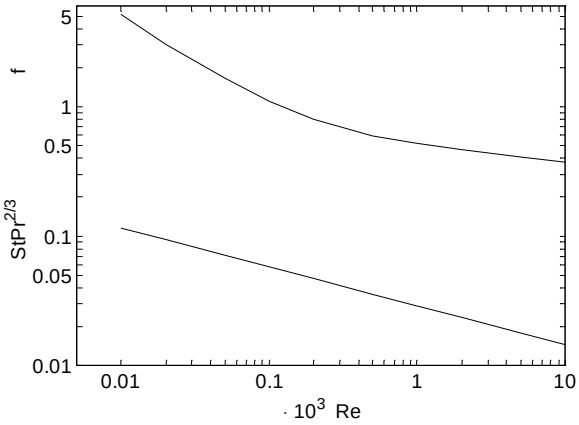

Figure 3.3: St $Pr^{2/3}$ and f versus Re for flow through a randomly stacked sphere matrix.

The f(Re)-relation for the pebble-bed is shown in figure 3.3, together with the St $Pr^{2/3}$(Re)-relation which will be used in the dynamic model.

The feedwater pump and the helium blower (which will be introduced in the design in the next paragraph) are described by the pump characteristics, which can be simplified to a one-dimensional correlation using a dimensionless head h_{nd}, a dimensionless flow ϕ_{nd} and the efficiency η.

$$h_{nd} = \frac{gh}{u^2} \qquad \phi_{nd} = \frac{\phi}{\rho u d_{imp}^2} \qquad h = \frac{\Delta p}{\rho g}$$

u = impeller speed in m s^{-1} = π d_{imp} ω
ω = pump speed in rev s^{-1}
d = diameter in m

The characteristics used in this model are given in figure 3.4 for the blower (Biesenbach, 1995) and in figure 3.5 for the feedwater pump (adapted from Perry, 1973). They are given in terms of scaled dimensionless head and flow:

$$h_{nd\ scaled} = \frac{h_{nd}}{h_{nd\ design}} \qquad \phi_{nd\ scaled} = \frac{\phi_{nd}}{\phi_{nd\ design}}$$

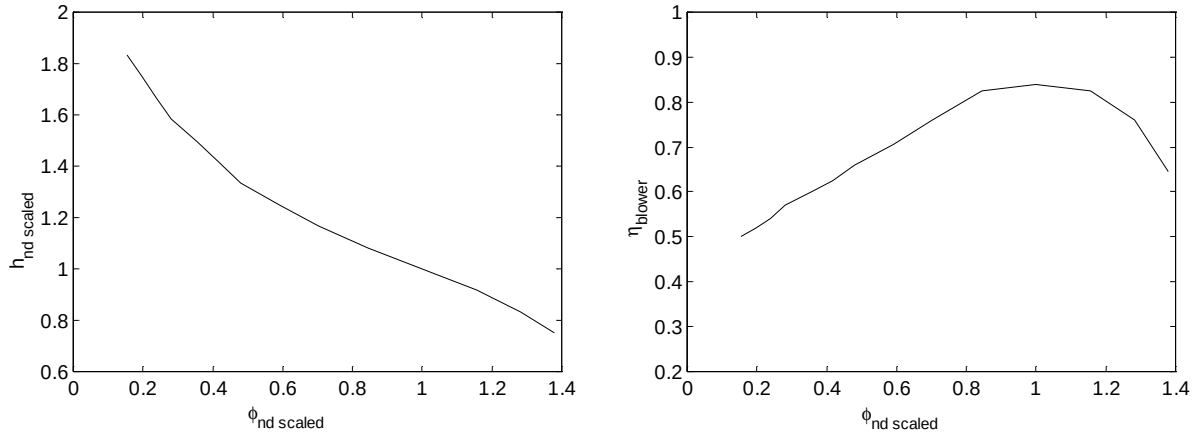

Figure 3.4: Blower characteristics.

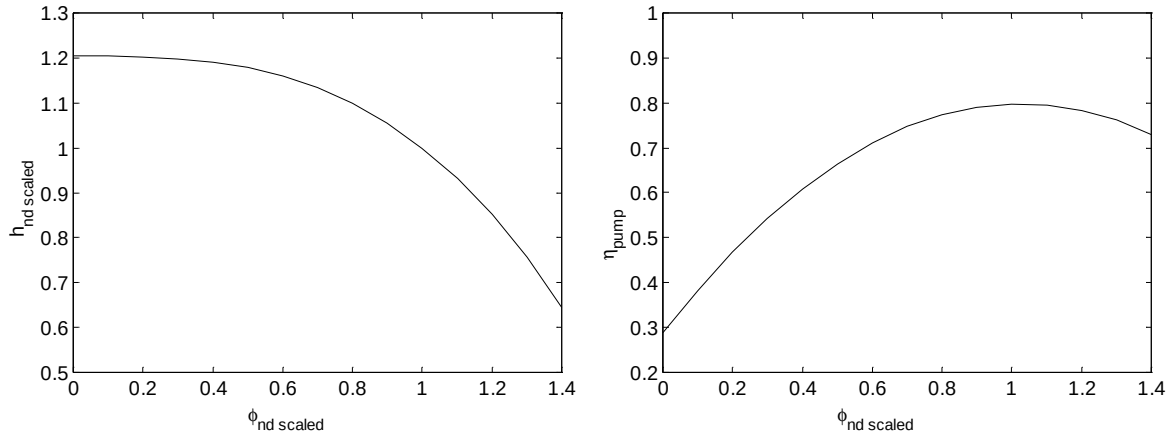

Figure 3.5: Pump characteristics.

The temperatures and pressures of the blower are related by:

$$p_{out} = p_{in} + \Delta p \qquad T_{out} = \frac{T_{in}}{\eta_{blower\ isen}} \left(\frac{p_{out}}{p_{in}} \right)^{\frac{\kappa - 1}{\kappa}} \qquad P_{blower} = \phi C_p (T_{out} - T_{in})$$

For the water pump, the outlet temperature is determined from the outlet enthalpy, which is calculated with:

$$P_{pump} = \phi (H_{out} - H_{in}) = \frac{h \phi g}{\eta_{pump}}$$

3.1.4 Physical Properties

In the steady-state model the deviation from ideal-gas behaviour for helium is taken into account. The density ρ [kg m^{-3}] and enthalpy H [J kg^{-1}] are calculated using a correction-factor B (Yan, 1990).

$$\rho = \frac{p}{RT + Bp} \qquad H = H_0 + C_p T + \left(B - T\frac{dB}{dT} \right) p \qquad B(T) = C_1 + \frac{C_2}{1 - C_3 T} + \frac{C_4}{1 + C_5 T}$$

The constants used are given in table 3.1:

Table 3.1: He properties.

C_1	$9.489433 \cdot 10^{-4}$ m^3 kg^{-1}
C_2	$9.528079 \cdot 10^{-4}$ m^3 kg^{-1}
C_3	$3.420680 \cdot 10^{-2}$ K^{-1}
C_4	$2.739470 \cdot 10^{-3}$ m^3 kg^{-1}
C_5	$9.409120 \cdot 10^{-4}$ K^{-1}
R	2077.22 J kg^{-1} K^{-1}
C_p	5193.0 J kg^{-1} K^{-1}
κ	1.666
h_0	5557 J kg^{-1}

The viscosity μ [kg m^{-1} s^{-1}] and thermal conductivity λ [W m^{-1} K^{-1}] of helium are calculated with:

$$\mu = 3.953 \cdot 10^{-7}\ T^{0.687}$$
$$\lambda = 2.774 \cdot 10^{-3}\ T^{0.701}$$

The water-steam properties are calculated using the IF97-formulation (Wagner, 1998).

3.2 Design

3.2.1 Cycle

In all electricity-only, large (>200 MW) HTGR-GT designs, the highest pressure is about 70 bar (Liebenberg, 1996, General Atomic, 1995, HHT, 1983). A high pressure reduces the pressure losses, the upper pressure limit is imposed by reactor vessel stress considerations. For the small CHP system however, another limit becomes important. In order to facilitate the turbo-machinery design (e.g. to reduce the relative influence of leakage-flows), the volume-flow should not be too small. The mass flow is set to approx. 25 kg/s by the thermal reactor power of 40 MW and the reactor inlet and outlet temperatures of 494 °C and 800 °C respectively. A reasonable volume-flow can be obtained by choosing a fairly low system pressure. Yan (1996) chooses a compressor inlet pressure of 10 bar for the similar INCOGEN-plant. From the basic model calculations it can be concluded that optimal conditions (pressure ratio, temperatures and mass flows) of the IS and DH plant are very similar to the INCOGEN-plant, therefore a lower pressure of 10 bar is chosen. The pressure ratio of 2.35 leads to a highest pressure of 23.5 bar, however, the pressure ratio can be optimised again with the steady-state model.

Direct positioning of the DH heat exchanger or steam generator in the primary cycle gives a higher plant efficiency, since the introduction of an intermediate loop will give exergy losses in the additional heat exchangers. However, the intermediate loop has two advantages in case of incidents:

1. Reduced risk of water ingress in the primary loop.
   Ingress of water in the reactor can lead to two problems:
   - 1.1 A reactivity excursion due to the additional moderation.
   - 1.2 Corrosion problems, which may be solved with an additional Si-C coating on the pebbles (Schröder, 1997).
2. No risk of transporting radio-active particles to outside the containment.

The second risk could be avoided in the DH-plant with an intermediate water-loop. However, the pressure would have to be high to achieve the temperatures needed without boiling. Given the low compressor inlet pressure, which is even lower at part-load, the intermediate loop pressure would be higher than the primary pressure, so that a leak would lead to water-ingress. For the IS-plant, an intermediate water-loop is of course no option. The highest temperature in the system during normal operation conditions is about 300 °C, which is approximately the upper limit for most thermal oils (Singh, 1985). Thermal oils give chemical stability-problems or explosion risks at higher temperatures, which may be expected during transients. The only remaining option is to use an intermediate gas-loop. The most logical choice would be to use helium, for the same reasons for which it is chosen in the primary loop. The pressure should be higher than the primary pressure, so that a leak leads to flow from the secondary to the primary loop. In order to minimise friction losses, a pressure of 70 bar is chosen for the intermediate helium loop.

The most simple configuration of the turbo-machinery is a single-shaft configuration, in which one turbine drives both the compressor and a generator. This can be done with a synchronous generator, but the frequency of 50 Hz severely complicates the turbine design and leads to inferior performance. A gear-box cannot be used, since the system has to be free of lubricant. The alternatives are (i) a two-shaft configuration with a synchronous generator (which complicates the design) or (ii) a single shaft with a variable speed asynchronous generator and power electronics for frequency conversion (which goes at the expense of efficiency). Because of the simplicity, the latter option is chosen. The one-shaft configuration has the additional advantage that the generator can be used to drive the compressor during startup.

With these choices the cycle is completely defined; the NGT-IS and NGT-DH cycles are shown in figures 3.6 and 3.7 respectively. The water/steam cycle consists of a deaerator, a feedwater pump, economiser, drum, evaporator and superheater. Most of the secondary helium (90% of the flow) by-passes the superheater, since the steam has to be only slightly superheated. In this plant a once-through boiler can not be used, because it is too expensive to de-salt the return water (this is only possible in a closed system). With a once-through system this leads to salt deposition in the tubes. A pool boiling type of steam generator (tube & shell heat exchanger with water on the shell side) in which the salt concentration can be regulated, is impossible because the helium would have to flow through the tubes leading to an extremely large number of tubes or very high gas speeds and consequently high pressure drops. The steam generator design is currently non-integrated, which means that it consists of three different shell-and-tube heat exchangers for the superheater, the evaporator and the economiser respectively. Given the high shell-side pressure an integrated design might be favourable, e.g. with all three steam generator heat exchangers and the precooler as helical coil tube bundles in a single vessel.

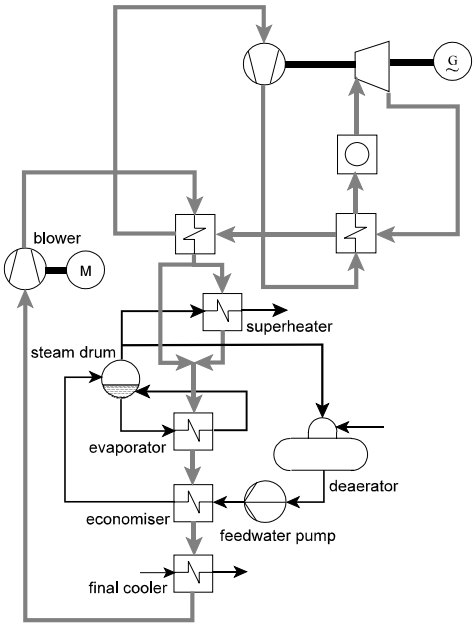

Figure 3.6: Cycle of the NGT-IS plant.

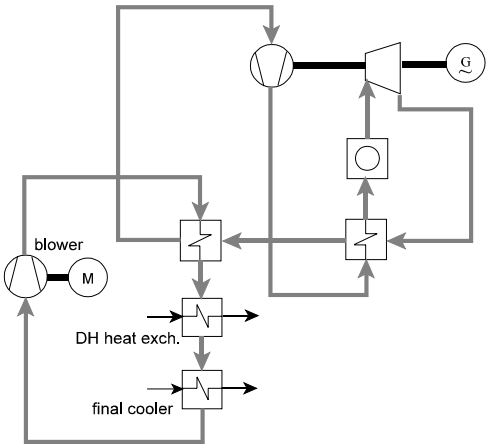

Figure 3.7: Cycle of the NGT-DH plant.

3.2.2 Heat Exchangers

The recuperator and precooler consist of a number of modular plate-fin strip-fin heat exchangers (equal to those used in the INCOGEN-design (Yan, 1996)) ducted in parallel. Figure 3.8 shows a recuperator module.

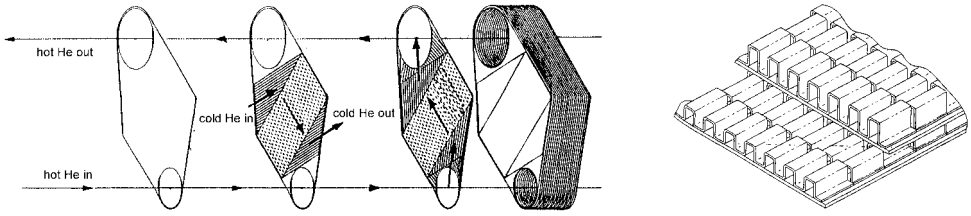

Figure 3.8: Recuperator module.

The recuperator and the precooler consist of five and seven modules respectively, leading to efficiencies of 90 and 94%. The sensitivity of the electric efficiency of the NGT-IS plant with regard to the number of modules is shown in figure 3.9.

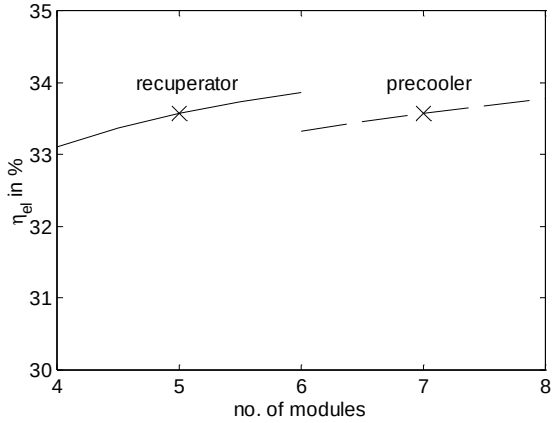

Figure 3.9: Sensitivity to no. of precooler and recuperator modules.

For helium-water heat exchangers, two geometries have been chosen: a staggered tube bank for the superheater, and a finned tube bank for all other heat exchangers, since the heat resistance is mainly on the helium side for the gas-liquid heat exchangers. The water flows

through the tubes in all heat exchangers. Data of the geometry and heat-transfer and friction-correlations are given in appendix A.

With the steady-state model, heat exchanger dimensions have been chosen which yield a good efficiency with acceptable pressure losses. For the evaporator, the resistance on the water-side is neglected. All heat exchangers have been modelled as a counterflow arrangement, which is true for the recuperator and precooler, irrelevant for the evaporator and a fair approximation for the other heat exchangers. The dimensions which resulted from this study are given in table 3.2. In the evaporator, a minimum temperature difference of only 7 °C is reached. A sensitivity-plot for the number of tubes is given in figure 3.10. In the NGT-IS design the only pinch-point at design conditions lies at the water-inlet of the evaporator, therefore no sensitivity-analysis is given for the other heat exchangers.

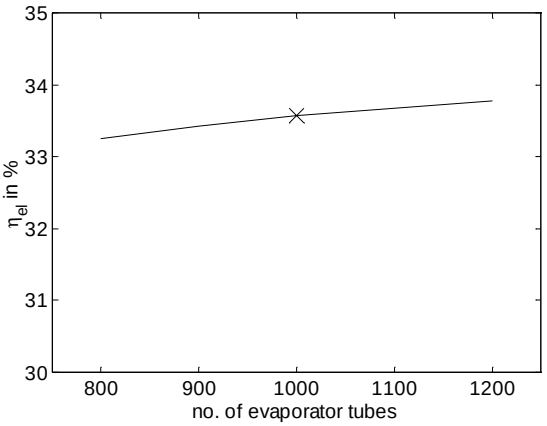

Figure 3.10: Sensitivity to no. of evaporator tubes.

Table 3.2: Heat exchanger-design.

	no. of tubes	tube length	no. of passes	no. of baffles
superheater	500	2 m	1	4
evaporator	1000	1.6 m	1	2
economiser	200	1.4 m	4	1
final cooler (NGT-IS)	500	2 m	1	1
DH heat exchanger	800	4 m	1	1
final cooler (NGT-DH)	1300	3 m	1	1

3.2.3 Turbo-machinery

With the performance of all the heat exchangers known, the sensitivity of efficiency to the pressure ratio for the IS-system has been established. The minimum pressure ratio (which gives a reactor inlet temperature of 494 °C) is 2.3. For pressure ratios up to 2.65, the efficiency increases slightly, as can be seen in figure 3.11. This is because a higher pressure ratio leads to a lower reactor inlet temperature and combined with the set reactor power this leads to a smaller mass flow through the system. A smaller mass flow leads to smaller pressure drops and to higher efficiency of heat exchanging equipment. However, the increase is so small that it does not justify the increased design-complexity due to the higher pressure ratio. Given the design-conditions, both radial and axial compressors can be built with reasonable performance (Op het Veld, 1998). Since the design conditions for the turbo-machinery are not too different from those in the

INCOGEN study (Heek, 1997a), the INCOGEN asynchronous single-shaft turbo-machinery design is slightly adjusted. The compressor and turbine (shown in figure 3.12) are designed for a rotational speed of 12000 rpm. The asynchronous generator however, allows for different rotational speeds at off-design conditions. Design conditions of the IS-system are given in table 3.3. Geometrical data of the turbo-machinery are given in appendix B.

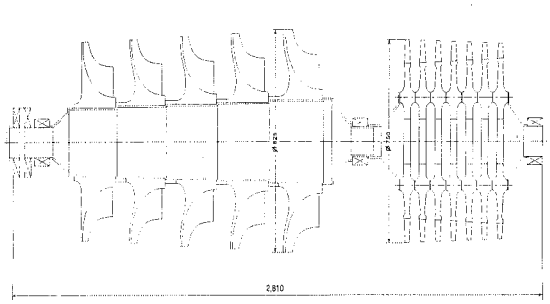

Figure 3.12: Turbo-machinery design.

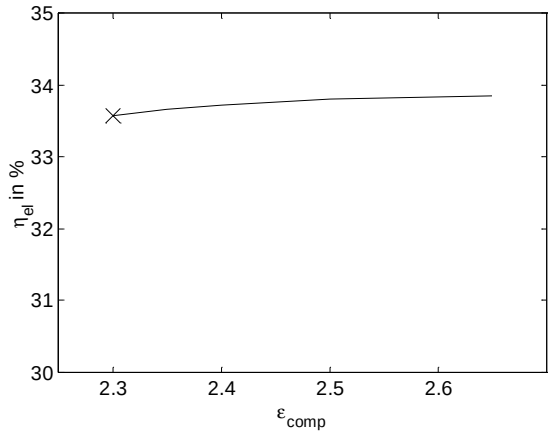

Figure 3.11: Sensitivity to pressure ratio.

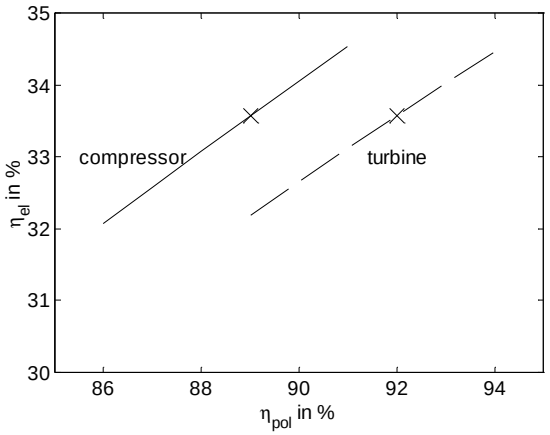

Figure 3.13: Sensitivity to turbo-machinery efficiency.

The sensitivity of electric efficiency with regard to polytropic compressor and turbine efficiencies are shown in figure 3.13. A deterioration of turbo-machinery does not drastically affect the electric efficiency. It leads to a higher heat production in the cycle, so that the same recuperator hot side outlet temperature can be reached with a lower compressor inlet temperature, which reduces the compression work again.

Table 3.3: Turbo-machinery design conditions.

	compressor	turbine
ϕ	25.4 kg/s	25.4 kg/s
T_{in}	93 °C	800 °C
p_{in}	10 bar	22.8 bar
ε	2.3	2.25
η_{pol}	89%	92%

Finally, given the heat exchanger design and the turbo-machinery efficiencies, the effect of the absolute pressure in primary and secondary pressure can be evaluated. Changing the pressure level over a wide range, without re-designing the heat exchangers gives a good indication of the achievable performance, since raising the pressure has no effect at all on the efficiency of the heat exchanging equipment. This is because of two reasons: (1) the Reynolds-number for a given design is only dependent on the mass flow (assuming helium to be a perfect gas), which is set by the choice of reactor power and temperatures, and (2) the thermal conductivity is pressure-independent. The absolute pressure affects the performance of the cycle in two ways: by the pressure drops in all equipment (which

has been evaluated) and by the effect on efficiency of compressor and turbine (which have been set to zero). The results which are shown in figure 3.14 and 3.15, suggest that the chosen design values of 10 and 70 bar are appropriate. With a primary system pressure twice as high, an electric efficiency gain of 1%-point is attained. From figure 3.13 one can see that if the isentropic efficiencies of the smaller compressor and turbine at this elevated pressure are each 1%-point lower, the effect is a 1%-point loss of electric efficiency. In that case there would be no gain in an increase of primary system pressure.

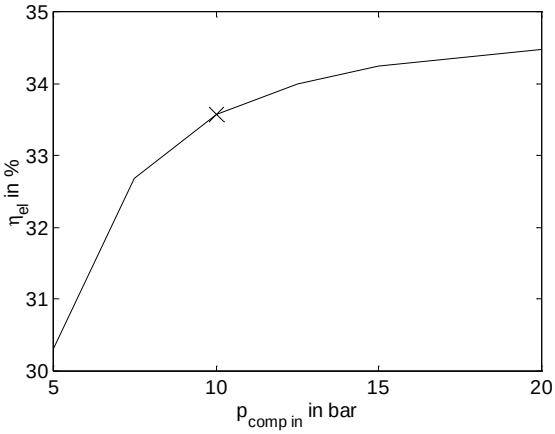

Figure 3.14: Sensitivity to compressor inlet pressure.

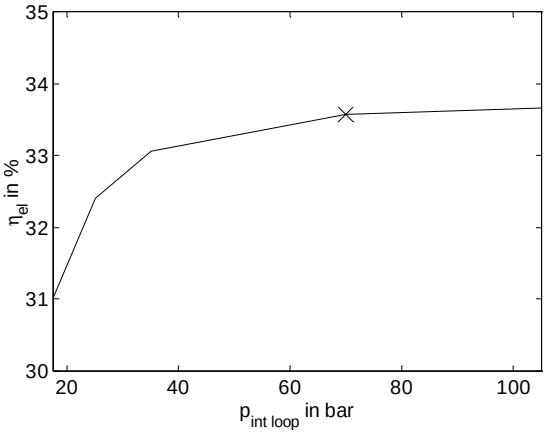

Figure 3.15: Sensitivity to intermediate loop pressure.

3.2.4 Layout

In figure 3.16 it is shown how the energy conversion system (ECS) fits into the plant. A description of the reactor design can be found in (Heek, 1997b). The layout of the ECS is shown in figure 3.18. The arrangement of the precooler modules is given in figure 3.17, a similar arrangement is used for the recuperator. The steam generator and final cooler are not shown in figure 3.18; they are situated on the same horizontal level as the gas-gas heat-exchangers and the turbo-machinery. The design of the secondary cycle is currently not integrated, it is simply a series-connection of tube & shell heat-exchangers.

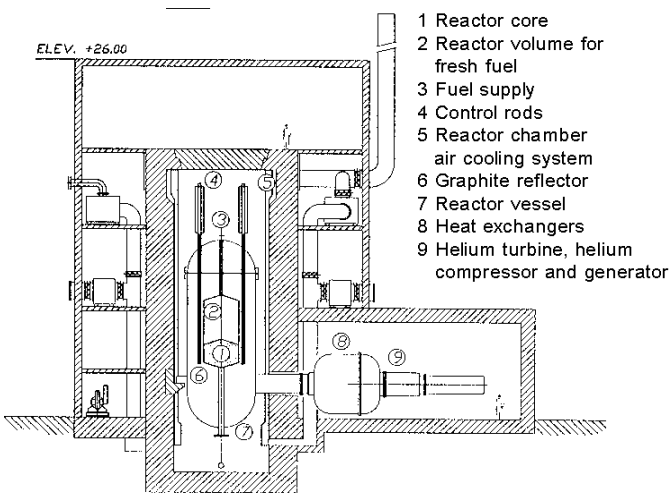

Figure 3.16: Plant layout.

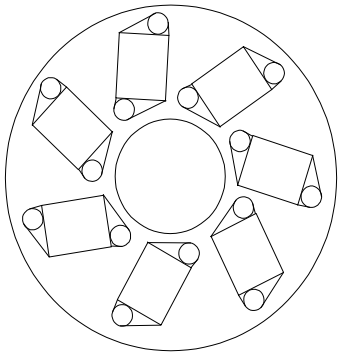

Figure 3.17: Precooler arrangement.

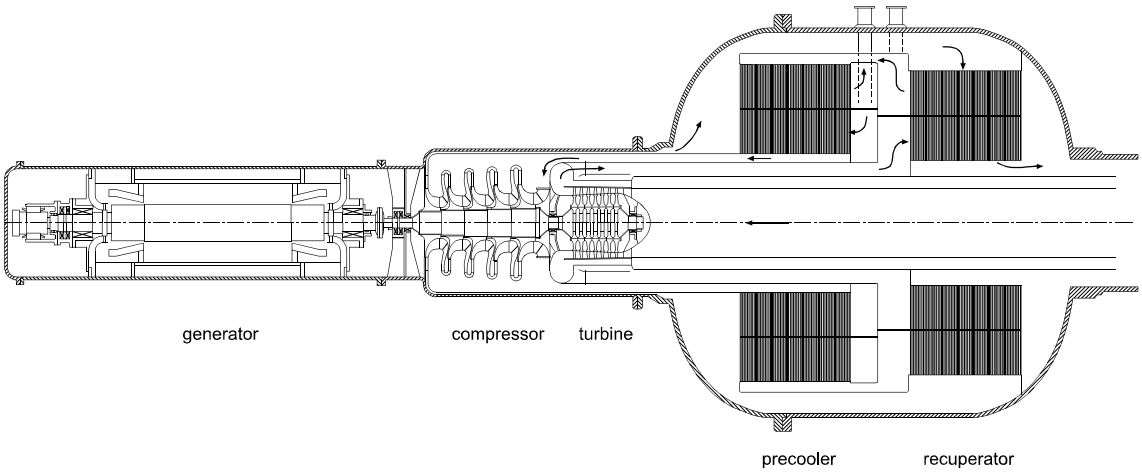

Figure 3.18: Energy conversion system.

3.2.5 Inventory Control System

A high part-load efficiency can be obtained by reducing the helium inventory. If at part load the pressure is halved and all temperatures are kept constant, the gas velocities are the same as at full load. The mass flows and the power are also halved. Since the velocity triangles in the turbo-machinery are unchanged, the efficiency stays high. The pressure losses are reduced and the heat exchanger efficiency increases, thus giving a slightly higher efficiency than at full load. It has been chosen rather arbitrarily that this high efficiency should be reached at part-load operation above 50%. The layout chosen leads to a helium inventory of approximately 127.5 kg at full load. The pressure reduction can be achieved by pumping helium in and out of the system with a positive discharge compressor. However, the compressor of the primary system can also be used to pump helium out of the system. A number of parallel tanks can be used to minimise the total tank volume. A method to calculate the tank volume needed in the limiting cases of isothermal or adiabatic emptying and filling of the tanks is given in appendix C. Normally, the vessels-behaviour would be approximately adiabatic, since the time-constant for heat-transport from or to the wall by natural convection is in the order of 15 minutes and a vessel can be filled or emptied much faster. In figure 3.19 the total vessel-volume and the corresponding total helium inventory as a function of the number of vessels is shown for the limiting cases of isothermal and adiabatic filling and emptying. Because of the large tank (and thus building) volume in case of adiabatic operation, the vessels should be designed with a large internal area, which leads to almost isothermal behaviour. The chosen inventory control system consists of two such tanks with a volume of 39 m^3 each and four valves.

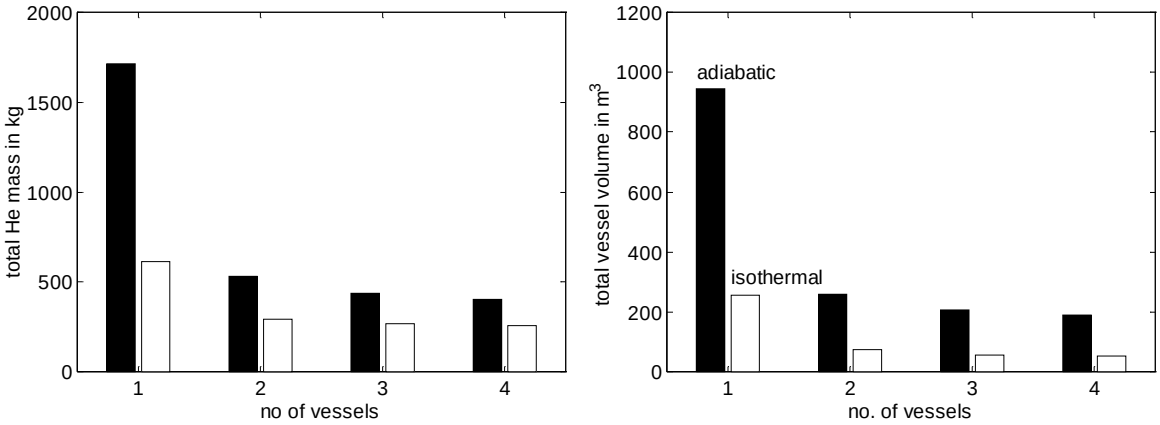

Figure 3.19: Total tank volume and helium mass versus no. of inventory vessels.

3.3 Optimal Operating Conditions

For the NGT-DH plant, the conditions which yield the highest efficiency for a given heat-demand are established with use of the steady-state model. With a constant reactor power and temperatures and a given DH-water flow, the blower speed and shaft speed have been optimised with regard to the efficiency. The shaft and relative blower speed, plant efficiency and compressor inlet temperature are shown in figure 3.20.

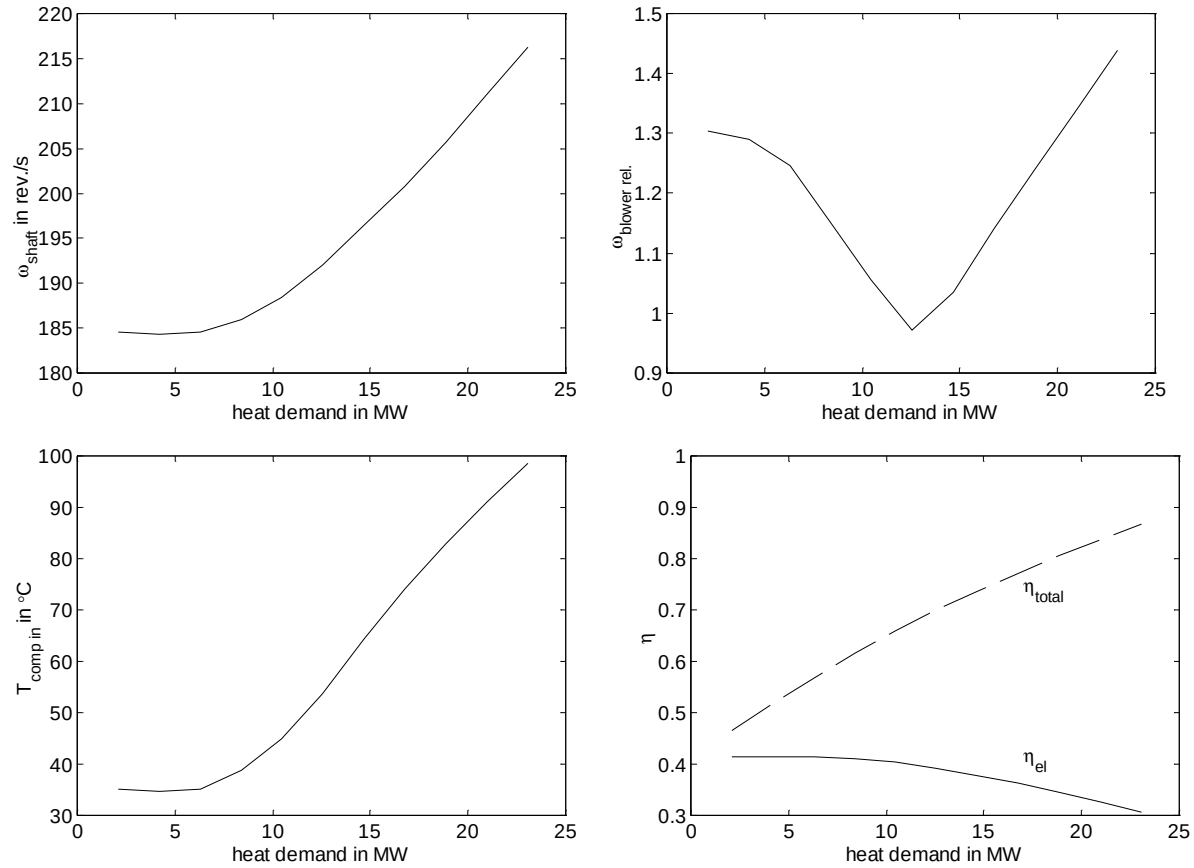

Figure 3.20: Optimised off-design conditions of NGT-DH plant.

The explanation of the curves is similar to that given for the basic model calculation in chapter 2. When the heat demand is low, the compressor inlet flow is cooled as far as possible to reduce compression work. For heat demands under 12 MW, the cooling water flow is maximal. At larger heat demands a higher temperature in the secondary loop, leading to a higher precooler temperature and thus a higher compressor inlet temperature is necessary. In order to keep the reactor temperatures and power constant, the primary mass flow is constant. The volume flow and gas velocities through the compressor then varies with the inlet temperature. In order to keep the compressor operating at the highest efficiency the shaft speed is adjusted accordingly. The blower speed influences the secondary mass flow and in that manner the temperature profiles of the heat exchangers in the secondary loop. When the compressor inlet must be cooled as far as possible the secondary helium flow can be high. When a large quantity of heat must be transported to the DH heat exchanger without too high temperatures, the secondary flow should also be high. For intermediate heat demands the heat transport in the precooler should be as effective as possible. This is achieved with the secondary flow approximately equal to the primary flow (parallel temperature lines in a Q-T diagram). Therefore the blower speed shows a minimum. Some of the optimal conditions, like the shaft speed, can be used as set-points for the control system.

3.4 Conclusions

A steady-state model has been produced which describes both design and off-design behaviour in detail. With this model, a conceptual design for the NGT-DH and NGT-IS plant has been made. The characteristic features of the plant are a single-shaft configuration with a low pressure (10-23 bar) and a secondary helium loop. The NGT-IS cycle with its design conditions is shown in figure 3.21. For the NGT-DH it has been shown, that the plant can operate with high-efficiency and constant reactor conditions throughout the whole range of heat-demands, by adjusting the compressor inlet temperature and shaft speed.

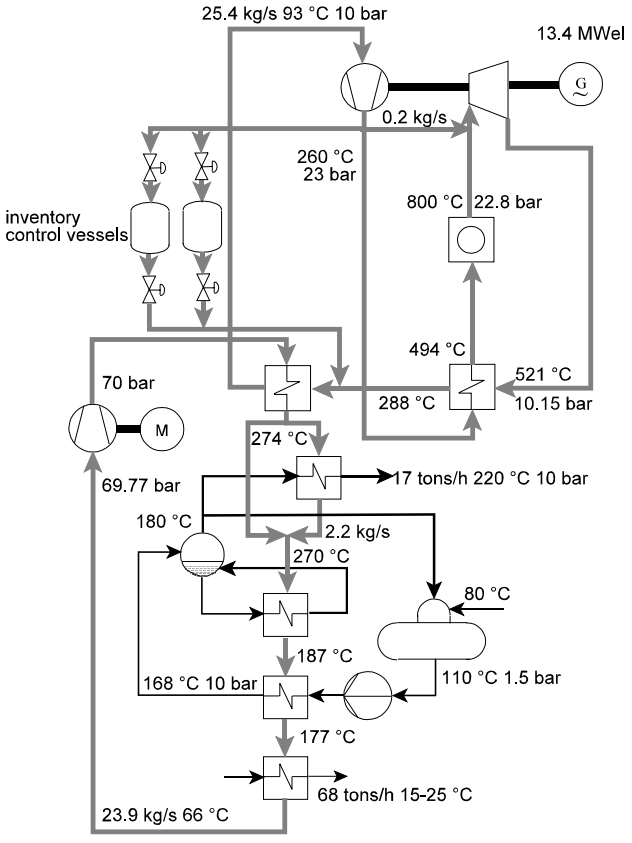

Figure 3.21: Conditions in NGT-IS plant.

Chapter 4

Dynamic Modelling

In this chapter the theory and implementation of a dynamic model of the NGT-CHP plant are described. First the state of the art of dynamic modelling for (nuclear) closed cycles and other gas turbine processes is discussed. A discussion of the goal, scope and design of the model follows. The theory of sub-systems (which are used in different components) and component-models is given in paragraph 4.3 and 4.4.

4.1 State of the Art

4.1.1 CCGT Dynamic Modelling

In recent history, several attempts to model the dynamic behaviour of Closed Cycle Gas Turbine plants have been undertaken. For the German HHT-project, Bammert (1971, 1978, 1980) and co-workers developed a model, which was compared with test results from the Oberhausen, externally fired closed cycle (with air as working fluid). Their work concentrated on the modelling of turbo-machinery with empirical algebraic relations and on heat exchange with pipes and equipment. The heat source and water side of heat exchangers were not modelled.

Rauhut (1982) developed a model which solves compressible gas-flow with the method of characteristics. This makes it possible to calculate shock waves and choked flow. The main goal was to calculate the transients following accidents like pipe breaks and loss of turbo-machinery blades, leading to shock-waves. The turbo-machinery behaviour has been modelled using a simple form of 4-Q characteristics (positive and negative flow and rotational speed) by Bammert (1974). The reactor is again considered as a simple heat source, core dynamics are not calculated. In the modelling efforts of General Atomic (Bardia, 1980) the core dynamics are taken into account. A point-kinetic model is used for the neutronics. The thermal hydraulics model of the reactor is one-dimensional. Much attention is paid to the control system and to flow at high Mach-numbers in valves connecting high and low pressure plenums.

Yan (1990) first introduces a flow model which is consistently used through the whole plant model. Unfortunately, the author makes a mistake by interchanging total and static enthalpy. The reactor is modelled with point-kinetic neutronics with one-group of delayed neutrons and reactivity feedback of one average temperature. However, the heat transport through the reactor by conduction, radiation and convection is modelled two-dimensionally and in great detail. The turbo-machinery is modelled with two-dimensional maps. Heat exchangers and the control

system are modelled with high accuracy.
Recently, Kullmann (1997) built a model of the South African PBMR system. The model consists of a point-kinetic core model and simple lumped relations for the heat exchangers and turbo-machinery.

4.1.2 Turbo-machinery Modelling

In nearly all simulations of power plants the compressor and turbine are each modelled with some simple algebraic empirical relations, based on characteristic relations between dimensionless numbers. For the compressor, outlet conditions are calculated in quasi steady-state manner from rotational speed and inlet conditions, using two two-dimensional performance maps (Yan,1990, Münzberg, 1977, Kreshman, 1992). In these models, the inertia of the shaft is the only dynamic influence. A possible refinement is to take the heat flow to the metal parts into account, which can simply be done by adjusting the map (Larjola, 1982). Performance maps only work in the region of normal operation; in order to investigate the dynamics of surge and stall problems, Greitzer (1976) has used two simplified (one-dimensional) empirical relations which are also valid at low and negative flows. For more detailed calculation of the dynamic behaviour, the compressor has to be modelled in a stage-by-stage (O'Brien, 1992) or even row-by-row manner (Schobeiri, 1994). Now for each stage relations have to be found between the source terms in the conservation equations and the shaft speed, flow and inlet conditions. These can be established from first-principle modelling (Attia, 1995, Bloch,1992, Schobeiri, 1992, Gravdahl, 1999) or empirical relations can be inserted (Garrard, 1995, Dalbert, 1988).

The turbine behaviour is quite often modelled as flow through a nozzle with an efficiency which is algebraically related to the ratio of dimensionless velocity and its design value (RELAP, 1995, MMS, 2000, Ray, 1980). Another approach is to give two two-dimensional empirical relations between efficiency and pressure ratio as outputs and flow conditions and rotational speed as inputs (Münzberg, 1977). For a safety-analysis of HTGR-GT plants in the German HHT-project, the behaviour of turbines under far off-design conditions like backflow has been studied (Bammert, 1974, Zehner,1978 & 1980). This resulted in a model which describes the turbine behaviour in a stage-by-stage manner from first-principles for both positive and negative flow and rotational speed. A row-by-row model for normal operation with a refinement for very low flow (the windmilling-region, in which the turbine consumes power) has been built by Schobeiri (1992).

4.2 Design of the Model

4.2.1 Goals

The main reasons for the development of the dynamic model of the NGT-CHP plant are (1) to investigate the interaction between design and dynamics, (2) to develop and test a control structure, (3) to determine the consequences of disturbances and accidents and (4) to establish start-up and shut-down procedures.

1. Investigation of interaction between design and dynamics
   Some design-decisions strongly affect the system dynamics. Examples are the size of equipment, volumes between equipment, choice for a single-shaft or a multi-shaft system and the position of control valves. With the dynamic model the influence can be checked

with some typical transients. In order to easily change the configuration, the model must be modular.

2. Development and testing of a control structure
   A dynamic model can be used to predict the responses of controlled variables (temperatures, pressures, etc.) on changes of manipulated variables like valve positions, pump speeds etc. When these interactions are mapped, a scientifically justified approach to the control system design can be followed. The control system can subsequently be implemented in the model, so that it can be tested and tuned to give stable and robust control. For this goal it is necessary to have a dynamic model which closely predicts the behaviour of the plant in its normal operating region.
3. Determining the consequences of disturbances and accidents
   In nuclear plants it is of great importance to predict the consequences of accidents, since it has to be guaranteed that accidents will not lead to major failures and the release of radio-activity. The accident transients that have to be calculated are:
   1. load rejection, sudden disconnection from the grid
   2. shaft break of turbo-machinery
   3. compressor surge and stall problems
   4. helium leakage, leading to reverse flow or complete depressurisation
   5. withdrawal of control rods
   6. loss of flow or mass of the intermediate loop

   To calculate the consequences of incidents the model should be able to predict the plant behaviour under unconventional conditions like negative flows.
4. Establishing start-up and shut-down procedures
   In order to establish start-up and shut-down procedures it is necessary to model the process behaviour in a wide region. The model should then be valid for low flows as well as normal flows.

4.2.2 Scope

The system which has to be simulated comprises the nuclear reactor, the primary and secondary cycle, the water/steam cycle and the cooling water system (only in the final cooler). The system boundary therefore completely surrounds figure 3.21. The variables which are of interest are pressures, temperatures, mass flows and rotational speeds of the shafts. The processes which must be modelled are therefore the transformation of energy (nuclear energy → heat → kinetic energy of gas → rotational energy of shaft → electricity), the storage and transport of mass and energy and momentum in all components. The model should concentrate on the interaction between different components and abstracts from detailed analysis of processes in the components.

The most rigorous way of modelling the system would be to solve the microscopic mass-, momentum- and energy-balance for the flowpath (with a CFD code), the microscopic energy balance of the solid constructions (with a CFD or FEM code), and the neutronics (with a diffusion or Monte Carlo code), all time-dependent and three dimensional. However, the computational effort needed is immense, insufficient information is available for the input of the models, and the level of detail of the information is unnecessarily high. Therefore a strongly simplified model will be constructed.

4.2.3 Assumptions

The most important assumptions used to simplify the rigorous model described above, have been listed in table 4.1 and are discussed below. Of course, many more assumptions have to be made regarding the effects simulated or discarded in models of different components. These assumptions are discussed in the description of the component-model.

Table 4.1: Simplifying assumptions.

Modelling Assumptions	
1	One-dimensional treatment of flowpaths
2	Discretisation of flowpath with staggered grid and method of lines
3	Point-kinetic neutronics model
4	Two-dimensional model of solid structure
5	Non-homogeneous two-phase flow with single momentum-balance

1. One-dimensional treatment of flowpaths

Under normal operating conditions, the flow is turbulent through the whole system, therefore radial differences are not very important. If the flow becomes laminar, calculations of properties like e.g. heat transfer coefficients and friction factors can nevertheless be based on radially averaged fluid properties. Because the rate of change of fluid properties perpendicular to the streamline is small compared to the rate of change along the streamline, the flow through the system can be modelled as one-dimensional, which means that all fluid properties are assumed to be uniform over any cross section.

2. Discretisation of flowpath with staggered grid and method of lines

Instead of solving the microscopic balance-equations, the flowpath will be divided in sections for which macroscopic alternatives will be solved. The flow path in the different components (recuperator, reactor, compressor etc.) is divided in a number of so-called thermal nodes, which are small volumes, assumed to be perfectly mixed and to have a constant cross-sectional area. For these thermal nodes, the mass- and energy-balances are solved. The mass flow between these volumes is determined by solving the momentum-balance for a so-called flownode, which consists of the two halves of neighbouring thermal nodes. This staggered grid (Patankar, 1980) is illustrated in figure 4.1 (page 41).

The mass- and momentum-balances will be solved with second-order central schemes. For the mass balance, this simple scheme may result in a response which is somewhat slower than in reality in case of large elements, but unlike higher order approximations physically unrealisable behaviour is not possible.

In the momentum-balance the effects of friction losses, area change, gravitational forces and forces in turbo-machinery and pumps will be taken into account. In modelling power plants or

chemical plants, the momentum-balance is very often simplified by neglecting the inertia of the fluid, which results in a static relation between the pressure on both sides of the element and the flow through the element. This is also a valid assumption for most components of the NGT-CHP plant. However, for the high velocities and large changes in flow which can appear in the turbo-machinery these terms are dominant. In order to build a general model, the unsimplified momentum-balance is used for all helium flowpaths. In the water/steam cycle, no rapid changes of velocities are expected. In order to enhance the numerical stability, the quasi steady-state solution of the momentum-balance will be used. The gravitational forces are negligible in the helium system. In the water/steam system however, they have to be taken into account since the difference in density between downcomer and evaporator is the driving force.

The discretisation with a second order central scheme is a valid approximation as long as the velocities stay well below the velocity of sound. If sonic or supersonic gas velocities are reached, only information of the upstream node can influence the flow in a given node, so the central difference scheme is no longer valid. The discretisation therefore results in a model which calculates the gas behaviour as if it where at a low speed up to the speed of sound. If an incident results in choking or shock-waves, the gas dynamics are not properly modelled. For a physically correct simulation, the time dependent microscopic balance equations have to be solved with the method of characteristics (Bergeron, 1908, Rauhut, 1982, Streeter, 1967), flux splitting (Garrard, 1995), the Godunov approach or a TVD scheme (Anderson, 1985). During normal operation, speeds approaching Mach one are not expected in the primary and secondary circuit. Choked flow is expected only in the valves connecting the inventory control vessels and the primary system, in the valves connecting high and low pressure plenums, and in case of a rupture. For these valves and the ruptures a different model will be developed.

The energy-balance will be modelled with an upwind scheme. The incoming energy is only influenced by the upstream node, which leads to physically realisable behaviour under all circumstances. A total energy-balance will be used, so internal, kinetic and potential energy are considered. Kinetic energy is of importance in the turbo-machinery only, and the potential energy is only relevant in the water/steam cycle. However, in order to keep the models general (so as to reduce the size of the code), all terms are taken into account in all components.

This method can be viewed as modelling of a flow through a sequence of perfectly mixed tanks. One can also consider it as a continuous system solved with the method of lines (Schiesser, 1991). As a result of this choice, the mass-, energy- and momentum-balance are all discretised with the same number of elements. The energy-balance needs the most fine-meshed discretisation. Especially in the high efficiency heat exchangers a large number of nodes is needed in order to correctly predict the heat transfer. This leads to an unnecessarily fine-meshed momentum-balance, but the extra computational burden can only be overcome with additional, less structured models.

3. Point-kinetic neutronics model

The behaviour of the reactor is only of interest as far as it influences the energy conversion system. Only the relation between input conditions, control rod-positions and outlet temperature needs to be modelled. This can be done with the zero-dimensional point-kinetic model (Duderstadt, 1986). It will be shown that a close agreement between the point-kinetic

approximation and a detailed neutronics code can be achieved, when the input parameters of the simple model are generated with the full-scope model.

4. Two-dimensional model of solid structure

For the metal parts of all components in the energy conversion system, a one-dimensional model is sufficient. However, in order to closely predict the reactor power, the temperature of the radial reflectors surrounding the pebble bed must be known. Therefore a two-dimensional model is produced.

5. Non-homogeneous flow with single momentum-balance for two-phase flow

At the pressures for which the water/steam sub-system model should be valid (1 to 20 bar), a water/steam mixture can not be modelled as a homogenous fluid, since there can be a considerable difference in velocity between the two phases. An alternative is to solve the balances for each phase separately, but in that case it will be difficult to describe the momentum exchange between the phases. A frequently used alternative is to assume thermodynamic equilibrium, to solve the momentum-balance for the two-phase mixture and to add an empirical relation between the relative velocities of both phases (Bourne, 1987).

4.2.4 Numerical solution

The fast phenomena in this model are those associated with the pressure dynamics. If the time advancement is calculated with an explicit scheme very small time-steps have to be used in order to obtain a stable calculation. According to the Courant-Friedrichs-Livey criterion the time step Δt is determined by:

$$(v_{sound} + |v_{gas}|)\frac{\Delta t}{\Delta x} \leq 1$$

With:

x = axial length of thermal node
v = velocity

Because this results in excessively small time-steps, an implicit method is used. The algorithm used is an implicit formulation of Gears method (ACM, 1999), using a re-initialization when discontinuities are encountered.

4.2.5 Structure

In order to make a process-model which can easily be adopted to changes in the process, it is necessary to build a generic model. In that way, changes in geometry, sizes or lay-out can easily be incorporated in the model. To develop such a model, the process is divided into components and sub-systems which can be described with a modular model.

The division of the total plant into components, which are interconnected with few relations, is analogous to the different pieces of equipment. Modelled components are compressor, recuperator, reactor, turbine, shaft etc. Within each component there exist sub-systems which behave similarly in different components. These sub-systems are:

1. One-phase flow
2. Two-phase flow
3. Solid structure
4. Neutronics

First a general model for these sub-systems will be developed, then the component specific source terms will be modelled.

4.3 Sub-system Models

4.3.1 One-phase Flow Model

The helium-system and single phase water and steam system are described with the same model. In figure 4.1 the division of the flowpath in ideally mixed thermal nodes and flownodes consisting of two half thermal nodes is illustrated. The mass-balance for thermal node i between the cross-sections j and j+1 in figure 4.1 is:

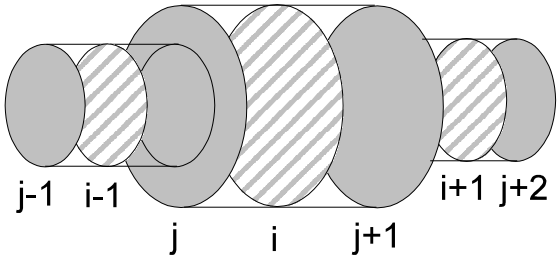

Figure 4.1: Flowpath divided in thermal nodes i-1, i and i+1 and flownodes j and j+1.

$$V_i \frac{d\rho_i}{dt} = \phi_j - \phi_{j+1}$$

V = A Δx = volume of the thermal node in m^3
A = cross-sectional area of the thermal node in m^2
Δx = axial length of the thermal node (between j and j+1) in m
ρ = density in kg m^{-3}
ϕ = mass flow in kg s^{-1}

The axial diffusion of heat is negligible compared to convective heat transport as long as the fluid is in motion and negligible compared to the heat flow through the wall if the fluid is in rest. Using this simplification, the total energy-balance for the same element can be written as:

$$V_i \frac{d(\rho_i E_i)}{dt} = \phi_j (H + K + \Phi)_j - \phi_{j+1} (H + K + \Phi)_{j+1} + Q_i + W_i$$

E = U + K + Φ = specific total energy in J kg^{-1}
U = specific internal energy in J kg^{-1}
K = ½ v^2 = specific kinetic energy in J kg^{-1}
v = velocity in m/s
Φ = g h = specific potential energy in J kg^{-1}
g = 9.81 = acceleration of gravity in m s^{-2}
h = height in m
H = U + p/ρ = specific enthalpy in J kg^{-1}
p = pressure in Pa
Q = heat source in J s^{-1}
W = work done on the fluid (by rotating equipment) in J s^{-1}

In most volumes the velocity is purely perpendicular to the cross-sectional area, therefore it can be calculated using:

$$v_i = v_{i\,perp} = \frac{\phi_i}{\rho_i A_i} \qquad \phi_i = \frac{\phi_j + \phi_{j+1}}{2}$$

The mass flow in the node is the average of the flow at inlet and outlet of that node which are calculated by means of the momentum-balance. In the turbo-machinery however, the velocity has also a large tangential component. The following correction can be applied, without violating the further one-dimensional approach:

$$v_i = \frac{v_{i\,perp}}{\cos(\theta)}$$

θ = angle between velocity and velocity perpendicular to the cross-sectional area

The angle θ is known from the geometry of turbo-machinery. This correction will lower the mass flow at which choking occurs and enlarge the difference between total and static temperature and pressure.

The energy of a flow crossing the cell-border is assumed to be equal to the value in the thermal node which lies upstream:

$$(H+K+\Phi)_j = \begin{cases} (H+K+\Phi)_{i-1} & \phi_j \geq 0 \\ (H+K+\Phi)_i & \phi_j < 0 \end{cases} \qquad (H+K+\Phi)_{j+1} = \begin{cases} (H+K+\Phi)_i & \phi_{j+1} \geq 0 \\ (H+K+\Phi)_{i+1} & \phi_{j+1} < 0 \end{cases}$$

The momentum-balance for flownode j consisting of half of thermal node i-1 and half of thermal node i is:

$$\frac{d\Delta x_j \phi_j}{dt} = \phi_{i-1} v_{i-1} - \phi_i v_i + A_{i-1} p_{i-1} - A_i p_i - (A_{i-1} - A_i) p_j + F_{friction\,j\,i-1} + F_{friction\,j\,i} + \frac{F_{rot\,i-1} + F_{rot\,i}}{2} + \frac{F_{grav\,i-1} + F_{grav\,i}}{2} + F_{comp}$$

Δx_j = axial length of flownode in m = $(\Delta x_{i-1} + \Delta x_i) / 2$
F_{rot} = forces on volume in rotating equipment in N
F_{grav} = gravitational forces on volume in N
F_{comp} = force compensating for effect of change in area on gravitational force in N
$F_{friction}$ = friction force in N

For p_j in the flownode the following relation is used, so that in case of $A_i \neq A_{i-1}$ the pressure acting on the wall in x-direction is balanced:

$$p_j = \begin{cases} p_{i-1} & A_{i-1} \geq A_i \\ p_i & A_{i-1} < A_i \end{cases}$$

The gravitational force can be written as:

$$F_{grav\ i} = g_x\ \rho_i\ V_i \qquad g_x = g\ \frac{-\Delta h_i}{\Delta x_i}$$

Δh = difference in height between inlet j and outlet j+1 in m

The gravitational and pressure forces on the wall in x-direction are compensated for changes in cross-sectional area by F_{comp}:

$$F_{comp\ j} = \begin{cases} F_{grav\ i-1}\ \dfrac{A_{i-1} - A_i}{2\ A_{i-1}} & A_{i-1} \geq A_i \\ F_{grav\ i}\ \dfrac{A_i - A_{i-1}}{2\ A_i} & A_{i-1} < A_i \end{cases}$$

In order to conserve the numerical stability of the staggered grid, the friction has to be calculated from the mass flow at the inlet and outlet. For the friction force applies (Bird, 1960):

$$F_{friction\ j\ i} = -\ \frac{e_{v\ i}\ |\dot{\phi}_j|\ \dot{\phi}_j}{4\ A_i\ \rho_i} \qquad F_{friction\ j+1\ i} = -\ \frac{e_{v\ i}\ |\dot{\phi}_{j+1}|\ \dot{\phi}_{j+1}}{4\ A_i\ \rho_i}$$

with:
e_v = friction loss factor

In pipes or heat exchangers with Fanning friction factor f the friction loss factor equals:

$$e_{v\ i} = \frac{4\ f_i\ \Delta x_i}{D_{e\ i}}$$

f = Fanning friction factor
D_e = equivalent hydraulic diameter in m

Since, this discretisation scheme is only valid for low Mach-numbers, it is checked whether the velocities stay well below the speed of sound. The acoustic velocity v_{sound} is calculated with:

$$v_{sound\ i} = Z\ \sqrt{\kappa R T_i} \qquad \left(Z = 1 + \frac{pB}{RT}\right)$$

Z = compressibility
B = correction for non-ideal gas behaviour, as defined in paragraph 3.1.4

These balances can be used to describe the behaviour of any homogenous fluid, only the equation of state and the relation between enthalpy, pressure and temperature have to be added. The relations used for helium are given in chapter 3, those for water are taken from Wagner (1998).

The set of equations will be closed when correlations for e_v, Q, F_{rot} and W_{rot} are added. These relations differ from component to component and will be described in the component models.

4.3.2 Two-phase Flow Model

For a two-phase model the mass-balance for thermal node i between the cross-sectional areas j and j+1 becomes:

$$V_i \frac{d\rho_i}{dt} = \phi_{L\,j} - \phi_{L\,j+1} + \phi_{G\,j} - \phi_{G\,j+1}$$

$$\rho_i = \alpha_i \rho_{G\,i} + (1-\alpha_i) \rho_{L\,i}$$

α = void fraction, time-averaged fraction of the volume occupied by the gas phase.
The subscript G refers to gas (steam) and L to liquid (water).

The energy-balance for the same volume is:

$$V_i \frac{d(\rho_i E_i)}{dt} = \phi_{L\,j}(H+K+\Phi)_{L\,j} - \phi_{L\,j+1}(H+K+\Phi)_{L\,j+1} + \phi_{G\,j}(H+K+\Phi)_{G\,j} - \phi_{G\,j+1}(H+K+\Phi)_{G\,j+1} + Q_i + W_i$$

In which the energy of the mixture is defined as:

$$\rho_i E_i = \alpha_i \rho_{G\,i} E_{G\,i} + (1-\alpha_i) \rho_{L\,i} E_{L\,i}$$

Some test runs in which the results of a steady-state version of the momentum balance are compared to those of a dynamic momentum-balance, show that the dynamic effects of the momentum-balance are much faster than those of energy- and mass-balances. Since the quasi steady-state approach was numerically more stable, the inertia of the fluid will be neglected. The momentum-balance for the two-phase flow system for flownode j consisting of half of thermal node i-1 and half of thermal node i is:

$$0 = \phi_{L\,i-1} v_{L\,i-1} - \phi_{L\,i} v_{L\,i} + \phi_{G\,i-1} v_{G\,i-1} - \phi_{G\,i} v_{G\,i} + A_{i-1} p_{i-1} - A_i p_i - (A_{i-1} - A_i) p_j + F_{friction\ j\ i-1} + F_{friction\ j\ i} + \frac{F_{rot\ i-1} + F_{rot\ i}}{2} + \frac{F_{grav\ i-1} + F_{grav\ i}}{2} + F_{comp\ j}$$

With:

$$v_{G\,i} = \frac{\phi_{G\,i}}{\rho_{G\,i} \alpha_i A_i} \qquad v_{L\,i} = \frac{\phi_{L\,i}}{\rho_{L\,i} (1-\alpha_i) A_i}$$

The friction force is now defined using a two-phase friction multiplier (Whalley, 1987) and the friction force in case of the complete flow having the properties (density and friction factor) of the liquid:

$$F_{friction\ j\ i} = - \frac{e_{v\,i} |\phi_j| \phi_j}{4 A_i \rho_{L\,i}} \qquad F_{friction\ j+1\ i} = - \frac{e_{v\,i} |\phi_{j+1}| \phi_{j+1}}{4 A_i \rho_{L\,i}}$$

$$\phi_j = \phi_{L\,j} + \phi_{G\,j} \qquad e_{v\,i} = \frac{4 \Phi_{LO}^2 f_{L\,i} \Delta x_i}{D_{e\,i}}$$

Φ_{LO}^2 = two-phase friction multiplier

The steam fraction x can be defined as:

$$x_i = \frac{\phi_{g\,i}}{\phi_i} = \frac{\phi_{g\,i}}{\phi_{g\,i} + \phi_{l\,i}}$$

The relation between x and α is as follows:

$$\alpha = \frac{1}{1 + \left(SR \frac{1-x}{x} \frac{\rho_g}{\rho_l} \right)}$$

SR = slip ratio, relative velocity of gas to liquid

The relations between (H+K+Φ) at the cross-sectional areas j and i both for water and steam are the same as the corresponding equations for the homogenous model. Calculation of p_j and all the forces is also similar to the helium model.

For the relations between density, specific energy, pressure and temperature of water and steam, and for the conductivity and viscosity, the IF-97 water/steam tables are used (Wagner, 1998).

Closure of the set of equations describing two-phase flow will be reached if empirical and/or component-specific relations for f_L, Q, W, SR and Φ_{LO}^2 are added. These will be introduced in the component models.

4.3.3 Solid Structure Model

The third sub-system which appears in all components is the solid structure. A two-dimensional lumped model will be described here. The two-dimensional form is only used to describe the reflectors of the reactor. For the wall in heat exchangers, a one-dimensional approach is sufficient. For the solids only the enthalpy balance needs to be solved. For an element c (centre) and its surrounding elements n, s, e and w (north, south, east and west) this results in:

$$\frac{d(V\rho H)_c}{dt} = \alpha_{n\,to\,c} S_{n\,to\,c}(T_n - T_c) + \alpha_{s\,to\,c} S_{s\,to\,c}(T_s - T_c) + \alpha_{e\,to\,c} S_{e\,to\,c}(T_e - T_c) + \alpha_{w\,to\,c} S_{w\,to\,c}(T_w - T_c) + Q_{from\ fluid} - Q_{to\ fluid} + Q_{generated}$$

$$\alpha_{n\,to\,c} = \frac{1}{\frac{\Delta x_n}{2\lambda_n} + \frac{\Delta x_c}{2\lambda_c}} \qquad \alpha_{s\,to\,c} = \frac{1}{\frac{\Delta x_s}{2\lambda_s} + \frac{\Delta x_c}{2\lambda_c}}$$

$$\alpha_{w\,to\,c} = \frac{1}{\frac{\Delta y_w}{2\lambda_w} + \frac{\Delta y_c}{2\lambda_c}} \qquad \alpha_{e\,to\,c} = \frac{1}{\frac{\Delta y_e}{2\lambda_e} + \frac{\Delta y_c}{2\lambda_c}}$$

With:

λ = thermal conductivity in J m^{-1} K^{-1} s^{-1}

S = area connecting solid elements in m^2
α = heat transfer coefficient in J m^{-2} K^{-1} s^{-1}

In figure 4.2 a piece of a solid structure is shown to clarify the nomenclature.

In none of the models all the terms are present, e.g. in the heat exchanger walls no heat is generated ($Q_{generated} = 0$), whereas in the pebble bed no hot fluid is present ($Q_{from\ fluid} = 0$).
The enthalpy can be written as:

$$H_s = H_{s\,0} + C_{p\,s} T_s$$

in which $H_{s\,0}$ can be set zero, since only changes in enthalpy are of interest.

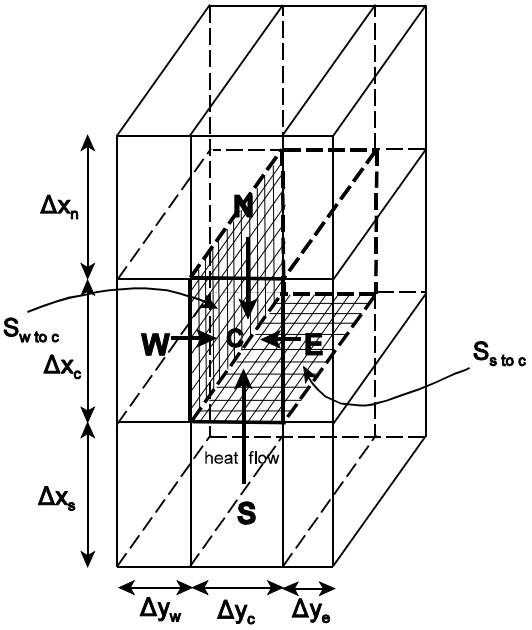

Figure 4.2: Solid structure.

The values used for the steel walls are (Marks, 1951):

ρ_{steel} = $7.77 \cdot 10^3$ kg m^{-3}
$C_{p\ steel}$ = 530 J kg^{-1} K^{-1}
λ_{steel} = 20 J m^{-1} K^{-1} s^{-1}

For the graphite, the changes of density and specific heat are not separated, but calculated using (Yan, 1990):

$$(\rho C_p)_{PB} = (1-\xi) \sum_{i=0}^{3} C_i \, (T_{PB} - 273.15)^i \quad [J m^{-3} K^{-1}]$$

ξ = porosity (0.39 for pebble bed, 0.114 for 'kohlenstein')

Table 4.2: Parameters for heat capacity pebbles.

C_0	$1.129 \cdot 10^0$
C_1	$5.495 \cdot 10^{-3}$
C_2	$4.916 \cdot 10^{-6}$
C_3	$1.678 \cdot 10^{-9}$

The effective thermal conductivity [J m^{-1} K^{-1} s^{-1}] (including radiation between pebbles) of the pebble bed is calculated using a empirical relation developed by General Atomic (Yan, 1990):

$$\lambda_{PB} = 1.1536 \cdot 10^{-4} \, (T_{PB} - 173.15)^{1.6622}$$

This relation is a strong simplifications, since in reality λ depends not only on the temperature but also on the fast neutron exposure and the temperature on which this occurred (VSOP, 1994). For the graphite reflector the thermal conductivity is calculated from:

$$\lambda_{graphite} = C_{\lambda\,gr} \, (1 + (1.5648 - 0.3162 \ln(T_{graphite} - 273.15)))$$

with $C_{\lambda\,gr}$ = 120 for solid reflectors and $C_{\lambda\,gr}$ = 115 if there are cooling channels in the reflector. Finally, λ of the outer reflector made of 'kohlenstein' is calculated with (VSOP, 1994):

$$\lambda_{kohlenstein} = 5.0 + 0.003 \, (T_{kohlenstein} - 273.15)$$

4.3.4 Neutronics Model

The neutronics model is kept simple. For rigorous core modelling, other dedicated models and software packages (VSOP, 1994) (PANTHER) can be used. A time-independent power-profile is assumed, which is valid for normal operation conditions. The actual power production $Q_{generated}$ in a section (axial slab) of the reactor can be calculated as the product of nominal power production Q_{nom} and normalised dimensionless total thermal power P_{norm}:

$$Q_{generated} = P_{norm} Q_{nom}$$

The reactor dynamics are modelled with the point-kinetic approximation using six delayed precursor groups (Duderstadt, 1976, Knief, 1992). The point-kinetic model is solved in a normalised form:

$$\frac{dP_{pr}}{dt} = \frac{\rho - \beta}{\Lambda} P_{pr} + \sum_{i=1}^{6} \lambda_i C_i$$

$$\frac{dC_i}{dt} = \frac{\beta_i}{\Lambda} P_{pr} - \lambda_i C_i \qquad (i = 1..6)$$

$$\frac{dP_j}{dt} = -\lambda_j P_j + \beta_j P_{pr} \qquad (j = 1..23)$$

With:

P_{pr} = normalised dimensionless prompt power
ρ = reactivity
β = $\Sigma\beta_i$
Λ = mean neutron generation time in s
β_i = delayed neutron fraction of precursor group i
λ_i = decay constant of precursor group i
C_i = scaled concentration of precursor group i
P_j = decay heat of group j
β_j = yield fraction of afterheat group j
λ_j = decay constant of afterheat group j

The normalised thermal power can be calculated as:

$$P_{norm} = \frac{P_{pr} + \sum_{k=1}^{23} \lambda_j P_j}{1 + \sum_{k=1}^{23} \beta_j}$$

The reactivity is calculated as the sum of contributions by the negative temperature coefficient, xenon-poisoning and external influences like control-rods or small absorber spheres (SAS).

$$\rho = \rho_{temp} + \rho_{Xe} + \rho_{external}$$

The reactivity resulting from temperature differences is calculated as the sum of the contributions of all axial layers of the core and all axial and radial layers of the reflector. These contributions are calculated from the difference between layer temperature T_k and its nominal value $T_{k\,nom}$. The

reactivity contributions are calculated with a full-scope model (Verkerk, 2000) and inserted in this model as an interpolation-table.

$$\rho_{temp} = \sum_{k=1}^{\#\ layers} \rho_k(\Delta T_k) \qquad \Delta T_k = T_k - T_{k\ nom}$$

The external reactivity-insertion is given as a function of rod-position or number of inserted SAS. The effect of xenon is calculated from the normalised Xe-concentration by:

$$\rho_{Xe} = \rho_{Xe\ zero}(1 - Xe)$$

with:

$\rho_{Xe\ zero}$ = xenon-reactivity at steady-state full power and Xe = 0
Xe = normalised Xe-concentration (normalised on steady-state value)

Xe is calculated based on a simplified decay scheme shown in figure 4.3.

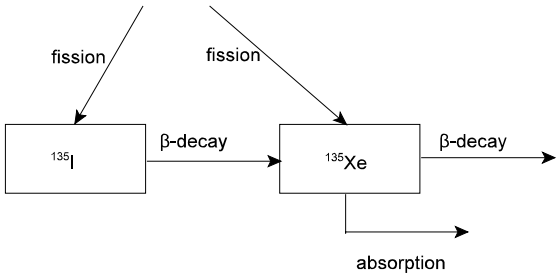

Figure 4.3: Simplified decay scheme of Xe.

According to this scheme iodine is produced as a fission product, which gives a production rate proportional to the neutron flux and thus to P_{pr}. Iodine decays to Xe with decay constant λ_{Xe}. This gives the following normalised I-balance:

$$\frac{dI}{dt} = C_1 P_{pr} - \lambda_I I$$

Xenon is produced as a fission-product and from I-decay. Xe disappears not only through decay, but also through neutron absorption. The absorption rate is proportional to both P_{pr} and Xe. The Xe-balance then reads:

$$\frac{dXe}{dt} = C_2 P_{pr} + \frac{[I]_0}{[Xe]_0}\lambda_I I - \lambda_{xe} Xe - C_3 P_{pr} Xe$$

At 100% power and steady-state conditions the rates of change are zero and P_{pr} = Xe = I = 1, therefore: $C_1 = \lambda_I$. To calculate C_2 one uses the fission-product fraction γ and steady-state full power concentrations $[Xe]_0$ and $[I]_0$: $C_2 = (\gamma_{Xe} / \gamma_I)\ ([I]_0 / [Xe]_0)\ C_1$.
Finally, $C_3 = C_2 + ([I]_0 / [Xe]_0)\ \lambda_I - \lambda_{Xe}$.

The point-kinetic parameters, Xe-poisoning parameters, the axial power-profile and the temperature-reactivity relations have been obtained from a rigorous core-model (Verkerk, 2000) and are given in the component model of the reactor.

4.4 Component Models

4.4.1 Compressor

In order to simulate the compressor behaviour, relations have to be found between the source terms (forces on, heat transport to and work done on the fluid), the inlet conditions and mass

flow, the speed, and the geometry of each stage. These relations have to be valid during normal operation, stalled operation and backflow (as it occurs in surge). In normal operation, the source terms are calculated from the changes in direction and magnitude of the velocity of the gas flow, using a method based mainly on the work of Gravdahl (1999). In the stalled region and for backflow a empirical relation based on the work of Greitzer (1976) is used for the calculation of the forces on the gas. The compressor flowpath is discretised with two thermal nodes for each stage: one for the impeller and the other for the diffusor and volute.

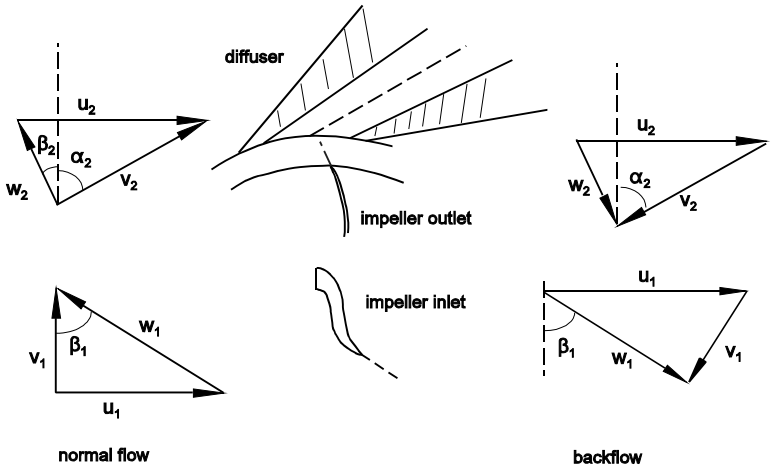

Figure 4.4: Velocity triangles in the radial compressor.

Figure 4.4 shows the velocity triangles at the impeller and diffuser inlet for positive and negative flow. v, w and u denote the absolute, relative and impeller velocity respectively.

The enthalpy rise ΔH over the impeller flowpath can be calculated from the Euler-equation:

$$\Delta H = u_{entr} v_{tang\ entr} - u_{ex} v_{tang\ ex}$$

entr = entrance of the rotor
ex = exit of the rotor
tang = tangential component of the gas velocity

For forward flow $v_{tang\ entr}$ is zero. u_{ex} can be calculated from the rotor speed ω and the impeller diameter d_{imp}:

$$u_{ex} = u_2 = \pi d_{imp} \omega$$

The tangential gas velocity at the impeller outlet is smaller than the impeller velocity, due to the backswept blades and slip:

$$v_{tang\ ex} = v_2 = u_2 - \Delta v_{backsweep} - \Delta v_{slip}$$

$\Delta v_{backsweep}$ can be calculated from the blade angle $\beta_{2\ blade}$ and the radial gas velocity which follows from the mass flow and the cross-sectional area at the impeller tip.

$$\Delta v_{backsweep} = v_{rad\ 2} \tan\beta_{2\ blade} \qquad v_{rad\ 2} = \frac{\phi_{imp}}{\rho A_{imp\ tip}}$$

Δv_{slip} is related to the impeller velocity with the definition of the slip factor μ_{slip}:

$$\mu_{slip} = \frac{u_2 - \Delta v_{slip}}{u_2}$$

There are a number of empirical correlations relating μ_{slip} to the number of impeller blades Z, the relation used here also corrects for the angle of backswept blades (Japikse, 1996)).

$$\mu_{slip} = 1 - \frac{\sqrt{\cos\beta_{2\ blade}}}{Z^{0.7}}$$

For backward flow u_{entr} and u_{ex} are related to the rotor speed by:

$$u_{entr} = u_2 = \pi d_{imp} \omega \qquad u_{ex} = u_1 = \pi d_{eye\ av} \omega$$

$d_{eye\ av}$ = average diameter of the eye in m = ($d_{eye\ inner}$ + $d_{eye\ outer}$) / 2

Now the tangential velocity at the exit (the eye) is not zero; it is calculated from the blade angle β_1 and the axial velocity at the eye. The gas angle is taken equal to the blade angle. This is a fair approximation since an exact prediction of the enthalpy rise is not very important in backflow transients. Likewise, the velocity at the tip is calculated from the diffuser inlet angle $\alpha_{2\,diff}$ and the radial velocity at the impeller tip.

$$v_{tang\ entr} = v_{rad\ 2} \tan\alpha_{2\ diff} \qquad v_{tang\ ex} = \frac{v_{ax\ 1}}{\cos\beta_{1\ blade}} \qquad v_{ax\ 1} = \frac{\phi_{imp}}{\rho A_{eye}}$$

The work done on the fluid is calculated from this enthalpy rise and $W_{disk\ fr}$, the work done by disk friction in the axial gap at the rear of the impeller:

$$W = \phi \Delta H + W_{disk\ fr}$$

$W_{disk\ fr}$ is calculated from the disk friction moment $M_{disk\ fr}$ (Vavra, 1960):

$$W_{disk\ fr} = 2\pi\omega\ M_{disk\ fr} \qquad M_{disk\ fr} = C_{disk\ fr}\ \rho d_{imp}^3 u_2^2$$

Pantell (1949) obtained an empirical relation for $C_{disk\ fr}$:

$$C_{disk\ fr} = \frac{1}{32}\frac{4\pi}{5}\left(\frac{0.9}{R_{sp}^2 \left(\frac{60}{2\pi}\right)^{1.2} Re^{1.2}} + \frac{0.51 + R_{sp}}{5(3 + R_{sp})\left(\frac{60}{2\pi}\right)^{0.182} Re^{0.182}} \right)$$

$$R_{sp} = \frac{\delta_{gap}}{d_{imp}} \qquad Re = \frac{v_{imp\ tip}\, d_{imp}/2}{\mu}$$

R_{sp} = ratio of axial gap and impeller diameter
δ_{gap} = width of the gap behind impeller disk in m
$Re_{disk\ fr}$ = disk friction Reynolds number

The isentropic enthalpy gain ΔH_{isen} over the impeller is obtained when a number of loss terms are deducted from the Euler enthalpy rise. The modelled losses are incidence losses $\Delta H_{inc\ eye}$ and

$\Delta H_{inc\ tip}$(due to a discrepancy between blade and gas angle at the impeller and diffuser inlet), clearance losses ΔH_{cl} (due to a leakage over the blades in the gap between impeller and house) and backflow losses $\Delta H_{backflow}$ (due to reinjection of gas into the impeller because of the pressure gradients in the impeller tip region).

$$\Delta H_{isen} = \Delta H - \Delta H_{inc\ eye} - \Delta H_{inc\ tip} - \Delta H_{cl} - \Delta H_{backflow}$$

The forces on the gas in the impeller are then calculated from ΔH_{isen} using:

$$\left(\frac{p_{in} + F_{rot}/A_{imp\ av}}{p_{in}} \right) = \left(\frac{T_{in} + \Delta H_{isen}/C_p}{T_{in}} \right)^{\frac{\kappa}{\kappa - 1}}$$

With:

$A_{imp\ av}$ = average cross-sectional area of the impeller in m = $(A_{eye} + A_{imp\ tip}) / 2$

The incidence losses are calculated according to the 'NASA shock loss theory' (Gravdahl, 1999). It is based on the assumption that the kinetic energy associated with the tangential component of the 'mismatch' in velocity is dissipated, as illustrated for the diffusor inlet in figure 4.5.

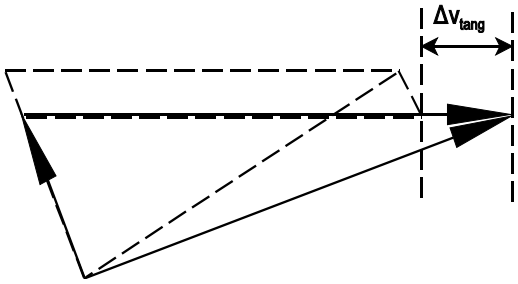

Figure 4.5 Incidence loss at impeller tip (dotted: design velocities, drawn: actual velocities).

$$\Delta H_{inc} = \frac{1}{2} \Delta v_{tang}^2$$

Insertion of trigonometric relations yields:

$$\Delta H_{inc\ eye} = \frac{(u_1 - v_1 \tan \beta_{1\,blade})^2}{2}$$

$$\Delta H_{inc\ tip} = \frac{(v_{tang\ 2} - v_{rad\ 2} \tan \alpha_{2\,diff})^2}{2}$$

The clearance loss and backflow loss are assumed to be a constant fraction of the enthalpy gain (Gravdahl, 1999):

$$\Delta H_{cl} = 0.3 \frac{\delta_{cl}}{b} \Delta H \qquad \Delta H_{backflow} = 0.03\ \Delta H$$

δ_{cl} = width of the clearance between impeller and house in m

b = impeller tip width in m (see appendix B)

The friction losses could be taken into account in the same manner. However, in the approach followed here, the friction forces (calculated from the friction loss factor e_v) are used in the momentum balance. In order to calculate the friction losses in the impeller, diffuser and volute, the friction factor-Reynolds relation for a smooth pipe is used (shown in appendix A). Moreover, the three 90 degrees bends in the volute give an extra pressure loss. For the chosen optimal ratio of 2.5 for bend and pipe radius, this yields a friction loss factor $e_{v\ bend}$ for each bend (Fox, 1994):

$$e_{v\ bend} = 4\ f_{pipe} \left(\frac{L}{D_e} \right)_{eq\ bend} \qquad \left(\frac{L}{D_e} \right)_{eq\ bend} = 12.5$$

Finally, an extra friction loss factor $e_{v\ desw}$ is associated with the deswirl vanes:

$$e_{v\ desw} = C_{desw} \frac{A_{frontal\ desw}}{A_{cr}} \qquad C_{desw} = 0.06$$

$A_{frontal\ desw}$ = frontal area of the deswirl blades in m^2
A_{cr} = cross sectional area of deswirl section in m^2

C_{desw} reaches the minimum value of 0.06 for a thickness/chord ratio of 0.25 (Fox, 1994).

When the isentropic and total enthalpy rise are non-dimensionalised through division by the square impeller velocity (yielding η and η) and plotted against η, the ratio of gas and impeller velocity, the curves approximately collapse on one line for a wide range of input conditions and shaft speeds (Casey, 1986). This is shown in figure 4.6.

$$\varphi = \frac{v_{inlet}}{u} \qquad \lambda = \frac{\Delta H}{u^2} \qquad \psi = \frac{\Delta H_{isen}}{u^2} \qquad \eta_{isen} = \frac{\psi}{\lambda}$$

The calculational method described above also gives a prediction in the stall region (dotted in figure 4.6). Due to the separation of the flow from the blades and local circulating flows, the calculation overestimates η. Therefore, an empirical fit measured by Greitzer (1976) is used for the stall- and backflow region. The parabolic fit used is shown as a dashed line in figure 4.6.

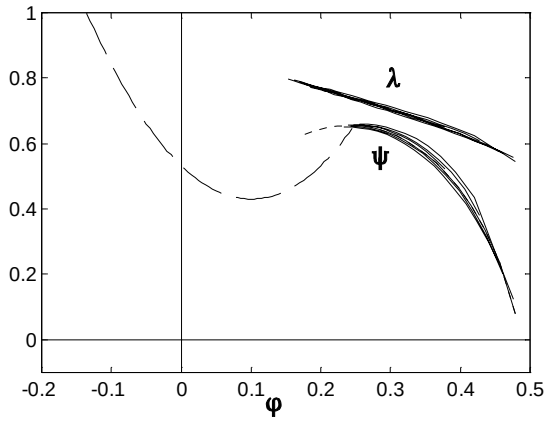

Figure 4.6: Dimensionless stage-curves with extension in stall- and backflow region.

In the stall-region, the steady state characteristic can not be used directly, because there is a delay induced by the development of stall cells in the stages. The time-constant τ_{stall} for this phenomenon is related to the rotational speed, a typical τ_{stall} corresponds to two revolutions (Greitzer, 1976). The applied force is therefore calculated from:

$$\frac{dF_{stall}}{dt} = \frac{1}{\tau_{stall}} (F_{ss} - F_{stall}) \qquad \tau_{stall} = \frac{2}{\omega}$$

The heat exchange between the compressor blades and the gas can also be taken into account. During steady operation, the temperatures are nearly equal and the heat flow is negligible, but during transients the heat flow can have a destabilizing effect. When the compressor is accelerated, the gas temperatures rise, and the blade temperatures are therefore heated. This results in a lower temperature rise than without the heat loss to the blades, thus a higher gas density results. The volumetric flow is therefore lower, which brings the compressor closer to or even into the stall-region. Unfortunately very little is yet known about the time-constants of

this effect, so only crude estimations can be made of input parameters like the effective blade mass (Crawford, 1985). The heat transfer coefficient is calculated from the St $Pr^{2/3}$-Reynolds relation for a smooth pipe. For the heat exchange area S and wall mass M of the impeller only the blade area and mass is used. For the diffuser, S and M are approximated with the area and mass of the triangular wall elements between the diffusor channels.
The heat flow is calculated from:

$$Q = \alpha S (T_{wall} - T_{fluid})$$

The energy balance of the blades is simplified from the wall sub-system model to:

$$M \frac{dH_{wall}}{dt} = -Q$$

The values for steel (given in the solid construction sub-system model) are used. Geometrical data of the compressor are given in appendix B.

4.4.2 Turbine

The turbine is modelled in a stage-by-stage manner. Just like for the compressor, the source terms are calculated from the changes in direction and magnitude of the velocity of the gas flow. These can be related to the geometry (size of annular space, blade angles and shape) using the work of Zehner (1978, 1980) and Bammert (1974, 1980) with an extension for the low flow region by Attia (1985). Work and force of each turbine stage are calculated using dimensionless η - η and η - η relations, which are valid for both positive and negative flow. η, η and η are related by studying the two-dimensional flow at a representative plane with a radius between inner and outer radius of the flow area. A sketch of the flow through a stator and rotor row with definitions of speeds and angles for positive and negative flow is given in figure 4.7.

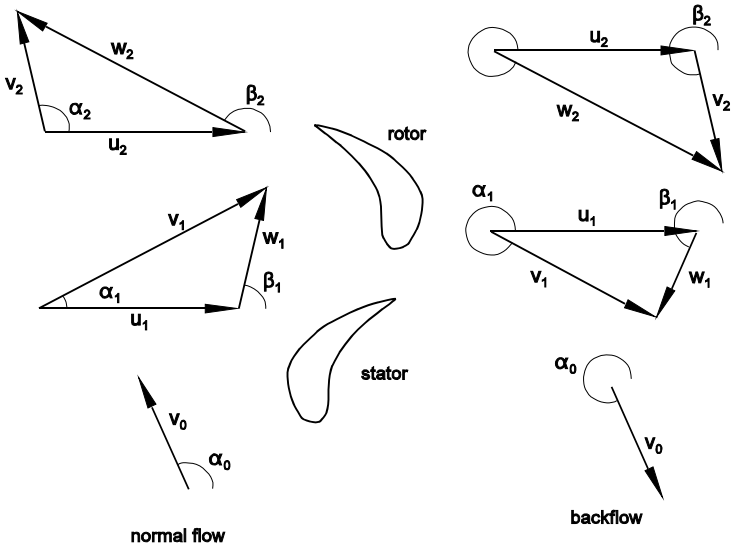

Figure 4.7 Velocity triangles in a turbine stage.

Insertion of some trigonometric relations from the velocity triangle in the Euler equation leads to:

$$\lambda = \varphi (\cot\alpha_{entr} - \cot\beta_{ex}) - 1$$

For forward flow $\alpha_{entr} = \alpha_1$ and $\beta_{ex} = \beta_2$, whereas for back-flow $\alpha_{entr} = \alpha_2$ and $\beta_{ex} = \beta_1$. The angles of the gas velocity are assumed to be equal to the corresponding blade angles within the turbine, whereas axial flow is assumed at the inlet. For forward flow this is a good approximation. For backward flow, it is not as accurate because of the blunt blade shape at the outlet (normally inlet).

Zehner (1980) uses an empirical correlation for the angles during backflow, which gives slightly better agreement with experiments. This more complicated relation is not used here, because backflow will only be encountered in very rare pipe-break accidents. For these accidents an approximation of the turbine behaviour is good enough, since other effects which can not be predicted (like size of the rupture) will have a stronger influence.

The isentropic enthalpy change for forward flow can be written as:

$$\Delta h_{isen} = \Delta h'_{isen} + \Delta h''_{isen} = \left(\frac{v_1^2}{2\eta'} - \frac{v_0^2}{2} \right) + \left(\frac{w_2^2}{2\eta''} - \frac{w_1^2}{2} - \frac{u_2^2}{2} + \frac{u_1^2}{2} \right)$$

where $'$ denotes the stator and $''$ denotes the rotor. The stator and rotor efficiency are here defined as:

$$\eta' = \frac{v_1^2}{v_{1\,isen}^2} \qquad \eta'' = \frac{w_2^2}{w_{2\,isen}^2}$$

When a constant axial velocity in the stage is assumed and with use of some trigonometric relations this can be rewritten to:

$$\psi_{first\ forward} = \frac{\varphi}{2} \left(\frac{\varphi}{\sin^2\alpha_1} \left(\frac{1}{\eta'} - 1 \right) + \varphi \left(\frac{1}{\eta'' \sin^2\beta_2} - 1 \right) + 2\cot\alpha_1 \right) - \frac{1}{2}$$

for the first stage (with axial flow at the inlet). For the subsequent stages applies:

$$\psi_{i\ forward} = \frac{\varphi}{2} \left(\frac{\varphi}{\sin^2\alpha_1} \left(\frac{1}{\eta'} - 1 \right) + \varphi \left(\frac{1}{\eta'' \sin^2\beta_2} - \frac{1}{\sin^2\beta_0} \right) - 2(\cot\beta_0 - \cot\alpha_1) \right) - 1$$

For backflow the following applies:

$$\Delta h_{isen} = \Delta h''_{isen} + \Delta h'_{isen} = \left(\frac{w_1^2}{2\eta''} - \frac{w_2^2}{2} - \frac{u_1^2}{2} + \frac{u_2^2}{2} \right) + \left(\frac{v_0^2}{2\eta'} - \frac{v_1^2}{2} \right)$$

For the last stage this can be rewritten to:

$$\psi_{last\ backward} = \frac{\varphi}{2} \left(\frac{\varphi}{\sin^2\beta_1} \left(\frac{1}{\eta''} - 1 \right) + \varphi \left(\frac{1}{\eta' \sin^2\alpha_0} - 1 \right) + 2\cot\beta_1 \right) - 1$$

and for the other stages to:

$$\psi_{i\ backward} = \frac{\varphi}{2} \left(\frac{\varphi}{\sin^2\beta_1} \left(\frac{1}{\eta''} - 1 \right) + \varphi \left(\frac{1}{\eta' \sin^2\alpha_0} - \frac{1}{\sin^2\alpha_2} \right) - 2(\cot\beta_1 - \cot\alpha_2) \right) - 1$$

For normal flow the angles α_0 and β_1 have to be related to the outlet angle of the preceding row, which is done by:

$$\alpha_{0\,i} = \begin{cases} \arctan\left(\dfrac{\varphi}{\varphi\cot\beta_{2\,i-1} + 1}\right) & \varphi \geq -\tan\beta_{2\,i-1} \\ \arctan\left(\dfrac{\varphi}{\varphi\cot\beta_{2\,i-1} + 1}\right) + \pi & \varphi < -\tan\beta_{2\,i-1} \end{cases}$$

$$\beta_1 = \begin{cases} \arctan\left(\dfrac{\varphi}{\varphi\cot\alpha_1 - 1}\right) & \varphi \geq \tan\alpha_1 \\ \arctan\left(\dfrac{\varphi}{\varphi\cot\alpha_1 - 1}\right) + \pi & \varphi < \tan\alpha_1 \end{cases}$$

The same can be done for β_2 and α_1 in backflow:

$$\beta_{2\,i} = \begin{cases} \arctan\left(\dfrac{\varphi}{\varphi\cot\alpha_{0\,i+1} - 1}\right) + \pi & \varphi \leq -\tan\alpha_{0\,i+1} \\ \arctan\left(\dfrac{\varphi}{\varphi\cot\alpha_{0\,i+1} - 1}\right) + 2\pi & \varphi > -\tan\alpha_{0\,i+1} \end{cases}$$

$$\alpha_1 = \begin{cases} \arctan\left(\dfrac{\varphi}{\varphi\cot\beta_1 + 1}\right) + \pi & \varphi \leq -\tan\beta_1 \\ \arctan\left(\dfrac{\varphi}{\varphi\cot\beta_1 + 1}\right) + 2\pi & \varphi > -\tan\beta_1 \end{cases}$$

A relation between the rotor and stator efficiency and the conditions and geometry has to be inserted. These relations are the same for stator and rotor, if all input variables are given in a relative frame. Hence, the relations given underneath for the rotor efficiency can be applied to the stator, simply by replacing β with α, w with v, 1 with 0 and 2 with 1. The efficiency can be calculated from three different loss-terms: 1) primary losses, which are due to losses over the blade profile, 2) secondary losses, due to disturbance of the velocity profile near the casing and 3) clearance losses, due to the leakage flow over the tip of the blades.

$$\eta = 1 - (\zeta_{prim} + \zeta_{sec} + \zeta_{cl})$$

A minimum efficiency of 0.03 is assumed; if the losses add up to more than 0.97, η is still kept at 0.03.

The primary loss coefficient can be calculated from the blade shape, the primary loss at design conditions and the difference between gas flow inlet angle and blade inlet angle (= design gas flow inlet angle). The influence of the blade shape is simplified with the construction of a dimensionless blade geometry parameter γ:

$$\gamma = \frac{f}{s}\sqrt{\beta_s\ \delta}$$

With:

f = camber in m (as shown in figure 4.8)
s = pitch in m
β_s = stagger angle in rad
δ = camber angle in rad

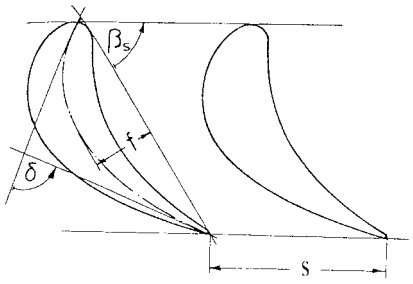

Figure 4.8: Blade geometry.

The primary loss coefficient is calculated as a Gaussian function from the difference in flow angle.

$$\zeta_{prim} = 1 - (1 - \zeta_{prim\ design})\ e^{-a(\Delta\beta^*)^b}$$

in which:

$$\Delta\beta^* = \begin{cases} \dfrac{\beta_1 - \beta_{1\ blade}}{2\pi - \beta_{1\ blade}} & \beta_1 \geq \beta_{1\ blade} \\ \dfrac{\beta_1 - \beta_{1\ blade}}{-\beta_{1\ blade}} & \beta_1 < \beta_{1\ blade} \end{cases}$$

Table 4.4: Constants C_i for calculation of a, b.

	$\beta_1 \geq \beta_{1\ blade}$		$\beta_1 < \beta_{1\ blade}$	
i	a	b	a	b
0	2.58	4.175	0.45	2.413
1	-0.4	10.802	3.82	10.38

The parameters a and b are dependent of the blade geometry parameter and from the sign of the difference in flow angle:

$$a, b = \sum_{i=0}^{2} C_i \gamma^i$$

The secondary losses can be calculated as a function of the aspect ratio s/h, velocity ratio before and after the row w_2/w_1 and deflection angle $\Delta\beta$ over the blade, using table 4.5:

$$\zeta_{sec} = \frac{s}{h} F \qquad F = \sum_{i=0}^{1}\sum_{j=0}^{2} C_{ij} \Delta\beta^i \left(\frac{w_2}{w_1}\right)^j$$

Table 4.5: Constants C_{ij} for calculation of F.

i, j	0	1	2
0	$4.422 \cdot 10^{-3}$	$7.4842 \cdot 10^{-2}$	$1.6170 \cdot 10^{-3}$
1	$7.647 \cdot 10^{-3}$	$2.0060 \cdot 10^{-3}$	$3.7016 \cdot 10^{-2}$

h = blade height in m
$\Delta\beta$ = $\beta_2 - \beta_1$ = deflection angle in rad

The clearance loss is also calculated according to Traupel (1982):

$$\zeta_{cl} = C_{cl} \frac{A_{gap}}{A_{axial}} \sin\beta_2 \qquad A_{gap} = \delta_{cl}\ \pi\ d_{gap}$$

$$C_{cl} = -0.382\ \Delta\beta + 0.850$$

d_{gap} = diameter of the gap in m (hub-diameter for the rotor, tip-diameter for the stator)

δ_{cl} = gap clearance in m

In figure 4.9 a typical variation of the three loss-terms with the relative inlet-angle is shown.

For the losses during backflow different relations, all found by Zehner (1980), will be used. The primary loss coefficient is calculated from the constants in table 4.6 with:

$$\zeta_{prim} = \sum_{i=0}^{4} \sum_{j=0}^{4} C_{ij} \gamma^i \beta_2^j$$

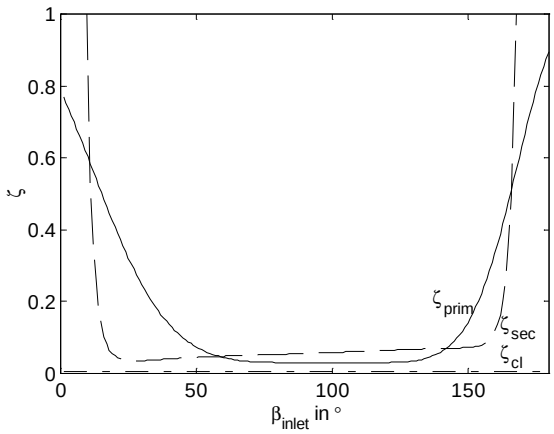

Figure 4.9: Turbine losses.

Table 4.6 Constants C_{ij} for calculation of ζ_{prim}

i, j	0	1	2	3	4
0	$1.448203 \cdot 10^{1}$	$-1.370380 \cdot 10^{1}$	$4.648633 \cdot 10^{0}$	$-6.478400 \cdot 10^{-1}$	$3.101000 \cdot 10^{-2}$
1	$5.749597 \cdot 10^{2}$	$-4.833603 \cdot 10^{2}$	$1.572941 \cdot 10^{2}$	$-2.350434 \cdot 10^{1}$	$1.352909 \cdot 10^{0}$
2	$-4.951008 \cdot 10^{3}$	$4.403119 \cdot 10^{3}$	$-1.484955 \cdot 10^{3}$	$2.248256 \cdot 10^{2}$	$-1.284760 \cdot 10^{1}$
3	$1.157481 \cdot 10^{4}$	$-1.049211 \cdot 10^{4}$	$3.580902 \cdot 10^{3}$	$-5.446983 \cdot 10^{2}$	$3.108084 \cdot 10^{1}$
4	$-7.249584 \cdot 10^{3}$	$6.621342 \cdot 10^{3}$	$-2.270661 \cdot 10^{3}$	$3.461037 \cdot 10^{2}$	$-1.974481 \cdot 10^{1}$

The secondary losses are simply related to the primary loss by:

$$\zeta_{sec\ stat} = 0.7\ (1 - \zeta_{prim\ stat}) \qquad \zeta_{sec\ rot} = 0.85\ (1 - \zeta_{prim\ rot})$$

The clearance loss during backflow is very small compared to primary and secondary losses, but is calculated using the same relation as for forward flow. Sin β_2 is replaced by sin β_1, so that the sinus of the exit angle is still used.

For very low flows, the turbine stage acts as an energy dissipation, in so-called windmilling operation. The η is therefore negative. For zero flow however, the calculation of the stage power consumption using

$$W_{theor} = \phi\ \lambda\ u^2$$

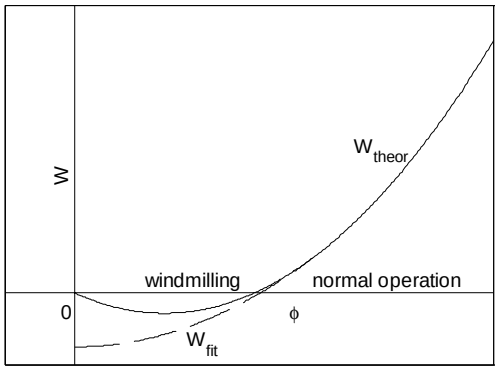

Figure 4.10: Theoretical solution and fit.

leads to a power consumption of zero, while in reality the turbine still consumes power. To overcome this discrepancy, Schobeiri (1992) uses a parabolic fit for W at low positive flow, as

illustrated in figure 4.10.

$$W_{fit} = a_W \phi^2 + b_W \phi + c_W$$

This fit is constructed in the following manner. The maximum power consumption occurs at zero flow, which leads to $b_W = 0$. A correlation is fitted to relate this measured ventilation power at zero flow to the blade velocity and geometry parameter:

$$W_{fit}(0) = c_W = 0.97121\ \gamma_{rot}\ \xi\ u^2 \qquad \xi = \rho A u$$

A smooth transition from the theoretical solution to the fit is obtained by the condition that at the transition flow ϕ_{trans}, the values of fit and theoretical solutions as well as their derivative with respect to ϕ are equal.

$$W_{fit}(\phi_{trans}) = W_{theor}(\phi_{trans}) \qquad \frac{dW_{fit}(\phi_{trans})}{d\phi} = \frac{W_{theor}(\phi_{trans})}{d\phi}$$

After rewriting η to a function of ϕ, this leads to:

$$\phi_{trans} = 2\ \rho\ A\ u\ 0.97121\ \gamma_{rot}^2 \qquad a_W = u^2 \left(\frac{\cot\alpha_{entr} - \cot\beta_{ex}}{\rho A u} - \frac{1}{2\phi_{trans}} \right)$$

The same procedure can be applied to small negative flows.

The force of the blade on the fluid is calculated with:

$$F_{theor} = -\psi\ u^2\ \frac{|\phi|}{v_{ax}}$$

The η - η relations give a good approximation of the behaviour for large positive and negative flows. For small flows, resulting in less accurate predictions of the very low row efficiencies however, the agreement is far worse. Therefore a parabolic fit is also made for the force on the fluid at low positive and negative flows.

$$F_{fit} = a_F \phi^2 + b_F \phi + c_F$$

At zero flow, the rotation will lead to a small pressure rise, so a small positive force should be calculated. No model and only measurements for one configuration of this pressure rise can be found in literature (Zehner, 1980), so only a crude estimation can be made. The force at zero flow is assumed to be a similar function of γ_{rot}, ξ and u as the work at zero flow. Dimensional analysis and the measurements suggest:

$$F_{fit}(0) = c_F = C_{force\ fit}\ \gamma_{rot}\ \xi\ u \qquad \xi = \rho A u$$

Extrapolation gives a value of approx. 1 for $C_{force\ fit}$. Because the derivative of F_{theor} with respect to ϕ can not be found easily, a smooth transition can not be made by calculating the transition-point from the condition of equal value and equal derivative. Therefore, the same transition-point ϕ_{trans} as for the work calculation is used, which leads to:

$$a_F = \frac{F_{theor}(\phi_{trans}) - F_{fit}(0)}{\phi_{trans}^2}$$

A typical plot of force and work of a stage for different mass flows (design value 25.4 kg/s) and design speed and inlet conditions is given in figure 4.11.

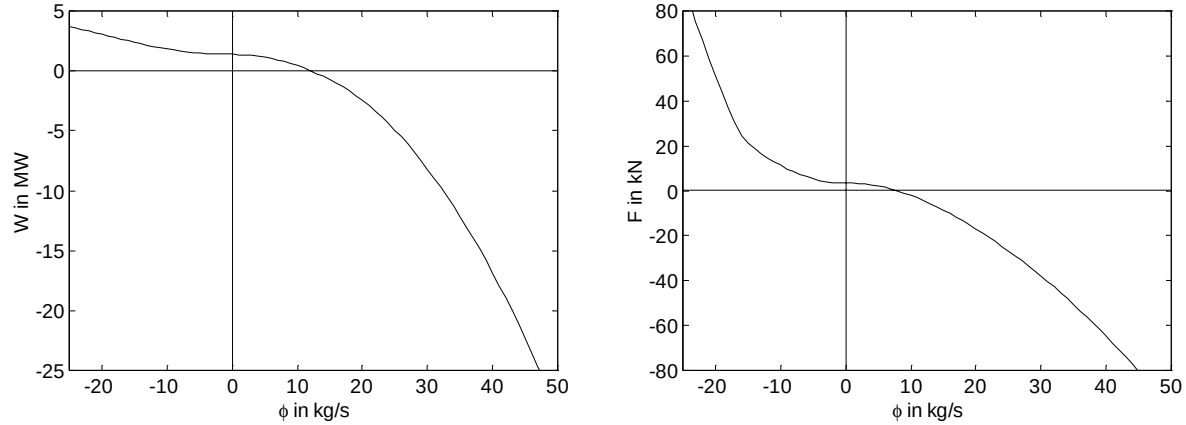

Figure 4.11: Typical force and work of a turbine stage.

The heat transfer from and to blades is modelled as described in the compressor model. The data used for the turbine model are given in appendix B.

4.4.3 Shaft and Generator

The shaft model relates the work performed in the turbine and consumed in compressor and generator to the shaft speed. The rotational energy balance reads:

$$\frac{d2\pi\omega}{dt} = \frac{W_{turb} - W_{comp} - W_{gen} - W_{mech\ loss}}{(I_{turb} + I_{comp} + I_{gen})\ 2\pi\omega}$$

I = inertia in kg m^2

The mechanical losses $W_{mech\ losses}$ and electricity P_{el} produced are calculated as:

$$W_{mech\ losses} = (1 - \eta_{mech})\ W_{gen} \qquad P_{el} = \eta_{gen}\ \eta_{FC}\ W_{gen}$$

η_{mech} = mechanical efficiency
η_{gen} = generator efficiency
η_{FC} = frequency converter efficiency

Table 4.7 shows the data used.

Table 4.7: Shaft data.

I_{comp}	10	η_{mech}	0.99
I_{turb}	10	η_{gen}	0.96
I_{gen}	30	η_{FC}	0.99

4.4.4 One-phase Heat Exchangers

The core model of all one-phase heat exchangers consists of a hot flow, a cold flow and a wall in between. For proper counterflow behaviour each flow is divided in a number of thermal nodes (and flownodes) and the wall is divided in the same number of elements. In order to reach closure of the equations describing the flow through the core relations have to be obtained for friction-

factor f and the heat exchange with the wall Q for both sides. Q can be written as:

$$Q = a\,\alpha S\,(T_{wall} - T_{fluid})$$

The correction factor a is used to adjust for the lower heat transfer due to the modelling with a number of ideally mixed nodes instead of a continuous model. The efficiency of a counterflow heat exchanger is considerably higher than the efficiency of a small number of ideally mixed heat exchangers with the same area and heat transfer coefficients. This is clarified in figure 4.12. With a ΔT in each node which is equal to that in the continuous model, the difference between the outlet temperatures of the discretised model is considerably larger than that of the continuous model. A correction can be made by enlarging the driving force with a factor a. The value of a is highly dependent on the number of mixed volumes which represent the heat exchanger; for small numbers no a can be found, whereas for large numbers a tends to one.

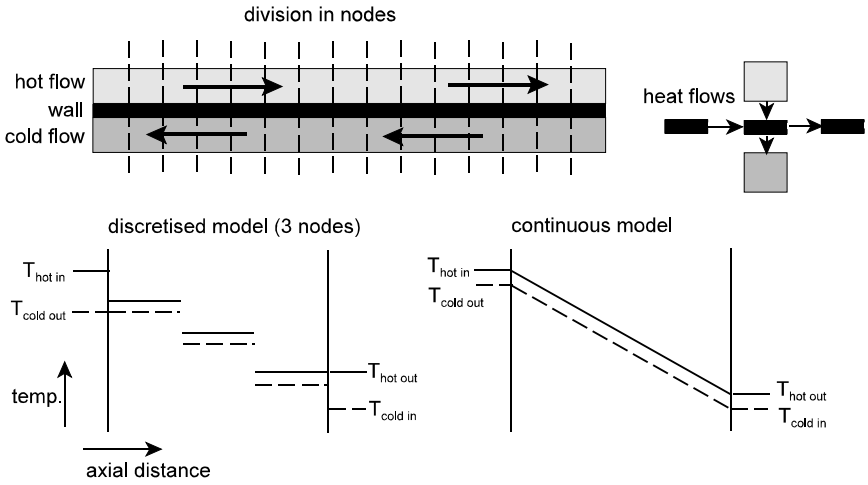

Figure 4.12: Heat exchanger discretisation.

Since the temperatures in a mixed volume are equal to the temperature at the exit, the following relations for the volume exist at steady-state:

$$Q_{node} = a\,(\alpha S)_{node}\,(T_{hot\ out} - T_{cold\ out}) = C_{cold}\,(T_{cold\ out} - T_{cold\ in}) = C_{hot}\,(T_{hot\ in} - T_{hot\ out})$$

Using the definition of heat exchanger efficiency η and NTU as given in paragraph 3.1.2 one can rewrite:

$$a = \frac{\eta}{NTU\left(1 - \eta\frac{C_{min}}{C_{max}} - \eta\right)}$$

η is a function of C_{min} / C_{max}, NTU and the flow arrangement, therefore a can be plotted against C_{min}/C_{max} and NTU for a counterflow arrangement. This is shown in figure 4.13.

The heat transfer coefficient for radial heat transport consists of a convective and a conductive

part. Both for the hot and cold side with different α_{fluid} holds:

$$\alpha = \frac{1}{\left(\frac{1}{\eta_{surf}\,\alpha_{fluid}} + \frac{\delta_{wall}}{2\,\lambda_{metal}}\right)}$$

η_{surf} and α_{fluid} are calculated as described in the steady-state model in paragraph 3.1.2

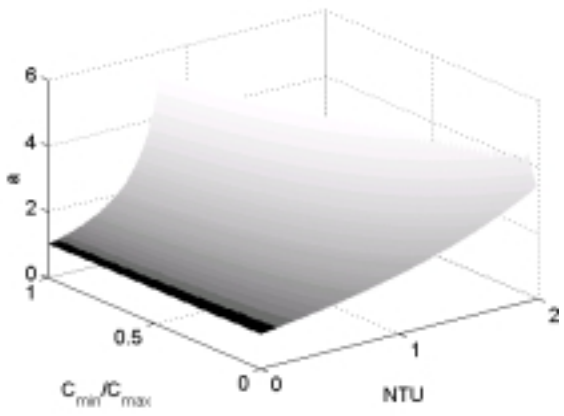

Figure 4.13: Correction factor a.

Heat transfer between the hot and cold flow and the headers is assumed to be negligible because of the relative small heat exchanging surface, therefore only heat transfer from the header to the core by conduction through the metal is taken into account in the energy-balance of the heads. The friction losses in the heat exchangers are also calculated in the same way as in the steady-state model.

The data used for all heat exchanger models are already given in appendix A and chapter 3 (table 3.2). The gas-gas heat exchangers are discretised with 20 axial nodes and 5 nodes are used for the other heat exchangers.

4.4.5 Evaporator, Steam Drum, Downcomer and Deaerator

For the two-phase flow models relations for the two-phase friction multiplier and slip ratio are necessary, as well as relations for friction-factor and heat-transfer.
Whalley (1987) states that the CISE correlation is the best general applicable relation for the slip ratio. The slip ratio is correlated to physical properties and a dimensionless Reynolds and Weber number with the following equations:

$$SR = 1 + E_1\left(\frac{y}{1+yE_2} - yE_2\right)^{\frac{1}{2}} \qquad y = \frac{\beta}{1-\beta} \qquad \beta = \frac{\rho_l x}{\rho_l x + \rho_g(1-x)}$$

$$E_1 = 1.578\,Re_{CISE}^{-0.19}\left(\frac{\rho_l}{\rho_g}\right)^{0.22} \qquad E_2 = 0.0273\,We_{CISE}\,Re_{CISE}^{-0.51}\left(\frac{\rho_l}{\rho_g}\right)^{-0.08}$$

$$Re_{CISE} = \frac{\phi\,D_e}{A\,\mu_l} \qquad We_{CISE} = \frac{\phi^2\,D_e}{A^2\,\sigma\,\rho_l}$$

σ = surface tension in N m^{-1}

Collier (1994) states that for fluids for which $\mu_f/\mu_g < 1000$ (which is the case for water), the Friedel correlation is the best relation for calculating a two-phase friction multiplier. Therefore this relation is implemented and described below:

$$\Phi_{LO}^2 = E_{Fr} + \frac{3.24\ F_{Fr}\ H_{Fr}}{Fr^{0.045}\ We_{Fr}^{0.035}} \qquad E_{Fr} = (1-x)^2 + x^2\ \frac{\rho_l\ f_{GO}}{\rho_g\ f_{LO}}$$

In which f_{GO} and f_{LO} are the friction factors calculated from Reynolds-numbers Re_{GO} and Re_{LO}, calculated from the whole mass flow with the properties of only gas and only liquid respectively.

$$Re_{GO} = \frac{\phi\ D_e}{A\ \mu_g} \qquad Re_{LO} = \frac{\phi\ D_e}{A\ \mu_l}$$

$$F_{Fr} = x^{0.78} + (1-x)^{0.224} \qquad H_{Fr} = \left(\frac{\rho_l}{\rho_g}\right)^{0.91} \left(\frac{\mu_g}{\mu_l}\right)^{0.19} \left(1-\frac{\mu_g}{\mu_l}\right)^{0.7}$$

$$Fr = \frac{\phi^2}{A^2\ g\ D_e\ \rho_h^{\,2}} \qquad We_{Fr} = \frac{\phi^2\ D_e}{A^2\ \sigma\ \rho_h} \qquad \rho_h = \left(\frac{x}{\rho_g} + \frac{1-x}{\rho_l}\right)^{-1}$$

The best correlation for the heat transfer in case of flow-boiling with upward flow through vertical pipes is the Chen correlation (Whalley, 1987). The Chen correlation describes two heat-transfer mechanisms working in parallel: 1) by forced-convection with an enhancement factor F_{Chen} and 2) by nucleate boiling, calculated from the Forster-Zuber equation with a suppression factor S_{Chen}. This correlation is written underneath in a form which is suitable for both sub-cooled and saturated boiling:

$$Q = F_{Chen}\ \alpha_l\ S_{wall}\ (T_{wall} - T) + S_{Chen}\ \alpha_{FZ}\ S_{wall}\ (T_{wall} - T_{sat})$$

F_{Chen} is calculated from the Martinelli-parameter X_{Mart} using the relation shown in figure 4.14.

$$X_{Mart} = \left(\frac{1-x}{x}\right)^{0.9} \left(\frac{\rho_g}{\rho_l}\right)^{0.5} \left(\frac{\mu_l}{\mu_g}\right)^{0.1}$$

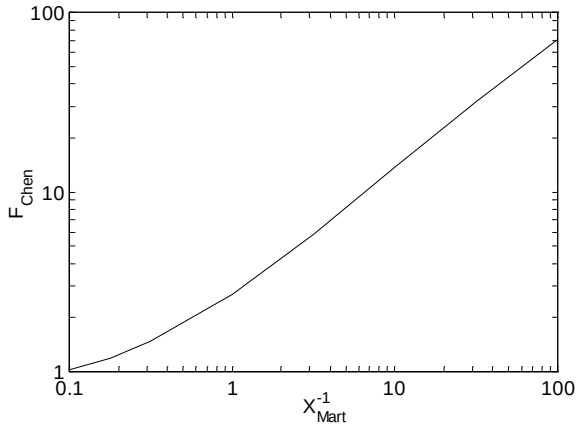

Figure 4.14 Relation between F_{Chen} and X_{Mart}.

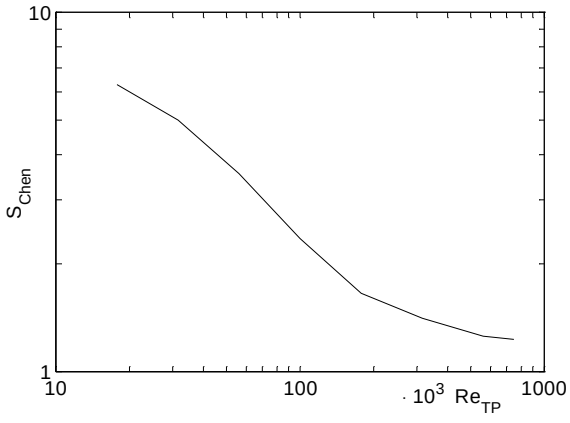

Figure 4.15 Relation between S_{Chen} and Re_{TP}.

α_l is calculated from the St-$Pr^{2/3}$-group using a Reynolds number based on only the fluid part of the flow:

$$Re_l = \frac{\phi_l \, D_e}{A \, \mu_l}$$

S_{Chen} is calculated using the relation shown in figure 4.15 from a two-phase Reynolds number Re_{TP}:

$$Re_{TP} = Re_l \, F_{Chen}^{1.25}$$

The Forster-Zuber heat transfer coefficient α_{FZ} is finally:

$$\alpha_{FZ} = \frac{0.00122 \; \Delta T_{sat}^{0.24} \; \Delta p_{sat}^{0.75} C_{pl}^{0.45} \; \rho_l^{0.49} \; \lambda_l^{0.79}}{\sigma^{0.5} \; \Delta H_{vap}^{0.24} \; \mu_l^{0.29} \; \rho_g^{0.24}}$$

With:

ΔT_{sat} = $T_{wall} - T_{sat}$

Δp_{sat} shown in figure 4.16

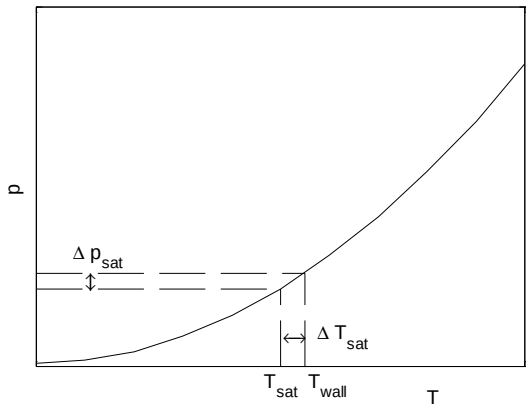

Figure 4.16: Saturation temperature and pressure showing ΔT_{sat} and Δp_{sat}.

10 nodes are used to discretise the evaporator. The discretisation in ideally mixed volumes leads to a non-physical discontinuity when a volume goes from a sub-cooled to a boiling state and vice versa. In reality the boiling front moves gradually, but in this model it moves with steps since a volume is either boiling or non-boiling, and not boiling in one part and non-boiling in the other. This leads to an increase of the mass flow leaving the volume which is too high due to the faster decrease of density at the onset of boiling.

The steam drum is modelled as a single thermal node in which water and steam are separated, but in thermal equilibrium. The velocity in the steam drum is negligible. Saturated water flows from the steam drum into the downcomer and saturated steam flows to the deaerator and the superheater. The liquid level (L) is calculated as:

$$L = \alpha \, d_{drum}$$

$_{drum}$ = diameter of the drum in m

This is a crude approximation since it does not take into account the change in area with level or volume changes of the water by bubble formation in case of a pressure reduction. However, in a real drum there are strong fluctuations in the measurement of the liquid level which can not be modelled anyway. Therefore, no attempt is made to correct for the effects mentioned above. Saturated water flows into the downcomer in which the hydrostatic pressure and velocity are higher than in the drum. The result is a decrease in static pressure which leads to steam formation. This steam is carried along with the water with the same speed (SR = 1). The flows to the superheater and to the deaerator contain saturated steam only.

The drum has a diameter of 0.5 m and is 3 m long, while the downcomer has a diameter of 0.25 m and a length of 2.35 m. The deaerator is an ideal mixer of water and steam, resulting in an one-phase water outlet flow. The deaerator is modelled as a frictionless and adiabatic volume of 3 m^3.

4.4.6 Reactor

A drawing of the reactor with the division of the solid structure in different elements is shown in figure 4.17 (adapted from (Verkerk, 2000)). The pebble bed (A) is divided in ten axial layers. 4 axially discretised reflector layers surrounding the pebble bed have been modelled: the inner reflector with channels for control-rods and the small absorber sphere-system (B), the middle reflector (C), layer consisting of the reflector with cooling gas channels and separator reflector (D) and outer reflector, made of 'kohlenstein' (E). The outer reflector is surrounded by a border in which heat loss to the surroundings is calculated (not shown since it has no heat capacity). The top and bottom reflector (F & G) above and beneath the pebble bed also contain cooling channels and are surrounded by four reflector-layers. The sizes of the elements are shown in figure 4.17. For the pebble bed, the distance for heat loss to the first reflector (Δy_c in paragraph 4.3.3) is not equal to the radius but much smaller, since the heat is not produced in the centre only but over the whole radius. This distance is varied to achieve the best agreement with the temperatures in the full scope model (Verkerk, 2000). The heat transfer coefficient for the heat loss to the surroundings is used to set the value of the steady-state heat loss to 433 kW, which is calculated with the full-scope model. The data of the helium channels are given in table 4.8.

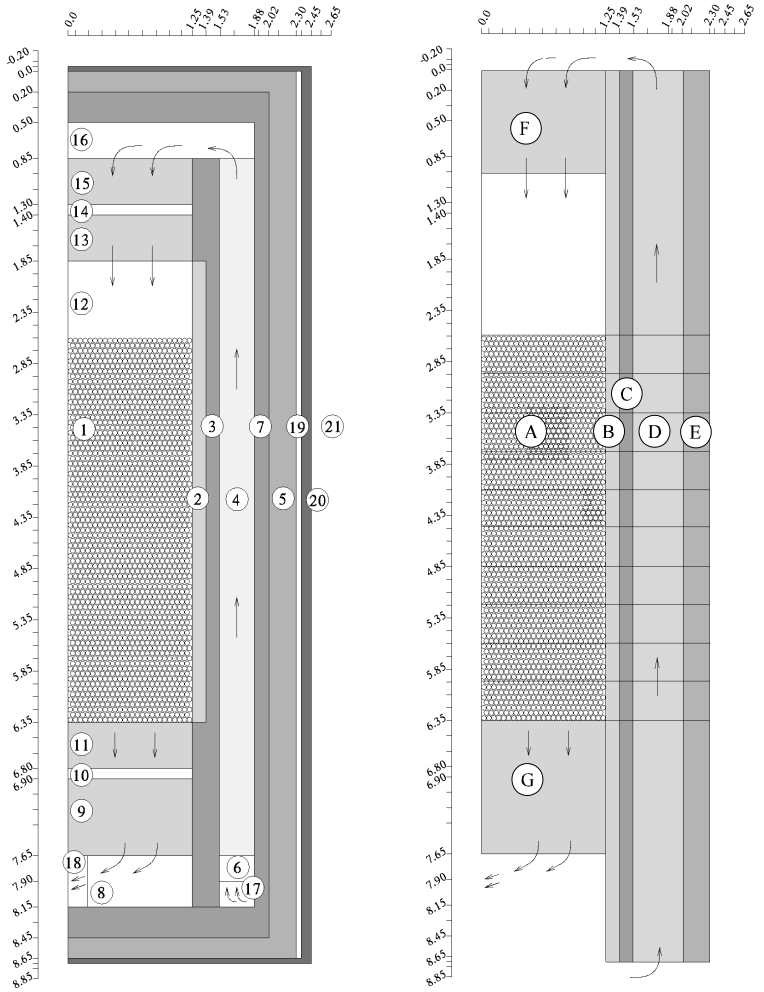

Figure 4.17: Reactor discretisation.

The heat transfer coefficient and friction-factor are calculated analogously to the heat exchangers, using the relation shown in figure 3.3. The heat production is calculated as described in the neutronics model (paragraph 4.4.4). The point-kinetic parameters, Xe-poisoning parameters, the

axial power-profile and the temperature-reactivity relations for the axial pebble-bed layers are given in table 4.9 and 4.10 and figures 4.18 and 4.19. Curves similar to those shown in figure 4.19 are used to calculate the reactivity contributions of all the reflectors.

Table 4.8: Data of reflector channels.

	no. of channels	diameter in m	length in m
top reflector	35	0.163	1
bottom reflector	155	0.075	1.3
reflector 1	20	0.1	8.65
reflector 3	72	0.13	8.65

Table 4.9: Point-kinetic parameters.

$\Lambda = 8.879 \cdot 10^{-4}$ s		
group i	β	λ in s^{-1}
1	$0.1807 \cdot 10^{-3}$	0.013
2	$1.237 \cdot 10^{-3}$	0.032
3	$1.192 \cdot 10^{-3}$	0.128
4	$1.972 \cdot 10^{-3}$	0.304
5	$0.6925 \cdot 10^{-3}$	1.35
6	$0.1314 \cdot 10^{-3}$	3.63

Table 4.10: Xe-poisoning parameters.

$\rho_{Xe\ zero} = 0.01718$		
fission product	I	Xe
γ	0.0603615	0.0077
λ in s^{-1}	$2.912 \cdot 10^{-5}$	$2.118 \cdot 10^{-5}$
$[C]_0$ in m^{-3}	$1.3732 \cdot 10^{20}$	$1.2887 \cdot 10^{20}$

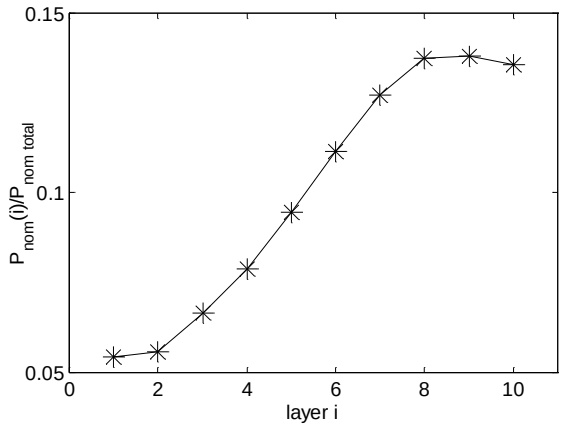

Figure 4.18: Reactor power distribution.

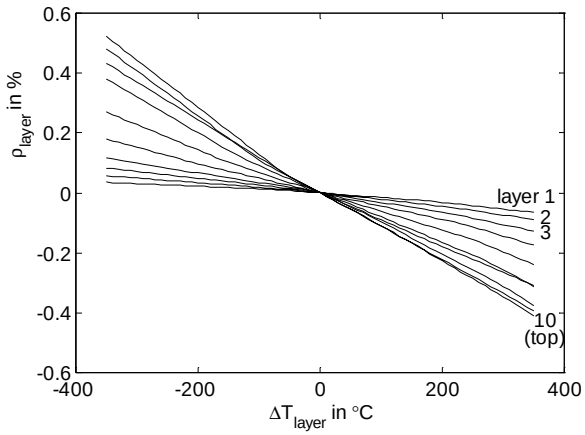

Figure 4.19: pebble bed reactivity.

4.4.7 Secondary Helium Blower and Feedwater Pump

In the helium blower and pump, two source terms have to be taken into account: the force exerted on the fluid F_{rot} and the corresponding work done W_{rot}. The friction forces can be neglected since they are small compared to the externally applied force, and heat transport from or to the wall is also negligible because of the small heat transferring area. F and W can be calculated from the pump head h and efficiency η:

$$F_{rot} = g\,h\,A \qquad W_{rot} = \frac{\phi\ g\ h}{\eta}$$

The head and efficiency under different operating conditions are described by the one-dimensional pump characteristics, which are given in chapter 3. No attempt is made to dimension the pump and blower.

4.4.8 Valves

For the valve, a relation has to be given between stem position and flow. This could be obtained by adjusting the cross-sectional area of the thermal node, but this would induce very high fluid speeds with corresponding high Mach-numbers and compressibility-problems when a valve is closed quickly.

For valves which operate at low Mach-numbers this would unnecessarily complicate the model. The flow through the valve can be influenced more easily by changing the friction loss factor in the following manner:

$$e_{v\ valve} = k_{valve}\ e_{v\ open\ valve}$$

No heat transfer from or to the fluid is modelled. The flow through an open valve is calculated using an e_v of 8 which is typical for a globe-valve (Bird, 1960). The flow through a closed valve is assumed to be 10^5 times smaller than the flow through an open valve. This approximation has to be made, since the numerical solver can not handle a stable zero-flow. For different types of valves, different relative flow versus valve stem position relations, so-called valve characteristics, are obtained (Stephanopoulos, 1984). For six frequently used types, these valve characteristics are plotted in figure 4.20. A relation between k_{valve} and the valve position is easily obtained: k_{valve} is inversely proportional to the square of the relative flow ϕ_{rel}.

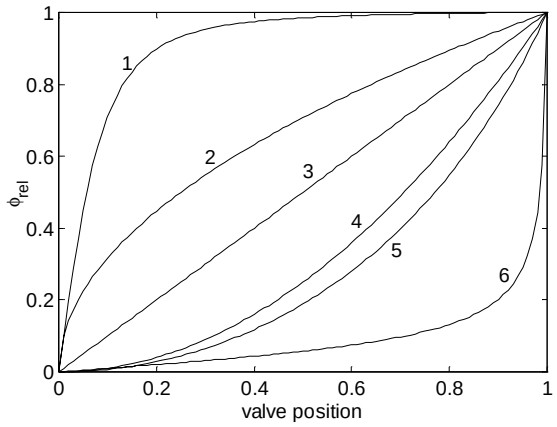

Figure 4.20: Valve characteristics for quick opening (1), square root (2), linear (3), parabolic (3), equal percentage (5) and hyperbolic valve (6).

Complex models for valve behaviour are readily available. One could take into account the second-order behaviour of the stem positioning and the maximum adjustment velocity (ACM, 1999). However, the goal of this model is to calculate the dynamics of the plant and not those of the control system. Therefore, only a first-order delay is built in to simulate the inertia of the valve:

$$\frac{dVP}{dt} = \frac{1}{\tau_{valve}} (VP_{target} - VP)$$

With:

τ_{valve} = valve time constant in s
VP = valve position

This approach leads to a correct prediction of the flow in case of low Mach-speeds (<0.7).

For valves in which higher Mach-numbers can be expected (like those connecting low- and high pressure plenums) a model based on Pool (1982) is used. He relates the forces on the fluid to the input and output conditions and two dimensionless numbers, in the form of area-ratios:

$$\frac{A_{fr}}{A_{in}} \left(= \frac{1}{\sqrt{e_v}}\right) \qquad \frac{A_{no}}{A_{in}}$$

A_{in} = area at inlet, cross-sectional area of connecting pipes in m^2
A_{fr} = fictional area for friction calculation in m^2
A_{no} = cross-sectional area at nozzle in m^2, see figure 4.21

These two ratios can be found experimentally as a function of the stem position. The behaviour for low Mach-numbers is determined by the first ratio, the behaviour for choked flow (Mach one at the 'nozzle') is determined by the second. In the intermediate regime, both numbers are used.

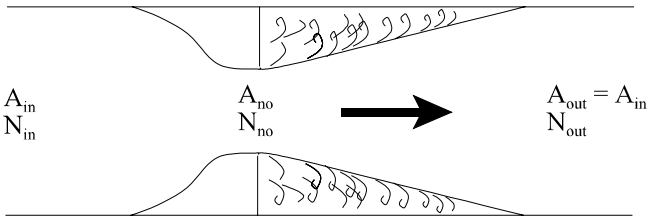

Figure 4.21: Model for high Mach-number valve.

The calculation is based on the flow-numbers N_{in} and N_{no} at the inlet and the nozzle, which are related to the Mach numbers as:

$$N_{in} = \sqrt{\frac{\kappa}{2}} M_{in} \qquad N_{no} = \sqrt{\frac{\kappa}{2}} M_{no}$$

The static flow-pressure relation is based on the formula (Bean, 1971):

$$\Delta p = - e_v \frac{1}{2} \rho \left(\frac{v}{Y}\right)^2$$

Y = expansion ratio

For Y=1 this formula reduces to the normal pressure-flow relation for flow with constant density, the variable Y corrects for the effects of compressibility. For flow through a pipe with constant cross-section, a theoretical expression for Y can be developed (Streeter, 1987).

$$Y = \sqrt{\frac{e_{v\ pipe}\ N_{in}^2}{1 - \frac{N_{in}}{N_{out}}\sqrt{\frac{\frac{\kappa}{\kappa-1} + N_{in}^2}{\frac{\kappa}{\kappa-1} + N_{out}^2}}}}$$

N_{out} = flow number at pipe outlet

Pool (1982) suggests that the expansion ratio Y for the valve can be taken equal to Y for a pipe which chokes at the same mass flow, thus avoiding the necessity to establish Y for different valves. This is a strongly simplifying assumption, which is supported by measurements. The flow number N_{in}^* for which the nozzle chokes is given by:

$$\left(\frac{A_{no}}{A_{in}}\right)^2 = \frac{2}{\kappa} N_{in}^* \left(\frac{\frac{\kappa+1}{2}}{1 + \frac{\kappa-1}{2} N_{in}^*}\right)^{\frac{\kappa+1}{\kappa-1}}$$

The equivalent friction loss factor $e_{v\ pipe\ eq}$ for which a pipe with the same inlet flow number chokes is:

$$e_{v\ pipe\ eq} = \frac{1}{2N_{in}^{*2}} - \frac{1}{\kappa} - \frac{\kappa+1}{2\kappa} \ln\left(\frac{\frac{1}{N_{in}^{*2}} + \frac{\kappa-1}{\kappa}}{\frac{\kappa+1}{\kappa}}\right)$$

With this equivalent friction loss factor, the outlet flow number N_{out} for the pipe with the same N_{in}^* as the nozzle can be calculated as a function of N_{in}:

$$e_{v\ pipe\ eq} = \frac{1}{2N_{in}^2} - \frac{1}{2N_{out}^2} - \frac{\kappa+1}{2\kappa} \ln\left(\frac{\frac{1}{N_{in}^2} + \frac{\kappa-1}{\kappa}}{\frac{1}{N_{out}^2} + \frac{\kappa-1}{\kappa}}\right)$$

From N_{out}, Y can be calculated and used in the pressure-flow relation. If the velocity reaches the speed of sound in the nozzle, a recompression shock-wave will occur just downstream of the nozzle. It is assumed that this leads to exactly Mach-number unity in the nozzle which is a fair approximation; the real Mach-number is just a little higher. From the mass flow through and the pressure difference over the valve calculated in this manner, a virtual friction loss factor is calculated and used in the momentum-balance downstream of the valve. Typical area ratios for a globe valve for different stem positions are given in figure 4.22 (Pool, 1982).

4.4.9 Plenums, Vessels and Pipes

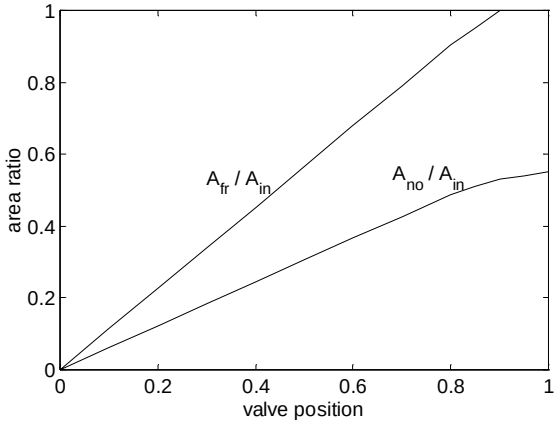

Figure 4.22: Area ratio for a globe valve.

Between the components, helium or water flows can be split or joint together. This is done in a plenum, a thermal node with several inputs and outputs. These thermal nodes all have relatively large cross-sectional areas and thus low velocities. Therefore, the incoming and outgoing flows are assumed to carry no momentum to the connecting flownodes. This is a valid simplification, since the difference in static and total pressure in these elements is negligible. The pressure loss within these plenums is also negligible. For numerical stability however, a very small friction loss factor is introduced. The plenums are all supposed to be adiabatic. This is a valid assumption since both the heat transfer to and the heat capacity of the the walls of the plenums is negligible compared to the heat transfer to and the heat capacity of walls in heat exchanging equipment. The dimensions of the plenums in the primary circuit are given in table 4.11.

The inventory control vessels are also modelled with plenums. The heat transfer to the surroundings is calculated from:

$$Q = -(\alpha S)_{vessel} (T_{He} - T_{surr})$$

T_{surr} = (constant) temperature of surroundings in K

The connecting pipes are assumed to be adiabatic on the same grounds as the plenums. The friction loss factor is calculated from the friction factor using the Re-fr relation for a pipe (given in appendix A). The reactor and energy conversion system are connected with a pipe and an annular space. The pipe from the reactor has a length of 4 m and a diameter of 0.95 m and the annulus to the reactor has a length of 11 m and an equivalent diameter of 0.7 m.

Table 4.11: Plenum volumes.

plenum	volume in m^3
between precooler and compressor	2
between compressor and recuperator	21
between recuperator and reactor	4
between reactor and turbine	0.5
between turbine and recuperator	4
between recuperator and precooler	10

4.5 Conclusions

A best-estimate code for the complete nuclear gas turbine plant has been produced. Its level of detail surpasses any model described in literature, except for the reactor neutronics. The setup of the code allows also for use as a design-code. For example, one can not only predict the pressure ratio for a compressor from its geometry during off-design operation, it is also possible to determine the impeller diameter necessary to achieve a certain pressure ratio.

Because of its modular approach it can easily be used for other power plants. If thermodynamic properties of air, fuel and off-gas are added, one can easily model a complete conventional power plant. The detailed description of the natural circulation evaporator makes the code with small adaption fit for the study of boiling instabilities, as they can occur in a boiling water reactor.

Chapter 5

Verification and Validation of the Dynamic Model

Generally, there are a number of options for verification and validation of a model. The most obvious option is comparison with data from the actual plant. Since the cogenerating NGT-plant has not been built, this option is not possible. Another method of validation is by comparison with another model. The reactor model has been validated with a 3-dimensional neutronics and thermal hydraulics model. The other component-models are verified by checking the simulated transients on e.g. the principles of conservation of energy. Moreover, the sensitivity of the model with regard to uncertain parameters and the spatial discretisation has been checked. Finally, some transients have been calculated with this dynamic model and with the nuclear thermal hydraulics code RELAP. The results are compared and discussed.

5.1 Compressor

In order to check the compressor model, first the compressor map shown in figure 5.1 has been produced. The map shows that the compressor model gives very realistic results. The most striking difference with the map used in the steady-state model (shown in figure 3.1) is that the design-point (marked with an asterisk) does not have the highest efficiency. Because the friction losses are high compared to the incidence losses, a higher efficiency is reached at lower mass flows.

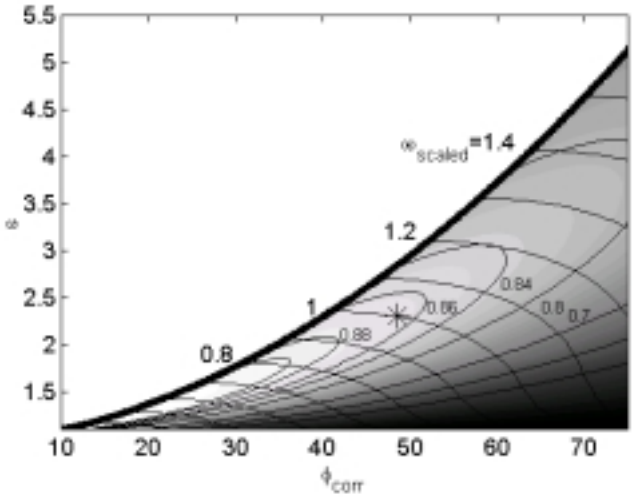

Figure 5.1: Compressor map.

The dynamic behaviour is tested in a configuration in which the compressor is connected with a plenum and a valve as shown in figure 5.2. When the valve is closed, the pressure ratio over the compressor rises. With the decreased flow the surge-line is passed and oscillatory behaviour results. Greitzer (1976) states that the shape and frequency of the flow oscillation is dependent of the plenum volume. A stable operation point in the rotating stall region can be found with a small plenum. For a larger volume high frequency oscillations without negative flow are expected. When the volume is enlarged further, a cycle including backflow

appears and the frequency decreases. The transitions are predicting using a parameter B:

$$B = \frac{u}{2 v_{sound}} \sqrt{\frac{V_{plenum}}{A_{comp} L_{comp}}}$$

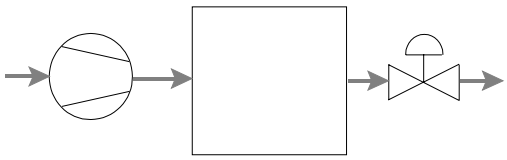

Figure 5.2: Surge test configuration.

u = rotational velocity in m/s
V = volume in m^3
A = cross-sectional area in m^2
L = length in m
v_{sound} = acoustic velocity in m/s

Greitzer predicts that for B = 0.45 an overdamped transition is expected, whereas with B = 0.6 the transition to stalled operation is underdamped. Classical surge appears for B = 0.7. At B = 1.58 the lowest mass flow is zero, and B = 5 leads to deep surge.

First a one-stage compressor is tested. In figures 5.3 to 5.6 the plenum pressure and compressor mass flow are shown for increasing plenum volumes (note the different time scales!). The valve has been closed to a position which brings the compressor just past the surge-line. If the throttle is closed further, the transitions occur at other values of B.

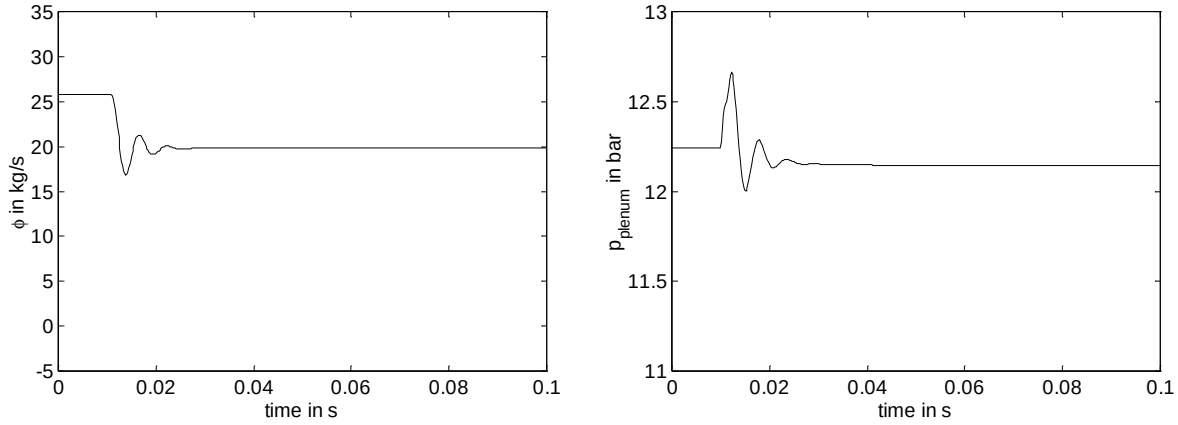

Figure 5.3: Single stage behaviour with 0.028 m^3 plenum, B = 0.1.

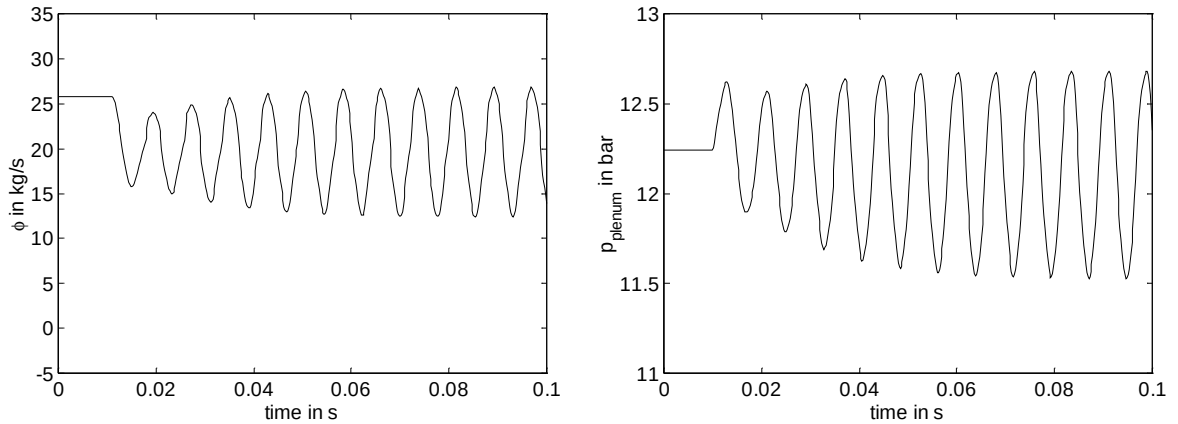

Figure 5.4: Single stage behaviour with 0.114 m^3 plenum, B = 0.2.

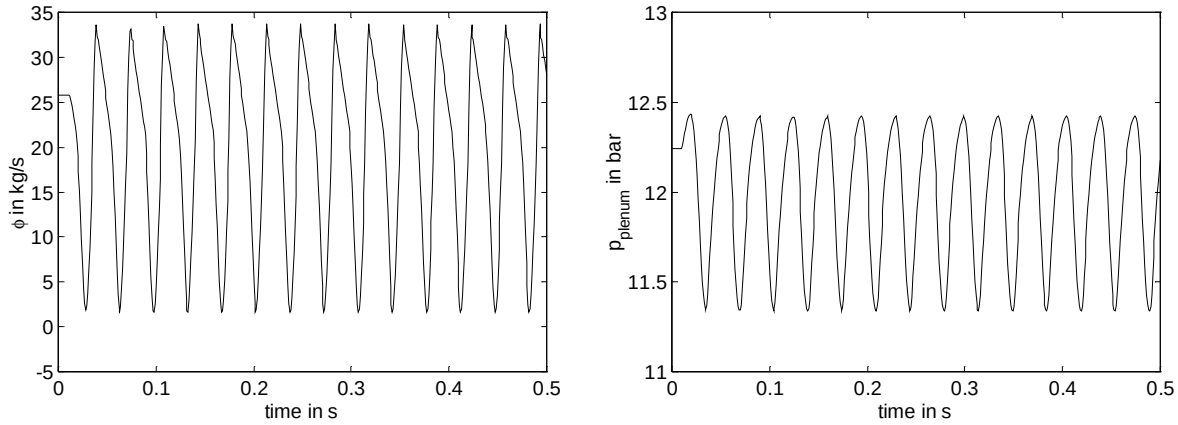

Figure 5.5: Single stage behaviour with 1.82 m^3 plenum, B = 0.8.

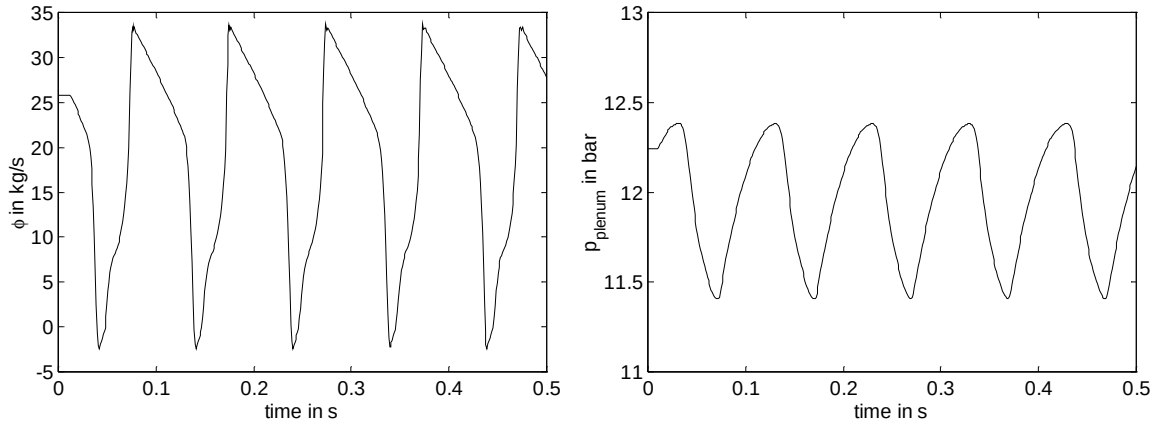

Figure 5.6: Single stage behaviour with 6.40 m^3 plenum, B = 1.5.

For B = 0.1 and smaller the transient gives an underdamped result. The damped transition which Greitzer observes is due to the fact that he ignores the inertia of the gas. When B is enlarged to 0.2, classical surge appears. If B is increased further, the lowest mass flow comes closer to zero, as shown in figure 5.5 with B = 0.8. Negative flow and the corresponding deep surge pattern appear when B is enlarged to 1.5. The qualitatively expected behaviour is exhibited, however the transition appear at lower values of B than Greitzer predicted.

When the multi-stage compressor is tested, the interaction between the stages leads to a chaotic pattern, resembling those Greitzer and Davis (1991) measured. Results are shown in figure 5.7 to 5.10 for a plenum size of 0.01, 0.1, 1 and 10 m^3. The transitions now take place at much lower B-values. This is because for L_{comp} the complete compressor length is taken, while the last stage alone already could establish the surge. If only the length of the last stage is used in the calculation of B, its value would increase approximately with a factor $\sqrt{5}$ which would bring them in the range expected.

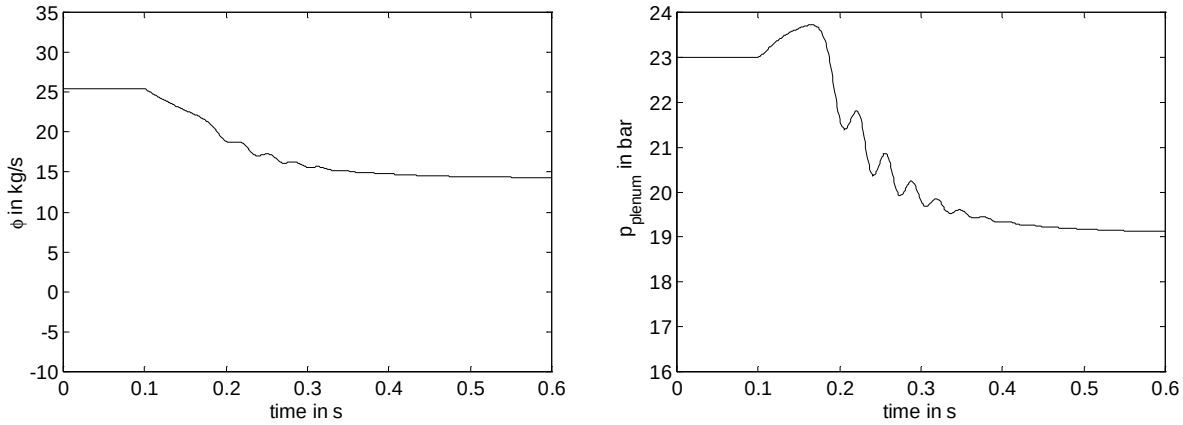

Figure 5.7: Compressor behaviour with 0.01 m^3 plenum, B = 0.024.

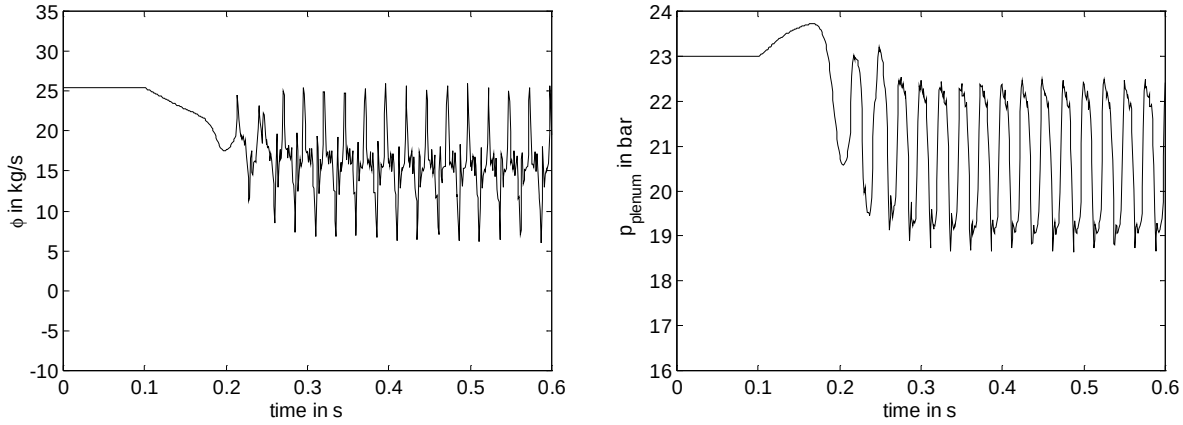

Figure 5.8: Compressor behaviour with 0.1 m^3 plenum, B = 0.077.

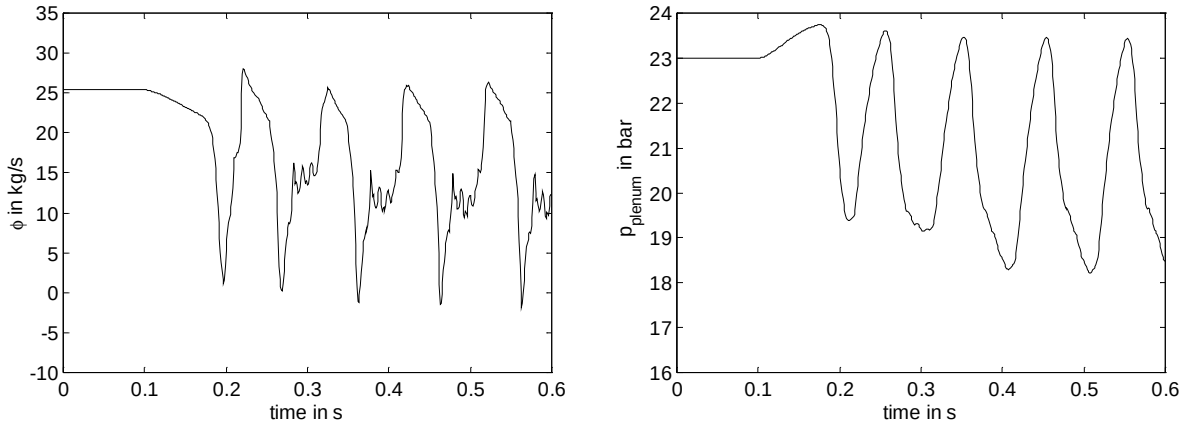

Figure 5.9: Compressor behaviour with 1 m^3 plenum, B = 0.24.

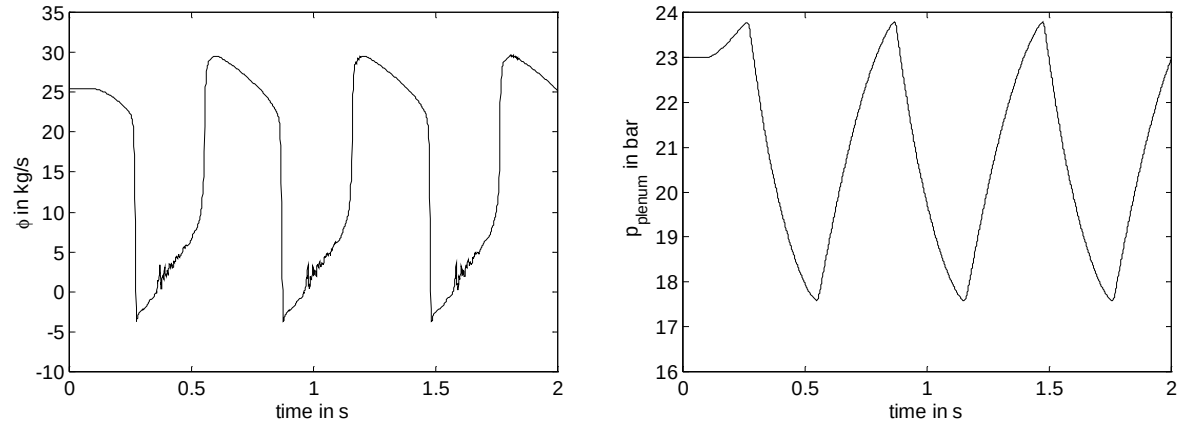

Figure 5.10: Compressor behaviour with 10 m^3 plenum, B = 0.77.

5.2 Turbine

In order to check the turbine-model, the steady-state results of the dynamic stage-by-stage model have been compared to the results of the simple steady-state model presented in chapter 3. In figure 5.11 the flow ϕ and isentropic efficiency η_{isen} are plotted against the pressure ratio ε for different rotational speeds ω. The mass flow of the simple model is hardly dependent on the rotational speed. This is consistent with the expectations, since the mass flow is calculated from an expression based on the similarity with a nozzle, in which there is no rotational speed. The stage-by-stage model does not model choking correctly; the mass flow does not level off at high pressure ratios. This was to be expected, since the discretisation-scheme cannot be used for choked flow. The 'nozzle'-model of course correctly predicts the choking. If a correct prediction of choking in the dynamical model is necessary, then a choking valve can be placed directly after the turbine. The efficiency curves are again similar but not the same. The simple model assumes a quicker decline of efficiency at off-design conditions than the stage-by-stage model. If the off-design efficiency relation shown in figure 3.2 is replaced with a curve which is flatter around the top, the results would be more similar.

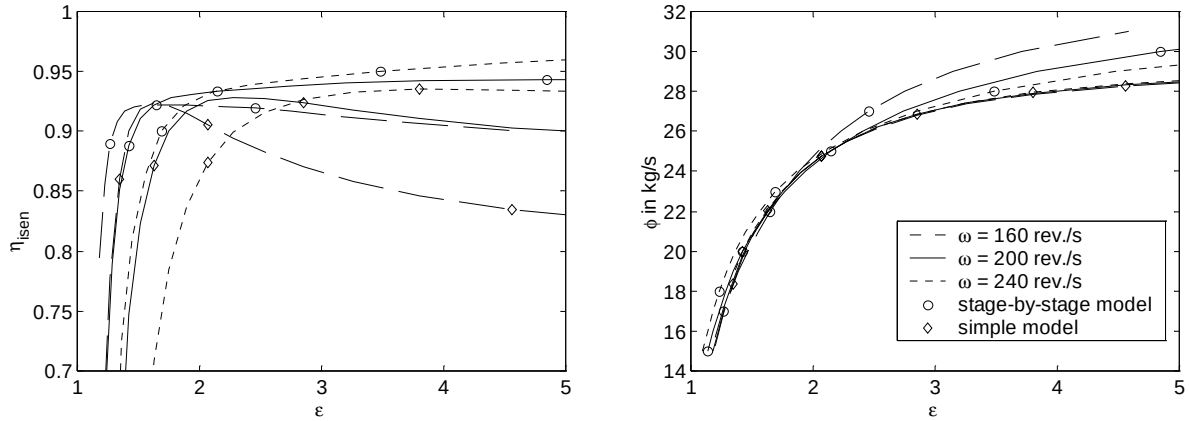

Figure 5.11: Comparison between stage-by-stage and simple model.

5.3 Heat exchangers

The heat exchanger dynamics have been verified with the energy-balance of the transient following a step change of 100 °C on the cold flow inlet temperature of the recuperator. The pressure on both inlets and outlets as well as the hot side inlet temperature were kept constant at their values at normal operating conditions. The response of the inlet and outlet temperatures and the mass flows are given in figure 5.12. The increased temperature and constant pressure gives a lower density. If the mass flow was constant, the velocity would increase, which leads to a higher pressure drop. However, the pressure difference over the heat exchanger is constant, therefore the mass flow decreases.

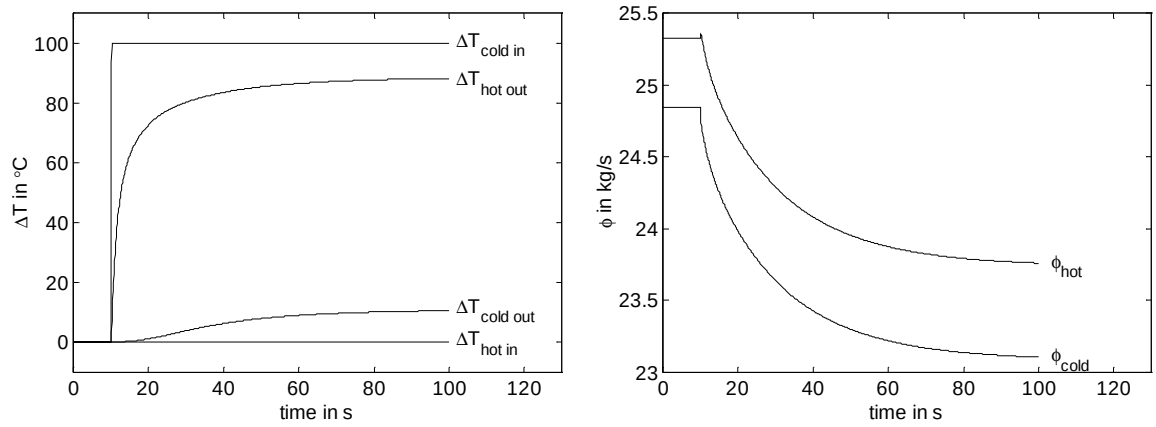

Figure 5.12: Response on a step change of the recuperator cold inlet temperature.

In figure 5.13 the heat flow to the heat exchanger body is shown:

$$Q_{to\ steel} = C_p[\dot{\phi}_{hot}(T_{hot\ in} - T_{hot\ out}) + \dot{\phi}_{cold}(T_{cold\ in} - T_{cold\ out})]$$

Integration of $Q_{to\,steel}$ gives the enthalpy difference of steel, from this the average steel temperature rise can be calculated.

$$\int_0^t Q_{to\ steel} = \Delta h_{steel}(t) = M\,C_p\,\Delta T(t) \qquad \rightarrow \Delta T(\infty) \approx \Delta T(100\ s) = 50\ °C$$

The mean wall temperature rise is again calculated to be 50 °C from comparison of the average wall temperature before and after the transient. This is also the expected behaviour when the inlet temperature on one side is raised with 100 °C while the other inlet temperature is kept constant.

This logical test shows that there are no modelling errors. However, the accuracy of the model depends on the accuracy of the empirical relations used and some modelling choices (like the number of thermal nodes used to discretise

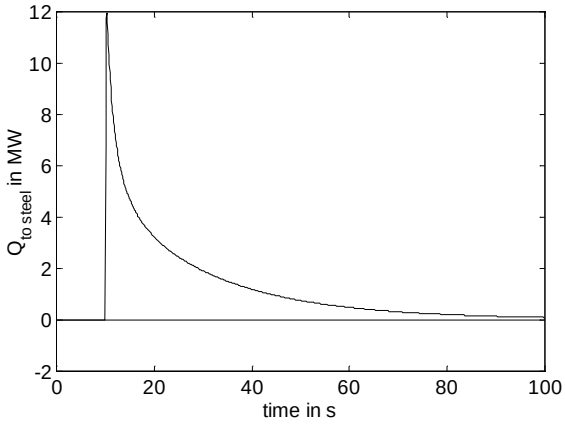

Figure 5.13: Heat flow to the recuperator steel during the transient.

a heat exchanger). Since a comparison with real data is not possible, a sensitivity analysis is the only way to assess the models. For the one-phase heat exchangers, the empirical relations for heat transfer coefficients and friction factors only influence the steady-state results (and thus the design). If the heat transfer coefficient turns out to be lower, the heat exchanger must be enlarged, but the dynamic behaviour is not directly influenced. (Indirectly it is: more steel leads to a slower response).

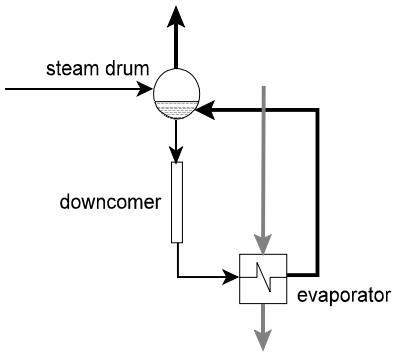

Figure 5.14: Steam generator.

For the evaporator-model, correlations for the slip-velocity and two-phase friction multiplier are added as well. The sensitivity of some output parameters to these two parameters has been tested with a model of the drum, downcomer and evaporator (shown in figure 5.14) and a transient in which the helium inlet temperature is increased with 50 °C. Whether the transient was simulated with a two-phase friction multiplier which was double or half the value of that calculated with the Friedel-correlation did not matter at all for the important output parameters like steam flow leaving the drum, drumlevel and pressure. The circulation ratio (of total water flow and steam production) is changed, because with a lower friction factor more water is dragged through the evaporator. Since the heat transfer is hardly dependent on conditions on the water-side (the helium side resistance against heat transfer is dominant) this does not influence the amount of water evaporated. A change of slip-velocity however, does affect the output parameters. In figure 5.15 the behaviour of the drumlevel, pressure and steam-production during the transient is shown for homogeneous flow (slip ratio = 1), the slip velocity as calculated with the CISE-correlation, and with a slip-velocity which is ten times as large. This strong overestimation is needed to obtain a visible effect.

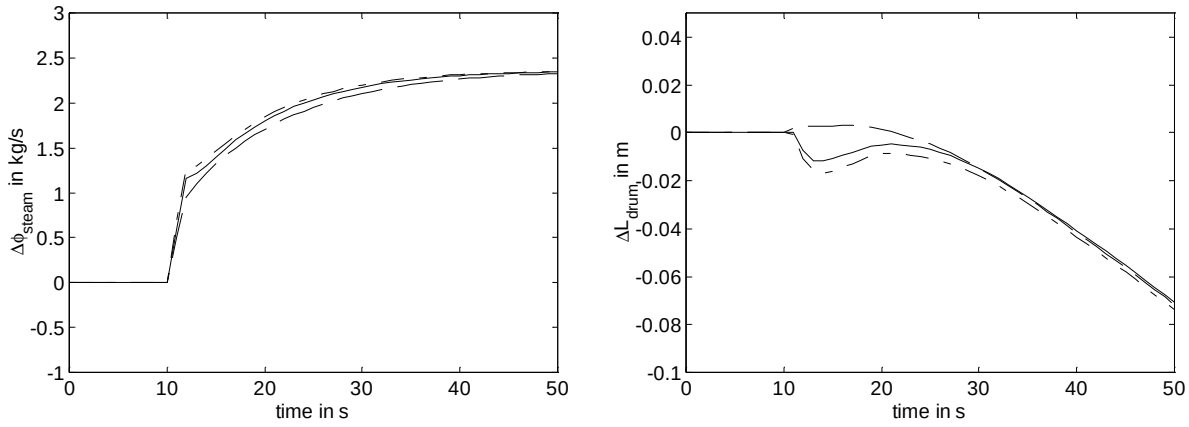

Figure 5.15: Behaviour with different slip velocities, +50 °C step on $T_{He\ in}$, drawn: CISE-correlation for slip-velocity, dotted: homogeneous flow, dashed: over-estimated slip-vel.

When THE helium temperature is increased, more steam is produced. Pressure builds up, until a new balance between inflow and outflow of the drum is reached. The drumlevel is a pure integrator, therefore no new equilibrium will be reached. The mass flows of water and steam are set by the heat-balance. With a larger slip velocity the comparatively higher steam velocity leads to a lower steam fraction in the evaporator. The total mass of the system is higher which gives a more sluggish response. The drumlevel is affected by the pressure dependent inlet flow from economiser and evaporator and outlet flow to downcomer and superheater. With a lower steam-fraction in the evaporator (due to a higher slip velocity) less mass can be accumulated in the evaporator. The reaction of the evaporator outlet flow on a change of the inlet is therefore faster and a balance between the flow to the downcomer and from the evaporator is reached earlier. Therefore, the homogeneous flow model does not exhibit the same fluctuation as the models with higher slip velocities.

The sensitivity to the discretisation is tested as well. For the high efficiency gas-gas heat exchangers, the number of thermal nodes should be fairly high, since otherwise the correction factor a (see paragraph 4.4.4) cannot be determined. The final cooler, economiser and superheater can be discretised with a few or even one node. The sensitivity of the accuracy to the number of nodes has been checked with the economiser model. The economiser was discretised with 1, 2 and 10 nodes and the same step change (+50 °C on the hot inlet) has been applied. The results shown in figure 5.16 are very similar. A small divergence can be seen between the single node and the two-node discretisation, but a finer discretisation makes little difference.

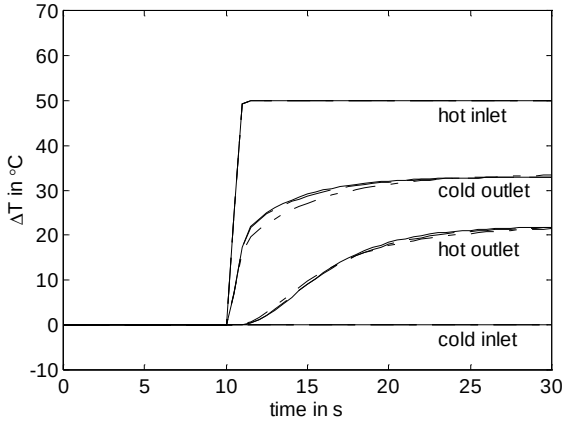

Figure 5.16: Sensitivity to economiser discretisation, drawn: 10 elements, dashed: 2 elements, dash-dotted: 1 element.

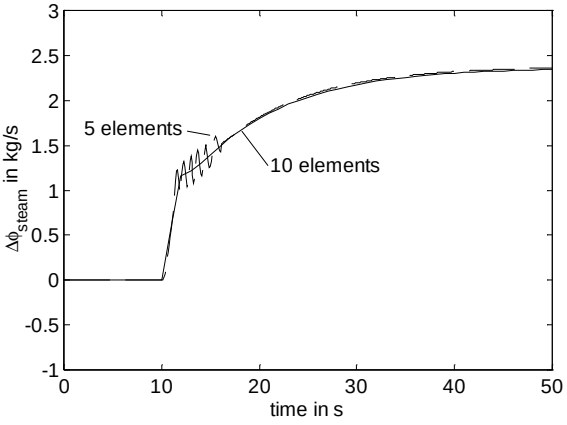

Figure 5.17: Sensitivity to evaporator discretisation.

For the evaporator, the discretisation also influences the stability. This is illustrated with figure 5.17. With a strong transient and too few nodes, the mass flows start to oscillate. This can be overcome by refining the mesh.

5.4 Choked Valve

The valve model with choking effects has been tested in a slow (quasi steady-state) transient. The pressure in plenum 1 of the model of figure 5.18 is kept constant, whereas the pressure in plenum 2 is slowly

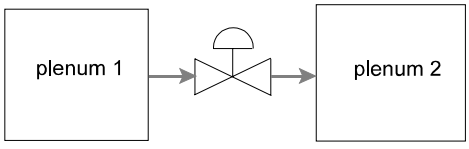

Figure 5.18: Valve test configuration.

raised. The resulting mass flow through the valve as a function of the pressure difference is shown in figure 5.19. A positive and large pressure difference results in a positive choked flow. In the choked regime the decrease of pressure drop does not affect the flow, the flow is only determined by the constant upstream pressure. With a small pressure drop, the choking effects are negligible and the valve friction determines the mass flow. For a large negative pressure difference the flow is choked again, however the increasing pressure in plenum 2 is now the upstream pressure. Therefore the density of the flow through the valve increases and with the constant (acoustic) velocity this results in a linearly increasing backflow. The analytical solutions for a high positive, high negative and small pressure difference have also been plotted and agree with the model.

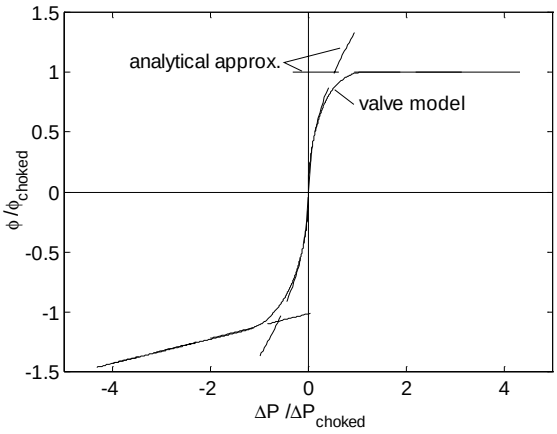

Figure 5.19: Pressure-flow relation for valve.

5.5 Reactor

The reactor-model has been validated with the three dimensional model with coupled neutronics and hydraulics built in Panthermix (PANTHER, 1995, Oppe, 1998). Results of four models will be given for some transients. The model developed here is first compared with the results of the complete Panthermix-model. Subsequently, another model is used, which has the same thermal hydraulics model as Panthermix (modelled with a code called Thermix-Direkt), but a point-kinetic neutronics model. In this manner the effects of different discretisation of flowpaths and heat structure on one hand and the different neutronics-models on the other hand can be separated. The results of a point-kinetic reactor model with yet another nodalisation of the heat-structure, modelled in RELAP are shown as well. The complete primary system response will be compared to those of the RELAP model in the next paragraph, therefore the reactor responses are compared first. In the comparison the models will be named after the code in which they were developed (Panthermix, Thermix-Direkt & RELAP), so the dynamic model developed in this thesis will be called the ACM-model (Aspen Custom Modeler).

In the first two transients the helium inlet temperature changes with -100 °C respectively +100 °C. The normalised reactor power and change in helium outlet temperature are plotted. The initial temperature and reactivity-effects are monitored during 500 seconds (figure 5.20), subsequently the Xe-transient is monitored during 50 hours (figure 5.21). The increase of inlet temperature leads to a negative reactivity, hence the power is reduced. Less heat is transferred to the helium, so its temperature rise is reduced. This effect is larger than 100 °C, so the outlet temperature decreases. This temperature fall at the outlet again leads to a reactivity and power increase, which explains the oscillations. With the lower power the xenon-concentration is too high; it initially even rises due to the decay of iodine. This leads to poisoning of the reactor, indicated by a lower power level. Only after about 40 hours, the Xe-concentration is in balance again.

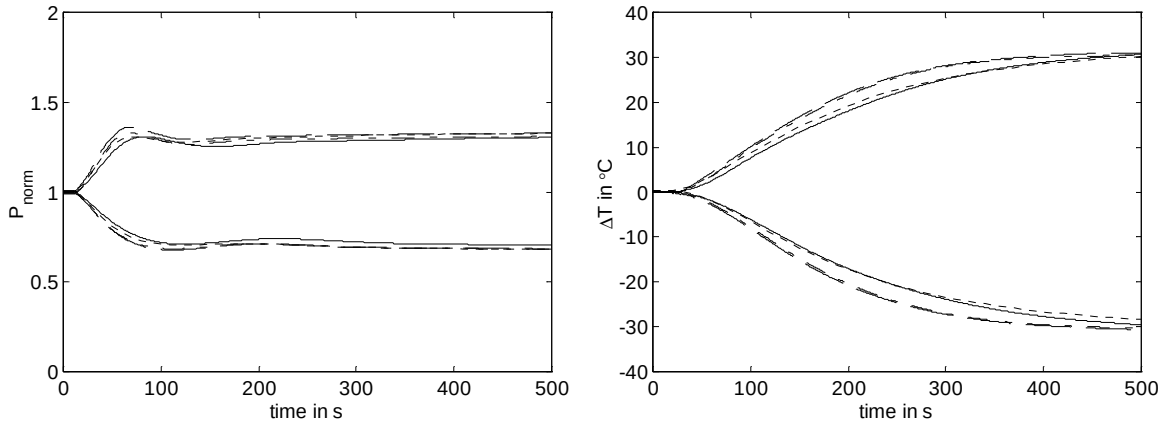

Figure 5.20: Comparison of short term transient after inlet temperature change, drawn: ACM, dashed: Panthermix, dash-dotted: Thermix-Direkt, RELAP: dotted.

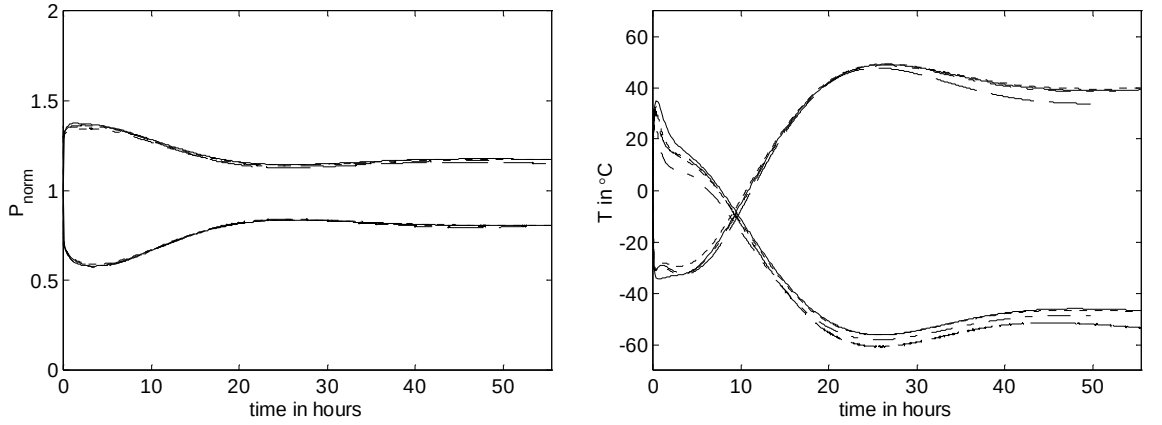

Figure 5.21: Comparison of long term transient after inlet temperature change.

It can be seen that the models are very consistent, with differences of a few percent. The point-kinetic approximation works very well, nearly all the differences are due to the different nodalisation of the heat structure. The speed at which heat is conducted through the structure and resulting temperature profile is slightly different for the models, hence the temperature-induced reactivity effects lead to a minor discrepancy in power production. The Panthermix model calculates a slightly lower power level, since the burnup over two days is taken into account.

A transient in which the coolant mass flow is reduced to 25% is also monitored (figure 5.22). The graphite temperatures rise slightly. This leads to a reduction of the power, again with some oscillatory behaviour. The oscillations are somewhat slower in the ACM model, but the models reach the same steady-state at 25% of the nominal power.

A more thorough discussion of the comparison between the point-kinetic model and the full-scope model can be found in Verkerk (2000).

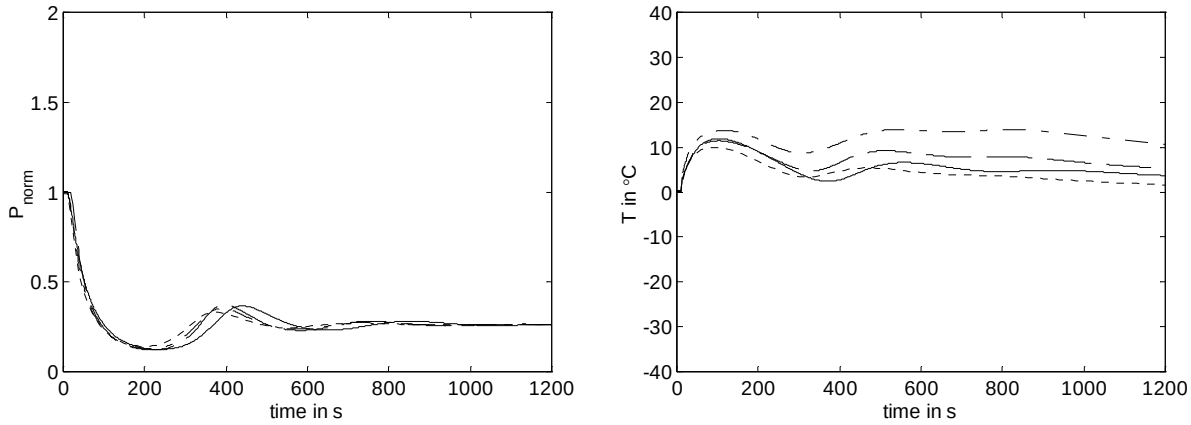

Figure 5.22: Comparison of transient after mass flow reduction.

5.6 Primary Cycle

Now that all the component models have been tested, the results of some transients of the integrated primary circuit are compared with those calculated with a model implemented in RELAP 5 MOD 3.2 (RELAP, 1995). RELAP is a nuclear thermal hydraulics code widely used for simulation of light water reactors. The code has been thoroughly validated and is accepted by licensing authorities. However, hardly any previous modelling and no validation of helium systems has been done with RELAP. Verkerk (2000) built a model of the primary system of the NGT-IS plant using RELAP component models. Since there was no standard RELAP model for a compressor it was modelled with a series-connection of pumps. The head and power curves were based on the φ-λ and φ-ψ curves produced with the ACM model. The curves are similar to those in figure 4.6, with inclusion of the friction losses in the diffuser in the calculation of ψ. THE plate-fin heat exchangers were modelled with flow of both the hot and cold flow through a high number of pipes with its walls joined together. THE number of pipes was chosen such that it yielded the right pressure drop and heat transfer coefficient, while the wall thickness was adjusted to achieve the thermal inertia calculated with the ACM-model. THE turbine was modelled with the RELAP steam-turbine model. THE RELAP model can be connected to the Panthermix reactor core simulation for a best estimate model or a point-kinetic neutronics model can be used for faster performance. The ACM and RELAP-model have been built with the same input-data. No fit-parameters have been tuned to improve the agreement of the two models. Some differences can be expected due to the different models of the reactor heat structure as well as different component models in the energy conversion system. The modelled circuit is shown in figure 5.23. In the RELAP model, the temperature at the compressor inlet is kept constant. In order to obtain the same boundary conditions for the ACM

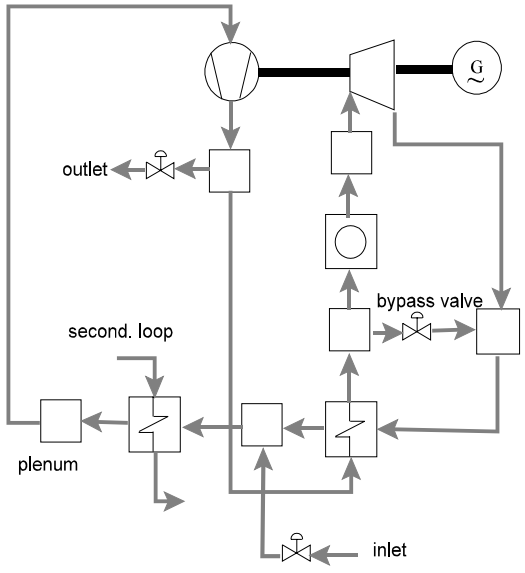

Figure 5.23: Modelled primary system.

model, the secondary flow through the precooler is made very large with a temperature nearly equal to that of the compressor inlet flow at design conditions. The inventory control system is simplified. Instead of the modelling of tanks, the helium flow leaving the system simply expands in an infinitely large volume at 1 bar, whereas the helium inlet is connected to an infinitely large volume at 70 bar and 20 °C.

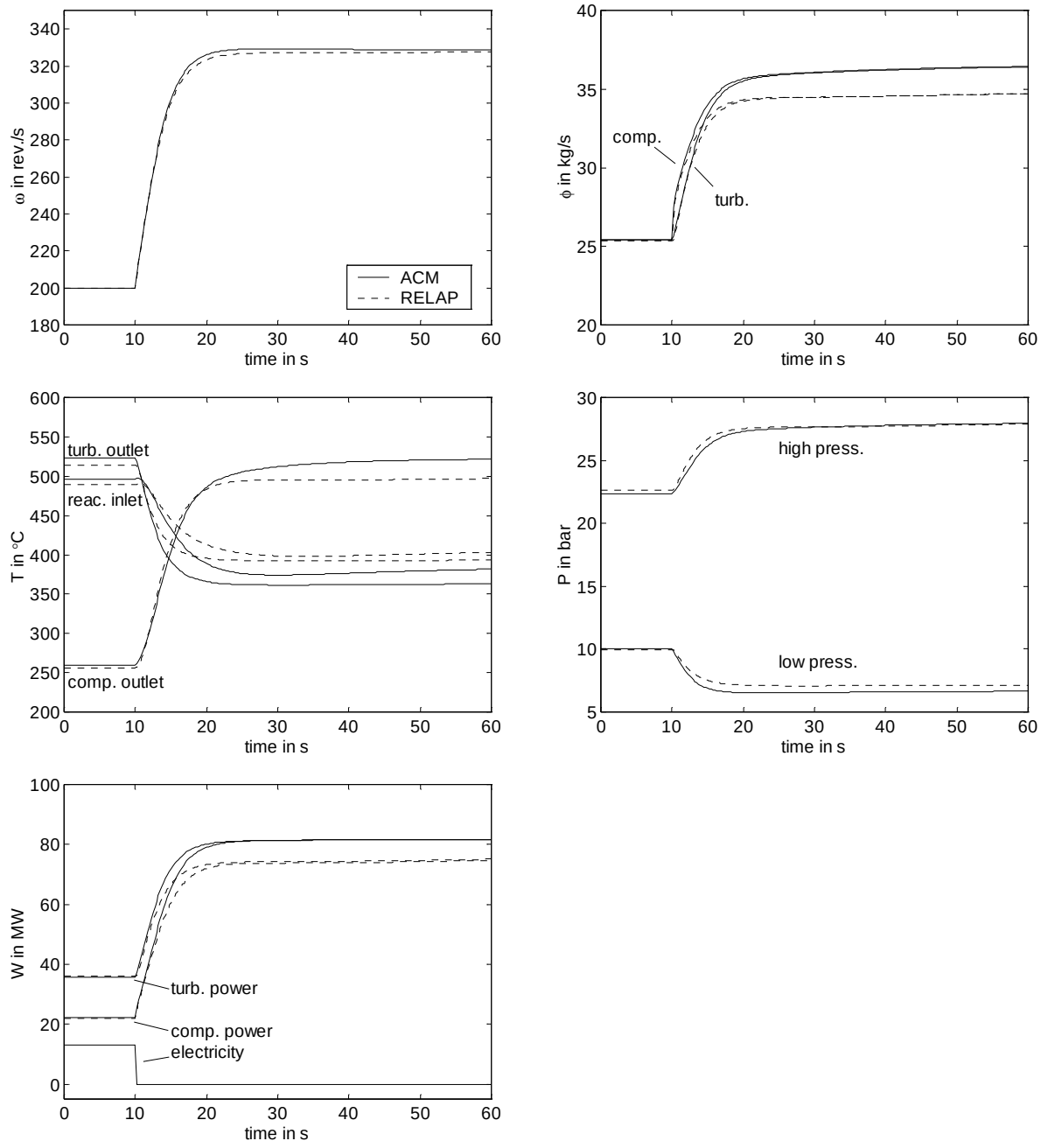

Figure 5.24: Comparison of transient after load rejection.

The models have been compared with three transients. In the first transient a load rejection (a generator trip) is simulated (figure 5.24). The generator-load is step-wise reduced to zero. The

shaft directly goes into overspeed. At a much higher speed and mass flow the compressor power balances the power produced by the turbine. At the higher final speed the pressure ratio is also increased, so the compressor inlet pressure is reduced while the outlet pressure increases. This of course leads to a fast increase of outlet temperature. The turbine outlet temperature is strongly decreased, since more power is produced at lower efficiency. Because of the strong coupling by way of the recuperator the reactor inlet temperature also decreases.

The models agree quite well. Due to the different compressor and turbine characteristics, the mass flow and rotational speeds at which the system is in steady-state again differ. This of course also leads to a different pressure ratio and temperatures. The differences between the two models are mainly due to the different turbine characteristics. One can see that the same compressor outlet temperature is predicted by both models, but the predicted turbine outlet temperatures differ by 40 °C, while both inlet temperatures hardly change. The decrease of turbine efficiency for this far off-design operation is not properly modelled in RELAP, so its efficiency estimation is too high. The RELAP model thus has the highest turbine power which leads to a higher shaft speed and mass flow.

The high rotational velocity of the shaft may lead to unacceptably high stresses due to centrifugal forces and the sudden increase of the recuperator cold inlet temperature leads to thermal stress which can reduce the life-time of the recuperator. Therefore, a valve can be used which bypasses the turbine. In similar systems, a valve between the reactor inlet and the turbine outlet is often proposed (General Atomic, 1995). In the second transient, at the same time the load is rejected and the bypass valve is opened stepwise (figure 5.25). This reduces the mass flow through the turbine and increases the mass flow through the compressor. Now the compressor and turbine power are balanced at the design rotational speed of 200 rev/s. A lower pressure ratio will result. In order to reach the corresponding pressures, the mass has to be redistributed over the high and low pressure plenums. This takes some time which explains why the shaft first goes in overspeed. The mass flows of the new steady-state are remarkably similar. The ACM model reacts somewhat faster, therefore the shaft exhibits a smaller initial overspeed.

With the third transient the long term behaviour is compared. Part-load operation can be achieved with a high efficiency when the helium inventory is reduced. In this transient, the inventory is reduced to 50% and after two days the system is filled again, after which the behaviour is again monitored for two days. For this test not the electricity output but the shaft speed is set. This corresponds to a very fast control loop in the asynchronous generator system. When the plant is grid-coupled (opposed to stand-alone electricity production) the amount of electricity produced can have any value. In this case the value which keeps the shaft speed at 200 rpm is chosen. The transient is started by opening the valve between the compressor outlet plenum and the helium outlet. The valve is kept open for approximately 300 s, until the helium inventory is reduced with 50%. The valve is choked during this time, so the mass flow through the valve reduces linearly with the system pressure. Now the system is monitored for 50 hours, until the xenon-transient is complete. After 50 hours, the helium inlet valve is opened until the system is filled again.

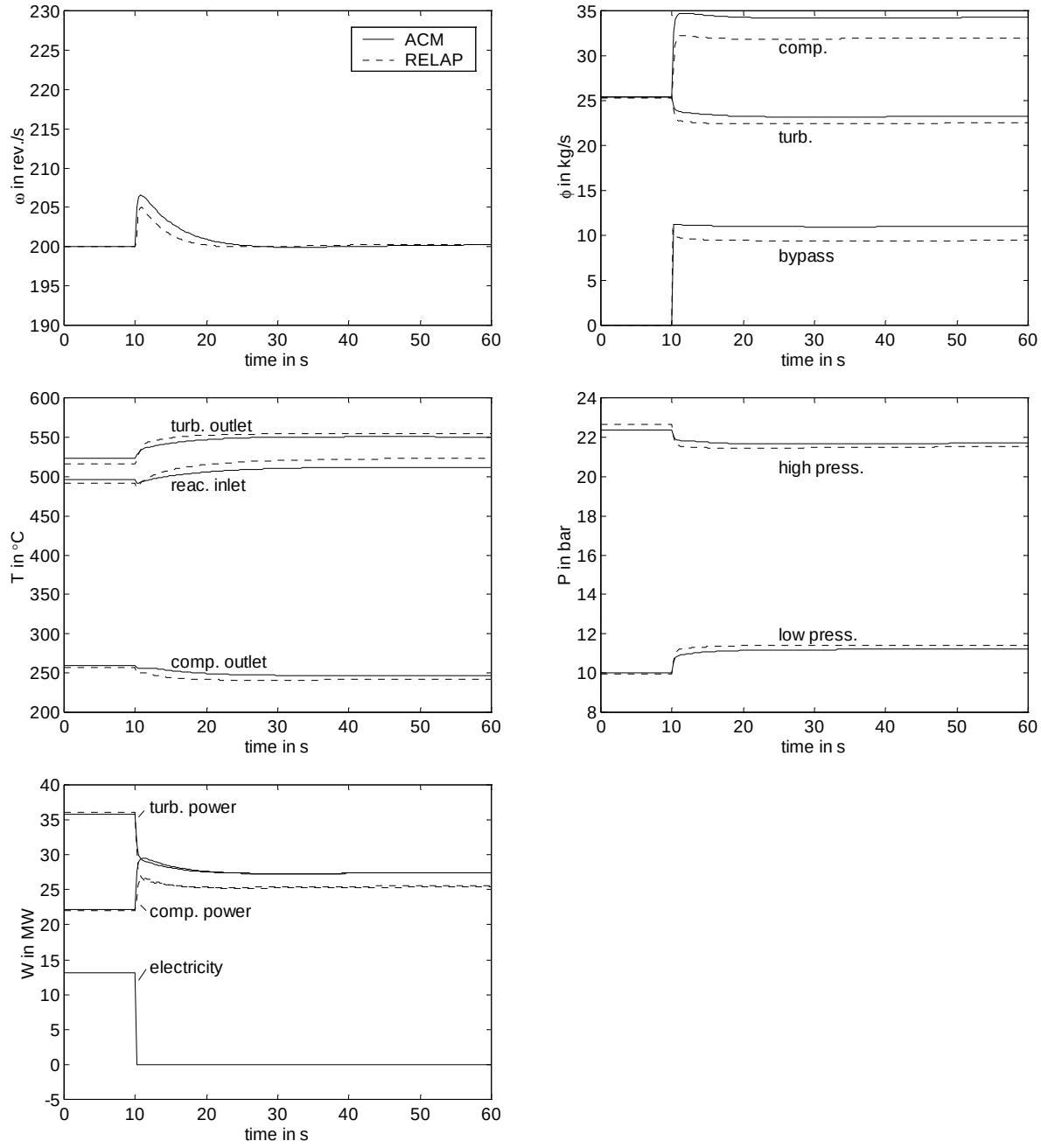

Figure 5.25: Comparison of transient after load rejection with opening of bypass valve.

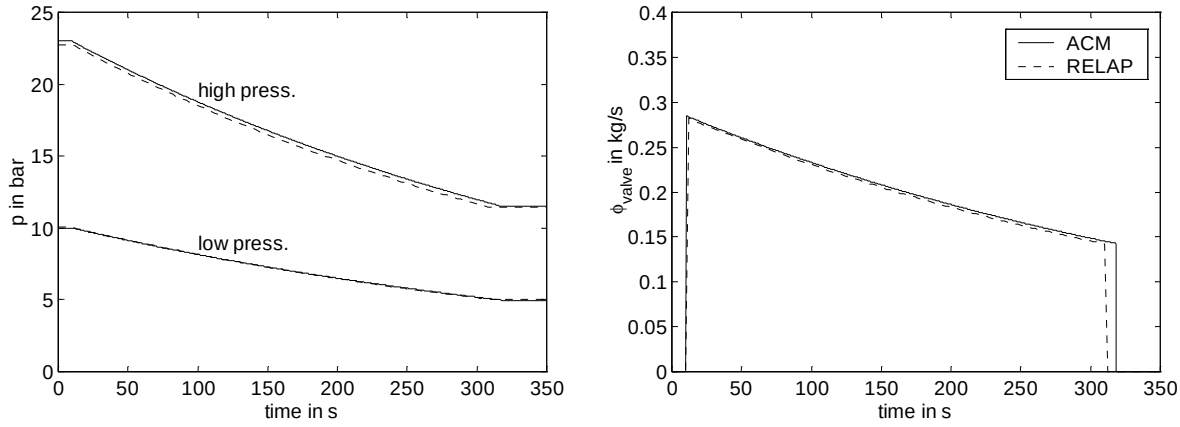

Figure 5.26: Comparison of inventory reduction.

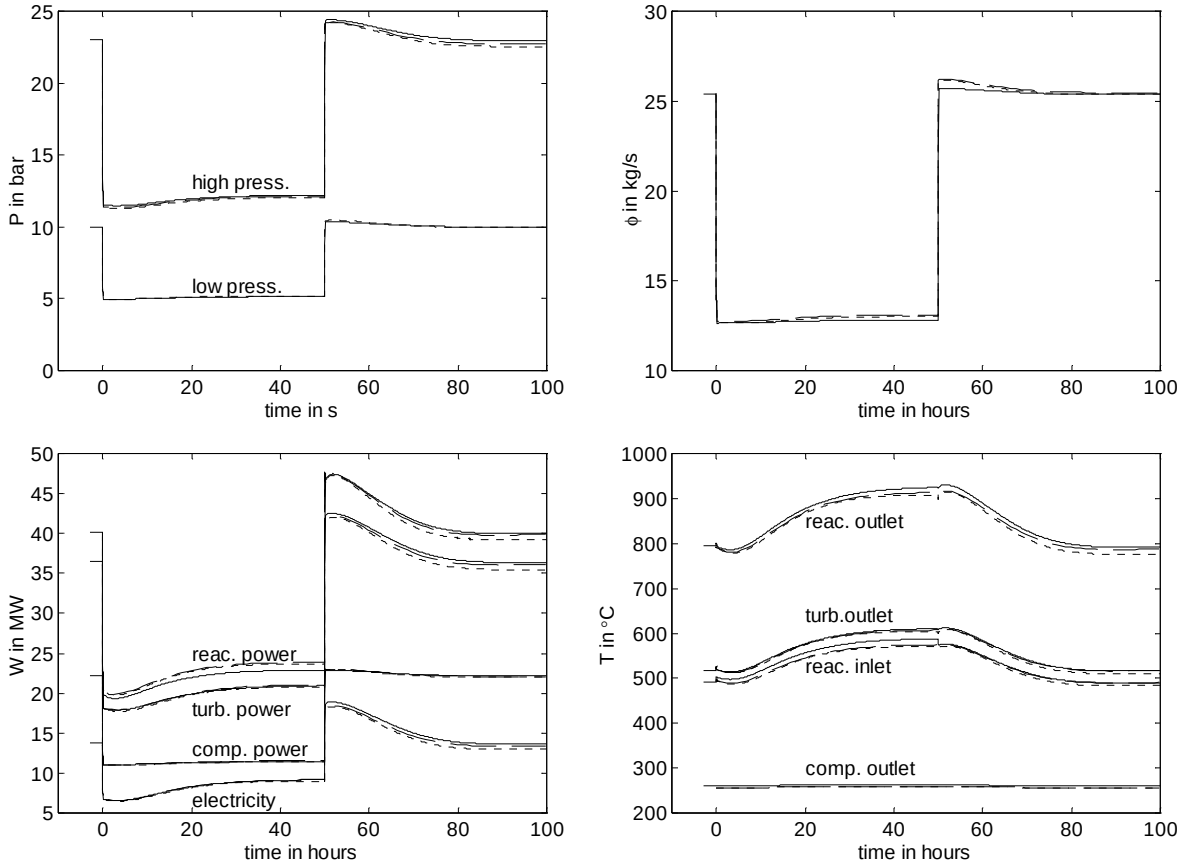

Figure 5.27: Comparison of long term transient with inventory reduction and elevation, drawn: ACM, dashed: RELAP, dotted: Panthermix.

When the inventory is halved, the pressures, mass flows, the reactor power and electricity production are also reduced to 50%. The transient behaviour during the inventory reduction is shown in figure 5.26. The behaviour during the full transient is shown in figure 5.27. At the lower mass flow the recuperator efficiency increases. This explains the sudden increase of reactor inlet and turbine inlet and outlet temperature. Subsequently, the initial increase of xenon is

compensated by a lower reactor temperature. When the xenon decays again (starting after 4 hours), the reactor power and temperatures rise again. With the constant shaft speed, the electricity production follows the reactor power.

The discretisation of the RELAP model of the recuperator is not very fine and the correction factor for the discretisation error (a) is not adjusted for different operating conditions. The efficiency does not increase with the decrease of mass flow, hence the recuperator outlet temperatures of the RELAP model differ from the ACM-prediction. The Panthermix model includes the burnup in its calculation, therefore the deviation in produced power increases during the transient.

5.7 Conclusions

It is impossible to prove that a dynamic model correctly predicts the transient behaviour under all conditions. However, by logical tests and comparison to analytical solutions and other models and codes, it is made plausible that the model developed gives a correct estimation of the system dynamics over a time-scale varying from fractions of a second to several days. The comparison of reactor transients show that the point-kinetic model gives an excellent approximation of the behaviour calculated with the full-scope model.

Chapter 6

Influence of Design on Dynamics

In chapter three a number of design-choices have been made, most of them based on thermodynamic grounds. Some of the design choices have an influence on the dynamic behaviour of the plant. No other configuration of the components in the flowsheet is conceivable, but for components designs, like sizes of heat exchangers, construction of the turbine etc, other choices are possible. In order to assess the influence on the dynamics, these alternative choices have been tested with typical transients. Moreover, several design parameters have been varied to test their significance with respect to the dynamic behaviour.

6.1 Turbo-machinery Design

An alternative for the single shaft system is a two-shaft system with a free-running power turbine (Op het Veld, 1998). When the turbine is split in two sections, each part can run at its optimal speed (with an asynchronous generator), which improves the efficiency. This possibility has been tested by simply splitting up the turbine. The first four stages are used to drive the compressor, whereas the last three drive the generator. Both turbines operate at a shaft speed of 12,000 rpm; to achieve this without redesigning the turbines, correction factors have been introduced for the turbine power and forces. The configuration is shown in figure 6.1.

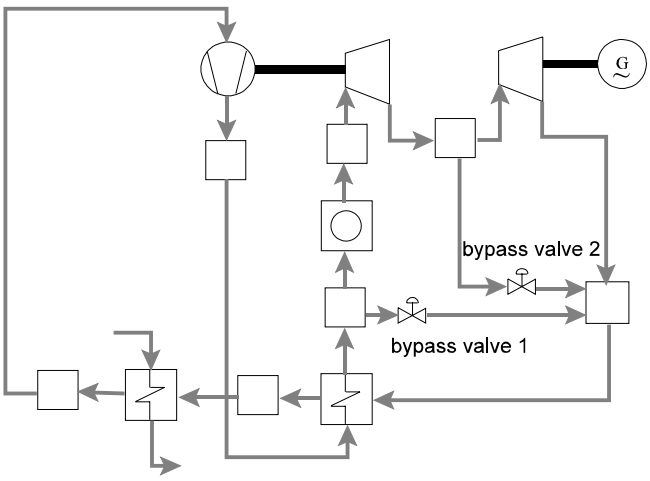

Figure 6.1: Two-shaft configuration.

In figure 6.2 the steady-state relation between generator rotational speed and produced electricity is shown for both the single shaft and the two shaft system. The results are produced with a constant compressor and turbine inlet temperature and constant helium inventory. For the single shaft plant, the electricity-production shows a maximum to the left of its design-point. At this speed the system works less efficient because the turbo-machinery does not operate at the design point and because the recuperator effectiveness decreases with the increased mass flow. However, the electricity production increases since the larger mass flow transports more energy from the

reactor to the energy conversion system. These counterbalancing effects yield a maximum power production at a shaft speed of approx. 230 rev/s. The nuclear gas turbine is in this respect completely different from a conventional gas turbine in which the energy input (by injection of fuel in the combustion chamber) is totally unaffected by the shaft speed.

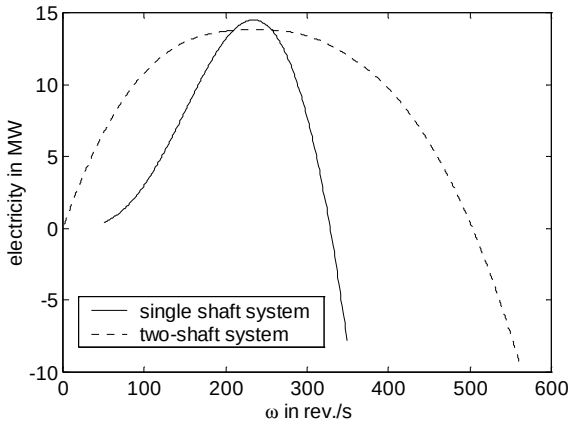

Figure 6.2: Steady-state relation.

At shaft speeds lower than the maximum no stable operation is possible without an active control-system. If the electricity-demand is not met, the shaft decelerates, since kinetic energy is consumed to produce electricity. At the lower shaft speed even less power is produced, so the shaft will decelerate until its speed is zero. If the shaft accelerates from its design speed, more work will be done in the turbine, which will further accelerate the shaft, until the maximum of the curve is reached. With a bypass valve opened or with different temperatures and pressures the position of the top of the curve changes. However, there will always be an unstable left half of the working line. The control system must stabilise the system. This can easily be achieved with a control loop using the electricity as the manipulated variable.

An increase of turbine speed in case of the two-shaft system does not lead to an increase of energy withdrawal from the reactor, because the compressor speed and thus mass flow remain unchanged. Since the two-shaft characteristic is extremely flat around the operating point, a small change of electricity demand has an enormous effect on the shaft speed. This is because there is no change of compressor load associated with the change of generator speed. Moreover, the asynchronous generator precludes the electrical network from limiting the speed. The only effect which reduces the power of the free running turbine, is its decreased efficiency. In figure 6.3 the responses to a load rejection and to a load reduction with 0.1% are shown. The shaft speed increases a lot, as expected.

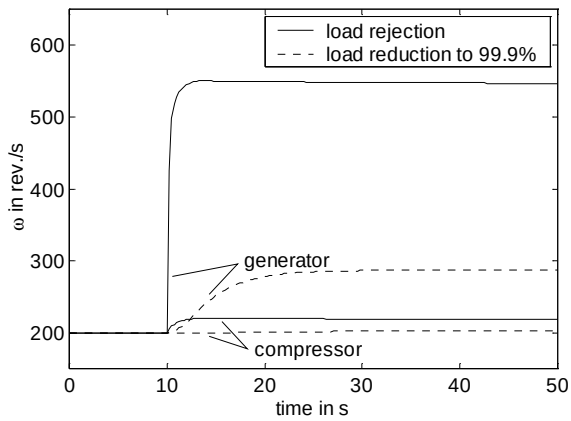

Figure 6.3: Effect on shaft speeds of large and small load reduction.

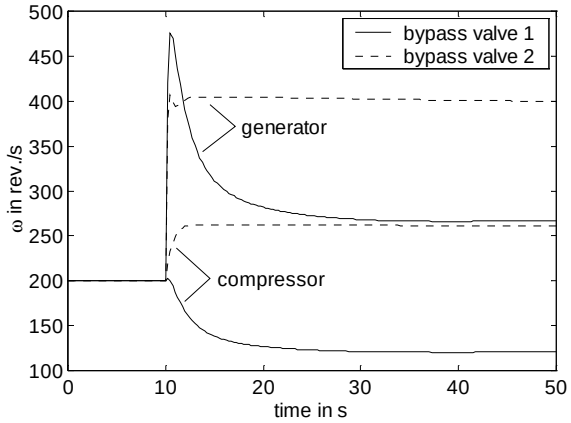

Figure 6.4: Effect of bypasses on shaft speeds.

In figure 6.4 the responses of the load rejection with opening of bypass valves is shown. In the first transient bypass valve 1 (20 cm diameter) is opened 30%, which leads to speed reduction of both shafts. In the second transient, bypass valve 2 (also 20 cm diameter) which bypasses only the power-turbine is fully opened. This leads to an increase of the compressor speed, while the generator speed is reduced. This shows that the combination of both valves can be used to control both shaft speeds. However, due to the strong sensitivity of shaft speed to electricity demand it will be complicated to control the speeds and large speed swings must be expected. Therefore, the possible improvement of efficiency due to more optimal shaft speeds does not outweigh the induced control problems.

A passive 'control-method' which keeps the shaft speed within bounds is choking of the compressor or turbine. In an air-breathing gas turbine, the mass flow cannot rise too much since the normal operating conditions are close to Mach one. The helium turbo-machinery does not have to work at these high Mach-numbers, but the outlet can be made small so that the machine chokes. In that manner, the overspeed can be reduced. With the turbo-machinery operating closer to choking, the helium has to be accelerated and decelerated further. This will increase the losses in the diffuser.

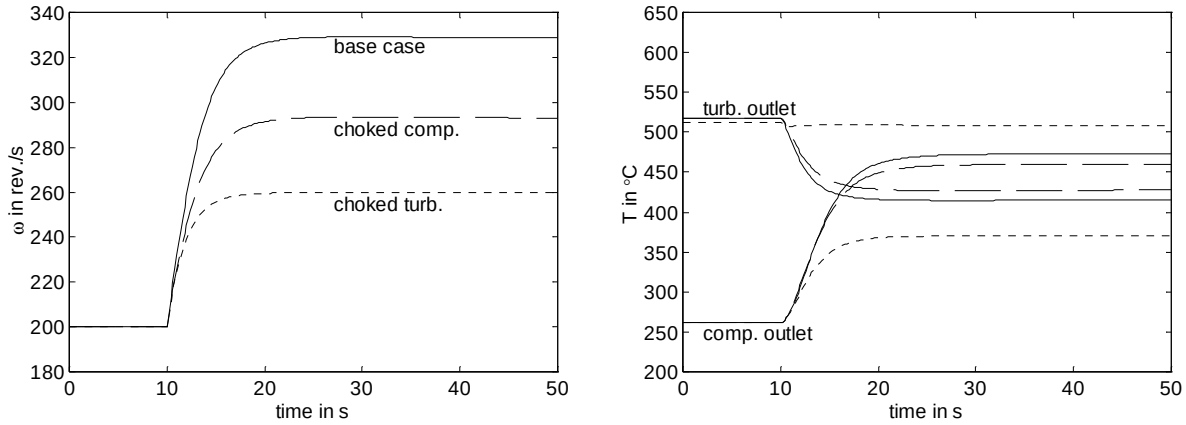

Figure 6.5: Influence of choking on load rejection transient.

In figure 6.5 the uncontrolled response of the load rejection is shown, together with those in which the turbine or compressor outlet is choked. This is accomplished with a nearly frictionless nozzle directly after the compressor or turbine which operates at Mach 0.9 during normal operation. The combination with both compressor and turbine choked has also been tested, but offers hardly any improvement over the transient with only the turbine choked. It can be seen that the shaft overspeed can be greatly reduced. With the turbine outlet choked, its outlet temperature (the hot recuperator inlet temperature) hardly changes, since the pressure ratio over the turbine stays the same. The additional pressure drop takes place in the choked section, which does not affect temperature. Unfortunately, it does not help to choke the turbo-machinery when bypass valves are used. The bypass valves reduce the primary mass flow, which prevents choking.

The shaft inertia is one of the most influential dynamic parameters of the system. Its influence is shown in figure 6.6, in which the response on a load rejection of shafts with 0.01, 0.5 and 2 times the normal inertia is shown. The time-constant (at which 63.2% of the new steady-state value is reached) as a function of the inertia is also shown. When the shaft inertia is negligible,

the shaft speed exhibits an overshoot. A new helium distribution over high and low pressure plenums is achieved almost immediately. However, the temperatures are slowly changing due to the recuperator. With the new temperatures a lower pressure ratio at a slightly lower shaft speed is reached. This effect is damped out by the shaft inertia.

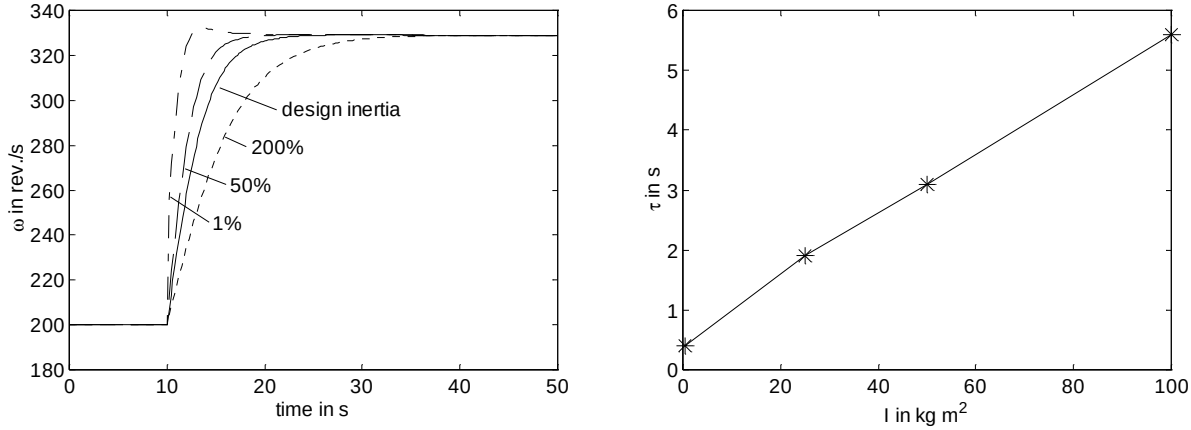

Figure 6.6: Influence of shaft inertia on load rejection transient.

With a larger inertia, the overshoot in case of speed control with a bypass valve is reduced. In figure 6.7 the load rejection with simultaneous opening of the bypass (time-constant of the valve: 0.5 s) is shown for different inertias. The slower response facilitates the control system design. The shaft inertia can be augmented quite simply, but this enlarges the forces on the bearings.

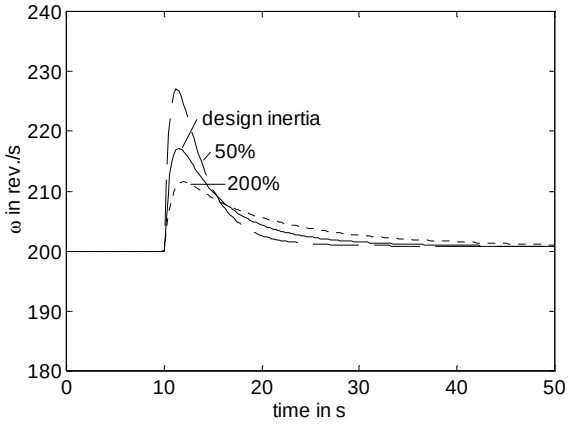

Figure 6.7: Load rejection with bypass opening for different inertias.

The effects of changed compressor characteristics are tested by assuming curves which are 1.5 times and half as steep as the normal curve, as shown in figure 6.8. The compressor design has not been changed, instead the compressor model has been replaced by a model based on characteristic curves. The responses on a load rejection are shown in figure 6.9. The responses with different compressor curves are hardly different. The steady-state shaft speed in case of the flat compressor curve is only 3 rev./s higher than that with the steep characteristic. This gives a slightly higher pressure ratio and a higher temperature change over the compressor and the turbine. The changes are small because the ratio of gas and rotor velocity φ changes with only 10% in the transient. One can conclude that the compressor

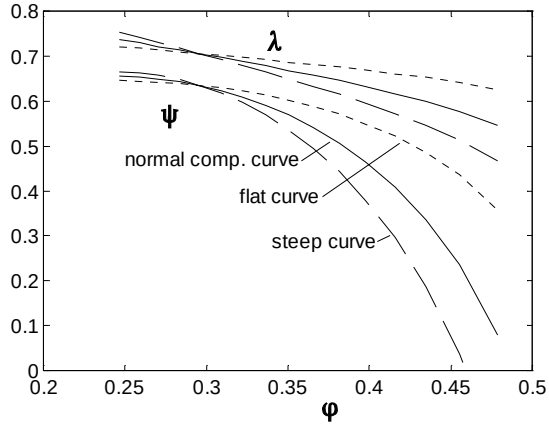

Figure 6.8: Diff. compressor characteristics.

characteristic does not have a pronounced influence on the dynamics of a load change.

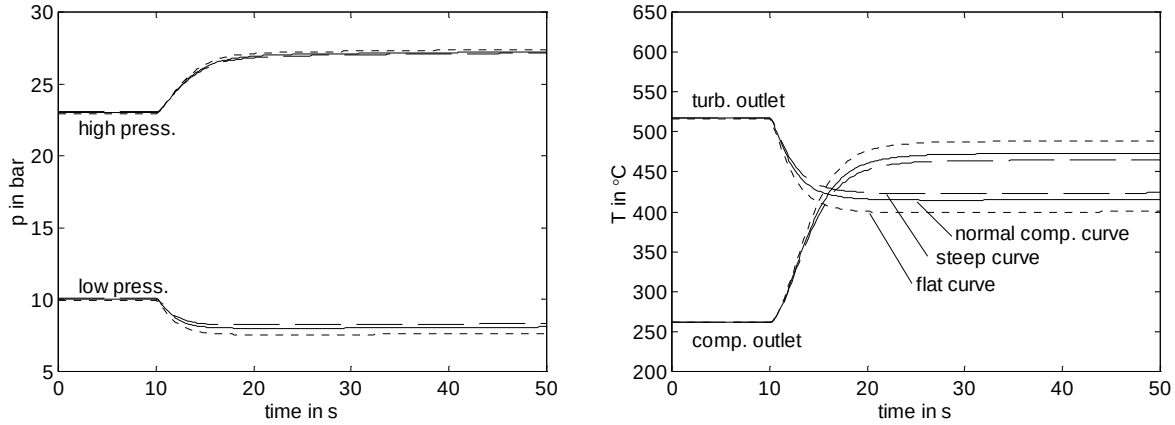

Figure 6.9: Influence of compressor characteristics on load rejection transient.

6.2 Reactor Design

The 100 hour transient in which the helium inventory is reduced to 50% and after 50 hours increased to its original value at constant shaft speed (described in paragraph 5.5) is used to investigate the influence of the reactor design. The run has been repeated with temperature-reactivity curves (as in figure 4.19) which are twice or half as steep. Results are shown in figure 6.10. With a stronger temperature dependancy of the reactivity, the temperature rise which compensates the xenon reactivity effect is smaller. The reactor outlet temperature therefore stays closer to its design value. The non-minimum phase response due to the Xe-concentration is hardly visible with the doubled steepness of the curves.

b

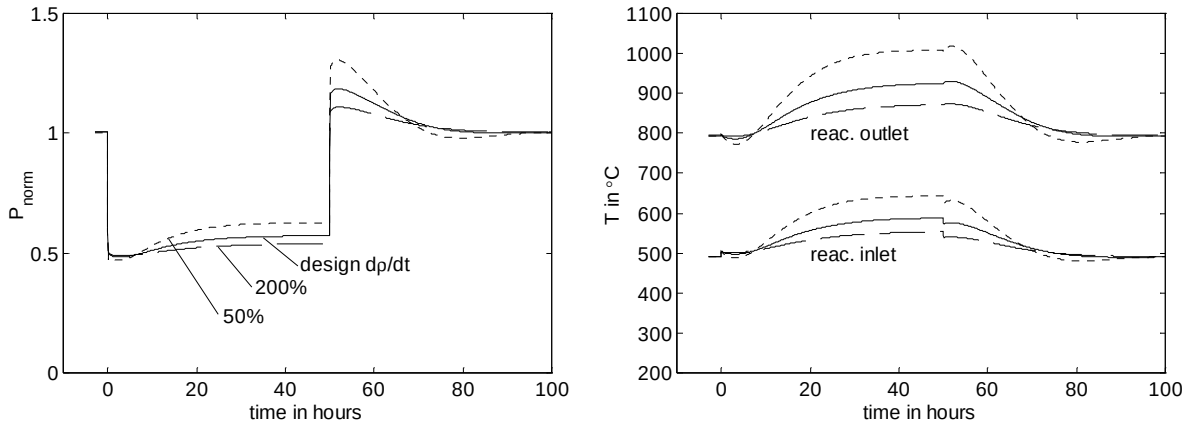

Figure 6.10: Influence of temperature-reactivity curves.

The influence of the thermal inertia of the reactor has also been assessed. With a doubled or halved reactor mass, the temperature and power curves of the 100 hours transients hardly change. On this time scale, the xenon effect dominates the dynamics, the thermal inertia effect is too fast to be noticed. The energy conversion system reacts much faster than the reactor temperature can change, so in the fast transients one can just as well assume a constant reactor temperature, instead of calculating it from the thermal inertia and energy balance.

It can be concluded that a strong negative temperature coefficient is not only favourable from the safety point of view, it also facilitates the temperature and power control. The reactor mass has no measurable influence on the dynamic behaviour for the operational transients.

6.3 Primary System Layout

Based on the layout (paragraph 3.2.4) the helium mass in low and high pressure plenums has been estimated at 24 and 103.5 kg respectively. The response of the shaft speed in case of a load rejection is shown in figure 6.11. The normal situation is called distribution A. With this unequal distribution, only a small amount of helium has to be transferred from the high pressure volume to the low pressure volume and vice versa to achieve a new pressure ratio. This makes the response in which the pressure ratio changes fast. The total helium mass and mass distribution obviously does not influence the steady-state results. In order to determine the influence of the helium distribution over the plenums, the load rejection transient has been calculated with different plenum sizes. First all plenums except the turbine inlet plenum are made very small, the turbine inlet plenum is sized at 69.7 m^3 to keep the total mass at 127.5 kg. In this way the mass on the low pressure side is minimised at 10.2 kg, which is situated in the recuperator and precooler. The mass on the high pressure side is concentrated in a plenum which has a constant temperature during the load rejection transient. In this manner the transient following a load rejection is made as fast as possible, as shown in figure 6.11, distribution B. There is hardly a noticeable difference with distribution A. An equal distribution over the high and low pressure side (distribution C: 62.75 kg on each side) is reached by setting the volume of the compressor and turbine inlet plenums at 40.6 m^3 and 16 m^3 respectively. This leads to a somewhat slower response. The response can be slowed down even further by concentrating the mass in the recuperator outlet plenums which are not constant in temperature, contrary to the compressor and turbine inlet plenums. This is shown with distribution D, which has plenum volumes of 12.8 m^3 and 62.3 m^3 for the reactor and precooler inlet plenums respectively, again leading to an equal distribution over the HP and LP side. The slow temperature change of these plenums leads to a change of density and therefore mass content, which slows down the transient. The last transient shown is with a 50% larger helium mass, again equally distributed over the recuperator outlet plenums (distribution E), which of course gives an even slower response.

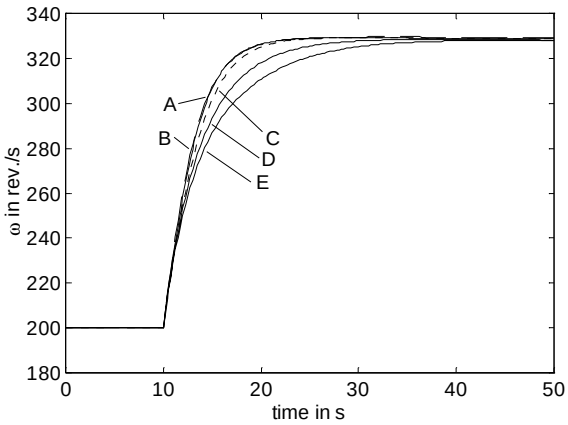

Figure 6.11: Influence of He mass distribution on load rejection transient.

Since a slower response is favourable, one would favour a larger inventory. However, this calls for larger inventory vessels and makes the inventory adjustment unnecessarily slow. The effect of the total helium mass of the plant on the transients in which the system is emptied or filled is tested with the system as shown in figure 6.12. The load reduction to 70% with inventory reduction by filling the first inventory vessel has been tested with a helium inventory which is 125% respectively 150% of the initial estimation. The inventory has been increased by enlarging

the compressor and turbine inlet plenums, thus keeping the ratio of HP and LP mass at one. The size of the inventory vessel is adjusted proportionally to the primary system inventory. The transient shown in figure 6.13 is produced by 10% opening of the 20 cm diameter inventory reduction valve at t = 10 s and closing it again when the pressure difference is equalised. In this way the inventory is reduced to 70%. The electricity load is reduced to 70% at t = 10s.

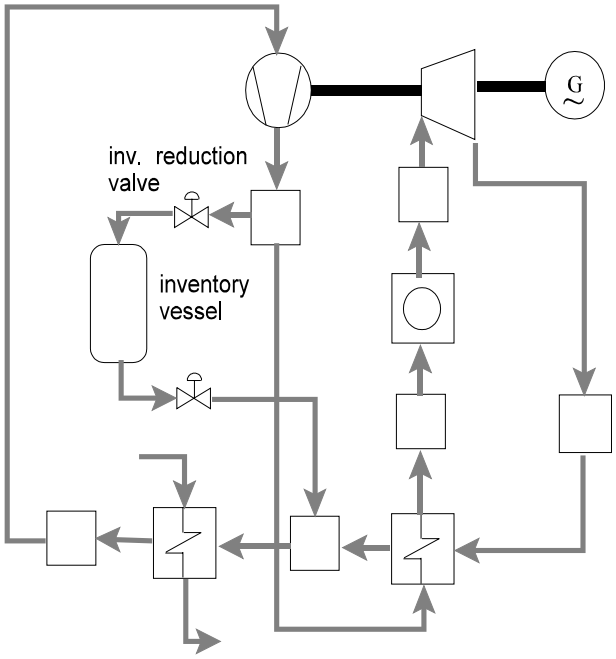

Figure 6.12: System with inventory vessel.

The flow through the inventory reduction valve and the shaft speed have been plotted. The shaft initially goes in overspeed because of the load reduction. With the reduced inventory less power is produced and the shaft speed is reduced. No new stable operating point at a shaft speed of 12000 rpm can be found, since this point is situated to the left of the top of the working line (as shown in figure 6.2). During the filling of the vessel the electricity production is reduced even further since helium is compressed which does not expand in the turbine. Therefore the shaft speed rises again after the vessel is filled for the largest inventory. With a larger inventory the valve has to be open for a longer time before the inventory is decreased to 70%. This leads to a somewhat larger overshoot of the shaft speed. The larger volumes of the primary system amplify the oscillatory behaviour of the pressures and shaft speed.

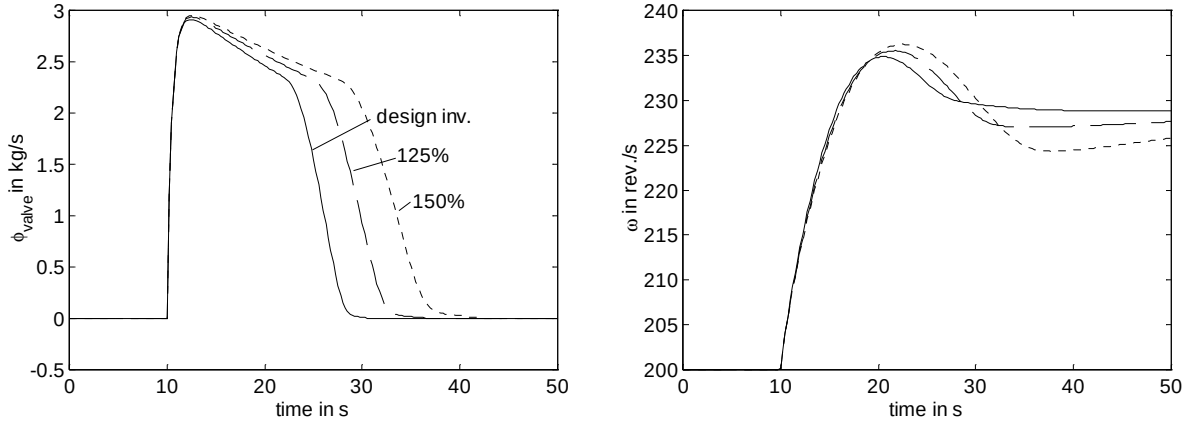

Figure 6.13: Influence of inventory size on inventory reduction transient.

6.4 Heat Exchanger Design

The major feature of the heat exchanger design which influences the dynamic behaviour is its mass. A higher mass gives an increased thermal inertia. The importance of this effect is tested with a complete model of primary and secondary cycle of the NGT-DH plant, shown in figure 6.14. The primary system conditions are kept at the same value as the NGT-IS plant in its design

point. The cooling water flow is controlled with a valve. In the test transient this valve is opened from 20% to 100%. This leads to an increase of cooling water flow from 73 kg/s to 324 kg/s. The transient behaviour of the final cooler hot outlet temperature, compressor inlet temperature and shaft speed are shown in figure 6.15.

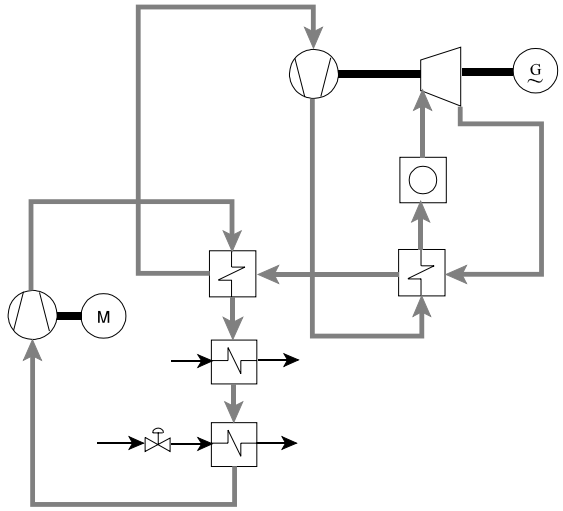

Figure 6.14: NGT-DH plant.

The increase of cooling water leads to a direct temperature drop of the final cooler helium outlet temperature and thus of the precooler hot outlet temperature. This reduces the compressor volume flow and therefore the needed compressor power which results in a higher shaft speed. With the changed pressure ratio, the recuperator slowly warms up. The consequence is a rise of precooler outlet temperature. The effect of the thermal inertia of the final cooler is assessed with a doubled and halved heat exchanger core mass. With an increased inertia the response is more damped. The influence of the thermal inertia of the DH heat exchanger is completely similar to that of the final cooler.

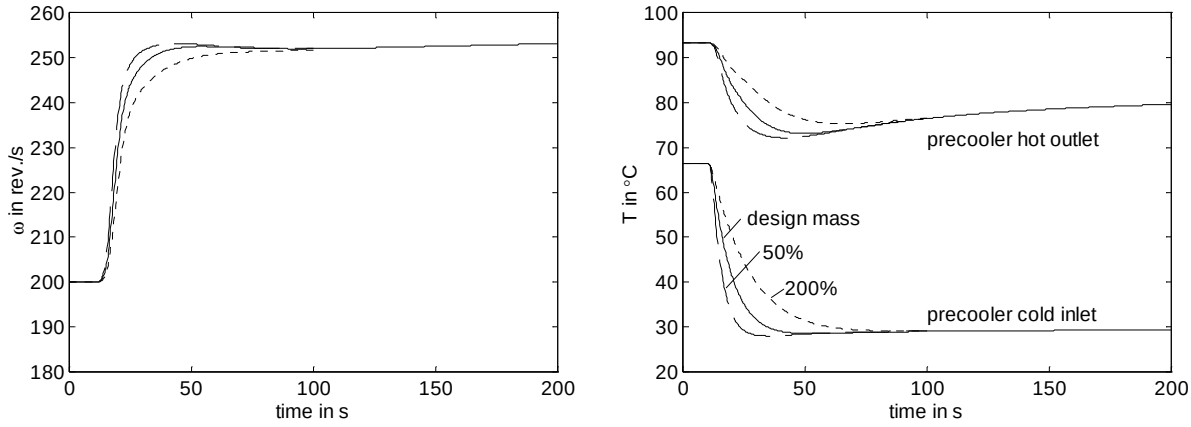

Figure 6.15: Influence of final cooler mass on transient with step change of cooling water flow.

The same test has also been performed with different precooler weights, results are shown in figure 6.16. It can be seen that the slight oscillation of the shaft speed is damped out with an increase of precooler mass.

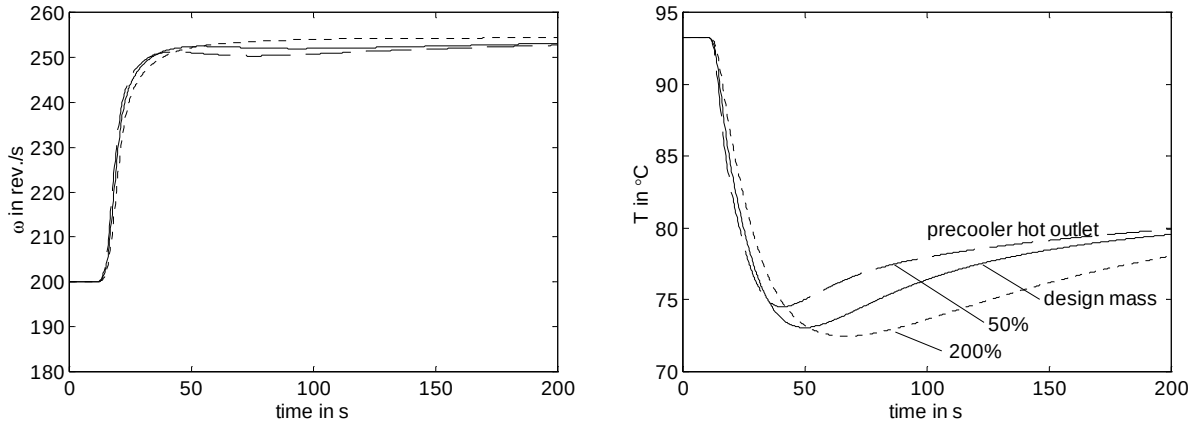

Figure 6.16: Influence of precooler mass on transient with step change of cooling water flow.

6.5 Steam Generator Design

The influence of the steam generator design on the dynamics has been tested with a model of the secondary loop of the NGT-IS plant as shown in figure 6.17. The results of a 50 °C increase of the primary inlet temperature of the precooler on the steam conditions have been monitored. The additional heat input leads to an increase of the steam temperature and extra steam production. In the actual plant the steam flow would be controlled by the customer, so the extra steam production will only lead to an increased pressure and not to an increased steam flow. In this test a valve with a high pressure drop has been situated in the steam line, so the temperature increase leads to both an increase of flow and pressure. The valve could be adjusted to yield the original steam flow, however the controller would only complicate the test and the behaviour would be very similar. The drum level is not controlled in this test which means that the drum is full or falls dry after a certain time. Then the test has to be stopped.

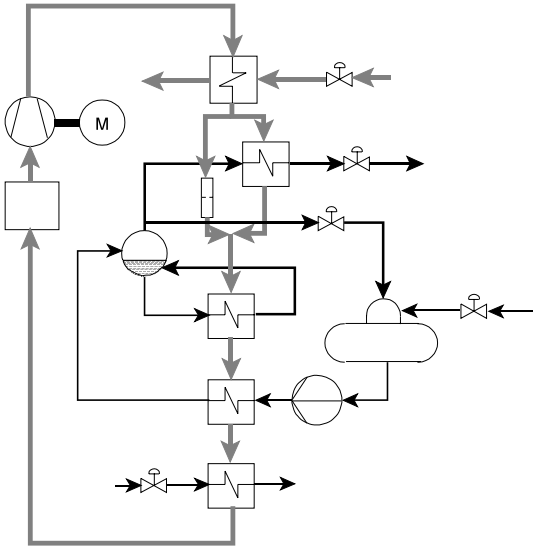

Figure 6.17: Secondary loop.

First the influence of the superheater thermal inertia has been tested by increasing and decreasing the core mass with 50%. The dynamics of the pressure and consequently the steam flow are hardly affected. The steam temperature dynamic behaviour is (in this test) almost completely determined by the superheater mass. One can see in figure 6.18 that the time-constant of the process would reduce greatly when the steel mass is negligible. This is because the steam and helium mass in the superheater are very small and the effect of the rest of the system (by means of the helium loop) is secondary.

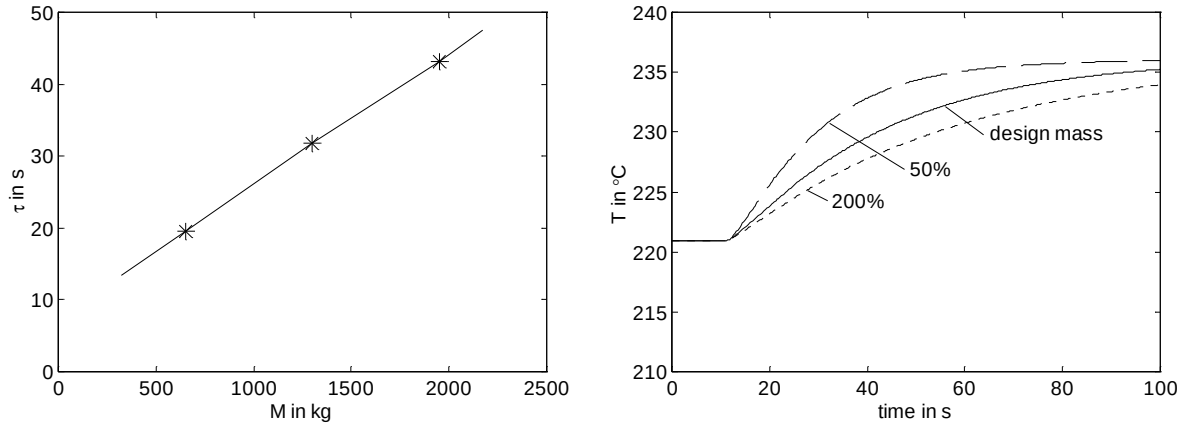

Figure 6.18: Influence of superheater mass on steam temperature transient.

The same test has been performed with an altered evaporator steel mass (50% and 150% of the normal value). The influence on the steam temperature dynamics is hardly visible, but the behaviour of the steam pressure changes slightly (fig. 6.19, A: normal steel mass, B: 50%, C:150%). With the changed pressure the evaporator, downcomer and drum temperature change, since the complete system is at the saturation temperature. The water mass in the system is approximately equal to the steel mass, but due to the much higher specific heat, its influence on the time-constant influence of the water mass is more pronounced. This is demonstrated by increasing the drum size leading to a total water mass which is 1.5 and 2 times the design value (D and E in figure 6.19 respectively). Decreasing was impossible, because with a smaller size the drum would be completely filled half way the transient.

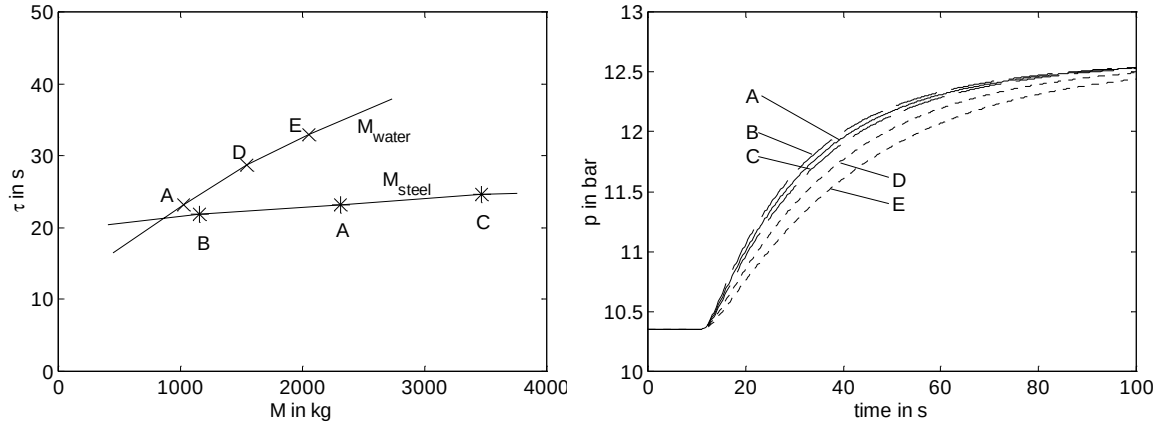

Figure 6.19: Influence of evaporator design on steam pressure transient.

Changes in the evaporator design quickly lead to a different circulation ratio. In a test transient, the circulation ratio of the evaporator has been lowered by adding a flow restriction in the downcomer. A decreased circulation ratio leads to a lower water mass in the evaporator. The influence on the time-constant is the same as with the increased drum-size and can therefore be read from figure 6.19. The helium outlet temperature of the final cooler rises with only 5 °C, therefore the influence of the design of the economiser and final cooler on the dynamics of the steam production is very small.

6.6 Conclusions

With regard to the turbo-machinery design one can conclude that:

1. The investigation of the dynamic behaviour shows that a free-running power turbine with an asynchronous generator is virtually impossible to control. This is due to the extremely small influence of the shaft speed on the power production near the operating point.
2. Choking of the turbine is very favourable in the uncontrolled situation, since it keeps both the shaft speed in the recuperator hot inlet temperature near its design value. Unfortunately one cannot make use of this effect when the shaft speed is controlled with a bypass, because with the decreased mass flow the turbine does not choke.
3. The shaft inertia is one of the most influential parameters for the dynamic behaviour. With a large inertia the overshoot in case of bypass control is reduced.
4. The compressor characteristics do not have a significant influence on the dynamic behaviour.

The reactor dimensions are hardly relevant for the dynamic behaviour during normal operation. The thermal inertia is so large that the outlet temperature is essentially constant during transients shorter than a couple of minutes, whereas during the long term transients the xenon effects are dominant.

Because of the small and unequally distributed helium inventory, the redistribution over high and low pressure plenums is very fast. Its dynamics are negligible compared to that of the shaft inertia. A smaller helium mass of course facilitates the inventory adjustment, since less helium has to be removed to achieve a pressure reduction. Moreover, with an increased inventory an oscillation in the shaft speed appears.

The steam generator and heat exchanger design influence the dynamics mainly through its thermal inertia. The thermal inertia of the steam generator is mainly determined by the water mass, while for all gas-gas heat exchangers the steel mass is dominant.

Chapter 7

Decentralised Feedback Control System Design

In this chapter first the possible operating strategies and the demands for the control system of the cogenerating NGT plant are examined. A typical control system proposed in literature will be discussed. Some possible valves for shaft-speed control will be identified and tested, after which a choice will be made. Then the position of the inventory valves is considered and two options for steam temperature control will be assessed. A set of control valves is chosen, after which the optimal steady-state operating conditions over the complete operating region are determined. The interaction between the inputs and outputs is then analysed and with this information a choice for pairing inputs and outputs with control-loops is made. Then single-loop feedback PI controllers have been tuned and tested.

7.1 Operation Strategies & Control Goals

For a cogeneration plant several operating strategies can be followed. If the plant supplies power and heat to a customer it simply has to meet both heat and power demand. If the plant operates grid-coupled, one could meet the heat demand and produce a suitable quantity of electricity. A possibility would be to operate at part-load at the HPR which yields the highest efficiency and thus to minimise operating costs. Another strategy could be to maximise the electricity-production. This would generate the highest revenues and thus lead to a shorter pay-back time. Given the comparatively high investment costs of nuclear power plants the second choice would probably be the most economical.

The strategy in which both heat and power demand are met obviously is the most difficult one. A much wider two-dimensional operation region exists. When only the heat demand is externally determined, one can produce a fixed amount of electricity. Alternatively, the electric load can be manipulated to control the shaft speed. In this manner the electric efficiency can be optimised. Moreover, the control system will be comparatively simple, since bypass valves can be omitted. In order to investigate both strategies, the NGT-DH will be operated heat-load following at constant reactor power, while the control system for the NGT-IS plant follows both the heat and electricity demand.

The demands on the control system (leading to the desired dynamic behaviour) are:

1. Conditions of heat produced near design values
   The temperature of district heating water or temperature and pressure of industrial steam must be close to their set-point. For industrial steam a correct saturation temperature and thus pressure is more important than the temperature. Unfortunately, no hard constraints can be given.
2. Stable compressor operation
   The compressor must not fall in surge or stall. Rapid flow and temperature fluctuations lead to too high blade stresses which may lead to failure. The problem is not as pronounced as with an axial compressor since the blade stresses are lower. When the asynchronous single shaft system is controlled with a bypass valve (and not with a throttle valve) it is virtually impossible to get the compressor in surge. This is because a reduction of the compressor mass flow (which brings the compressor closer to the surge limit) directly leads to a reduced turbine flow. The reduced turbine power leads to a reduction of the shaft speed which again moves the operating point in the compressor map away from the surge line. In a conventional gas turbine the compressor can go in surge when the turbine is speeded up through injection of additional fuel. This gives a fast rise of turbine inlet temperature, which causes the imbalance of power and thus the compressor surge. In the nuclear gas turbine plant such a fast temperature rise is impossible due to the reactor thermal inertia.
3. Constrained shaft speed
   The centrifugal forces in turbine, compressor and generator increase quadratically with the rotational speed of the shaft. In order to avoid over-dimensioning of the rotating equipment the shaft speed must be constrained.
4. Constrained thermal stress in heat exchangers
   Fast temperature gradients in heat exchangers can lead to fatigue or direct failure (Lu, 1998). The thin-walled gas-gas heat-exchanger might be vulnerable. It would be convenient if the dynamic model could predict the thermal stresses, but in order to calculate the thermal stresses the complete geometry must be known and a three-dimensional finite element model is necessary (Nakaoka, 1996, Carter, 1996). However, in order to minimise thermal stresses the speed and magnitude of temperature changes can be limited.
5. Constrained temperatures
   The reactor and turbine inlet temperatures have been chosen in view of material limitations. At elevated temperatures creep accelerates. It is desirable to keep the temperature at or under its set-point, but for shorter periods of time it is acceptable to operate at higher temperatures. The main problem for temperature control is the xenon effect. In figure 5.22 it can be seen that during part-load operation the reactivity deficiency due to lower xenon levels are compensated by higher temperatures. With a constant compressor inlet temperature the steady-state reactor inlet and outlet temperature at 50% load are approximately 50 °C and 100 °C higher respectively. The reactor inlet temperature can be reduced with a reduction of the compressor inlet temperature, however at the cost of an increase of the outlet temperature due to the compensation of reactivity. Figure 5.16 showed a change of +50 °C of the outlet for a -100 °C change of the inlet temperature. The turbine inlet temperature could be decreased using a bleed flow from the

compressor. Note that in order to effectively lower the temperature of the turbine blades good mixing between the small bleed flow and the reactor outlet flow must be achieved.

6. High efficiency
   Especially for prolonged operation at a certain power-level and heat-to-power ratio the installation must operate at high efficiency. The optimal values for some parameters which can be used as set-points for the control system can be calculated with the steady-state model (paragraph 3.3) or with the dynamic model (paragraph 7.3.2).
7. Drum level within boundaries
   The steam drum must not flood or dry out. In order to have a good separation of water and steam the level must be somewhere in the middle of the drum.
8. Deaerator near saturation temperature
   In order to deaerate the feedwater, the temperature in the deaerator must be just below the saturation temperature. The easiest way to achieve this is with both pressure and temperature control.
9. Economiser outlet temperature below saturation temperature
   No boiling should occur inside the economiser.

The demand of nuclear safety has deliberately been omitted in this list. This is because there are no incidents conceivable which bring the reactor in an unsafe condition. Therefore the control system has no task in the safety plan.

7.2 Control System Strategy

7.2.1 Literature

In literature, some different control system designs for nuclear gas turbine plants can be found; Yan (1990) gives an overview of these methods. However, all those designs are for electricity production only. A typical control system is that of the MGR-GT (Yan, 1990), shown in figure 7.1. For prolonged part-load operation the helium inventory is reduced. The inventory of the vessels is calculated from temperature and pressure measurement. Deviations from the set-point (SP M_{vessel}) which is calculated from the power demand, are corrected using the four inventory control

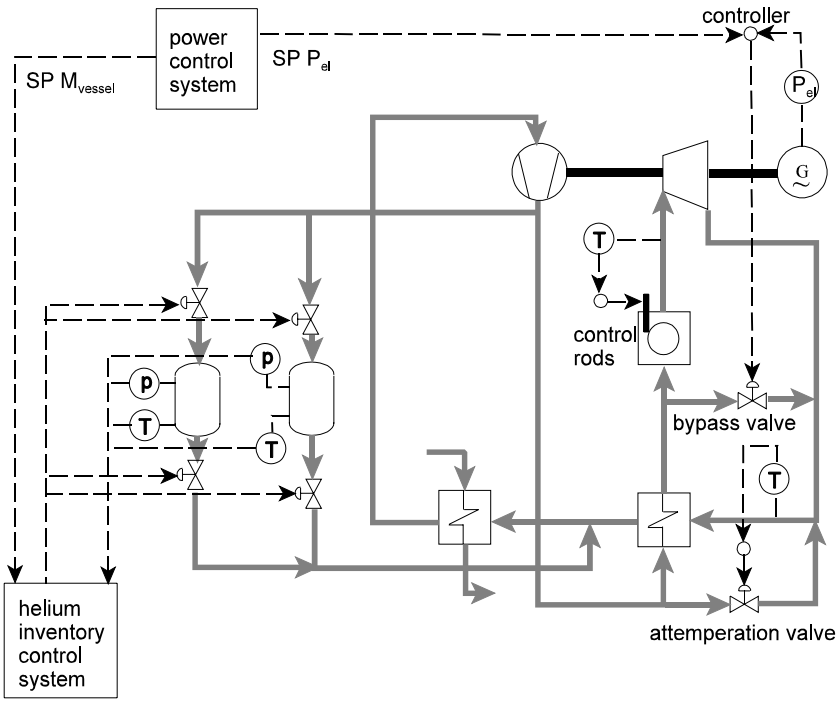

Figure 7.1: Typical NGT control system.

valves. Since the large plants have a large inventory, the inventory reduction is fairly slow. Therefore there is a bypass-valve between reactor inlet and turbine outlet which can be opened to reduce the shaft speed. In order to have control at full power as well, the bypass has to be always slightly open. The opening of the bypass leads to a lower pressure and temperature drop over the turbine. The fast temperature rise of the recuperator can lead to thermal overstressing. This can be reduced by mixing the turbine outlet flow with 'cold' helium from the compressor outlet. For this reason an attemperation valve is added. The reactor temperature is regulated with control-rods. The compressor inlet temperature is not controlled, the system is simply cooled as far as possible.

Another control method proposed in literature is throttling (Adams, 1994). A throttle valve in the primary flow can be closed partly in order to reduce the mass flow through the system. Similarly to the inventory reduction, less heat is transported from the reactor to the energy conversion system. A throttle valve either has to be very large or consist of many valves ducted in parallel since otherwise it gives a significant pressure drop (leading to a poor efficiency), even when it is fully opened.

Yet another method for turbo-machinery control is the use of variable-geometry inlet vanes (Cohen, 1996). The stator-vanes are rotated so that in off-design operation the blade-angles better fit the angles of the gas flow. Only small adjustments can be made in this manner without loss of efficiency. In the control system of the PBMR large adjustments of the vane-positions are used to control the shaft speeds in case of a load rejection (Nicholls, 1998). This actually has the same effect as throttling. The use of variable-geometry is not considered for this study since it strongly complicates the turbo-machinery design and the benefits are small.

The control of the NGT-CHP plant will be different in two aspects: (1) The reactor outlet temperature control-loop will be omitted, since the self-regulation capacity by virtue of the negative temperature coefficient is sufficient for the temperature control and (2) the compressor inlet temperature determines the heat-to-power ratio, so it must be controlled in a CHP plant. The turbine inlet temperature of about 900 °C (which appears at lowest part-load) is considered acceptable for some time, since in the PBMR design 900 °C was chosen as the design-temperature (Liebenberg, 1996). Note that this is the total temperature, the static temperature at the first rotor inlet and thus the moving blade temperature is approximately 25 °C lower.

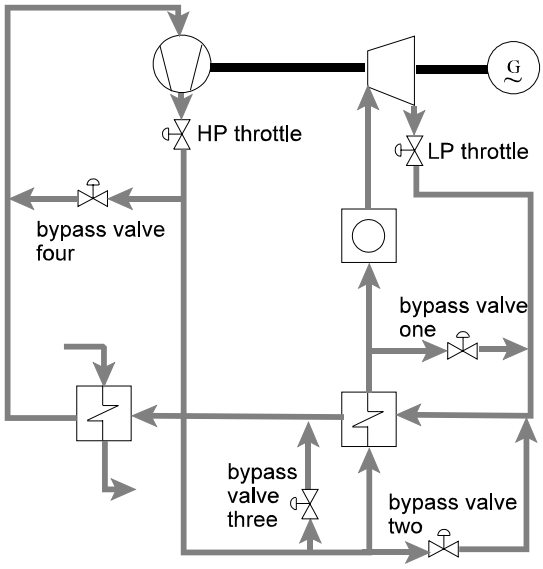

Figure 7.2: Possible control-valves.

7.2.2 Shaft Speed Control Options

In figure 7.2 a number of alternative control-valves is shown. Valves one and two are the bypass and attemperation valve mentioned above. The bypass valve is situated in a high temperature environment, which might complicate the design. An alternative position for the bypass valve would be between the cold (instead of the hot) inlet and outlet of the

recuperator (valve three). This might make a cheaper valve feasible, since the temperature would be 260 °C instead of 494 °C. Yet another possible position is between compressor outlet and inlet (valve four). In this manner the compressor inlet temperature is increased and the density is decreased. The compressor mass flow is therefore reduced. This is favourable for the efficiency, since the the heat transport from the reactor is decreased. Two possible throttle-valves are conceivable, either positioned in the high pressure (HP) or low pressure (LP) side.

The influence of these valves is tested with a transient in which the shaft speed is reduced to its nominal speed after a load rejection. This is done in a system with constant compressor inlet temperature, with bypass valves of 20 cm diameter with a time-constant of 0.5 second. In one transient no stable operating-point can be reached at nominal speed and zero electricity-production, as explained in paragraph 6.1. In this cases the control valves are adjusted so that the lowest stable shaft speed is reached.

In order to assess the different control-possibilities a number of output parameters have been monitored. The shaft-speed must be reduced with as little overshoot as possible. Figure 7.3 shows the transients of the shaft speed ω during 50 s. The recuperator temperature profile has been monitored to estimate the thermal stresses. The profile should preferably change as little as possible. Moreover, an increase of temperature (both in flow direction and perpendicular to it) is worse than a decrease. Figure 7.4 shows the original temperature profile of the recuperator (hot and cold helium temperature) dotted while the profile at the end of the transient (after 50 s) is drawn solid. Finally, the heat flows Q to and from the primary helium flow in the reactor respectively the precooler are plotted in figure 7.5. In order to minimize the disturbance of the secondary system, both the heat flow to it and the precooler hot inlet (recuperator hot outlet) temperature must be as constant as possible. The heat from the reactor becomes equal to the heat supplied to the secondary system, the difference is used to heat the recuperator and precooler core. A small and short deviation between both heat flows shows that the heat exchangers operate at constant temperature.

It can be seen that in case of a load rejection without any control action the recuperator actually cools the low pressure flow instead of heating it. The temperature profile changes a lot, but the temperature differences are reduced. The heat flow to the secondary cycle becomes 2.4 times as large, which leads to a poor efficiency. The fact that the compressor inlet temperature is constantly kept low is responsible for the high heat transport. The strong increase of the precooler hot inlet temperature will normally also lead to a rise in compressor temperature and thus to a decrease of the heat transport. If necessary, the temperature can be increased further by reduction of the cooling flow. With the turbine choked, the behaviour is essentially the same, albeit much less pronounced as can be seen in figure 6.5.

With the LP throttle (in the turbine outlet) the mass flow is reduced to 23 kg/s. This leads to a hardly changed energy transport to the secondary cycle and a well controlled shaft speed. Unfortunately the temperature difference over the recuperator increases. The HP throttle can only limit the increase of mass flow to 29 kg/s (no control gives an increase from 25.4 to 33 kg/s). Throttling further brings the system in the unstable left half of the electricity versus speed curve (fig. 6.1). The increased recuperator hot outlet temperature gives a strong increase of heat transport to the intermediate helium loop.

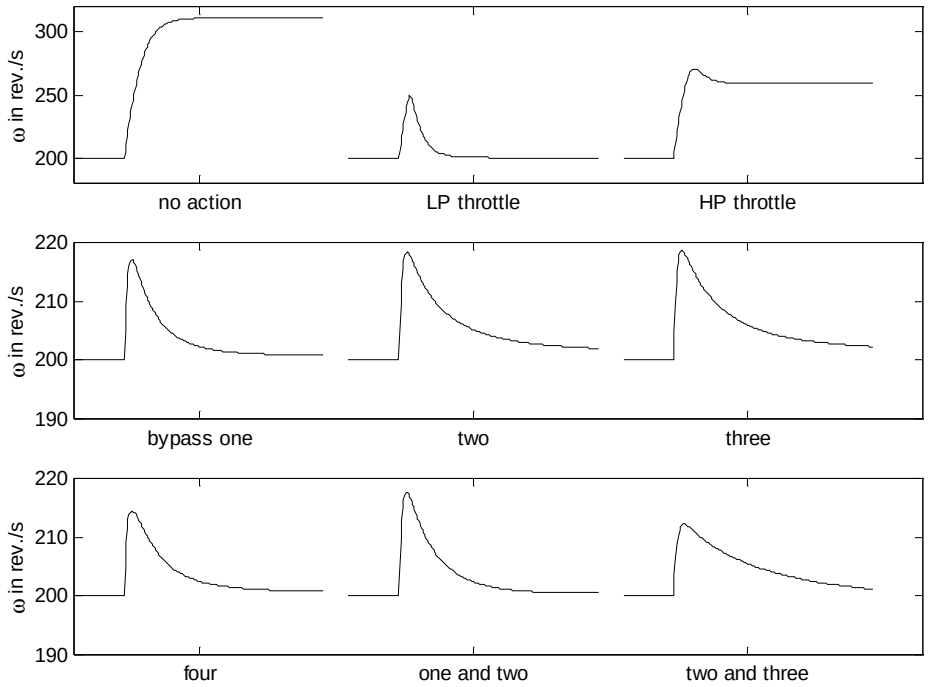

Figure 7.3: Shaft speed response during 50 s after different control actions.

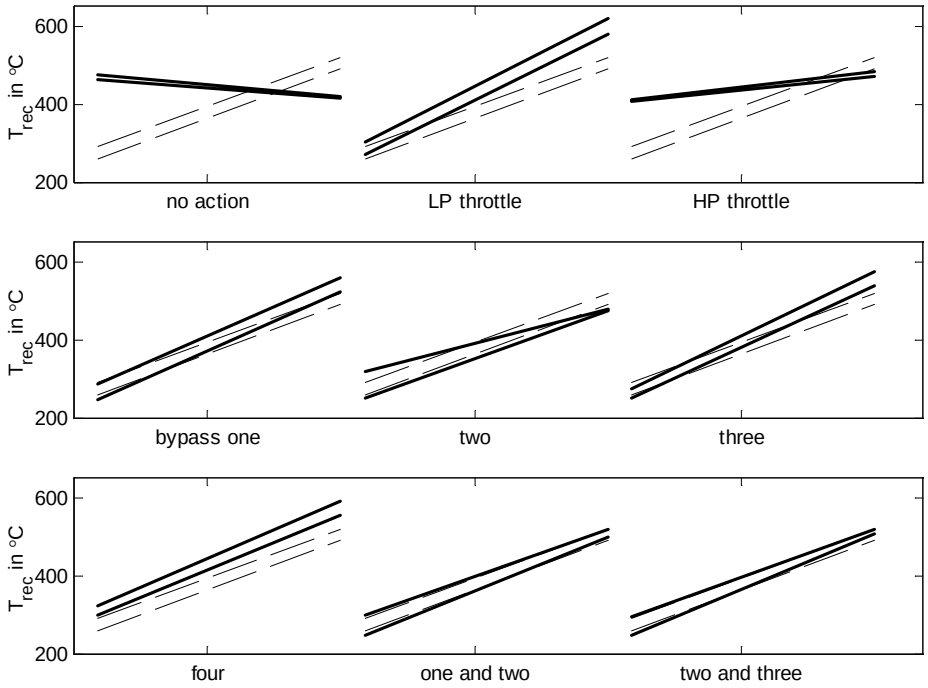

Figure 7.4: Recuperator axial temperature profile response on different control actions (dotted: profile before transient, drawn: after transient).

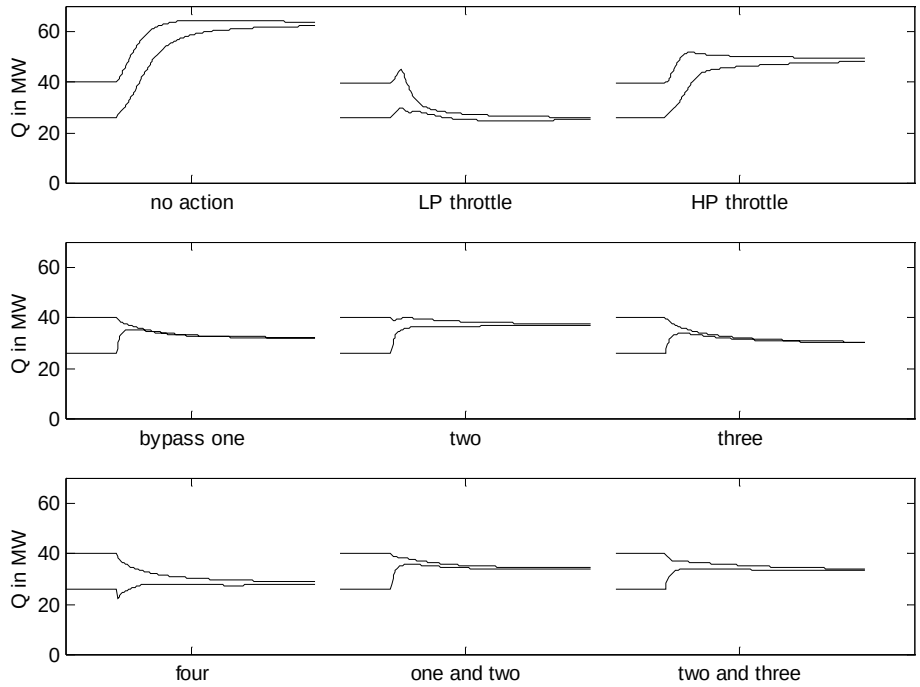

Figure 7.5: Heat flow response during 50 s after different control actions (upper: heat to primary system in reactor, lower: heat to secondary system).

For control with a bypass flow, valves one to four have to be opened to 38.5%, 31.2%, 31.5%, and 25.3% respectively, so that the shaft speed returns to 200 rev./s. This has hardly any effect on the recuperator cold inlet temperature for valves one, two and three. The reason is that the compressor inlet temperature is kept constant with the large secondary flow through the precooler (simulating perfect control of the secondary loop) and the pressure ratio over the compressor does not change very much. When valve four is opened hot helium is mixed with the compressor inlet flow so the compressor outlet temperature rises. This rise could also be accomplished by decreasing the final cooler water flow. The increase of temperature leads to a decrease of heat transport from the reactor.

For valves one, two and four, the mass flow on both sides of the recuperator is equal. This keeps the temperature lines parallel, which is favourable because it keeps the temperature difference and thus the thermal stresses perpendicular to the flow direction small. Opening of valves one, three or four leads to an increase of the turbine outlet temperature. This increase is the smallest with the 'normal' bypass valve no. 1. A load decrease with opening of the attemperation valve (valve two) leads to a decrease of the recuperator hot inlet temperature. This shows that the combination of the bypass and attemperation valve can be used to keep the temperature constant.

Finally, the results for a transient in which two bypass valves are opened simultaneously are shown. This can lead to a hardly changed recuperator temperature profile. Figure 7.5 shows that the energy transport to the secondary cycle is still too high. It can be reduced further with an

increase of the compressor inlet temperature. This will again raise the temperature at the cold side of the recuperator. In figure 7.6 the recuperator inlet temperature transients in case of opening of valve one, two or three are shown. From the dynamic behaviour (the faster response and slight overshoot of valve two) one can see that opening two valves in perfect ratio will not work perfectly; unnecessary temperature swings will occur. This can be overcome by adding a first-order filter with a time constant of approx. three seconds in the signal path to valve two, which of course will make the total response a bit more sluggish leading to higher overshoots of temperature and shaft speed. An alternative for the opening in perfect ratio is to use valve one or three for shaft speed control and valve two for temperature control as shown in figure 7.1. This can keep the recuperator temperature perfectly constant during a fast load following transient (Kikstra, 2000). However, the goal of the control structure is not to keep the temperature constant, but only to limit the rate of change of the temperature. Trying to keep the temperature constant will lead to an unnecessarily opened bypass which reduces the efficiency. Moreover, a temperature above the set-point can still not be corrected because the valve is closed during normal full power operation, in other words: the controller operates very close to saturation.

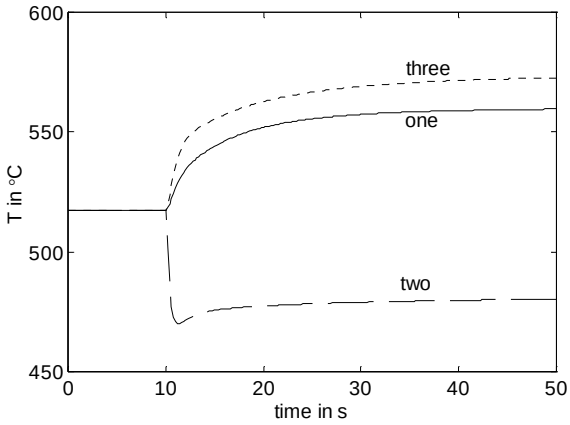

Figure 7.6: Turbine outlet temperature response for valve one, two and three.

It can be concluded that bypass-control is preferred over throttle-control. The disadvantages of throttling are the additional pressure losses, the larger shaft-speed overshoot and the increased temperature differences over the recuperator. Its only asset is the unchanged heat input at the constant compressor inlet temperature. Moreover, it can be concluded that valve three works just as good as valve one. A slightly higher recuperator hot side temperature results when the valve is used solitarily. If the combination with the attemperation valve number is used, valve three is favoured because of its lower shaft speed overshoot and smaller change in heat transport to the secondary cycle. Valve three operates at a much lower temperature which might lead to a cheaper design. The valve can also be 20% smaller, because of the increased density at the inlet. The goal of the control system is not to keep the recuperator temperature constant, but merely to limit the rate of change of the temperature. Moreover, in order to operate at the highest efficiency the valves should be closed. Therefore, operating valve three and two in a given ratio to control shaft speed only is preferred over feedback control of both recuperator temperature and shaft speed.

7.2.3 Inventory Control Valve Position

The inventory valve between vessel and primary system (which is used to empty the tanks and fill the primary system) is in all previous designs situated before the precooler, see figure 7.1. However, the injection of cold helium before the precooler could be undesirable in case of cogeneration, because of the sudden change of temperature in the precooler. The helium from the inventory vessel could also be injected between the precooler and compressor. In this case the compressor inlet temperature will decrease which brings the operating point closer to the surge-line.

Both options have been tested in a transient in which the system is emptied and subsequently filled again. The first vessel is filled by opening the vessel inlet valve 10% at t = 10 s and closing it when the inventory is reduced to 70%. Starting at t = 50 s one of the two possible vessel outlet valves is also kept open at 10% until the system inventory is back at 100%. In order to simplify the analysis the transient has been calculated with a constant shaft speed and a variable electricity production. Some results are shown in figure 7.7.

The flow through the valves is equal in both cases. The transients of the low pressure and the heat flows only show a minor difference between the two cases with different vessel outlet valves. Adding the helium to the primary system before the precooler leads to a deeper temperature dip because of the larger temperature difference between plenum and vessel temperature. However, the dip in the temperatures in the secondary and water or water/steam circuit are not as pronounced due to the thermal inertia of the heat exchangers. The temperature dip of the compressor inlet in case of opening of the alternative valve brings the compressor hardly closer to the surge-limit, because the absolute temperature only decreases with 3%. The valve position between precooler and compressor therefore gives the least disturbance of the temperatures and power and is slightly favoured. However, the difference is very minor and from construction point-of-view the position between recuperator and precooler is preferred, as can be seen in figure 3.18. This option will therefore be chosen.

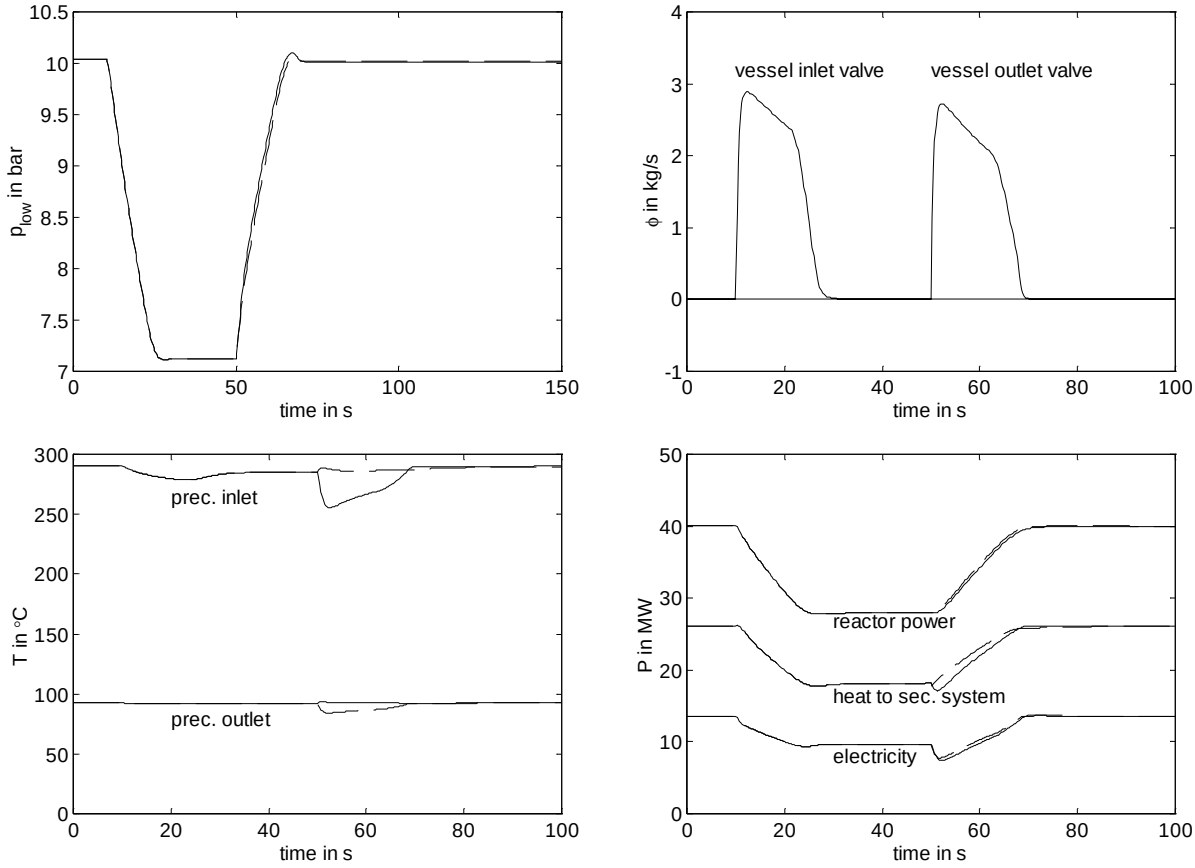

Figure 7.7: Inventory adjustment transient with two vessel outlet valves. Drawn: injection before precooler, dashed: injection after precooler.

When the inventory is reduced, an almost instantaneous drop of electricity results, additional to the ramp down proportional to the inventory. This is due to the imbalance of the mass flow through the compressor and the turbine during the emptying. The compression work used to fill the vessel does not contribute to the turbine power, hence the decrease of electricity production. A similar explanation holds for the non-minimum phase behaviour of the electricity production during the increase of the inventory. The helium is added at the low pressure side, therefore the compressor work is increased before the turbine power increases. An extra 'kick' (sudden increase) will result instead of this initial dip in power production if the helium is added to the high pressure side. This would call for a different inventory control system with a separate reciprocating compressor. The electric power will increase completely proportional to the inventory without these initial and final effects if equal amounts of helium enter the primary system at the high and low pressure side.

Unlike, the larger systems studied in literature, the inventory of the plant under consideration can be reduced very quickly. Therefore a control system which does not use bypass valves for fast control might be conceivable. The non-minimum phase behaviour of the electricity during the inventory increase poses a problem, which can be overcome by redesigning the inventory system to inject helium at the high pressure side. Another problem is that with power control by inventory adjustment only, the heat-to-power ratio is constant given a constant compressor inlet temperature. The only way to change the heat-to-power ratio, thus to independently control steam and electricity production, is to change the compressor inlet temperature by means of changing the cooling water flow. This control method is not only very slow due to the thermal inertia of the heat exchangers in the secondary cycle, it is also bounded due to the limited duty of the final cooler and because heat can only be withdrawn but not added in the cooler.

7.2.4 Steam Temperature Control Possibilities

Two possible control strategies for the control of the steam temperature of the NGT-IS have been identified: superheater bypass-control and spray attemperation, both shown in figure 7.8. The superheater bypass valve gives a slight pressure drop, so it is not favourable from efficiency point-of-view. This effect can be overcome by placing the valve in the bypass parallel, but than it must be larger, because the helium flow bypassing the superheater is larger than the flow through the superheater. Control by means of spray attemperation can be applied without loss of efficiency because the pinch-point is situated at the entrance of the evaporator, and not at the high temperature side (see figure 2.4). Steam can easily be overheated and subsequently cooled by water injection.

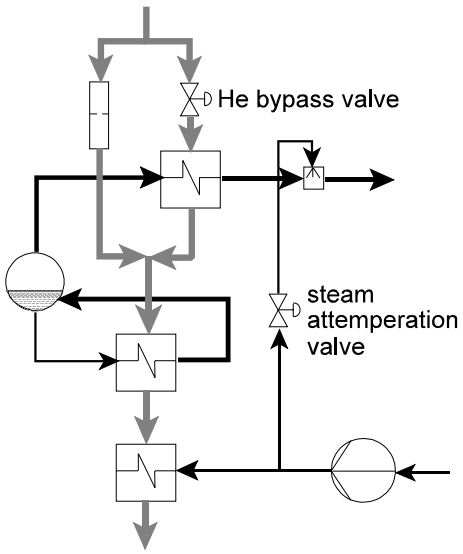

Figure 7.8: Steam temperature control options.

The transients of the steam conditions following adjustments of these two valves are shown in figure 7.9. If the superheater bypass valve is closed, the helium flow through the superheater as well as the total secondary helium flow is reduced. This leads to a reduced heat flow to the superheated steam and initially to an increased heat flow to the evaporator. The latter occurs faster due to the better heat transfer in the evaporator. This

leads to the non-minimum phase behaviour of the superheater outlet temperature. The thermal inertia of the superheater leads to a sluggish response. The increased evaporation-rate of water due to the higher evaporator helium inlet temperature gives an initial increase of pressure. However, more energy is used for further superheating of the steam, so eventually less heat is available for the evaporator. Therefore the pressure decreases again to a value which is slightly below the starting-point.

Since the temperatures of the heat exchangers stay constant when spray attemperation is applied, the transient is very fast. The flow through the attemperation valve for this transient is less than 1% of the total steam flow, so the steam pressure and flow are hardly influenced. It is therefore obvious from the dynamic behaviour that spray attemperation is the best method for steam temperature control, since it is fast and it does not influence the steam pressure.

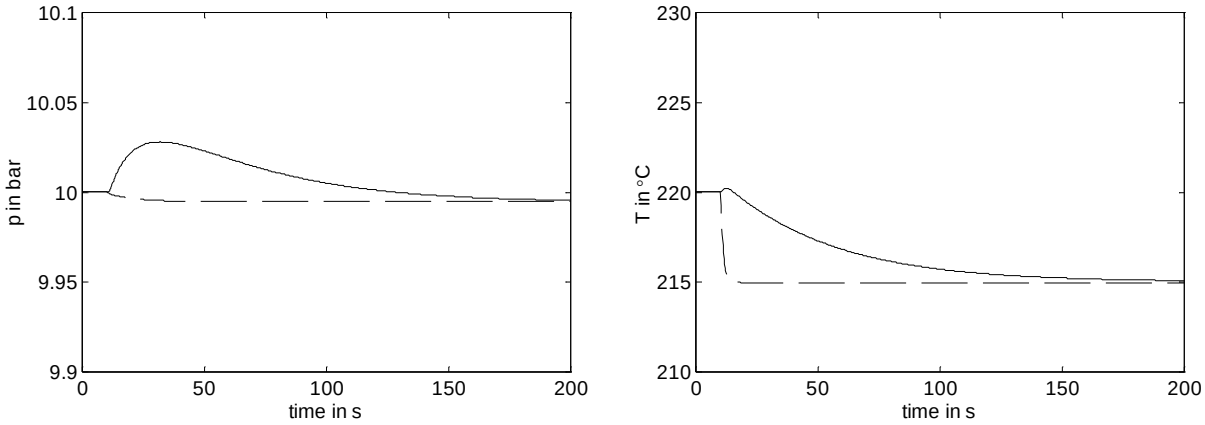

Figure 7.9: Comparison of steam temperature control with helium bypassing or attemperation. Drawn: helium bypass valve, dashed: attemperation valve.

7.3 NGT-DH Plant Control System Design

The control system design for the NGT-DH plant will be kept as simple as possible. Only the heat-load will be followed, while operating at constant reactor power and maximum efficiency. The result of the opening of a bypass valve is a reduced efficiency of the energy conversion system in order to reduce the electricity produced. If one is prepared to continuously vary the electric load, the bypass valves can be omitted. Since no part-load operation of the reactor is required, the inventory system can be omitted as well. This has the additional benefit that the temperature swings associated with xenon hardly appear. Optimal values for the blower speed and the generator speed for different heat demands were determined in paragraph 3.3. This optimal generator speed is given as a set-point to the control system, the blower speed is directly manipulated.

The shaft speed can be controlled using the generator load. The DH-water return temperature and especially the flow are set by the customer, this is modelled by considering the DH-water valve position (VP) a disturbance. The delivered temperature must be controlled, this can be done with the cooling water valve position. When the cooling water flow is reduced all the temperatures in the secondary loop are increased. This gives an increase of DH delivery temperature. The blower

speed cannot be used to control the temperature because, for low heat demands an increase of speed leads to an decrease of DH water delivery temperature, while the opposite response appears at high heat demands. The proposed control system is summarised in figure 7.10.

In order to keep the design simple, only PI feedback is used. The response of the shaft speed on a change of electric load is unstable during normal operating conditions, as described in paragraph 6.1, therefore the controller cannot be tuned using step responses. Figure 7.11 shows the response on an unit step-change of set point for different proportional gains G (in MW/(rev./s)). The performance improves with an increasing gain up to a gain of 2.5, which is therefore used. In order to reduce the steady-state error, integral action with a time-constant τ_I of 1 second has been added.

Figure 7.12 shows the step responses of the DH water temperature on change of cooling water valve position with the shaft speed control loop closed. The DH water flow has been varied between 20 and 120 kg/s, corresponding to a heat demand variation between 4 and 23 MW. The non-linearities are due to the changing heat capacities of the two water flow and intermediate helium flow. With either the DH valve or the cooling water valve almost closed, (at a DH water flow below 20 kg/s respectively above 80 kg/s) a small absolute change in valve position yields a large relative change in heat rejection which gives a large gain in the step response of the DH water temperature. When both valves are in the middle of their range (at a DH water flow of 60 kg/s) the sensitivity of

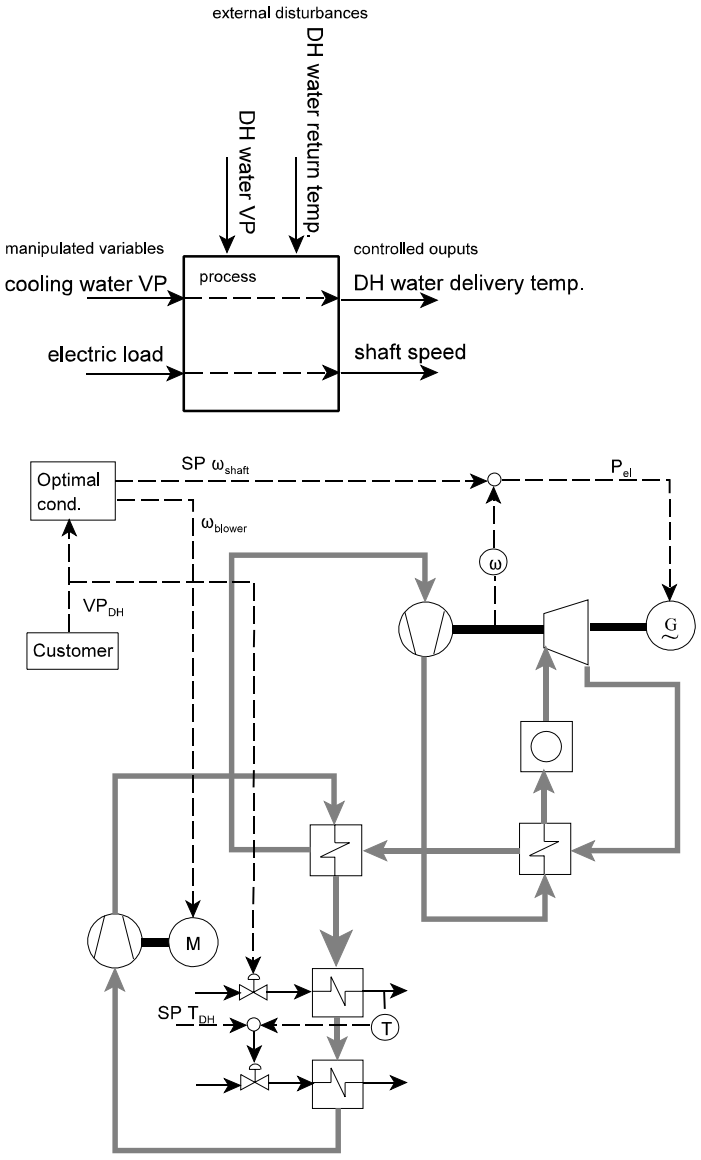

Figure 7.10: NGT-DH control system.

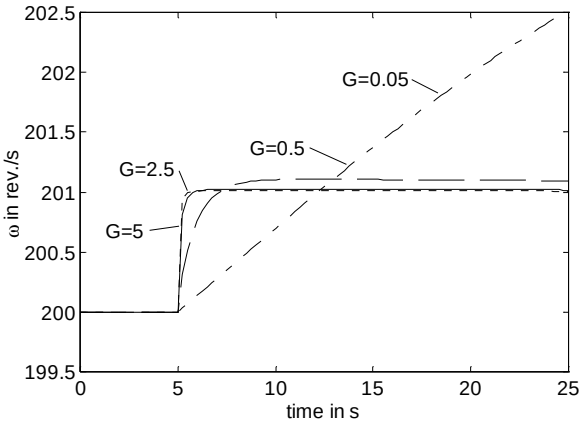

Figure 7.11: Shaft speed control loop tuning.

the temperature to the cooling water flow is low.

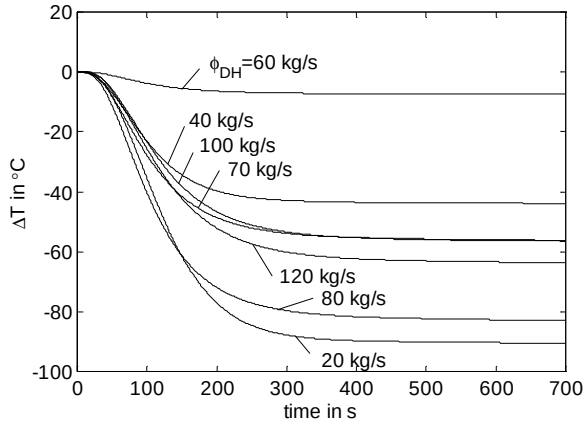

Figure 7.12: Step responses at different DH water flows.

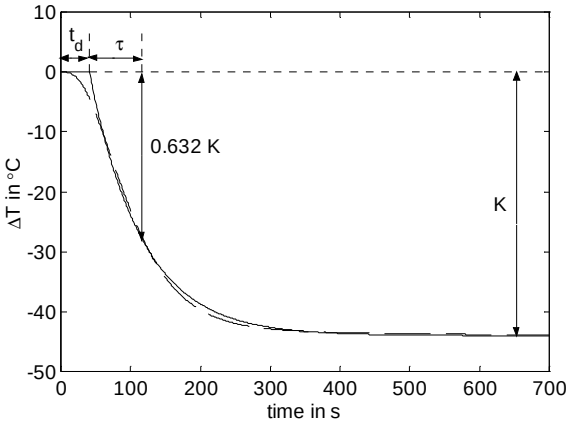

Figure 7.13: Approximation of step response (dashed) with first order + dead time process (drawn).

Figure 7.13 shows that the step responses can be approximated very well with a 'first-order + dead-time' response, characterised by the process gain K, the dead time t_d and the time constant τ. Cohen and Coon calculated the following 'optimal' PI-settings for such a process (Stephanopoulos,1984):

$$G = \frac{1}{K}\frac{\tau}{t_d}\left(0.9 + \frac{t_d}{12\tau}\right) \qquad \tau_I = t_d\frac{30 + 3t_d/\tau}{9 + 20t_d/\tau}$$

The optimal value of τ_I is for all responses approximately equal to 65 s, while the optimal gain G varies between 0.02 and 0.25. Therefore, various gains have been tested over the operational range. The results are shown in figure 7.15. The DH water flow has been decreased from 120 to 20 kg/s with a step-change of 20 kg/s every thousand seconds. Simultaneously, the shaft speed set-point and the blower speed have been changed to their optimal steady-state values. The responses of the DH water temperature for four values of the controller gain G are shown. A gain of 0.15 gives a good response over the whole operational range. Improved performance could be obtained with gain-scheduling.

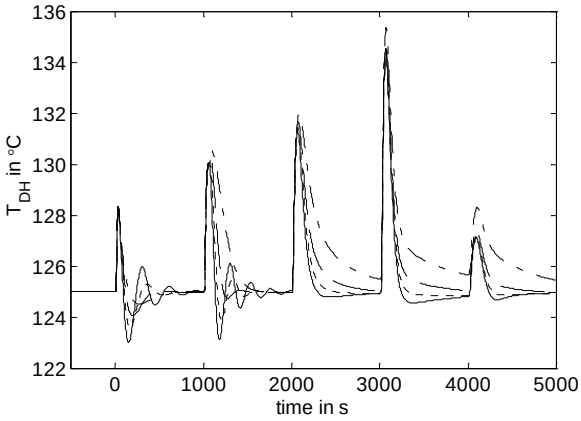

Figure 7.15: DH water temperature response for different controller gains. Drawn: G = 0.2, dotted: G = 0.15, dashed: G = 0.1 and dash-dotted: G = 0.05.

7.4 NGT-IS Plant Control System Design

7.4.1 Choice of Manipulated and Controlled Variables

A possibility for pairing of control system inputs and outputs for the NGT-IS plant is shown in

figure 7.16. Just like in the NGT-DH plant, the electric load will be used to control the shaft speed in the NGT-IS plant. However, in this plant the customer will give a set-point for the electricity production. This set-point will be tracked using bypass valves for fast control. In paragraph 7.2.2 it is shown that a combination of valve two and three is the best choice for simultaneous control of electricity (or shaft speed) and recuperator temperature.

In order to efficiently operate at low heat and power demands, the NGT-IS uses the helium inventory system. Given the power and heat demand, the optimal reactor power and thus the optimal helium inventory can be calculated and used as the set-point. Alternatively, the inventory system could be used to drive the bypass valve positions to zero.

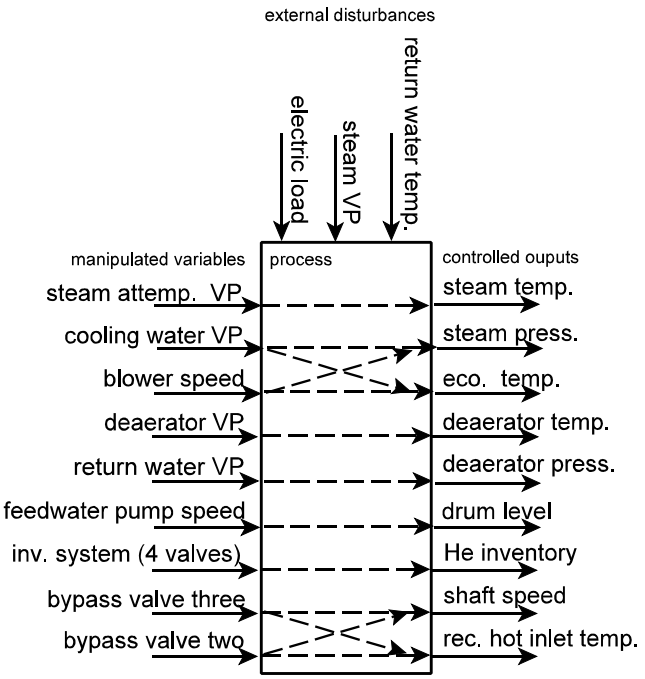

Figure 7.16: A priori choice of input-output pairing for NGT-IS control system.

The blower speed can be used to control the energy transport to the secondary system. In order to efficiently transport energy to the secondary circuit, the temperature lines of the precooler must be approximately parallel. With a reduced inventory in the primary circuit, the secondary mass flow through the precooler must be reduced to obtain the same ratio of heat capacities between primary and secondary side. This can be achieved by reduction of the blower speed. The temperatures in the secondary cycle and heat flow are also influenced by the cooling water flow. The blower speed and cooling water valve position therefore can be used to control the steam pressure and economiser outlet temperature. It is not easy to see a-priori which manipulated variable should be used for which controlled variable in Single Input - Single Output (SISO) loops. This will be investigated below.

In paragraph 7.2.4 it has been shown that the steam temperature can best be controlled with a spray attemperator. The steam pressure for a given steam flow to the customer is strongly dependent on the temperature in the secondary circuit, therefore the cooling water valve can be used to control the steam pressure. The drumlevel will be controlled with the feedwater pump speed, and the deaerator can be kept at the saturation temperature using the deaerator valve (in the steam flow from the drum). The deaerator pressure can simply be controlled with a valve in the return water inlet.

7.4.2 Operating Conditions

With the choice of inputs and outputs (but not necessarily the connecting loops) one can calculate the optimal steady-state working conditions. The NGT-IS plant has a two-dimensional operation region. Optimal conditions are shown in figure 7.17. At optimal conditions the bypass valves are of course closed. The shaft speed is always kept at 200 rev./s. The conditions are calculated for

a reactor outlet temperature of 800 °C, so they do not reflect real steady-states, only steady-states for the energy conversion system. At high electricity and heat production the area is bounded because otherwise the helium inventory and thus the pressure become too high. The 'left' and 'right' boundaries in figure 7.17 are due to saturation the cooling valve. At the left boundary the valve is fully closed, whereas it is fully opened at the right boundary. With the bypass valves opened, the plant can operate in steady-state at much lower electricity demands.

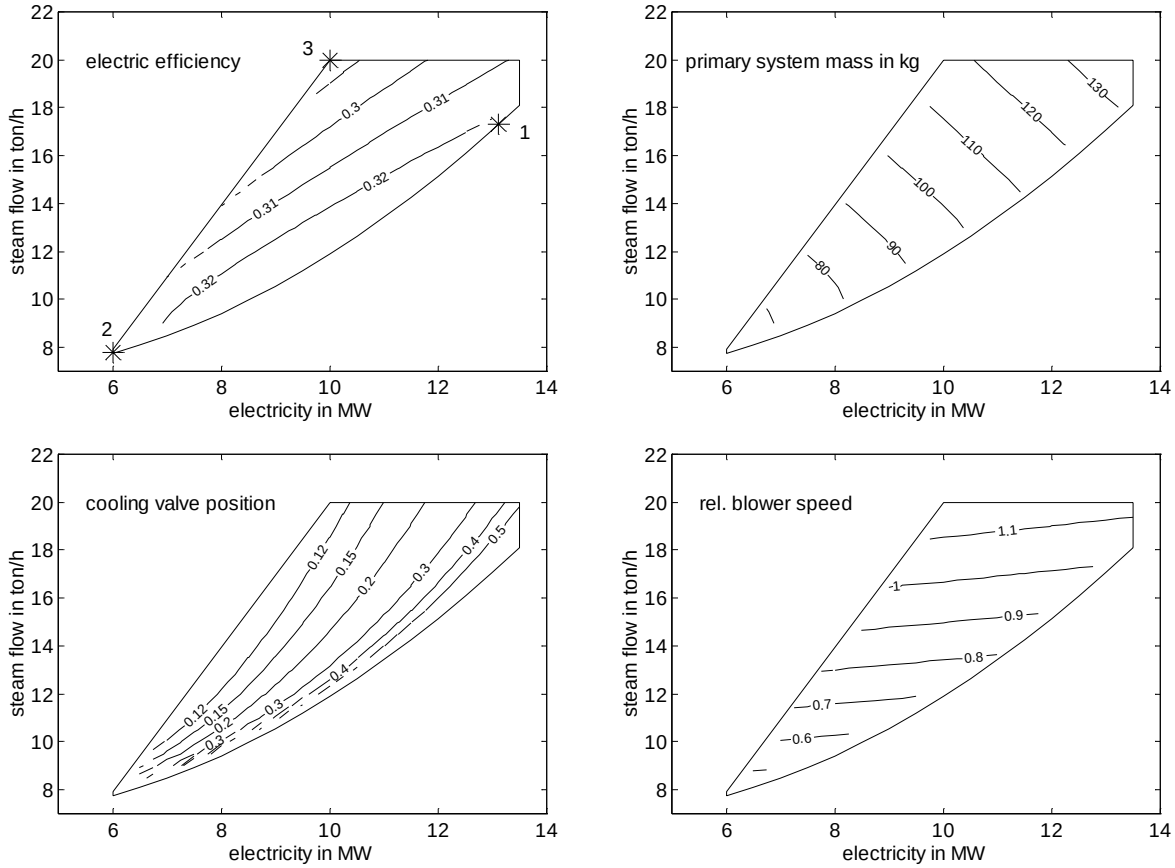

Figure 7.17: Optimal operating conditions of NGT-IS plant.

7.4.3 Analysis of Step Responses

In order to map the interaction between inputs and outputs, step responses have been produced at the three operating points indicated with an asterisk in figure 7.17. With all other inputs constant, a small step is applied to one input. The output is monitored during 700 s, after which steady-state is reached for most input-output combinations. Only for a small step on the steam input to the deaerator, it takes longer to reach steady-state than the time-scale shown, because of the large thermal inertia of the deaerator. Linearity has been checked by applying a step of opposite sign or, if this is not possible, a step twice as large. In order to obtain stable responses, perfect control is assumed for the shaft speed. The responses under full load conditions (✳1 in fig. 7.17) are shown in figure 7.18.

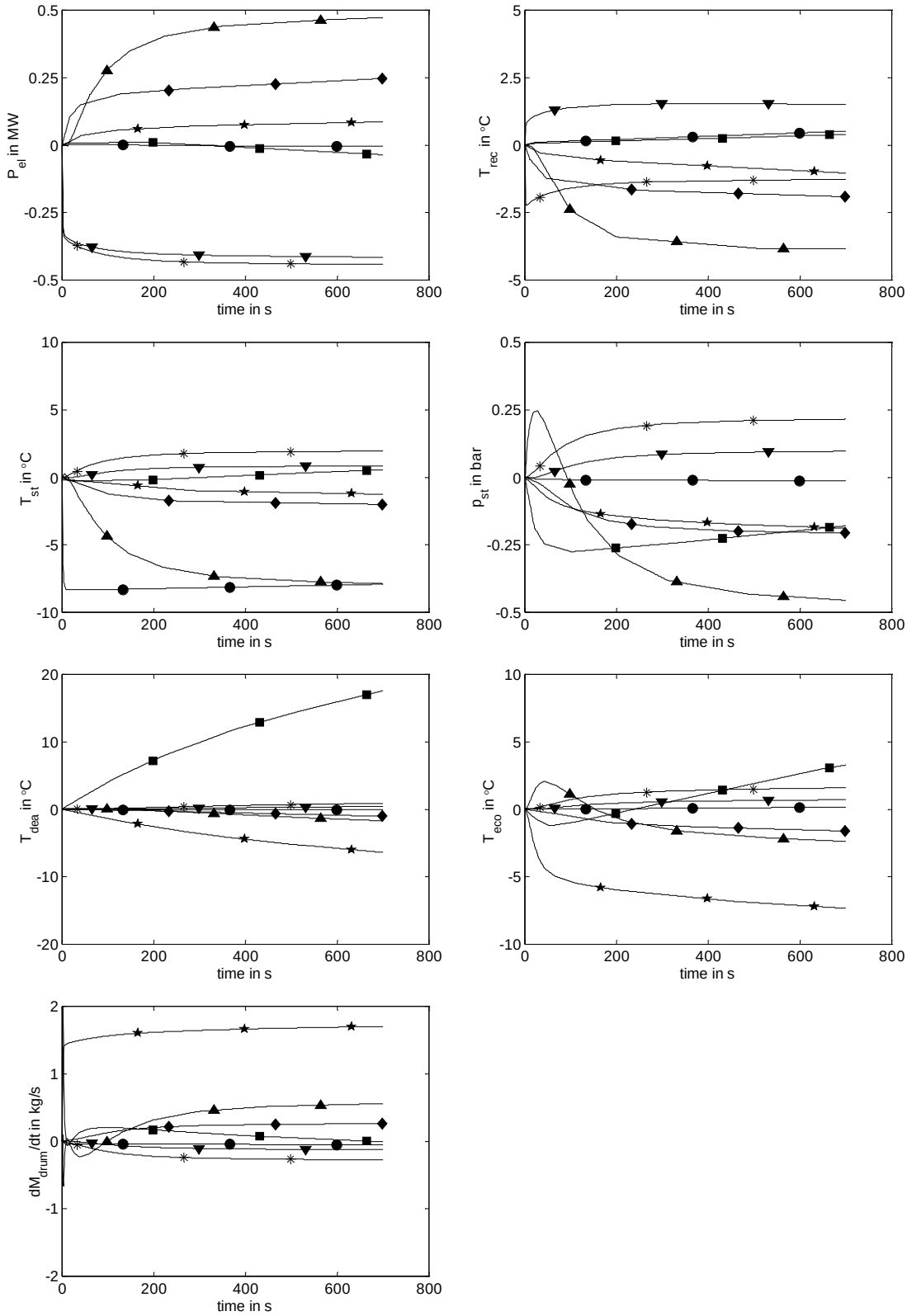

Figure 7.18: Response on 'unit' step of manipulated variables under normal operating cond. ✳ bypass valve two + 1%, ▼ bypass valve three + 1% , ▲ blower + 10%, ● attemperation valve + 30%, ★feedwater pump + 10%, ■ deaerator valve + 40%, ♦ cooling valve + 20%.

Three of the inputs and outputs shown in figure 7.16 have been omitted in figure 7.18, namely the electric load, the inventory system and the return water valve. Step responses on the electric load could not be simulated because they would not result in a stable response. If a small step-change is applied to a valve of the inventory system, an integrating response results in which the system is slowly emptied (or filled). Moreover, obviously it is the only input available for control of the primary system mass. The return water valve finally is omitted, because a priori it can be concluded that the control loop of this valve and deaerator pressure shows no interaction with other loops. The steam drum level is a pure integrator. In order to easily obtain a state-space model from the step responses the time-differential of the drum mass is shown in figure 7.18 and used in the following analysis of input-output interaction. The transient behaviour of this output yields the same information, but has the advantage of being stable.

Some conclusions can be drawn from the step responses:

1. The attemperation valve position hardly influences any other output than the steam temperature. This is because the water flow diverted from the feedwater pump for attemperation is very small, so that it does not influence the drumlevel or economiser temperature.
2. Similarly, the deaerator valve position only strongly affects the deaerator temperature, with smaller influence on the economiser temperature and the drum level.
3. The responses of the steam pressure and economiser output temperature on the blower speed show non-minimum phase behaviour. Changing the secondary mass flow changes the temperature profiles in all heat exchangers in the loop. The speed at which a heat exchanger reaches a new steady-state depends on its thermal inertia. This thermal inertia and the sign of the response are different for different heat exchangers. Directly after an increase of blower speed more heat is transported from the precooler to the evaporator, leading to a pressure rise, because more water is evaporated. After a while more heat is removed in the final cooler, which has the opposite effect.

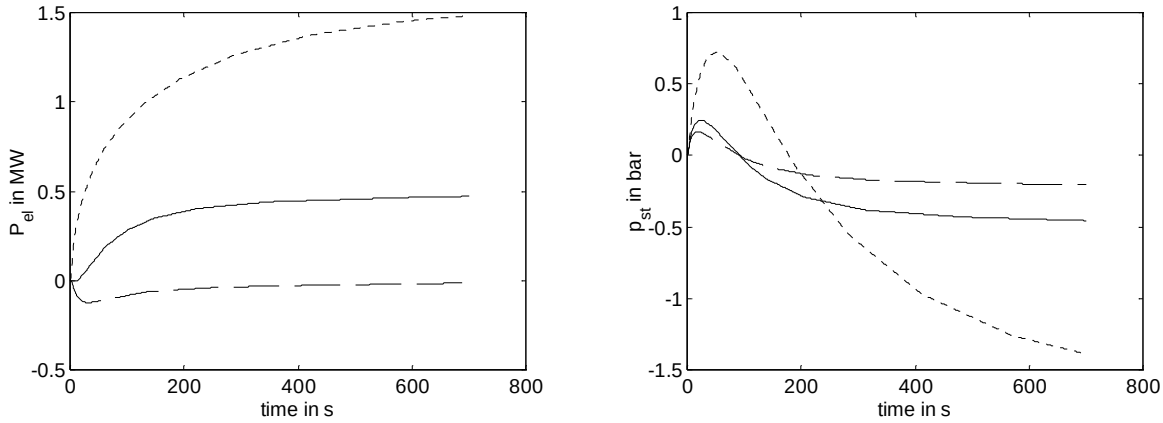

Figure 7.19: Response to step on blower speed, drawn: at normal operating conditions (point 1), dotted: at operating point 2, dashed: at operating point 3.

Figure 7.19 and 7.20 show some important step-responses in the other two operating points. A strong non-linearity over the operational region exists. The non-linearity of the response on a step-change in blower speed is due to the counterbalancing effects of the changed temperature

profiles in the heat exchangers. The effect of the blower speed on the temperatures and the pressure is dependent on the ratio of duties of the heat exchangers. The magnitude of the step response on the cooling water flow strongly depends on the initial valve position. When the valve is almost closed (in operating point 3), a small absolute change gives a fairly large relative change which gives the response a high gain.

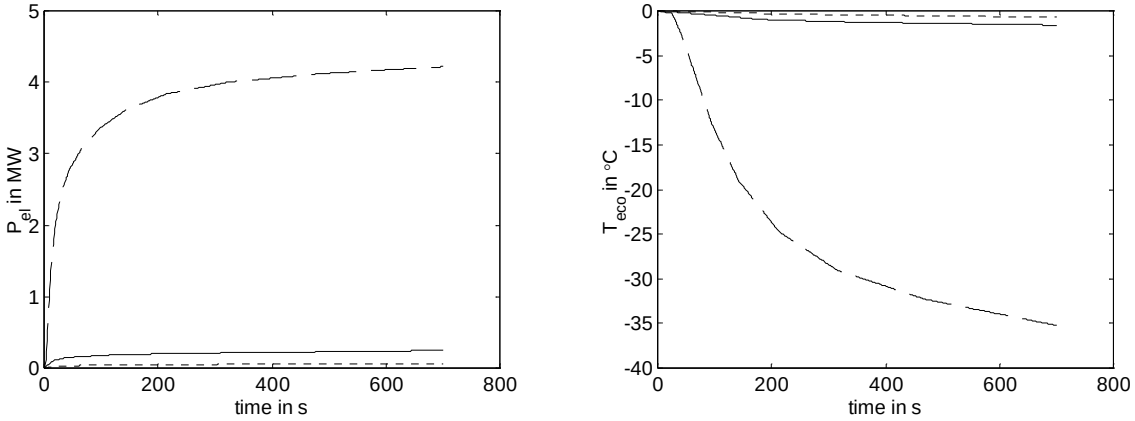

Figure 7.20: Response to step on cooling water valve, drawn: at normal operating conditions (point 1), dotted: at operating point 2, dashed: at operating point 3.

7.4.4 Relative Gain Analysis

More insight into the optimal choice of input-output pairing for a SISO feedback control structure can be made based on analysis of the Bristol Relative Gain Array (Stephanopoulos, 1984). The RGA matrix has as its elements the ratio of open-loop gain with all other loops open and open-loop gain with all other loops closed for every input-output combination. One element of a column close to one with all the other elements close to zero indicates that this is a good input-output pair; the control-loop shows little interaction with other loops. Negative elements indicate that a difference of sign between the response with the other loops open or closed, which of course complicates the use of this pair for control. The RGA at operating point 1 is shown underneath. The elements indicating strong interaction have been underlined.

	byp. v. 2	byp. v. 3	att. v.	blower	dea v.	cool. v.	pump
P_{el}	1.1435	0.3023	- 0.0001	0.0024	- 0.0001	- 0.4473	- 0.0006
T_{rec}	0.2955	0.3417	0.0012	0.0379	0.0000	0.3224	0.0013
T_{st}	0.0092	- 0.0129	0.9618	0.1051	- 0.0010	- 0.0680	0.0058
p_{st}	- 0.4811	0.4579	- 0.0123	1.4716	0.0027	- 0.2838	- 0.1550
T_{dea}	- 0.0159	0.0500	0.0178	0.7237	0.8341	- 0.6456	0.0359
T_{eco}	- 0.0149	- 0.1546	- 0.0373	- 2.8260	0.0733	3.9454	0.0141
dM_{drum}/dt	0.0638	0.0156	0.0688	1.4854	0.0910	- 1.8231	1.0985

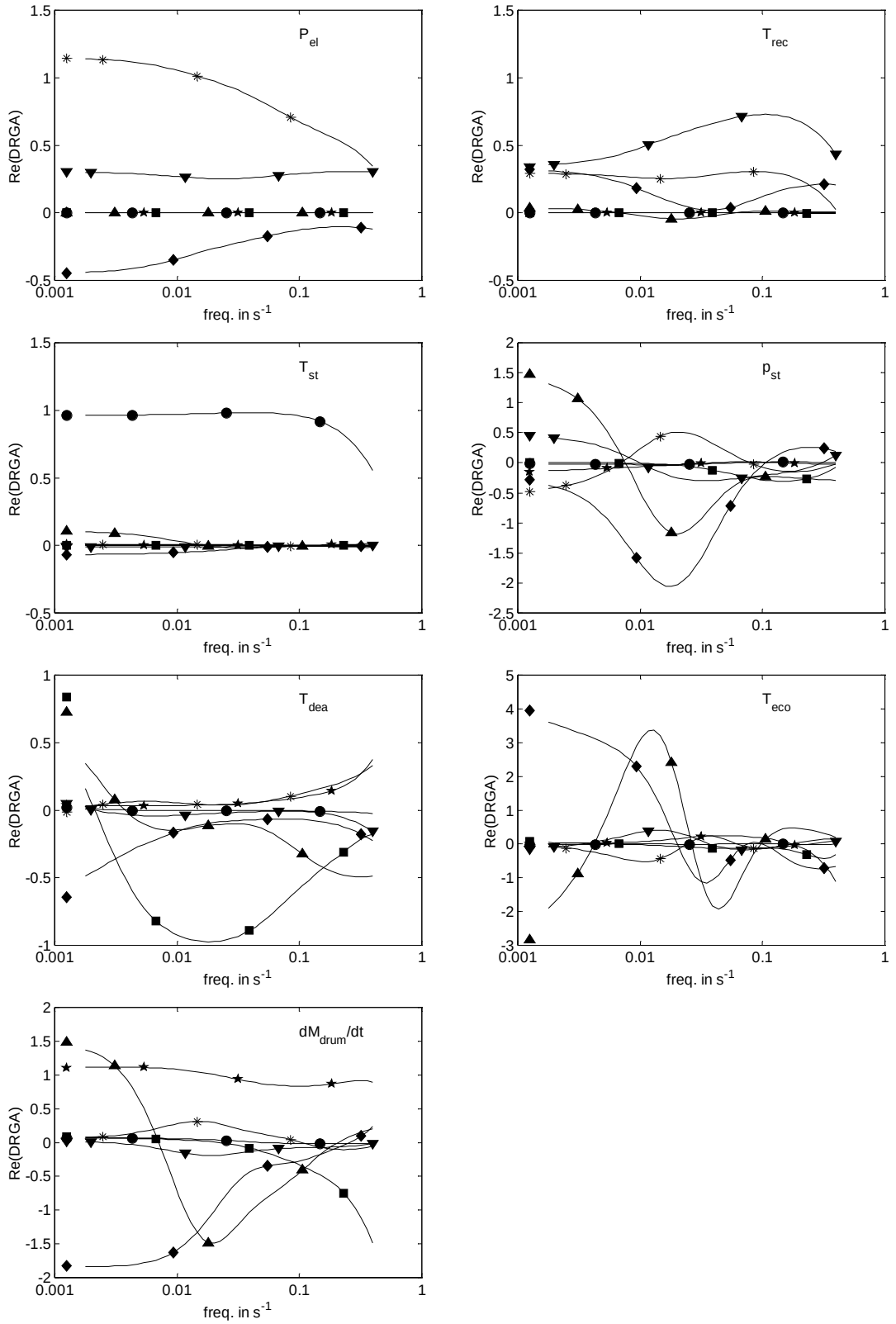

Figure 7.21: Dynamic Relative Gain Analysis. ✳ bypass valve two, ▼ bypass valve three, ▲ blower, ● attemperation valve, ★ feedwater pump, ■ deaerator valve, ♦ cooling valve.

The RGA does not show dynamic interaction. Dynamic Relative Gain analysis (Maciejowski, 1989) is an extension which overcomes this shortcoming. Assuming perfect control, the frequency response at different frequencies can be calculated from the transfer function or a state-space model. This state-space model is obtained from a model reduction using Hankel Singular Value Decomposition based on the step-weights (Zee, 1979) obtained from figure 7.18. Using input and output scaling, a tenth order state-space realisation could be obtained of the model with 700 step-weights (sample time 1 second) for each input-output pair. Figure 7.21 shows the real part of the response at different frequencies. At the low frequency end an extra symbol indicates the RGA at zero frequency.

The only loop which shows no interaction with the rest of the system, is the steam temperature control with the attemperation valve. The two topmost figures suggest that the best pairing for the bypass valves is the control of electric power with valve three and recuperator temperature with valve two. However, as discussed at the end of paragraph 6.2.2, ratio control is preferred. Therefore the electricity production is controlled with valve three and valve two is operated in ratio with valve three. The a-priori guess of using the feedwater pump for drumlevel control and the deaerator valve for control of the deaerator temperature is confirmed.

The blower speed shows interaction with almost all output variables. Moreover, as expected from the non-minimum phase behaviour, the sign of response changes with frequency. Some tests proved that closed loop control using the blower speed is extremely difficult if not impossible, due to the slow non-minimum phase behaviour. If the steam pressure is tightly controlled, the economiser temperature will not change much either. Even without a closed-loop temperature control the economiser remains subcooled, therefore this control loop can be omitted. This leaves the cooling water valve as the remaining manipulated variable for steam pressure control.

7.4.5 Decentralised PI-Control Structure

With the choice of input-output pairs, a decentralised PI-control structure can be designed. In order to obtain a fast and stable response to load variations, some feed forward loops have been added.

If the helium inventory is not adjusted or directly adjusted to its optimal steady-state value after a change in electric load, the heat input to the secondary cycle changes quickly. The heat removal in the final cooler cannot be adjusted equally fast, due to its thermal inertia. This results in unacceptably large swings in steam pressure during load changes. The problem can be overcome by first adjusting the helium inventory to such a value that the primary mass flow through the precooler is kept constant. Since the temperatures are also fairly constant due to the operation of bypass valves, the heat flow to the secondary cycle remains in balance. In case the bypass valve is opened in order to reduce the electricity production, the compressor flow and thus the primary precooler flow increase. To counterbalance this effect the inventory is reduced. This is accomplished by ramping up or down the set-point simultaneously with the electricity demand. Subsequently the inventory can be reduced very slowly to the optimal value shown in figure 7.17, this is done with a 1000 s ramp. The reduction in heat input into the secondary cycle leads to a steam pressure reduction, after which the controller closes the cooling water valve. The compressor inlet temperature rises which through an increased power consumption of the compressor gives a reduced electricity production. This is balanced by closing the bypass valves,

thus raising the efficiency.

The inventory of the primary system is calculated from the constant total inventory and the vessel inventory which is calculated from the pressure and temperature in both vessels. This value is sent to a PI-controller. If the primary mass is too low, one of the two vessel outlet vessels is opened. If the pressure in the LP vessel is higher than the compressor inlet pressure its outlet valve is opened, otherwise the signal from the PI-controller is sent to the HP outlet valve. In case of an increase of primary mass, an inlet valve is opened. If the compressor outlet pressure is higher then the HP vessel pressure the HP vessel inlet valve is opened, otherwise the LP vessel inlet valve is used.

The control structure is depicted in figure 7.22. The PI-controllers have been tuned heuristically with various transients.

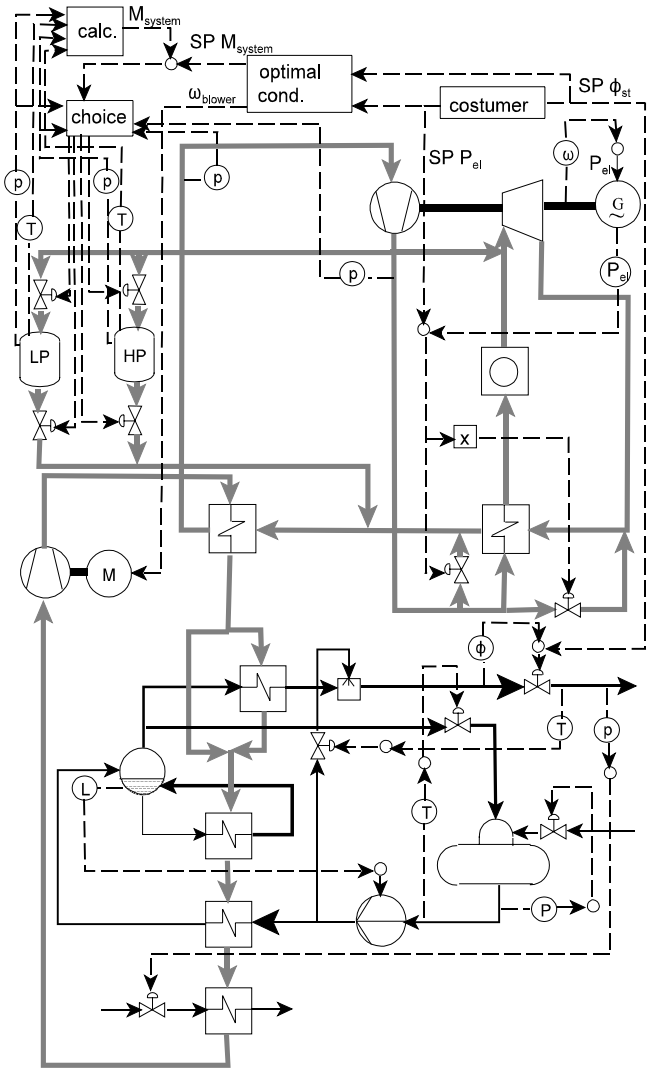

Figure 7.22: NGT-IS control structure.

In order to test the control strategy, a transient in which both electricity and heat demand are changed has been simulated. The time history of some important variables is shown in figure 7.23. Starting At t = 10s the electricity demand is ramped down with 25% in 10 s. As a result, the inventory is directly adjusted and during the next 1000 s ramped down to its optimal value. At t = 2000 s the heat demand is decreased with 15%. The blower speed is directly adjusted.

The electricity production exactly meets the demand, while the steam flow and pressure show only small deviations from their set-point (shown as dotted line). The steam temperature and the deaerator conditions are almost the same as their set-points. Ratio control of bypass valve two cannot keep the recuperator temperature completely constant, but the changes are small. The drumlevel is kept in the middle of the drum. The controller is not set very aggressively since that would lead to short and large deviations of the steady-state pump speed, which would unnecessarily upset the system. Because of the integrating nature of the drumlevel response to both the pump speed and disturbances, longer small differences in pump speed work equally well. The bypass valves are almost closed during the heat load following transient. If they are completely closed (as could happen in larger load-swings), either the electricity set-point cannot be attained, or the inventory must be adjusted to secure the electricity production. It can be concluded that the overall response of the system is satisfactory.

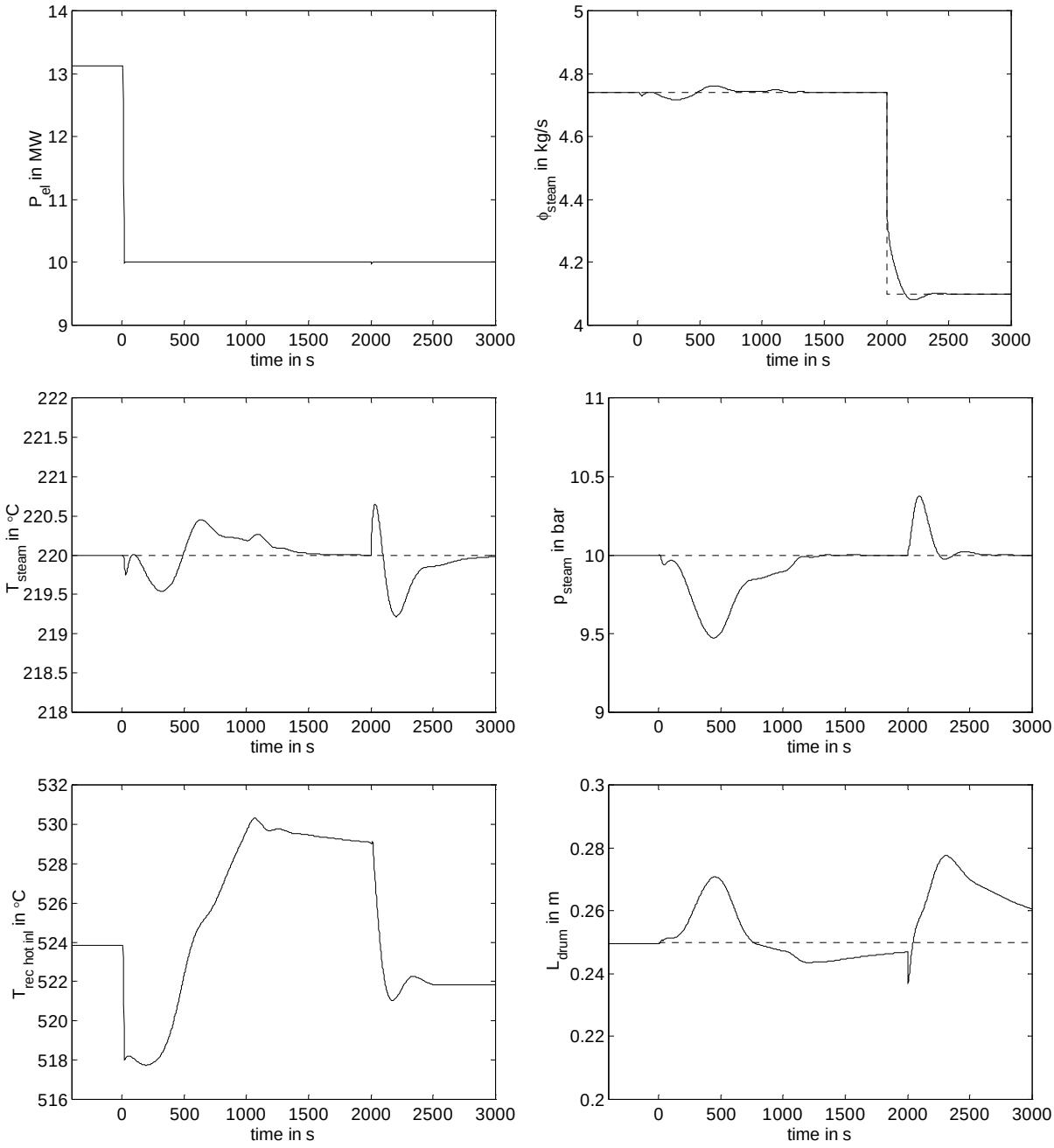

Figure 7.23: Results of NGT-IS control system test transient.

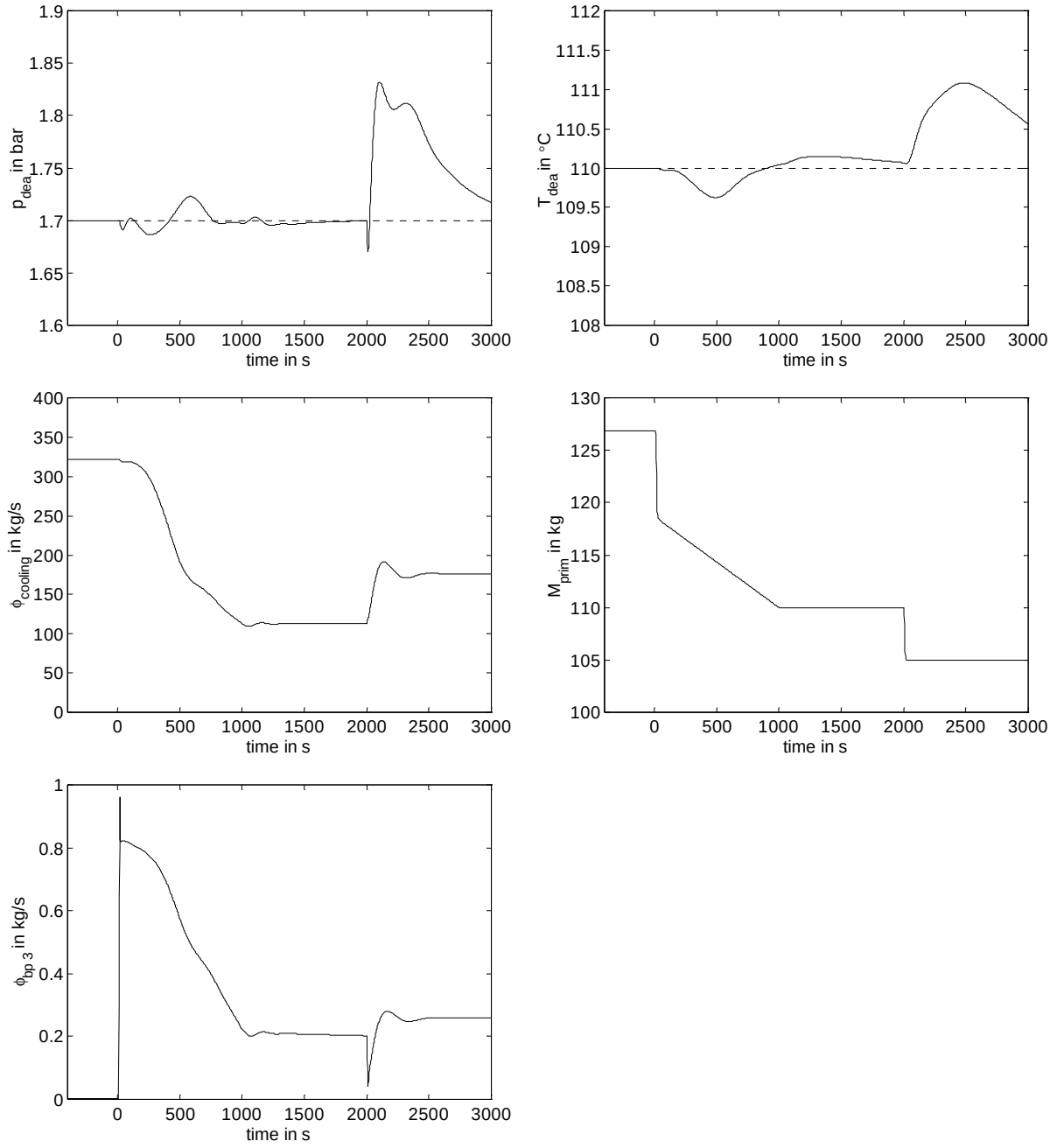

Figure 7.23: Results of NGT-IS control system test transient (continued).

7.5 Conclusions

The operating strategy and demands for the control system for the CHP plant are different from those for the designs for electricity generation only, therefore the control system design will be quite different from those found for NGT plants in literature. Because of the small reactor with a strong negative temperature coefficient, the temperature control with control-rods can be omitted. In order to control the quality and quantity of heat, a number of control loops must be added.

With the dynamic model, the effect of various control valve positions in the flowsheet has been compared. Bypass valves proved to work more efficient then throttle valves. Moreover, it was found that not bypass valves one and two (referring to figure 7.2), as proposed in literature, but valves two and three are the optimal combination for shaft speed and recuperator temperature control. The position of the valve between inventory vessel and primary system, before or after the precooler, does not heavily influence the dynamic behaviour. Consequently, the position which gives the easiest mechanical construction is chosen. For steam temperature control, the attemperation valve clearly gives the tighter control than the helium superheater bypass valve.

With this choice of control valves, the operational region and optimal working conditions is found. Then the optimal pairing of controlled and manipulated variables was investigated. For the NGT-DH plant this was very straight-forward. Two SISO control loops are sufficient to control the plant. For the NGT-IS plant however, it has been shown that there exist strong non-linearities in the operational region, that there is a strong interaction between control-loops and that some important responses show non-minimum phase behaviour. This complicated the control system design. Nevertheless, the implemented control structure was capable of heat and power load following with acceptable deviations from the set-points.

Chapter 8

Simplified Non-Linear Model

In this chapter a simplified model for use in a control scheme is developed. First the reasons for the model development and its goals are listed. Then the assumptions on which the simplification is based are discussed and the model is presented. Finally it is shown that this low-order model gives the same results as the model developed in chapter 4 in a wide region of normal operation.

8.1 Goals and Demands

A dynamic model can not only be used to tune and test a control scheme, it can also be incorporated in the control structure, in order to optimise the dynamic plant behaviour. Such a structure can be advantageous over the decentralised feedback structure presented in chapter 7. Based on an measured and/or estimated state of the plant and a plant model, a number of future control moves of all manipulated variables can be optimised with regard to a criterium based on the weighted performance of all controlled variables. Various methods with varying complexity have been presented in literature, e.g. single input-single output or multi input-multi output, linear or non-linear, using different state-estimators, etc. (Garcia, 1989, Morari, 1999). The assets of model-based control include the multi-input multi-output approach, the use of feed-forward control, taking into account constraints on inputs and outputs, the formalised way of weighing several control goals and its unified approach to plant wide control.

Model-based control structures call for a fairly simple dynamic model, most methods therefore use linear state-space or step-response models. The optimisation is preferably done with a linear model because of the availability of robust numerical recipes and computational efficiency. However, in chapter 7 it was shown that over the operational region a large non-linearity can be observed. A work-around could be to use locally linearised models in the optimisation step. A way to produce such models is to measure step-responses in a number of operating points and to estimate the models between operating points by e.g. gain scheduling or interpolation (Kikstra, 1998). A more elegant way however, would be to start with a dynamic low-order first-principle model which can be used in its non-linear formulation for prediction of future outputs and which can be linearised at any given state (Prasad, 2000).

The model developed in chapter 4 is obviously far too complex for using it online; its calculation time is too high, since the system of differential and algebraic system is large and implicitly formulated. Therefore a low-order explicit model will be developed in this chapter. This model

only needs to be valid in the normal operational range. It will not be used for design, so the preprocessing part which translates sizes and geometry into the model parameters does not have to be included.

8.2 Simplifying Assumptions

In order to achieve a low-order model, strong simplifications have to be made to the full-scale model of chapter 4. The most important are discussed underneath.

1. Simplified material properties
   Helium and steam are treated as ideal and perfect gases. Helium almost behaves as an ideal gas, the disagreement in the operational region being lower than 2%. Steam at the pressures and temperatures of interest shows very different behaviour. Nevertheless, ideal gas behaviour can be assumed using a local gas constant R. Since steam pressures and temperatures in a certain plenum or component vary very little this approach can give reasonable results. For the same reason one can work with a constant specific heat C_p in a component, even though for example the C_p of steam varies between 2690 and 2270 J kg^{-1} K^{-1} when the temperature varies between 180 and 230 °C at a pressure of 10 bar (the inlet and outlet temperature of the superheater). Liquid water is almost incompressible, which gives very stiff dynamic mass balances. Therefore a constant density is assumed and the mass balances are solved statically. For the same reasons as steam, a constant C_p is applied. Although temperatures in the final cooler vary more over the operational region then those in the superheater, the C_p is less sensitive to temperature and very insensitive to pressure. In the drum, downcomer and evaporator, the pressure, temperature, densities and some partial derivatives of state-variables are calculated from the gas density, using locally fitted fourth order polynomials.

2. Simplified balance-equations
   The helium mass in all components is negligible compared to the helium mass in the connecting plenums. Moreover, due to the large velocities and small distances, the residence-time in components is small compared to the dynamic effects of importance. Therefore static energy-, momentum- and mass-balances can be solved for the components. This results in instantaneous changes of outlet conditions for a change of inputs. For the plenums, dynamic mass- and energy-balances are solved. In the energy-balance, only internal energy is taken into account. Kinetic energy can be neglected because the velocities in the places of interest are low. Potential energy can be neglected because it was only of interest in the natural convection evaporator. In this component the waterside flow phenomena are hardly of interest as was shown in paragraph 5.3. The simplification of the evaporator model will be discussed later. The corresponding terms are also removed from the momentum-balance. Moreover, since the momentum-balances are always solved between two plenums, the incoming and outgoing momentum is also negligible and changes in the cross-sectional area are not of interest. This results in a simple relation between flow, and pressure drop. For the drum, downcomer and evaporator, the mass and energy balances for a mixture of saturated water and steam are solved. For the deaerator a dynamic energy balance is solved, while the assumption of incompressibility gives a static mass balance.

3. Map-based simulation of rotating equipment
   Both the compressor and turbine model are based on two two-dimensional maps correlating dimensionless groups. Since the maps are produced using the stage-by-stage models, they give the same result under the condition of adiabatic operation. The groups have been re-ordered compared to the usual representation to yield an explicit calculation. The blower and feedwater pump forces are calculated from the same relation as in the full-scale model, but the temperature rises are neglected.

4. Coarsely nodalised heat-exchanger model
   In literature, no simple low-order model for gas-gas heat exchangers with a large temperature rise compared to temperature difference can be found. In the modelling tool MMS for example, either a constant temperature difference between gas and wall is assumed, or the efficiency-NTU relation (Kays, 1985), which only holds for steady-state, is used. Therefore a new method must be developed. The assumption of a constant temperature in a node of the heat exchanger wall in the full-scale model called for a fine-meshed discretisation, otherwise the correct steady-state solution can not even be found (see paragraph 4.4.4). In order to reduce the number of differential equations now a linear temperature profile is assumed between the points for which a temperature is calculated from the dynamic wall energy-balance. Given this temperature profile and a static energy-balance for the fluids, an analytic solution for the fluid temperature is obtained. With a low number of nodes, the correct dynamic behaviour can be simulated.

5. No reactor model
   The model for the calculation of reactor power can be omitted completely. With a fixed graphite temperature, the heat transfer to the helium flow can be calculated. The change of power only slowly leads to a change of solids temperature, on the time scale of interest for the control system, the effect is trivial.

8.3 Component Models

8.3.1 Gas Plenums

In the plenums the local density, pressure and temperature are calculated from the temperature and mass flows of incoming and outgoing streams and heat transfer with the surroundings by means of mass- and energy balances. Application of the ideal and perfect gas properties, neglecting kinetic and potential energy and assuming perfect mixing gives:

$$\frac{d\rho}{dt} = \frac{1}{V}\left(\Sigma\phi_{in} - \Sigma\phi_{out}\right)$$

$$\frac{dT}{dt} = \frac{1}{V\rho C_v}\left(\Sigma\phi_{in} C_p T_{in} - \Sigma\phi_{out} C_p T + (\alpha S)\left(T_{surr} - T\right)\right)$$

$$p = \frac{\rho}{RT}$$

8.3.2 Rotating Equipment

The most common compressor model is a two-dimensional map relating efficiency and pressure ratio to dimensionless speed and mass flow, as explained in paragraph 3.1.1. For steady-state calculations, this is a practical form. However, in order to achieve an explicit dynamic calculation, the dimensionless groups have been re-ordered. From the upstream and downstream plenums, the pressures and temperatures are known. The shaft speed is calculated in a mechanical energy balance of the shaft, exactly the same as in the full scale model, see paragraph 4.4.3. Using the input-conditions pressure ratio and dimensionless speed, the resulting outlet temperature and mass flow are known from efficiency and dimensionless mass flow which are the outputs of the map. The re-ordered map is shown in figure 8.1. Because the speed is always controlled, its range in the map is fairly small.

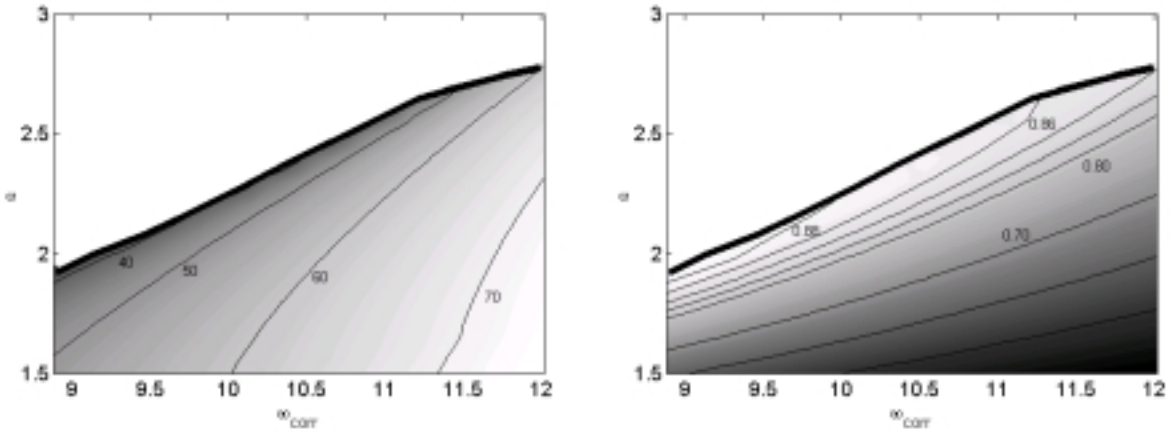

Figure 8.1: Compressor map showing dimensionless mass flow (left) and isentropic efficiency (right) as a function of dimensionless shaft speed ω_{corr} and pressure ratio ε.

The turbine map can be represented using exactly the same structure, as shown in figure 8.2. This is again not a normal representation, but it allows for a explicit calculation of output parameters.

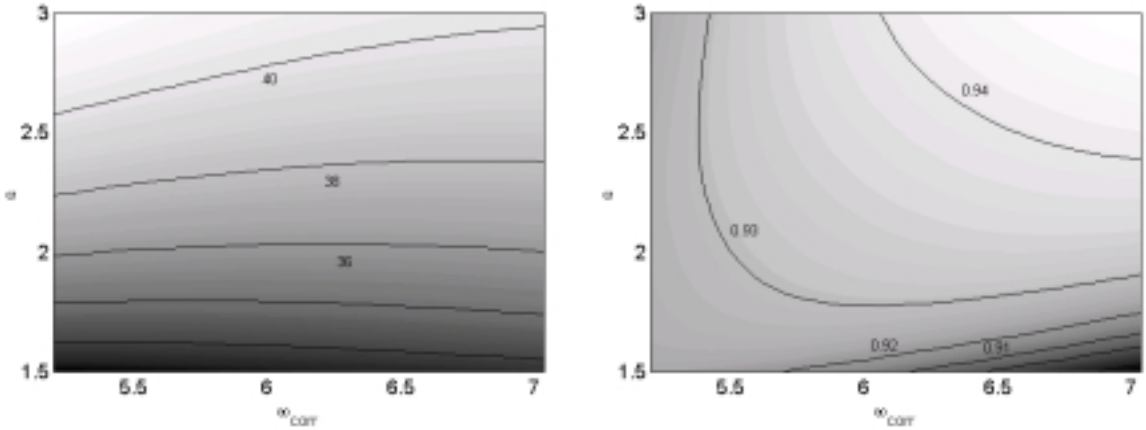

Figure 8.2: Turbine map showing dimensionless mass flow (left) and isentropic efficiency (right) as a function of dimensionless shaft speed ω_{corr} and pressure ratio ε.

In the blower and feedwater pump model, the mass flow is calculated from the dimensionless head, (which is known from the pressure difference) using the relations shown in figure 3.4 and 3.5. The temperature rise is neglected.

8.3.3 Valves

The flow through a valve is calculated from the upstream density and temperature, pressure difference and stem position VP. For a linear non-choking valve it is simply known from:

$$\phi_{\text{non choked}} = C_{f\,\text{open}}\ VP\ \sqrt{\rho\,\Delta p}$$

For a choking valve it is assumed that the flow area also varies linearly with stem position, figure 4.22 shows that this is approximately the case. In that case the choked flow can be calculated from:

$$\phi_{\text{choked}} = A_{f\,\text{open}}\ VP\ \rho\ v_{\text{sound}} \qquad v_{\text{sound}} = \sqrt{\kappa R T}$$

A common approximation (e.g. in the nuclear code RELAP (1995)) is to use $\phi_{\text{non choked}}$ unless it grows beyond ϕ_{choked}, in which case it is 'chopped off' at ϕ_{choked}:

$$\phi = \min(\phi_{\text{non choked}}, \phi_{\text{choked}})$$

From 5.19 it can be seen to that the error made by this approximation is not too large, it only yields an abrupt change.

8.3.4 Heat Exchangers

In the heat exchanger model the flows and outlet temperatures are calculated from the inlet and outlet pressure and temperatures. The mass flows are calculated from the momentum-balance which has been simplified to a pressure drop-flow relation by means of neglecting the inertia and all forces but friction losses. The friction loss factor e_v is proportional to the fanning friction factor which approximately scales with the negative fractional power -a of the Reynolds-number. This corresponds with a linearisation (on log-log scale) of e.g. figure 3.3. If the influence of change of viscosity with temperature is neglected, Re scales with $\phi/\phi_{\text{design}}$. This gives:

$$\phi = C_f\sqrt{\rho\,\Delta p} \qquad C_f = \frac{A}{\sqrt{2\,e_v}} \qquad e_v = C\,Re^{-a} \qquad C_f = C_{f\,\text{design}}\left(\frac{\phi}{\phi_{\text{design}}}\right)^{a/2}$$

Substitution yields:

$$\phi = \left[\left(\frac{C_f}{\phi^{a/2}}\right)_{\text{design}}\sqrt{\rho\,\Delta p}\right]^{\frac{1}{1-a/2}}$$

Due to the low residence time and the small heat capacity of the fluid compared to the wall in the gas-gas heat exchangers, the energy balance can be solved statically. The calculation of wall and fluid temperature profiles is illustrated in figure 8.3. The wall temperature is calculated in a number of nodes, shown with dots. At both ends, a negligible length and therefore also negligible heat capacity and heat transfer area of the wall is associated with the node. The wall is

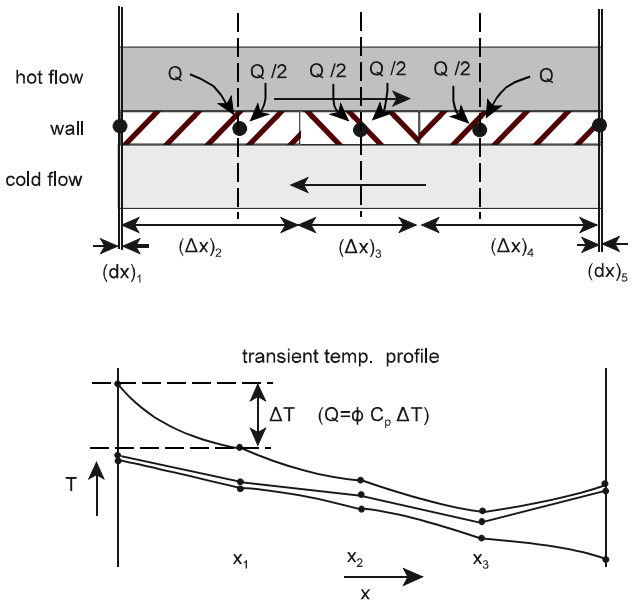

Figure 8.3: Heat exchanger discretisation.

further divided in a number of equi-distant nodes (here three, but any number is possible), the hatched areas in figure 8.3 show which part of the heat capacity is associated with each nodes. It can be seen that the first and the last centre nodes have a larger heat capacity than the other(s). Given the assumption of a linear temperature profile of the wall the energy balance of the fluid between the nodes becomes:

$$\phi C_p \frac{dT}{dx} = \frac{\alpha S}{L}(T_{wall}(x) - T) \qquad T_{wall} = T_{wall\ i} + \frac{x - x_i}{x_{i+1} - x_i}(T_{wall\ i+1} - T_{wall\ i})$$

Integration and application of boundary conditions gives:

$$T_{i+1} = T_{wall\ i} + \frac{\phi C_p}{\alpha S}(T_{wall\ i} - T_{wall\ i+1}) + \left(T_i - T_{wall\ i+1} + \frac{\phi C_p}{\alpha S}(T_{wall\ i} - T_{wall\ i+1}) \right) e^{-\frac{\phi C_p}{\alpha S}}$$

The energy input over the section between i and i+1 is of course known from:

$$Q_{i\ to\ i+1} = \phi C_p (T_{i+1} - T_i)$$

The end-nodes both have a negligible heat capacity and surface area, however, their ratio is the same as that of the complete heat exchanger. Therefore energy balance for the end-nodes using local gas temperatures using total the heat capacity and surface area is:

$$\frac{dT_{wall\ end}}{dt} = \frac{1}{(MC_p)_{steel}} \left((\alpha S)_{hot} (T_{hot\ end} - T_{wall\ end}) - (\alpha S)_{cold} (T_{wall\ end} - T_{cold\ end}) \right)$$

The energy-balance of the interior nodes is using the local wall heat capacity:

$$\frac{dT_{wall\ i}}{dt} = \frac{1}{(MC_p)_{steel\ i}} \left(c_1 Q_{i-1\ to\ i\ hot} - c_1 Q_{i-1\ to\ i\ cold} + c_2 Q_{i\ to\ i+1\ hot} - c_2 Q_{i\ to\ i+1\ cold} \right)$$

Generally, c_1 and c_2 are ½, however for the first and last interior node c_1 respectively c_2 is 1, which is apparent from fig. 8.1. M C_p of the first and last interior is also 1.5 times larger than those of the other nodes.

In literature a variation of the overall heat transfer with fractional power of the Reynolds-number is frequently assumed (MMS, 2000). However, this assumption no longer holds for a non-negligible heat resistance in the wall and extended surface. Since most heat exchangers in the plant under consideration have extended surface, a more precise alternative is used. Analogous to the frictional losses, the Stanton-number scales with $(\phi/\phi_{design})^{-b}$, under the assumption of negligible influence of temperature on viscosity and Prandtl-group. Consequently, the heat transfer coefficient of the fluid α_{fluid} varies with $(\phi/\phi_{design})^{1-b}$ and the (ml_{eff})-group introduced in the fin efficiency calculation (paragraph 3.1.2) varies with $(\phi/\phi_{design})^{(1-b)/2}$. The heat resistance in the wall R_{wall} is of course constant. The off-design heat transfer coefficient can be calculated from:

$$\alpha S = \frac{1}{R_{wall} + \frac{1}{\eta_{surf}\,\alpha_{fluid}\,S}} \qquad \eta_{surf} = 1 - \frac{S_{fin}}{S_{total}}\left(1 - \frac{\tanh(ml_{eff})}{ml_{eff}}\right)$$

$$ml_{eff} = (ml_{eff})_{design}\left(\frac{\phi}{\phi_{design}}\right)^{(1-b)/2} \qquad \alpha_{fluid} = \alpha_{fluid\ design}\left(\frac{\phi}{\phi_{design}}\right)^{(1-b)}$$

For the waterside in the economiser and the final cooler, the assumption of negligible heat capacity of the flow does not hold. In order to use the same approach, the heat capacity of the flow has been lumped together with the wall. For the fluid side this yields a response which is instantaneous, which is of course not a good approximation. However, the cooling water outlet temperature is not of interest at all and a correct prediction of the response of the economiser outlet temperature is not crucial.

The model has been validated with a transient in which the recuperator hot inlet temperature drops 300 °C and becomes lower than the cold side inlet temperature. Figure 8.4 shows the resulting hot and cold outlet temperatures of the recuperator for the full scale model and the simplified model with 3, 4, 5 and 10 wall nodes. In order to correctly simulate this transient with strong changes, a number of wall nodes over 5 should be used. In that case, the simplified model performances very well.

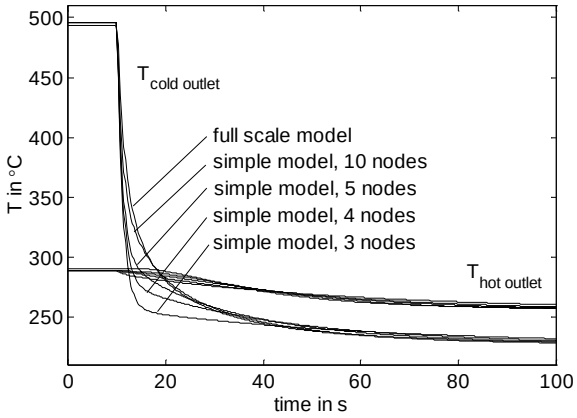

Figure 8.4: Recuperator response of the simplified model.

8.3.5 Steam Generator

In the analysis in paragraph 5.3 it was already concluded that the discretised waterside model of the steam generator with a number of empirical relations does not have a pronounced influence on the behaviour of outputs on input-changes. This is due to the fact that the resistance against heat flow lies almost solely at the helium side. If one is not interested in the internal variables, like velocities, steam fractions etc., a much simpler model of the drum, downcomer and evaporator is sufficient. Schoen (1993) formulated a combined mass- and energy balance for these three components, based on the state-variables saturated steam density ρ_G and liquid phase water volume V_l. The model assumes one mixed saturated water/steam mixture. All material properties needed are locally fitted using a fourth order polynomial in ρ_G. The temperature difference between the water and the wall is a fraction of a degree centigrade, therefore the liquid water mass has been enlarged with a constant term to take the thermal inertia of the steel mass into account.

$$\frac{d\rho_G}{dt} = \frac{1}{\Phi_2\Phi_3 - \Phi_1\Phi_4}\left(\Phi_3\left(\phi_{L\ in} - \phi_{G\ out}\right) - \Phi_1\left(\phi_{L\ in}h_{L\ in} - \phi_{G\ out}h_G + Q\right)\right)$$

$$\frac{dV_L}{dt} = \frac{1}{\Phi_1\Phi_4 - \Phi_2\Phi_3}(\Phi_4(\phi_{L\,in} - \phi_{G\,out}) - \Phi_2(\phi_{L\,in}h_{L\,in} - \phi_{G\,out}h_G + Q)$$

$$\Phi_1 = \rho_L - \rho_G \qquad \Phi_2 = V_{total\ corr} - V_L + V_L\frac{d\rho_L}{d\rho_G} \qquad \Phi_3 = u_L\rho_L - u_s\rho_G$$

$$\Phi_4 = (V_{total\ corr} - V_L)\left(\rho_G\frac{du_G}{d\rho_G} + u_G\right) + V_L\left(\rho_L\frac{du_L}{d\rho_G} + u_L\frac{d\rho_L}{d\rho_G}\right)$$

$$V_{total\ corr} = V_{drum} + V_{downcomer} + V_{evaporator} + \frac{M_{steel}\,C_{p\ steel}}{C_{p\ L\ water}\,\rho_{L\ water}}$$

In Schoen (1989) the water fraction in the evaporator is calculated. The model used here is further simplified by the assumption of a constant liquid water mass in the downcomer and evaporator. This of course is not the case but the changes in filling only have a short term effect on the drumlevel (see for example fig. 5.15: after 15 seconds the effect of a different distribution over the two phases of the evaporator and downcomer is negligible). Due to the strongly fluctuating nature of the level measurement such short term effects can not even be measured; in order to smooth the signal a filter with time-constant in the order of perhaps half a minute might be used. The drumlevel is calculated as:

$$L_{drum} = \frac{V_{L\ drum}}{A_{drum}} \qquad V_{L\ drum} = V_L - (V_{L\ downcomer} + V_{L\ evaporator} + \frac{M_{steel}\,C_{p\ steel}}{C_{p\ L\ water}\,\rho_{L\ water}})$$

The helium outlet temperature and consequently the transferred heat Q are calculated from the helium inlet temperature and the uniform wall temperature equal to the saturation temperature using the method introduced in paragraph 8.3.3.

The steam generator model has been tested by comparison of the responses of the high-order model of chapter 4 and the simplified model on a step-change of the helium inlet temperature. In order to use consistent boundary conditions the water inlet and steam outlet of the drum are ducted with a valve with a pressure drop of five bar. The helium mass flow is kept constant. The responses of the drum level, the pressure and the inlet and outlet flow are shown in figure 8.5. The dynamic behaviour is approximately correct, but the steady-state gains are clearly different. The reason for this error is that the step-responses of the simplified model are extremely sensitive to some parameters. Figure 8.5 also shows the response of the simplified model in case of a constant pressure drop for the helium side. This gives a mass flow which is 0.1% lower due to the decreased density at the higher inlet temperature. The resulting difference in gain of the step-responses is almost 10%! The reason is that the step-response is now a result of two input changes, a change of temperature and a change of flow. The magnitude of the effect of a 1% change in mass flow is approximately the same as a 1 K change of inlet temperature. This very high sensitivity makes it very difficult to tune the simplified model to the high-order model.

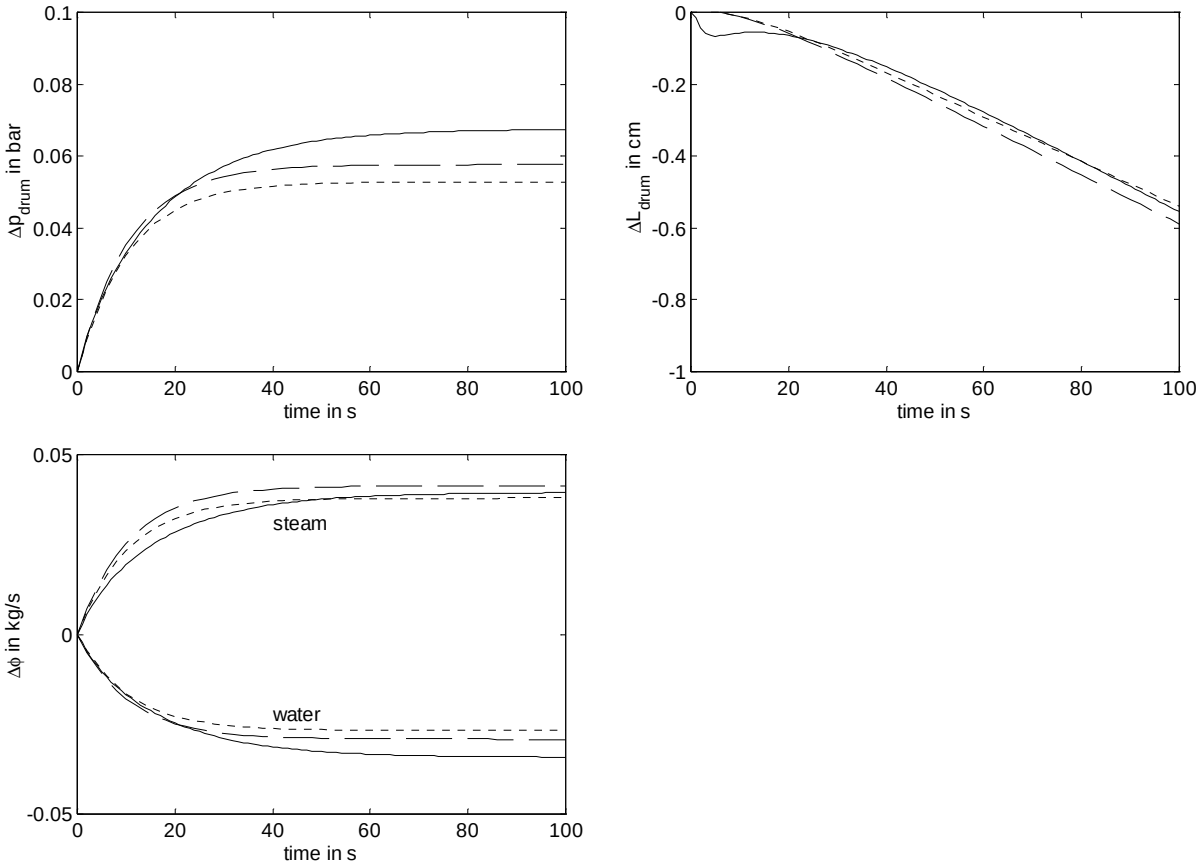

Figure 8.5: Response on 1 °C step in helium inlet temperature, drawn: high-order model, dotted: simplified model, constant mass flow, dashed: simplified model, constant pressure drop.

8.4 Balance-Of-Plant Model

The component models described above are implemented in so-called S-functions in Matlab. In Simulink they are combined to form a balance-of-plant model. The information flow in the model is clarified in figure 8.6. Some components are combined and represented by one model, because this allows for explicit calculation. This is shown by a dotted rectangle around the components. The combination of drum downcomer and evaporator is already discussed in paragraph 8.3.4. Because of the assumed incompressibility of water, the final cooler and cooling water valve are combined in one model. The series-connection yields a combined C_f:

$$C_{f\,total} = \sqrt{\frac{1}{\left(\frac{1}{VP\ C_{f\,valve\ open}}\right)^2 + \left(\frac{1}{C_{f\,hx}}\right)^2}}$$

If the variation of $C_{f\,hx}$ with flow is taken into account direct substitution into the flow-pressure drop relation is not feasible. Therefore first the flow is calculated using $C_{f\,hx} = C_{f\,hx\,design}$ and from that flow $C_{f\,hx}$ is corrected for the variation of the Reynolds-number. Subsequently a new flow is calculated. Three iterations of this kind are made to obtain the flow. This approximation is good enough, since a large deviation from the design flow can only be obtained by closing the valve, in which case the pressure drop over the heat exchanger is only of minor importance. The

feedwater pump, attemperation valve and economiser are also combined in one model because of the assumption of incompressible liquid water. The pressure drop over the economiser is negligible, therefore the pump flow can be calculated from the drum and deaerator pressure. Similarly, the attemperation valve flow is known from the drum and attemperator pressure. The economiser flow is the difference of these flows. In the deaerator the pressure is assumed constant at 3 bar, which makes the mass balance static. The return water flow is therefore calculated, which corresponds to the assumption of perfect control of the pressure with this flow.

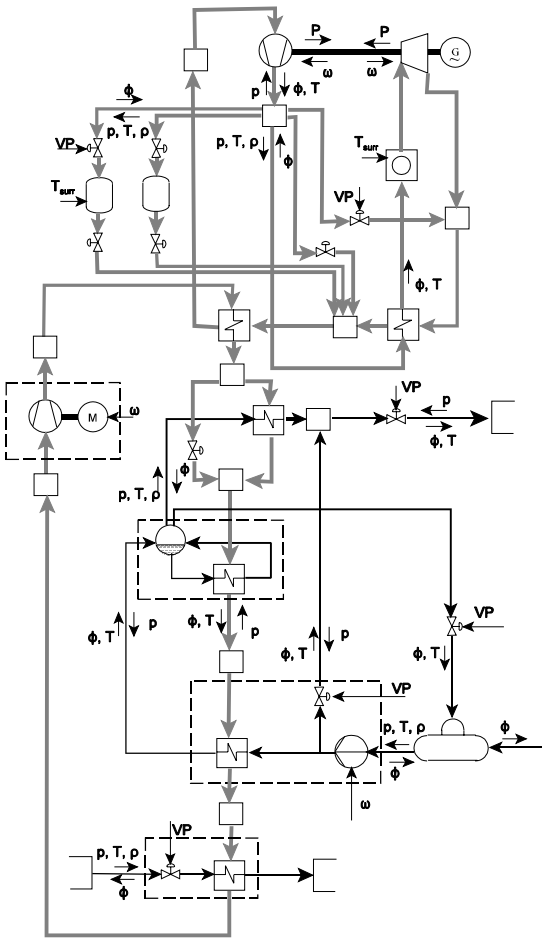

Figure 8.6: Structure of simplified model.

The Balance-Of-Plant model has also been tested by comparison of step responses of the high-order and simplified model. Because of the extreme sensitivity to a number of input parameters, no attempt has been done to tune the simplified model based on the step-responses. Figure 8.7 shows the step-responses of the most important input-output combinations of both models. The step responses are slightly different from those in figure 7.18, because of the different boundary conditions. For the transients in fig. 7.18 the return water valve position was fixed, and the deaerator pressure was uncontrolled. The simplified model assumes perfect control, so in order to make a fair comparison, the high-order model simulations were carried out with this pressure tightly controlled using the return water valve. As expected the steady-state gains do not exactly match, but the dynamic behaviour (time-constants and non-minimum phase behaviour) is correctly predicted by the simplified model. MPC algorithms tend to be fairly forgiving for errors of this magnitude in step-responses (otherwise control over a region of conditions with one linearised model, which is only correct in one working point, would always fail). When the model is used for online prediction it can be continuously corrected, for example by using an extended Kalman filter (Prasad, 2000).

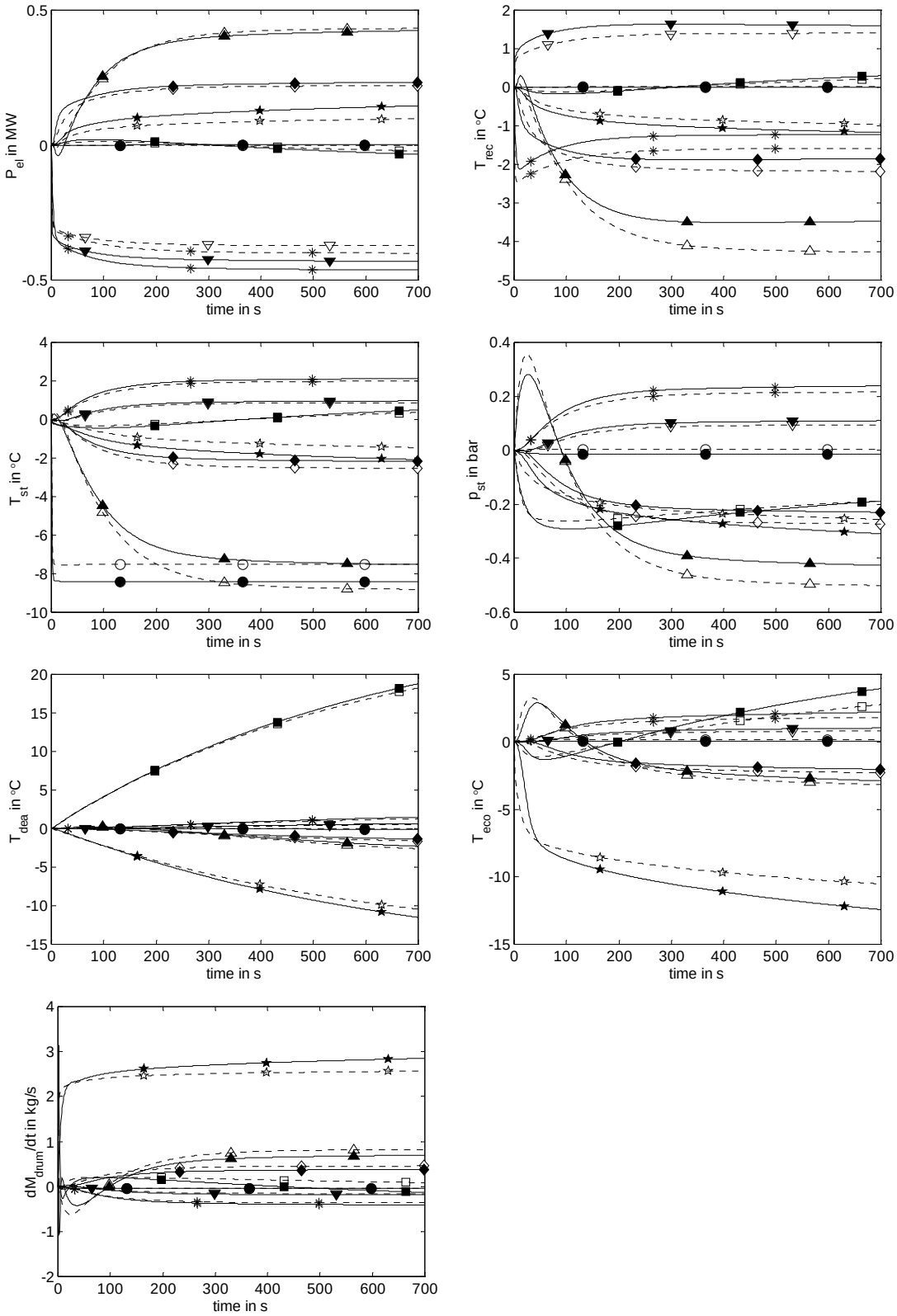

Figure 8.7: Step responses of: ✳ bypass valve two, ▼ bypass valve three, ▲ blower, ● attemperation valve, ★ feedwater pump, ■ deaerator valve, ♦ cooling valve, drawn lines and filled symbols: high-order model, dashed lines and open symbols: simplified model.

8.5 Conclusions

In this chapter, a simplified physical plant model has been constructed. A heat exchanger model especially fit for the high-efficiency gas-gas heat exchangers is developed. Tests show its good performance in modelling this type of heat exchangers with a coarse nodalisation. The Balance-Of-Plant model is robust and is capable of very quickly calculating operational transients. Its steady-state gains of step-responses are unfortunately very sensitive to certain parameters. The model is nevertheless fit for use in a model-based control scheme.

Chapter 9

Concluding Remarks

9.1 Conclusions

This thesis describes investigations into the modelling, design and control of a Nuclear Gas Turbine (NGT) plant for Combined Heat and Power (CHP) production. Four different plant wide models were developed and used to assist in the design and control of the plant.

With help of the thermodynamic model, the major design parameters were chosen. Based on the characteristics of CHP, it is decided that a direct, recuperated cycle without bottoming steam cycle is optimal for the NGT-plant for cogeneration. The plant should produce electricity and Industrial Steam (IS), or electricity and hot water for District Heating (DH). In order to separate the primary system and the high pressure water cycle, an intermediate high pressure helium system is introduced. The reactor power, pressure ratio mass flows and temperatures were optimised over the operational region of different heat-to-power ratios and power levels. In order to simplify the design, the reactor and primary cycle design were kept the same for both the IS and DH-cogeneration plant. The most striking difference with a non-cogenerating design is the fact that the compressor inlet flow is not cooled as far as possible. In order to obtain a substantial heat production of a certain quality, the temperature level of the waste heat of the primary cycle must be high. This is achieved with an elevated compressor inlet temperature. The primary system pressure is low compared to other designs for larger plants. This simplifies the turbo-machinery design. An often encountered assumption is that an elevated pressure increases the heat transfer in the reactor and the recuperator, but this is not the case. If one keeps the geometry of the heat exchanging equipment the same and one increases the pressure level, the only positive effect on the cycle efficiency is by means of the decreased pressure losses. A DH-cogeneration plant is favourable over a steam-coproducing plant. A cycle which has been optimised for electricity production only, gives a waste-heat flow which still can be used for water heating. On account of to the recuperator however, the heat-content of the recuperator hot outlet flow is too low to produce a decent amount of steam.

With use of a steady-state model, a preliminary design is produced. It can be concluded that a high efficiency can be obtained over a large operating region. By means of reduction of the pressure level one can operate at part-load with hardly altered gas velocities and thus constant turbo-machinery efficiency. The heat-to-power ratio can be changed by altering the compressor

inlet temperature.

In order to analyse the influence of design choices on the dynamic behaviour and to develop and test a control structure, a best-estimate dynamic code is developed. The level of detail of the code exceeds all previous attempts described in literature, except for the reactor neutronics. It has been proved that the point-kinetic approximation for neutronic calculations works excellent for the whole operational region of interest. Comparisons with analytical solutions and with simulations performed with the nuclear code RELAP show that the dynamic plant behaviour is predicted correctly over a wide range of conditions and at time scales varying from a fraction of a second to several days. The implicit formulation of the problems makes it possible not only to calculate the system behaviour from its design, but also to deduce the geometry needed to obtain the requested performance. For example, the compressor geometry is obtained by fixing its pressure ratio and a set of velocities through the compressor.

Investigations of the dynamic behaviour of different designs led to the conclusion that a single shaft configuration is preferred if one wants to apply an asynchronous generator. With a free-running power turbine, the generator speed would be very difficult to control due to the small influence of the power turbine speed on its power production. This is very different from the situation with an ordinary gas turbine. In that case the heat input (by means of fuel) can be regulated separately. In case of a nuclear heat source, the large thermal inertia of the reactor core, leads to a linear increase of heat input with mass flow. Another difference between a conventional turbine and the helium turbine is the fact that the latter operates far removed from choking. Therefore, a load rejection leads to a much higher mass flow and thus to a very high shaft speed. Alternatively, one could choke to turbine or compressor outlet flow and reduce the overspeed in this passive manner.

The thermal inertia of the reactor is so large that the influence of its dimensions on the dynamic behaviour is hardly visible. During short term transients the outlet temperature is virtually constant, while during long term transients the xenon effects are dominant. A strong negative temperature coefficient is shown to be not only favourable from a safety point of view, it also reduces temperature variations during off-design operation and is as such beneficent to the reduction of creep due to operation at elevated temperatures.

Unlike previous NGT plants, the helium inventory of the primary system is so small that the dynamics associated with the redistribution of high and low pressure plenums are very fast compared to the mechanical shaft dynamics. The small inventory also allows for quick adjustments using the inventory control system.

The dynamic model has also been used to assess the effect of various control options. In most previous designs a bypass valve in a high temperature environment is used for speed or power control. It was found that a valve at another position in the flowsheet, operating at much lower temperatures, gives the same performance. Control with throttle valves instead of bypass valves is also feasible. Two disadvantages are the pressure losses even when the valve is fully opened and the comparatively high temperature changes in the recuperator. The main advantage is the unchanged heat transport to the secondary cycle, which simplifies the control of the quality and quantity of heat delivered.

The optimal working conditions were also be established using the dynamic model. Then the pairing of controlled and manipulated variables was investigated using Relative Gain Analysis. The NGT-DH can easily be controlled with two SISO control loops. The NGT-IS plant shows a lot of interaction between the control loops, strong non-linearities in the process and non-minimum phase behaviour which seriously complicates the control system design. Nevertheless, the distributed control system was capable of following both heat and power demand with acceptable deviations from the set-points.

A dynamic model can not only be used to develop and test a control structure, it can also serve as an online estimator of the plant behaviour, integrated in the control scheme. This calls for a robust model, which allows for fast calculation. Such a model has been developed in the last chapter. The model is developed from first principles but highly simplified compared to the high-order dynamic model, in order to allow for explicit calculation with a minimum number of states. Because of the use of an analytical solution, the high-efficiency gas-gas heat exchanger can be modelled with a very coarse discretisation. The results of the simplified model are similar to those of the high-order model, but their final gains are not exactly the same. Luckily, model-based control schemes tend to be forgiving for this type of discrepancy.

Overall, it can be concluded that the NGT plant is technically well suited for combined heat and power production. The plant can quickly follow widely different heat and power demands, with a high efficiency. This can be achieved with a simple design and control system. Moreover, the economic investment can easily be protected against failure through thermal stress or load rejections.

9.2 Recommendations

The dynamic model can easily be adapted to simulate the transient behaviour of conventional power plants. Thermodynamic properties of air, fuel and off-gas have to be implemented, this work is currently underway. The level of detail of the compressor and the turbine model make it a useful tool for preliminary designs. A model dedicated to axial compressors is also under construction. In future, a radial turbine model and simple combustion chamber model could be added, so that a complete conventional gas turbine can be modelled.

Boiling instabilities as they can occur in a boiling water reactor, could also be studied, using the detailed description of the natural circulation evaporator. Addition of a moving boundary formulation for the transition from liquid water to a water/steam mixture would improve the capabilities in this field.

The model described in the last chapter is intended for use in an online optimising control structure. This method should be implemented and tested in future. The scheme could use the non-linear model for calculation of the free response (response following current initial conditions and no future control moves), while a locally linearised model could be used for the optimisation step. This is expected to give better performance than the distributed control system. Moreover, it should be easier to tune the control system to specific demands, like e.g. minimisation of thermal stresses.

References

- Adams, R., Adams Atomic Engines, Inc., U.S. Patent number 5,309,492, 1994, USA.
- Agazzani, A. et al., An Assessment of the Performance of Closed Cycles With and Without Heat Rejection at Cryogenic Temperatures, Journal of Engineering for Gas Turbines and Power, Vol. 121 No. 3, July 1999, USA.
- Anderson, J.D., Computational Fluid Dynamics, 1985, New York, USA.
- Aspen Custom Modeler 10.1 User Manual, 1999, Cambridge MA, USA.
- Attia, M.S., Development of Axial Compressor and Turbine Simulation Modules for Integration into the Dynamic Simulation Code GETRAN, May 1998, Texas, USA.
- Bammert, K, A General Review of Closed-Cycle Gas Turbines Using Fossil, Nuclear and Solar Energy, 1975, München, Germany.
- Bammert, K, Operating Experiences and measurements on Turbo Sets of CCGT-Cogeneration Plants in Germany, ASME paper, No. 86-GT-101, 1986.
- Bammert, K. and G. Krey, Dynamic Behaviour and Control of Single-Shaft Closed-Cycle Gas Turbines, Journal of Engineering for Power, Vol. 93, No.4, October 1971.
- Bammert, K. and H. Pösentrup, Das Verhalten einer geschlossenen Gasturbine bei Zeitlich veränderlichen Betriebszuständen, VDI-Forschungsheft 588, 1978.
- Bammert, K. and H. Pösentrup, The Behavior of a Closed-Cycle Gas Turbine with Time Dependent Operating Conditions, Journal of Engineering for Power, Vol. 102, No. 3, July 1980.
- Bammert, K. and P. Zehner, Back flow Characteristics of Turbine Cascades, Atomkernenergie, Vol. 24, No. 4, 1974.
- Bammert, K. and P. Zehner, Measurements of the Four-Quadrant Characteristics on a Multi-Stage Turbine, Journal of Engineering for Power, Vol. 102, No. 2, 1980.
- Bammert, K. et al., Nuclear Power Plants with Closed-Cycle Helium Turbine for Industrial Energy Supply, Journal of Engineering for Power, Vol. 93 No. 1, January 1971, USA.
- Bardia, A., Dynamics and Control Modeling of the Closed-Cycle Gas Turbine (GT-HTGR) Power Plant, in: Katz, E.M., Proceedings of the Fourth Power Plant Dynamics, Control and Testing Symposium, March 1980, Tennessee, USA.
- Barnert, H. and J. Singh, Future Applications of HTR: Electricity Production and Process Heat Applications, Proceedings of the IAEA Technical Committee Meeting, November 1994, Petten, the Netherlands.
- Barnert, H. and K. Kugeler, HTR Plus Modern Turbine Technology for Higher Efficiencies, Proceedings of the IAEA Technical Committee Meeting, October 1995, Bejing, China.
- Bean, H.S., Fluid Meters, Their Theory and Application, 1971, New York, USA.
- Bedenig, D., Gasgekühlter Hochtemperaturreaktoren, January 1972, München, Germany.

- Bergeron, L., Sy Coup de Bélier en Hydraulique au Coup de Foudre en Electricité, 1908, Paris, France.
- Biegler, L.T., I.E. Grossmann and A.W. Westerberg, Systematic Methods of Chemical Process Design, 1997, Upper Saddle River, USA.
- Biesenbach, R.,Untersuchungen zum Instationären Verhalten eines Geregelten HTR-Modul-Kraftwerks, June 1995, Jülich, Germany.
- Bird, R.B., Stewart, W.E. and Lightfoot, E.N., Transport Phenomena, 1960, Madison, USA.
- Bloch, G.S. and W.F. O'brien, A Wide-range Axial-Flow Compressor Stage Performance Model, ASME paper, No. 92-GT-58, 1992.
- Bourne, J.A., Two-Phase Flow Models: the Closure Issue, in: Hewitt, G.F., Delhaye, J.M. and Zuber N., Multiphase Science and Technology, Vol 3, 1987, USA.
- Carter, P. et al., Failure Analysis and Life prediction of a Large, Complex Plate Fin Heat Exchanger, Engineering Failure Analysis, Vol. 3, No. 1, 1996.
- Casey, M.V. and F. Marty, Centrifugal Compressors - Performance at Design and Off-Design, The Proceedings of the Institute of Refrigeration, Vol. 82, 1986, Surrey, UK.
- Cohen, H., G.C.F. Rogers and H.I.H. Saravanamuttoo, Gas Turbine Theory, 1996, London, UK.
- Collier, J.G. and J.R. Thome, Convective Boiling and Condensation, 1994, Oxford, UK.
- Crawford, R.A. and A.E. Burwell, Quantitive Evaluation of Transient Heat Transfer on Axial Flow Compressor Stability, AIAA Paper, No. 85-1352, July 1985.
- Dalbert, P. et.al., Development, Testing and Performance Prediction of Radial Compressor Stages for Multi-Stage Industrial Compressors, ASME paper, No. 88-GT-34, 1988.
- Davis, M.W. Jr and W.F. O'Brien, Stage-by-Stage Post Stall Compression System Modeling Technique, Journal of Propulsion, Vol. 7, No. 6, Nov 1991.
- Davis, W.K., Energy and the Environment, Chemical Engineering Progress, Vol. 86, No. 7, July 1990, New York, USA.
- Douglas, J.M., The Conceptual Design of Chemical Processes, 1988, New York, USA.
- Drbal, L.F. et al., Power Plant Engineering, 1996, New York, USA.
- Duderstadt, J.J. and L.J. Hamilton, Nuclear Reactor Analysis, 1976, New York, USA
- El-Hinnawi, E.E., Review of the Environmental Impact of Nuclear Energy, IAEA Bulletin, Vol. 20, No. 2, 1978, Vienna, Austria.
- Fox, R.M. and A.T. McDonald, Introduction to Fluid Dynamics, 1994, New York, USA..
- Gal, P., Vergelijking van HTGR CCGT-Systemen op Basis van Economische en Rendementsbeschouwingen, TUD EV-report, EV-1990, August 1998, Delft, The Netherlands.
- Gao, Z. et al., Investigation of GT-ST Combined Cycle in HTR-10 Reactor, Proceedings of the IAEA Technical Committee Meeting, October 1995, Bejing, China.
- Garcia, C. and M. Morari, Model Predictive Control: Theory and Practice - a Survey, Automatica, Vol. 25 No. 3, 1989.
- Garrard, G.D., ATEC: The Aerodynamic Turbine Engine Code for the Transient and Dynamic Gas Turbine Engine System Operations, August 1995, Knoxville, USA.
- General Atomic, GT-MHR, conceptual design description report, January 1995, San Diego, USA.
- Gravdahl, J.T. and O. Egeland, Compressor surge and rotating stall : modeling and control, 1999, London, UK.
- Greitzer, E.M., Surge and Rotating Stall in Axial Flow Compressors Part I: Theoretical

Compression System Model, Journal of Engineering for Power, Vol. 98, No. 2, April 1976.
- Greitzer, E.M., Surge and Rotating Stall in Axial Flow Compressors Part I: Theoretical Compression System Model, Journal of Engineering for Power, Vol. 98, No. 2, April 1976.
- Halzl, J. et al., Application of the HTGR-CCGT System in Dual-Purpose Nuclear-Power Plants, Proceedings of the IAEA Symposium on Nuclear Desalination, November 1968, Madrid, Spain.
- Heek, A.I. van, ed. (a), INCOGEN Pre-Feasibility Study, Nuclear Cogeneration, PINK-rapport, April 1997a, Petten, the Netherlands.
- Heek, A.I. van, et. al. (b), Influence of Power Level and Fuel Type on Safety and Economy of the Simplified Pebble Bed HTR Concept, Proceedings of the IAEA Technical Committee Meeting, November 1997, Petten, the Netherlands.
- HHT-project Ergebnisse der Entwicklung und Planung des Hochtemperaturreaktors mit Heliumturbine von 1969 bis 1982, March 1994, Germany.
- Hicks, T.G., Power Plant Evaluation and Design Reference Guide, 1986, New York, USA.
- Japikse, D., Centrifugal Compressor Design and Performance, 1996, Vermont, Canada.
- Kays, W.M. and A.L. London, Compact Heat Exchangers, 1985, USA.
- Kikstra, J.F. , B. Roffel and P. Schoen, Model Predictive Control of a Combined Heat and Power Plant Using Local Linear Models, Journal of Engineering for Gas Turbines and Power, Vol. 120, No. 4, 1998.
- Kikstra, J.F., and A.H.M. Verkooijen, Dynamic Modelling of a Cogenerating Nuclear Gas Turbine Plant for Control System Design, Proceedings of the 10th International Conference on Emerging Nuclear Energy Systems, 2000, Petten, the Netherlands.
- Kikstra, J.F., E's Overnight van Mogelijke HTGR-GT Systemen voor Produktie van Elektriciteit en Warmte, ECN report, ECN-I-97-045, 1997, Petten, the Netherlands.
- Knief, R.A., Nuclear Engineering, 1992, Mechanicsburg, USA.
- Kreshman, H. et. al., Modelling an Simulation of the Dynamic Behaviour of a Stationary Gas Turbine, in: Tsafestas, S. et.al., Parallel and Distributed Computing in Engineering Systems, 1992, The Netherlands.
- Kugeler, K. and R. Schulten, Hochtemperaturreaktortechnik, 1989, Berlin, Germany.
- Kuljian, H.A., Nuclear Power Plant Design, 1968, New York, USA.
- Kullmann, B.A. and M.L. Dams, Development of an Engineering Simulator as a Design Tool for the Pebble Bed Modular Reactor, in: Ades, M., Simulators International XIV, Proceedings of 1997 Simulation Conference, April 1997, Atlanta, USA.
- Larjola, J., Transient Simulation of Gas Turbines Including the Effects of Heat Capacity of the Solid Parts, 1982, Otaniemi, Finland.
- Li, K.W., and A.P. Priddy, Power Plant System Design, 1985, New York, USA.
- Lidsky, L.M. and X.L. Yan, Modular Gas-Cooled Reactor Gas Turbine Power Plant Designs, Proceedings of the 2nd JAERI Symposium on HTGR Technologies, October 1992, Ibaraki, Japan.
- Lidsky, L.M. et al., A Direct-Cycle Gas Turbine Power Plant for Near-Term Application: MGR-GT, Proceedings of the 10th International HTGR Conference, September 1988, San Diego, USA.
- Lidsky, L.M., Overview of Gas Turbine Cycles and Technology, Proceedings of the International Workshop on the Closed-Cycle Gas-Turbine Modular High-Temperature Gas-Cooled Reactor, June 1991, Cambridge MA, USA.
- Liebenberg, L., Power Conversion Unit for the SA Direct Cycle HTGR, Proceedings of the

IAEA Technical Committee Meeting, November 1996, Johannesburg, SA.
- Lu, S. and B. Wilson, On-line Stress Calculation and Life Monitoring Systems for Boiler Components, Transactions of the Institute of Measurement and Control, Vol. 20, No. 1, 1998.
- Maciejowski, J.M., Multivariable Feedback Design, 1989, Wokingham, UK.
- Marks, L.S., Mechanical Engineers' Handbook, 1951, London, UK.
- MATLAB manual, 1992, Natick MA, USA.
- McDonald, C.F. (a), The Key Role of Heat Exchangers in Closed Brayton Cycle Gas Turbine Power Plants, ASME-paper, 1996.
- McDonald, C.F. (b), The Indirect Cycle - A Logical and Practical Nuclear Gas Turbine Power Plant Concept, ASME-paper, 1996.
- McDonald, C.F., Enabling technolologies for Nuclear Gas turbine (GT-MHR) Power Conversion System, ASME-paper, No. 94-GT-415, 1994.
- McDonald, C.F., Gas Turbine Power Plant Possibilities with a Nuclear Heat Source - Closed and Open Cycles, ASME-paper, No. 90-GT-69, 1990.
- McDonald, C.F., The Nuclear Gas Turbine - Towards Realization after Half a Century of Evolution, ASME-paper, No. 95-GT-262, 1995.
- Miedema. J.A., Cycle: a General Computer Code for Thermodynamic Cycle Computations-Studies of Cogeneration in District Heating Systems, 1981, Delft, the Netherlands.
- MMS, User Manual Release 5.1, 2000, Lynchburg, USA.
- Morari, M. and J.H. Lee, Model Predictive Control: Past, Present and Future, Computers and Chemical Engineering, Vol. 23 No. 4-5, May 1999.
- Morse, F.T., Power Plant Engineering and Design, 1946, New York, USA.
- Münzberg, H.G. and J. Kurzke, Gasturbinen-Betriebsverhalten und Optimierung, 1977, Berlin, Germany.
- Nakaoka, T. et al., Evaluation of Fatigue Strength of Plate-Fin Heat Exchanger under Thermal Loading, Proceedings of the ASME International Conference on Pressure Vessel Technology, Vol. 1, 1996.
- Nicholls, D.R., Eskom Sees a Nuclear Future in the Pebble Bed, Nuclear Engineering International, December, 1998.
- O'Brien, W.F., Dynamic Simulation of Compressor and Gas Turbine Performance, AGARD Lecture Series 183-5, Steady and Transient Performance Prediction of Gas Turbine Engines, 1992.
- Op het Veld, R. and J.P. van Buijtenen, An Empirical Approach to the Preliminary Design of a Closed Cycle Gas Turbine, ASME paper, No. 98-GT-393, 1998, USA.
- Op het Veld, R. and J.P. van Buijtenen, An Empirical Approach to the Preliminary Design of a Closed Cycle Gas Turbine, ASME paper, No. 98-GT-393, 1998, USA.
- Oppe, J. et al., Panthermix (Panther-thermix) User Manual, ECN Report ECN-I-98-019, 1997, Petten, the Netherlands.
- Pantell, K., Versuche über Scheibenreibung, Forschung auf dem Gebiete des Ingenieurswesens, Vol. 16, No. 4, 1949.
- PANTHER Reference Manual, Nuclear Electric Technology Division.
- Patankar, S.V., Numerical Heat Transfer and Fluid Flow, 1980, Washington, USA.
- Perry, R.H. et. al., Perry's Chemical Engineers' Handbook, 1973, New York, USA.
- Pool, E.B., Friction Area and Nozzle Area for Valves and Fittings As New All-purpose Flow Parameters, in: Lyons, J.L., Lyons' Valve Designer's Handbook, 1982, New York, USA.
- Prasad, M. et al., Plant-wide Predictive Control for a Thermal Power Plant Based on a

Physical Plant Model, Control Theory and Applications, Vol. 147 No. 5, September 2000.
- Rauhut, K.H., Bruchstörfallrechnungen Gasgekühlter Kernreaktoranlagen, July 1982, Aachen, Germany.
- Ray, A., Dynamic Modelling of Power Plant Turbines for Controller Design, Applied Mathematical Modelling, Vol. 4, April 1980.
- RELAP, Code Manual RELAP 5 /Mod 3, June 1995, Idaho, USA.
- Sanokawa, K., et al., Status of HTGR Development Program in Japan, Proceedings of the IAEA Technical Committee Meeting, November 1997, Petten, the Netherlands.
- Schiesser, W.E., The Numerical Method of Lines, 1991, San Diego, USA.
- Schobeiri, T. and M. Abouelkheir, Row-by-Row Off-Design Performance Calculation Method for Turbines, AIAA Journal of Propulsion and power, Vol. 8, No. 4, July 1992.
- Schobeiri, T. et. al., GETRAN: A Generic, Modularly Structured Computer Code for Simulation of Dynamic Behavior of Aero- and Power Generation Gas Turbine Engines, Journal of Engineering for Gas Turbines and Power, Vol. 116, No. 3, July 1994.
- Schoen, P., Dynamic Modeling and Control of integrated Coal Gasification Combined Cycle Units, September 1993, Delft, The Netherlands.
- Schoen, P., Vereenvoudigd Niet-Lineair Dynamisch Model voor Kolengestookte Wervelbedketels, TUD EV-report, EV-1510, Januari August 1989, Delft, The Netherlands.
- Schoene, T.W. et al., The Gas Turbine HTGR Plant - Economical Dry Cooling or a Wet-Cooled high Efficiency Binary Configuration, Proceedings of the 37th American Power Conference, 1995, Chicago, USA.
- Schröder, B. et. al., Research on SiC-coatings for Graphite Surfaces in HTRs, Proceedings of the OECD/NEA Workshop, November 1997, Petten, the Netherlands.
- Simon, U., Der Radialverdichter bei Rükwärtsdurchströmung, Brennstof-Wärme-Kraft, Vol. 20, No. 7, July 1958.
- Singh, J. Heat Transfer Fluids and Systems for Process and Energy Applications, 1985, New York, USA.
- Smith, E.S.C. et al., Applied Atomic Power, 1947, London, UK.
- Stephanopoulos, G., Chemical Process Control, an Introduction to Theory and Practice, 1984, New Jersey, USA.
- Streeter, V.L. and E.B. Wylie, Fluid Mechanics, 1987, New York, USA.
- Streeter, V.L. and E.B. Wylie, Hydraulic Transients, 1967, New York, USA.
- Traupel, W., Thermische Turbomachinen, 1982, Zürich, Switzerland.
- Vavra, M.H., Basic Elements for Advanced Design of Radial-Flow Compressors, 1960, California, USA.
- Veen, W. van der, personal communication, 1997, Arnhem, the Netherlands.
- Verkerk, E.C., Dynamics of the Pebble-Bed Nuclear Reactor in the Direct Brayton Cycle, 2000, Petten, the Netherlands.
- VSOP (‘94) Computer Code System for Reactor Physics and Fuel Cycle Simulation, Input Manual and Comments, April 1994, Jülich, Germany.
- Wagner, W. and A. Kruse, Properties of Water and Steam, IAPWS-IF97, 1998, Berlin, Germany.
- Wees, F.G.H. van, et. al., GEIN-studie: Grootschalige Energieopwekking in de Industrie, ESC-35, October 1986, the Netherlands.
- Whalley, P.B., Boiling Condensation and Gas-Liquid Flow, 1987, New York, USA.

- Woudstra, N., Exergie interessant bij beoordeling warmte/kracht, Mechanische Technologie, June 1993, the Netherlands.
- Xu, Y. and Y. Sun, Status of HTR Programme in China, Proceedings of the IAEA Technical Committee Meeting, November 1997, Petten, the Netherlands.
- Yan, X.L. and L.M. Lidsky, Design Study for an MHTGR Gas Turbine Power Plant, Proceedings of the 53rd American Power Conference, April 1991, Chicago, USA.
- Yan, X.L. and L.M. Lidsky, HTR-GT Nuclear Cogeneration, Conceptual Design of the HTGR Gas Turbine Cogeneration Plant, April 1996, Cambridge MA, USA.
- Yan, X.L., Dynamic Analysis and Control System Design for an Advanced Nuclear Gas Turbine Power Plant, May 1990, Cambridge MA, USA.
- Zee, G.A. van and O.H. Bosgra, The Use of Realization Theory in the Robust Identification of Multivariable Systems, Proceedings of the fifth IFAC Symposium on Identification and Parameter Estimation, 1979, Darmstadt, Germany.
- Zehner, P., Vier-Quadranten Charakeristik einer Turbinenstufe, Atomkernenergie, Vol. 32, No. 4, 1978.
- Zehner, P., Vier-Quadranten Charakeristiken Mehrstufiger Axialer Turbines, Fortschritt-Berichte der VDI Zeitschriften Reihe 6, No. 75, 1980.
- Zhang, Z. and Z. Jiang, Design of Indirect Gas Turbine Cycle for a Modular High Temperature Gas Cooled Reactor, Proceedings of the IAEA Technical Committee Meeting, October 1995, Bejing, China.

Appendix A

Heat Exchanger Data

For the plate-fin strip-fin heat exchangers, a number of identical modules is used. The hot and cold side geometry of the modules are identical. The geometry-data of a module and heat transfer and friction correlations are given in table A.1 and figure A.1.

Table A.1: Recuperator module data.

L_{flow}	0.85 m
$A_{frontal}$	0.903 m^2
M_{core}	894 kg
l_{fin}	3.24 mm
δ_{fin}	0.1 mm
δ_{wall}	0.5 mm
β	1803 m^2/m^3
σ	0.42
S_f/S	0.85
D_e	2.11 mm

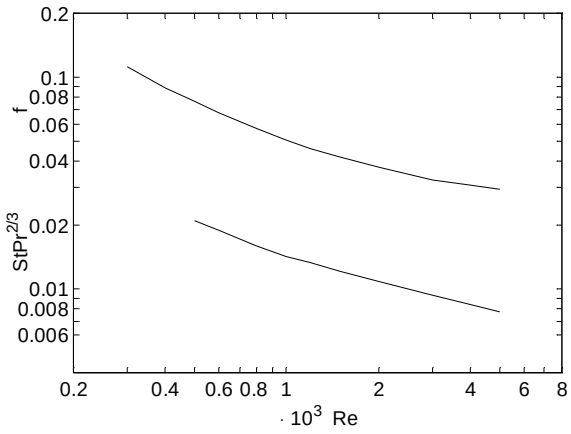

Figure A.1: St $Pr^{2/3}$ and f versus Re for the plate-fin strip-fin heat exchanger.

For finned tube banks, the contraction σ, specific area β, area ratio S_f/S and equivalent hydraulic diameter D_e of the shell and tube side can be calculated from longitudinal, transversal and fin pitch (x_{long}, x_{trans}, x_{fin}) and tube and fin diameter and thickness (d_{outer}, d_{fin}, δ_{wall}, δ_{fin}) by considering a unit cell as shown in figure A.2.

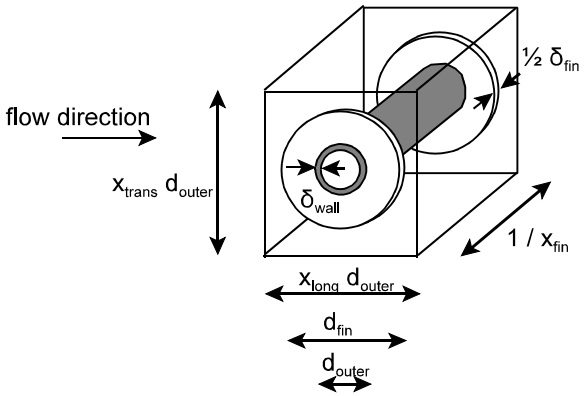

Figure A.2: Finned tube bank unit cell.

For the shell-side applies:

$$S_{fin\ u} = 2\frac{\pi}{4}(d_{fin}^2 - d_{outer}^2) \qquad S_{tube\ u} = (\frac{1}{x_{fin}} - \delta_{fin})\pi d_{outer}$$

$$V_u = \frac{1}{x_{fin}} x_{long} x_{trans} d_{outer}^2 \qquad S_u = S_{fin\ u} + S_{tube\ u}$$

$$\left(\frac{S_f}{S}\right) = \frac{S_{fin\ u}}{S_u} \qquad \beta_{shell} = \frac{S_u}{V_u} \qquad A_{contr\ u} = A_{frontal\ u} - A_{bank\ u}$$

$$A_{frontal\ u} = \frac{1}{x_{fin}} x_{trans} d_{outer} \qquad A_{bank\ u} = (\frac{1}{x_{fin}} - \delta_{fin}) d_{outer} + \delta_{fin} d_{fin}$$

$$\sigma_{shell} = \frac{A_{contr\ u}}{A_{frontal\ u}} \qquad D_e = \frac{4 A_{contr\ u} x_{trans} d_{outer}}{S_u}$$

And for the tube-side:

$$\sigma_{tube} = \frac{\pi d_{inner}^2}{4 x_{long} x_{trans} d_{outer}^2} \qquad \beta_{tube} = \frac{\pi d_{inner}}{x_{long} x_{trans} d_{outer}^2} \qquad d_{inner} = d_{outer} - 2\delta_{wall}$$

Now L, A and S of both shell and tube side can be related to the no. of baffles and passes ($N_{baffles}$, N_{passes}) as indicated in figure A.3, and shell length and diameter (l_{shell}, d_{shell}):

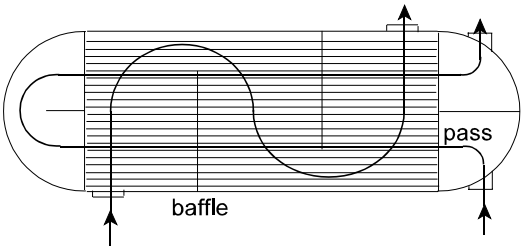

Figure A.3: Tube & shell heat exchanger with two passes and two baffles.

$$L_{tube} = l_{shell} N_{passes} \qquad L_{shell} = (N_{baffles} + 1) d_{shell}$$

$$A_{tube} = \sigma_{tube} \frac{\pi}{4} \frac{d_{shell}^2}{N_{passes}} \qquad A_{shell} = \sigma_{shell} d_{shell} \frac{l_{shell}}{N_{baffles} + 1}$$

$$S_{tube} = \beta_{tube} \frac{\pi}{4} d_{shell}^2 l_{shell} \qquad S_{shell} = \beta_{shell} \frac{\pi}{4} d_{shell}^2 l_{shell}$$

Finally, the mass of the tube-bank M_{bank} can be calculated using:

$$V_{fin\ u} = \delta_{fin}\frac{\pi}{4}(d_{fin}^2 - d_{outer}^2) \qquad V_{pipe\ u} = \frac{1}{x_{fin}}\frac{\pi}{4}(d_{outer}^2 - d_{inner}^2)$$

$$V_u = \frac{1}{x_{fin}} x_{long} x_{trans} d_{outer}^2 \qquad V_{hx} = l_{shell}\frac{\pi}{4} d_{shell}^2$$

$$M_{bank} = \frac{V_{fin\ u} + V_{pipe\ u}}{V_u} V_{hx}\rho_{steel}$$

The relations for non-finned tubes can be deducted from these finned tube-relations.

The data of the two bank geometry which are used are given in table A.2, and the heat-transfer and friction characteristics are given in figure A.4 to A.6.

Table A.2: Tube bank data.

	staggered tube bank	finned tube bank
δ_{wall}	2.5 mm	2.5 mm
d_{outer}	2.6 cm	2.6 cm
x_{trans}	1.5	1.9
x_{long}	1.25	2
x_{fin}		346 fins/m
δ_{fin}		0.3 mm
d_{fin}		4.4 cm

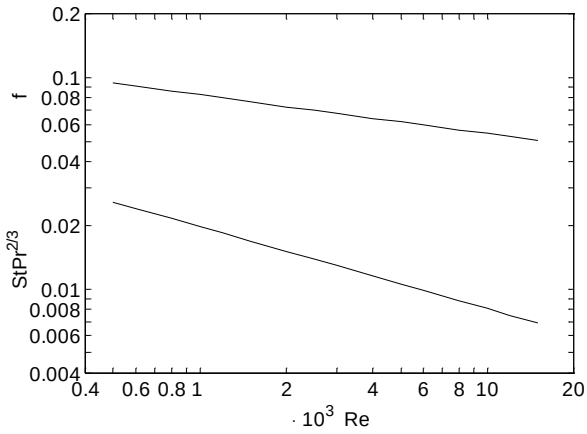

Figure A.4: St $Pr^{2/3}$ and f versus Re for the staggered tube bank.

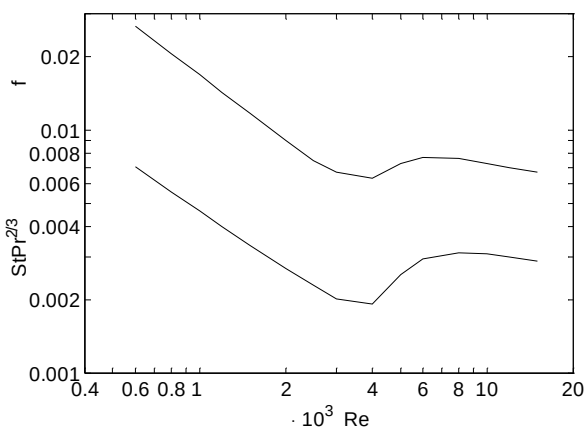

Figure A.5: St $Pr^{2/3}$ and f versus Re for the tube side.

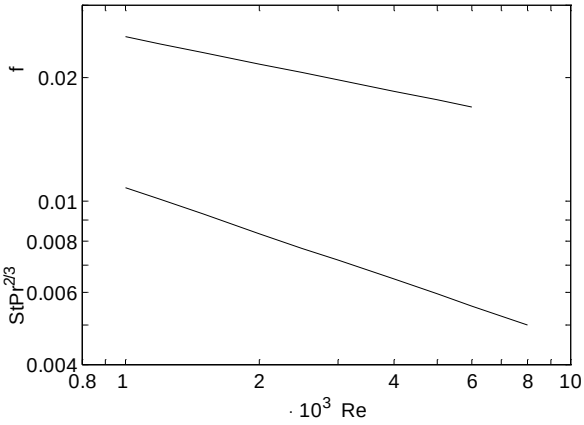

Figure A.6: St $Pr^{2/3}$ and f versus Re for the finned tube bank.

Appendix B

Turbo-Machinery Data

The compressor-design is based on a method published by Vavra (1960). The five congruent stages all have an axial inlet and radial impeller outlet velocity of 150 m/s. The impellers have twenty backswept blades with an angle of 32 ° and a ratio $r_{eye\ outer}/r_{imp}$ of 0.6. With a constant impeller radius of 0.399 m, the pressure ratio of 2.3 is achieved. The diffuser inlet is square and has a diffusion angle γ_{diff} of 5 °. Its length is chosen such that it decelerates the velocity to 150 m/s. The volute bends have a ratio of 2.5 for r_{bend}/b yielding minimal friction losses. 20 deswirl blades with a thickness/chord ratio of 0.25 are used to redirect the flow in the next impeller.

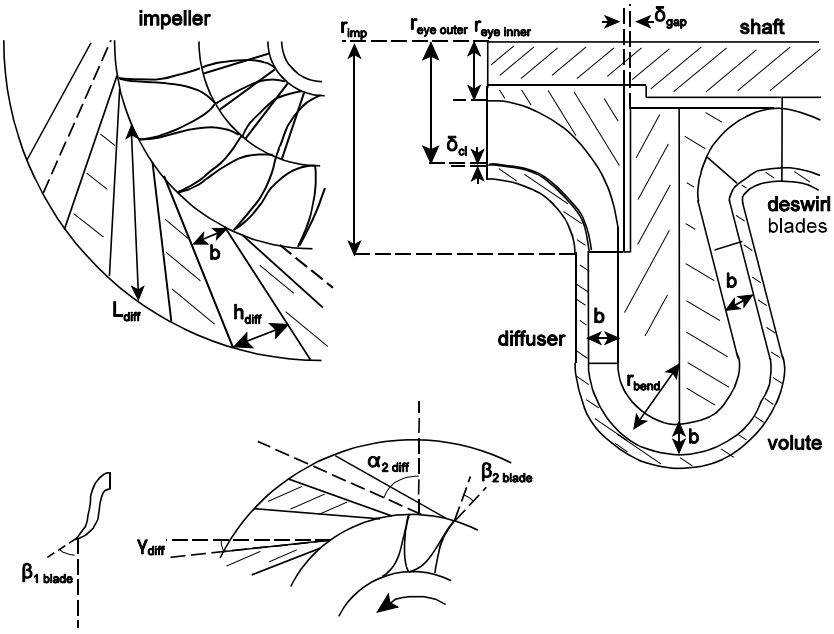

Figure B.1: Compressor geometry.

Table B.1 and B.2 list the main dimensions, shown in figure B.1.

Table B.1: Stage-specific compressor data.

	Stage 1	Stage 2	Stage 3	Stage 4	Stage 5
no. of diff. channels	14	15	17	19	21
$r_{eye\ inner}$ in m	0.098	0.124	0.138	0.149	0.157
b in m	0.052	0.047	0.043	0.04	0.037
h_{diff} in m	0.178	0.166	0.147	0.131	0.118

The flow length of the impeller has been approximated as a quarter of the circumference of a circle with radius r_{imp} - ($r_{eye\ inner}$ +$r_{eye\ outer}$) / 2. The equivalent hydraulic diameter, which is necessary for the calculation of the friction losses is by definition known from the perimeter P and area A of the eye:

$$D_{e\ imp} = \frac{4\ A_{eye}}{P_{eye}}$$

The hydraulic diameter of the diffuser and the volute is also known from this definition, using the perimeter and area at the diffuser outlet. The diffuser length can be calculated from:

$$L_{diff} = \frac{h_{diff} - b}{2\ \tan \gamma_{diff}}$$

Table B.2: Compressor data common to all stages.

no. of impeller/deswirl blades	20
$\beta_{1\ blade}$ in °	63.5
$\beta_{2\ blade}$ in °	32
$\alpha_{2\ diff}$ in °	66.9
γ_{diff} in °	5
r_{imp} in m	0.396
$r_{eye\ outer}$ in m	0.238
δ_{cl} in mm	1
δ_{gap} in mm	10

The flow length of the volute comprises half the circumference of a circle with radius r_{bend}, the straight section with length L_{diff} cos $\alpha_{2\ diff}$ and the section with the third bend which is assumed to be equally long as the flowlength of the next impeller. The cross-sectional and frontal area of the deswirl blades are known from the thickness/chord ratio and the number of blades.

The turbine is designed with a constant axial inlet velocity, a constant mean diameter and a degree of reaction of 0.5. The diameter is calculated from the desired pressure ratio, while the blade height follows from the axial design velocity of 210 m/s. The main data are shown in table B.3, the nomenclature is clarified in figure B.2. Other geometrical parameters like cross-sectional area, pitch, hydraulic diameter, heat exchange surface etc. can easily be calculated from the data in table B.3.

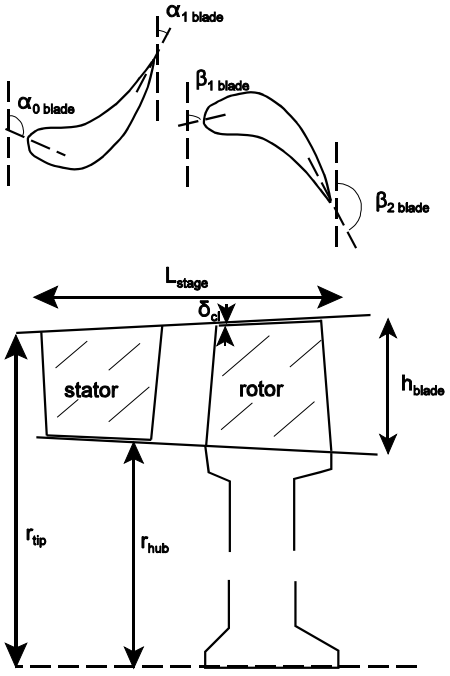

Figure B.2: Turbine geometry.

Table B.3: Turbine data.

all stages	
L_{stage} in m	0.08
$\gamma_{stat, rot}$	0.4
no of stator blades	173
no of rotor blades	174
δ_{cl} in mm	0.25
$\alpha_{0\ design}$ in °	99
$\alpha_{1\ design}$ in °	25
$\beta_{1\ design}$ in °	81
$\beta_{2\ design}$ in °	155
$\zeta_{prim\ stat, rot\ design}$	0.03

stage	d_{tip} in m	h in m
1	0.722	0.058
2	0.726	0.062
3	0.73	0.067
4	0.734	0.072
5	0.739	0.077
6	0.744	0.083
7	0.75	0.089

Appendix C

Inventory Control Vessel Sizing

The primary system helium inventory can be changed without use of a dedicated compressor if a number of vessels is connected to both the high and low pressure side (as shown in figure 3.21). In this case, if n vessels are consecutively filled and emptied, each vessel reduces the helium inventory with an equal factor f. If the ratio of lowest part-load inventory and design inventory pressure is X, then:

$$f = X^{\frac{1}{n}}$$

The mass which is displaced with the first vessel is therefore:

$$\Delta M_v = (1 - f) M_{s\ \text{full load}}$$

In which the subscript v indicates the first vessel and s the primary system.
The vessel size can be calculated in the extreme processes of adiabatic and isothermal behaviour, considering helium a perfect gas, and making use of the perfect mono-atomic gas relation:

$$\frac{5}{3} C_v = \frac{5}{3} R = C_p \quad \rightarrow \quad \frac{\kappa - 1}{\kappa} = \frac{2}{5}$$

For the isothermal process the qualitative behaviour of the tank states mass M, pressure and temperature are shown in figure C.1. Note that the processes refer to the tank, filling means filling of the tank and thus emptying of the primary loop.

The vessel size follows from a mass-balance between states 1 and 2.

$$\Delta M_v = (1 - f) M_{s\ \text{full load}} = M_{v\,2} - M_{v\,1} = \frac{V}{RT} (p_{v\,2} - p_{v\,1})$$

When the first vessel is full, its pressure equals the compressor discharge pressure, and when it is ‘empty’, its pressure equals the full load lowest system pressure.

$$p_{v\,2} = p_{s\ \text{high}\ 2} = f p_{s\ \text{high full load}} \qquad p_{v\,1} = p_{s\ \text{low}\ 1} = p_{s\ \text{low full load}}$$

The temperature is in the isothermal case equal to the temperature of the surroundings T_{surr}. The vessel volume V can now be calculated.

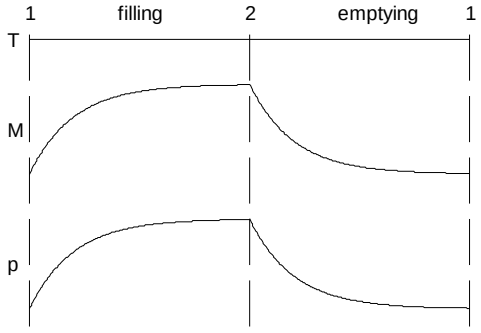

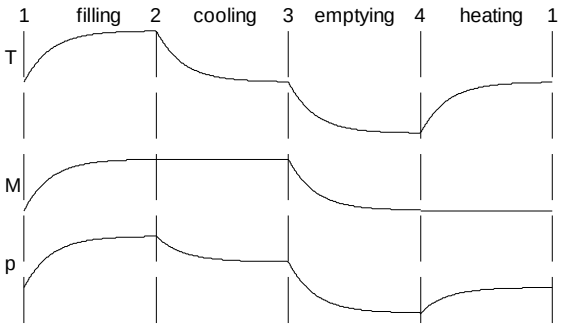

Figure C.1: Isothermal emptying and filling. *Figure C.2: Adiabatic emptying and filling.*

The states and processes of the adiabatic filling and emptying are shown in figure C.2. Similar to the isothermal case:

$$p_{v\,2} = f\,p_{s\ \text{high full load}} \qquad p_{v\,4} = p_{s\ \text{low full load}} \qquad T_{v\,1} = T_{v\,3} = T_{surr} \qquad \Delta M = \frac{V}{R\,T_{surr}}(p_{v\,2} - p_{v\,1})$$

Applying the ideal gas law to the heating and cooling yields:

$$\frac{p_{v\,2}}{T_{v\,2}} = \frac{p_{v\,3}}{T_{v\,3}} \qquad \frac{p_{v\,4}}{T_{v\,4}} = \frac{p_{v\,1}}{T_{v\,1}}$$

An energy-balance over the filling-process gives:

$$\frac{d\rho UV}{dt} = \phi_{in} H_{in} \qquad \frac{d\frac{p}{RT}C_v TV}{dt} = \phi_{in} C_p T_{s\ in}$$

Insertion of the ideal gas law and integration yields:

$$\frac{VC_v}{R}(p_{v\,2} - p_{v\,1}) = \Delta M\, C_p\, T_{s\ in}$$

The last relation can be obtained by considering the helium mass that stays in the vessel during emptying. This mass expands adiabatically and frictionless. For the isentropic process the following relation holds:

$$\frac{T_{v\,3}}{T_{v\,4}} = \left(\frac{p_{v\,3}}{p_{v\,4}}\right)^{\frac{\kappa-1}{\kappa}} = \left(\frac{p_{v\,3}}{p_{v\,4}}\right)^{\frac{2}{5}}$$

Combination of all equations gives:

$$\frac{D^5 A^2}{C^5} p_{v\,1}^5 - (A-B)^2 p_{v\,1}^2 + 2BE(B-A)p_{v\,1} - B^2E^2 = 0$$

with:

$$A = \frac{2}{3}\Delta M C_p T_{in} \qquad B = \Delta M R T_{surr} \qquad C = p_{v\,4} T_{surr} \qquad D = p_{v\,4}^{\frac{2}{5}} T_{v\,4} \qquad E = p_{v\,2}$$

The real root $p_{v\,1}$ between $p_{s\,low\,full\,load}$ and f $p_{s\ high\,full\,load}$ is the correct solution, backsubstition gives the vessel volume.

Nomenclature

variables:

α = heat transfer coefficient in J K^{-1} m^{-2} s^{-1}, void-fraction or angle in rad or °
β = delayed neutron, decay-heat group fraction or angle in rad or °
γ = yield fraction or blade geometry parameter
δ = thickness in m, gap clearance in m or camber angle in rad or °
Δ = difference
ε = pressure ratio
ζ = efficiency loss
η = efficiency
θ = angle between axial and absolute velocity
κ = ratio of specific heats (C_p/C_v)
λ = thermal conductivity in J m^{-1} K^{-1} s^{-1}, work input coefficient or decay constant in s^{-1}
Λ = mean neutron generation time in s
μ = dynamic viscosity kg m^{-1} s^{-1}
μ_{slip} = slip factor
ξ = porosity
ρ = density in kg m^{-3} or reactivity
σ = area ratio (A_{small} / A_{large}) or surface tension in N m^{-1}
τ = time constant in s
ϕ = mass flow in kg s^{-1}
Φ = specific potential energy in J kg^{-1}
Φ^2_{LO} = two-phase multiplier
$\Phi_{1..4}$ = terms in steam generator mass and energy balance
φ = velocity ratio
ψ = isentropic work coefficient
ω = rotational speed in s^{-1} or rpm

a = correction factor for discretisation in heat transfer or power of Reynolds in calc. of f
A = (cross-sectional) area in m^2
B = correction factor for non-ideal-gas behaviour
b = blade height in m or power of Reynolds in friction
$c_{1,2}$ = constant in division of Q over different nodes = ½ or 1
C = heat capacity in J $K^{-1}s^{-1}$, scaled precursor concentration or constant
C_p = specific heat at constant pressure in J kg^{-1} K^{-1}
C_f = flow resistance factor in m^2

d = diameter in m
D_e = equivalent hydraulic diameter in m
e_v = friction loss factor
Ex = exergy in J kg^{-1}
f = friction factor, camber in m or factor used in division of inventory over vessels
F = force in N
Fr = Friedel-number
g = gravitational constant = 9.81 m s^{-2}
G = controller gain
h = head in m, turbine blade height in m
H = specific enthalpy in J kg^{-1}
I = normalised Iodine concentration or inertia in kg m^2
K = specific kinetic energy in J kg^{-1} or process gain
L = flow length in m
l = length in m
M = mass in kg, Mach-number or moment in Nm
N = flow-number or number of passes or baffles
n = number of vessels
p = pressure in bar
P = power in J s^{-1} or dimensionless (in point-kinetic model)
Pr = Prandtl-number
Q = heat flow in J s^{-1}
r = radius in m
R = gas constant in J kg^{-1} K^{-1} or resistance against heat flow in J^{-1} K s
Re = Reynolds-number
R_p = price ratio of electricity to heat
s = blade pitch in m
S = entropy in J kg^{-1} K^{-1} or heat transfer surface area in m^2
SR = slip ratio
St = Stanton-number
t = time in s
T = temperature in K or °C
u = impeller speed in m s^{-1}
U = specific internal energy in J kg^{-1}
v = velocity in m s^{-1}
V = volume in m^3
VP = valve position
w = relative velocity in m s^{-1}
W = work done in rotating equipment in J s^{-1}
We = Weber-number
x = distance in flow direction in m, pitch or steam quality
Xe = normalised Xe-concentration
X_{Mart} = Martinelli-parameter
Y = expansion ratio
Z = number of impeller blades

abbreviations, acronyms and subscripts:

ACACIA	= AdvanCed Atomic Cogeneration for Industrion Applications
atm	= atmospheric
att	= attemperation
av	= average
ax	= axial
CCGT	= Closed Cycle Gas Turbine
CHP	= Combined Heat and Power
cl	= clearance
comp	= compensation (for gravitational force with area change) or compressor
contr	= contraction
corr	= corrected (for compressor off-design input conditions)
cr	= cross-sectional
d	= dead (time)
dea	= deaerator
desw	= deswirl
DH	= District Heating
diff	= diffuser
DRGA	= Dynamic Relative Gain Array
ec	= economic
eco	= economiser
ECS	= Energy Conversion System
eff	= effective
el	= electric
entr	= entrance
eq	= equivalent
ex	= exit or exergetic
exp	= expansion
FC	= frequency converter
fr	= friction
FZ	= Forster-Zuber
G	= gas
gen	= generator
GO	= gas only
grav	= gravitational
GT	= Gas Turbine
He	= helium
HP	= High pressure
HPR	= Heat to Power Ratio
HTGR	= High Temperature Gas-cooled Reactor
HX	= Heat eXchanger
imp	= impeller
inc	= incidence
INCOGEN	= Inherently safe Nuclear Cogeneration
IS	= Industrial Steam

isen	= isentropic
L	= liquid
LO	= liquid only
long	= longitudinal
LP	= low pressure
mech	= mechanical
MIMO	= Multi Input - Multi Output
nd	= dimensionless
NGT	= Nuclear Gas Turbine
no	= nozzle
nom	= nominal
norm	= normalised
NTU	= Number of Tranfer Units
PB	= pebble bed
PBMR	= Pebble Bed Modular Reactor
PI	= proportional-integral
PINK	= Programme for Intensification of Nuclear Competence
perp	= perpendicular
pol	= polytropic
pr	= prompt
prim	= primary
rad	= radial
rec	= recuperator
RGA	= Relative Gain Array
rot	= rotating equipment or rotor
s	= system
sat	= saturation
sec	= secondary
SG	= Steam Generator
SISO	= Single Input - Single Output
SP	= setpoint
ss	= steady-state
st	= steam
stat	= stator
surf	= surface
surr	= surroundings
tang	= tangential
temp	= temperature
th	= thermal
theor	= theoretical
TP	= two-phase
trans	= transition or transversal
turb	= turbine
u	= unit cell of finned tube
v	= vessel
vap	= vaporisation